PLAXIS LE
Slope Stability
2D/3D LIMIT EQUILIBRIUM SLOPE STABILITY ANALYSIS

Theory Manual

Written by:
The Bentley Systems Team

Last Updated: Tuesday, September 14, 2021

Bentley Systems Incorporated

COPYRIGHT NOTICE

TRADEMARK NOTICE

1 SLOPE STABILITY INTRODUCTION

Slope stability problems in geotechnical and geo-environmental engineering involve the solution of equilibrium equations of force and moment. This is traditionally accomplished through traditional method of slices techniques or more progressive stress-based methods.

The PLAXIS LE - Slope Stability software was designed to be a technically comprehensive slope stability set of software tools which implements cutting-edge searching and solution techniques as well as classic limit equilibrium methods of slices. As such, the software combines the best of the old and new technologies and provides a comprehensive set of tools to the geotechnical consultant.

The purpose of the theory manual is to provide the user with details regarding the theoretical formulation of each of the solution techniques implemented in the PLAXIS LE - Slope Stability software. The intent is not to provide an exhaustive summary of all theories associated with slope stability. Rather, the intent is to clearly describe specific details of the theory used in the PLAXIS LE - Slope Stability software.

Throughout this theory manual the term "the software" will refer to the software product "PLAXIS LE - Slope Stability", unless otherwise noted.

The software allows input from various finite element software modules in the PLAXIS product line. The user may import pore-water pressures from PLAXIS LE - Groundwater or stress states from PLAXIS 2D.

Some of the features of the software are as follows:

- Advanced stochastic analysis (Monte Carlo, Latin Hypercube, APEM)
- Spatial variability (1D, 2D)
- Unsaturated soil analysis
- Advanced critical slip surface searching algorithms
- Finite element analysis methods
- Comprehensive help systems

Covering the historical development of slope stability calculation methods and the latest advances, the software provides the following list of solution methodologies:

- Ordinary Method (also referred as Conventional or Swedish Method)
- Bishop Simplified Method
- Janbu Simplified Method
- Corps of Engineers Methods 1 and 2
- Lowe-Karafiath Method
- Spencer Method
- GLE (Fredlund) Method
- Morgenstern-Price Method
- Sarma Method
- Sarma Non-Vertical Slices Method
- Kulhawy Method
- SAFE-DP Method

2 OVERVIEW OF SLOPE STABILITY

Slope Stability is designed as a comprehensive and theoretically advanced slope stability package. The package is designed to contain a mix of classic limit equilibrium methods of slices as well as other newer, more rigorous slope stability methods that use optimization and other computational techniques.

Figure 1 provides an overall classification of slope stability methods of analysis. A distinction should be made between analysis methods and searching techniques. In 1977, Fredlund and Krahn classified the limit equilibrium methods of slices according to the elements of static equilibrium that were satisfied when solving for the factor of safety. This included categorizing the assumptions used to render the analysis determinate.

In 1981, Fredlund, Krahn and Pufahl further extended the comparison of slope stability method of slices to include additional methods (Fredlund et al, 1981). Most of the limit equilibrium methods of slices made an assumption regarding the interslice forces (e.g., the interslice force function). Consequently, most of the methods of slices differed in the manner by which the normal force at the base of a slice was calculated. Common to all the methods of slices was the way the factor of safety was defined and the fact that the normal force was computed from static considerations of one slice through a potential sliding mass.

Figure 1 indicates that it is now possible to also take into consideration the search technique associated with the determination of the shape and location of the critical slip surface. The finite element stress analysis method can also be used to determine the normal force at the base of a slice, giving rise to the Enhanced (Kulhawy) Limit method as well as other optimization techniques (e.g., Dynamic Programming).

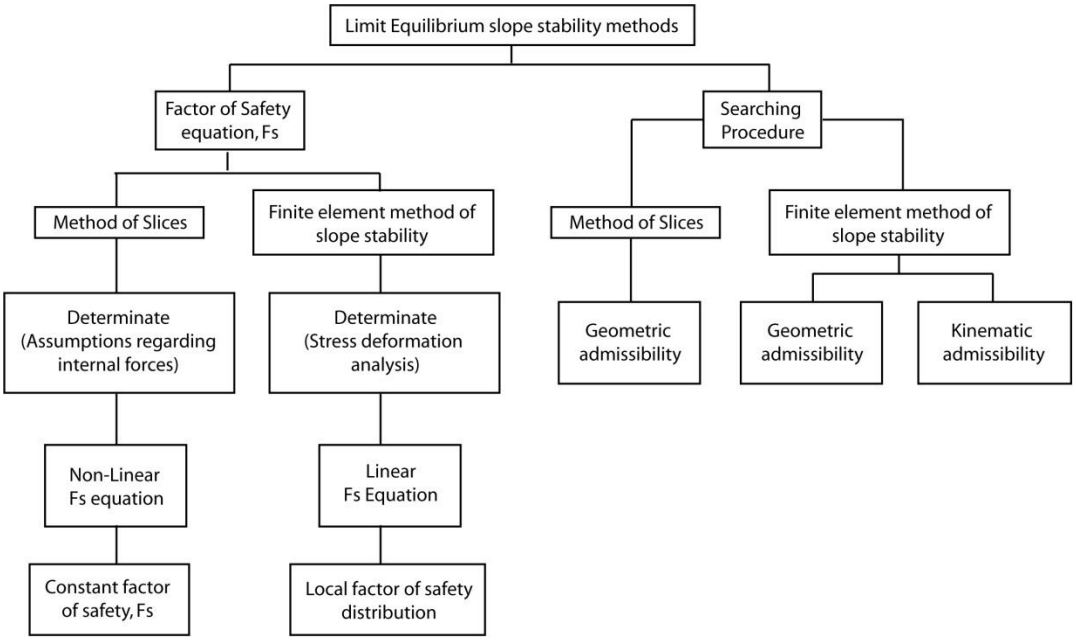

Figure 1 Overall classification of slope stability methods of analysis

3 LIMIT EQUILIBRIUM METHODS

3.1 INTRODUCTION

Limit equilibrium methods of slope stability analysis have been widely used for computing the factor of safety since the advent of the digital computer in the 1960s. The methods can be classified and understood in terms of the principles involved and assumptions used in formulating each analysis.

The general principles that have historically applied to all limit equilibrium methods of slices state that:

1. Plasticity conditions are developed only along the slip surface and the moving slope mass behaves as a solid,
2. The shape of the slip surface is to be selected by the end-user, and
3. The location of the critical slip surface is found by trial and error.

The assumptions common to all limit equilibrium methods of slices are as follows:

1. The materials behave in a Mohr-Coulomb manner (i.e., each material has friction, ϕ ', and cohesion, c', component of the shear strength) and the material fails in accordance with the Mohr-Coulomb failure criterion,
2. The factor of safety, F_s, is the same for all slices, and
3. The factor of safety, F_s, for the cohesive component is equal to the factor of safety for the frictional component as shown in the following shear force mobilized equation for a saturated soil.

$$S_m = \frac{c'\beta}{F_s} + \frac{\left[\left(\sigma_n - u_w\right)\tan\phi'\right]\beta}{F_s} \qquad \textbf{[1]}$$

where:

c' = effective cohesion,

ϕ' = effective angle of internal friction

u_w = pore-water pressure at the base of a slice,

β = length along the base of a slice,

σ_n = normal stress acting on the base of a slice,

F_S = overall factor of safety,

S_m = shear force mobilized at the base of a slice,

S_{soil} = shear strength of the soil expressed as a force (i.e., $S_{soil} = \tau\beta$),

S_c = cohesion strength expressed as a force (i.e., $S_c = c'\beta$), and

S_f = frictional strength expressed as a force (i.e., $S_f = [(\sigma_n - u_w)\tan\phi']\beta$).

All the methods of slices implemented in Slope Stability are based on the limit equilibrium principles and assumptions except for the SAFE method, which evaluates the factor of safety based on stress conditions determined from an independent finite element stress analysis (i.e., normal stresses and actuating shear stresses).

The shape of a potential slip surface can be assumed to be circular, composite (i.e., combined circular and linear portions) or non-circular (i.e., fully specified or block specified slip surfaces). The slip surface passes through the material mass and the inscribed portion of material is subdivided into slices.

Figure 2 and Figure 3 show the forces involved for circular and composite slip surfaces, respectively. Note that the fully specified slip surfaces and the block specified surfaces are somewhat similar in the linear portion of a composite slip surface. The variables are defined as follows:

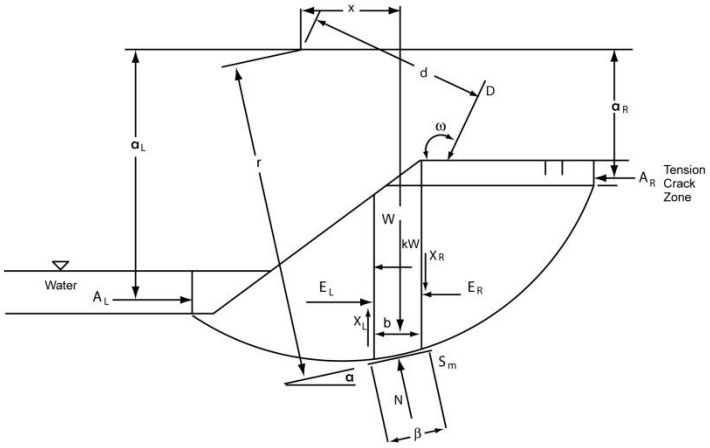

Figure 2 Definition of forces and slope geometry variables for a circular slip surface

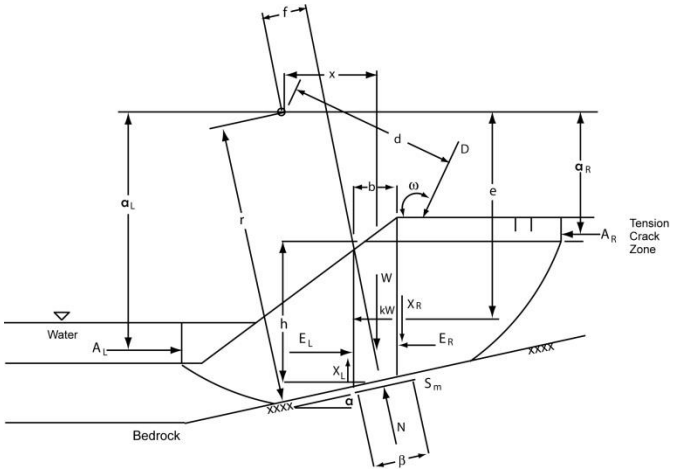

Figure 3 Definition of forces and slope geometry variables for a composite slip surface

where:

W = weight of a slice,

N = normal force on the base of the slice,

S_m = shear force mobilized on the base of each slice,

E = horizontal interslice normal forces. The *'L' and 'R'* subscripts indicate the left and right sides of the slices, respectively,

X = vertical interslice shear forces. The *'L'* and *'R'* subscripts indicate the left and right sides of the slices, respectively,

D = external line load is applied only to the slice on which it acts. A distributed load can also be converted into an equivalent line load for each slice,

k = horizontal seismic load coefficient applied through the centroid of each slice,

r = radius (or the moment arm) associated with the mobilized shear force, S_m,

f = perpendicular offset of the normal force from the center of rotation (or from the axis point). It is assumed that the *'f'* distance on the right side of the center of rotation of a negative slope (i.e., a left-to-right slope) is negative and those on the left side of the center of rotation are positive,

x = horizontal distance from the centroid of each slice to the center of rotation (or to the axis point),

e = vertical distance from the centroid of each slice to the center of rotation (or to the axis point),

d = perpendicular distance from a line load to the center of rotation (or to the axis point),

d_r = perpendicular distance from a reinforcement load to the center of rotation (or the axis point),

h = vertical distance from the center of the base of each slice to ground surface,

$a_{L,R}$ = perpendicular distance from the resultant external water force to the center of rotation (or the axis point). The *'L'* and *'R'* subscripts indicate the left and right sides of the slope, respectively,

$A_{L,R}$ = resultant external water forces. The *'L' and 'R'* subscripts indicate the left and right sides of the slope, respectively,

ω = angle of the line load from the horizontal. This angle is measured counterclockwise from the positive x-axis,

θ = angle of the reinforcement load from the horizontal. This angle is measured counterclockwise from the positive x-axis, and

χ = angle between the tangent to the center of the base of each slice and the horizontal. The sign conversion for a slope is as follows: positive when the angle of the slice base is in the same direction as overall slope of the geometry, and negative when the angle of the slice base is opposite to the overall slope of the geometry.

3.2 DEFINITION OF FACTOR OF SAFETY

The factor of safety is defined as: "*that factor by which the shear strength must be reduced to bring a material mass into a state of limit equilibrium along a specified slip surface*". The shear force mobilized for a saturated soil can be written in terms of the failure criterion for any given slice.

$$S_m = \frac{\beta}{F_s}\left\{c' + \left(\sigma_n - u_w\right)\tan\phi'\right\} \quad \textbf{[2]}$$

where:

S_m = shear force mobilized,

c' = effective cohesion of the material,

ϕ' = effective angle of internal friction,

u_w = pore-water pressure at base of a slice,

β = length along the base of a slice, and

σ_n = normal stress acting on the base of a slice.

3.2.1 Unsaturated Soil Phi-b Method

For an unsaturated soil, the effect of matric suction needs to be included in the equation for the mobilized shear force (Fredlund et al., 1978).

$$S_m = \frac{\beta}{F_s}\left\{c' + \left(\sigma_n - u_a\right)\tan\phi' + \left(u_a - u_w\right)\tan\phi^b\right\} \quad \textbf{[3]}$$

where:

u_a = pore-air pressure at the base of a slice,

$u_a - u_w$ = matric suction, and

ϕ^b = the angle defining the rate of increase of strength due to an increase in suction.

Equation [3] is a linear form for designating the shear strength of an unsaturated soil. The shear force mobilized equation is later written in terms of the soil-water characteristic curve, SWCC, for an unsaturated material. The component of shear strength related to matric suction then becomes nonlinear. This equation has the effect of increasing the shear strength in the unsaturated zone of a soil profile.

3.3 GENERAL LIMIT EQUILIBRIUM METHOD

A *General Limit Equilibrium Method (GLE)* was proposed by Fredlund at the University of Saskatchewan in the 1970's (Fredlund and Krahn 1977; Fredlund et al 1981). This method is based on the calculation of two factors of safety equations and allows for

the incorporation of a variety of interslice force assumptions. The GLE method can then be specialized to other methods of slices available in the software.

3.3.1 Static Equilibrium Equations

The following equations of Newtonian statics are used to formulate two factors of safety equations.

$\sum M_0 = 0$: equation is applied for the overall slope and is the basis of the moment equilibrium factor of safety, $(F_s)_m$ equation,

$\sum F_h = 0$: equation is applied for the overall slope and is the basis of the force equilibrium, $(F_{s)\,f}$ equation,

$\sum F_v = 0$: equation is applied to each slice for defining the normal force on the base of each slice, *N,* and

$\sum F_h = 0$: equation is applied for each slice when using an integration across the slope for defining the interslice normal forces, *E.*

The GLE method can be viewed as independently solving two factors of safety equations. One equation gives the factor of safety with respect to moment equilibrium, $(F_{s)\,m}$, and the other equation provides the factor of safety with respect to overall horizontal force equilibrium, $(F_s)_f$.

3.3.2 Factor of Safety Equations for Moments and Horizontal Equilibrium

The factor of safety equation with respect to moment equilibrium is:

$$\left(F_s\right)_m = \frac{\sum\left[c'\beta r\cos a + \left[W + \left(X_L - X_R\right) + \left[D\sin\omega\right] + \left[D_r\sin\theta\right] - u_w\beta\cos a\right]r\tan\phi'\right]/m_a}{\pm Aa + \sum Wx - \sum Pf + \sum kWe \pm \left[Dd\right] \pm \left[D_r d_r\right]} \quad \textbf{[4]}$$

The factor of safety equation with respect to horizontal force equilibrium is:

$$\left(F_s\right)_f = \frac{\sum\left[c'\beta + \left(\frac{W}{\cos\alpha} + \frac{\left(X_L - X_R\right)}{\cos\alpha} + \frac{\left[D\sin\omega\right]}{\cos\alpha} + \frac{\left[D_r\sin\theta\right]}{\cos\alpha} - u_w\beta\right)\right]/m_\alpha}{\pm A + \sum\left\{W + \left(X_L - X_R\right) + \left[D\sin\omega\right] + \left[D_r\sin\theta\right]\right\}\tan\alpha + \sum kW - \left[D\cos\omega\right] - \left[D_r\cos\theta\right]} \quad \textbf{[5]}$$

where:

c' = effective cohesion of the material at the base of a slice,

u_w = pore-water pressure,

N = normal force on the base of a slice,

W = self-weight of each slice,

D = load (line load and/or distributed load),

D_r = reinforcement load,

A = hydrostatic water force acting at the left, L, or right, R, extremities of the slip surface,

r = radius (or moment arm) associated with the mobilized shear force, S_m,

x = horizontal distance from the centroid of each slice to the center of rotation (or to the axis point),

f = perpendicular offset of the normal force from the center of rotation (or from the axis point),

d = perpendicular distance from a line load to the center of rotation (or the axis point),

d_r = perpendicular distance from a reinforcement load to the center of rotation (or the axis point),

X_R = vertical interslice shear forces on the right side of a slice,

E_R = horizontal interslice normal forces on the right side of a slice,

ω = angle of the line load from the horizontal. This angle is measured counter-clockwise from the positive x-axis,

λ = lambda value representing the percentage of the interslice force used in the analysis,

ϕ' = effective angle of internal friction of the material at the base of a slice,

β = length along the base of a slice,

θ = angle of the reinforcement load from the horizontal. This angle is measured counterclockwise from the positive x-axis, and

α = angle between the tangent to the center of the base of each slice and the horizontal.

3.3.3 Normal Force at the Base of each Slice

The normal force at the base of each slice is obtained by summing forces in a vertical direction.

$$N = \frac{W + (X_L - X_R) - \frac{c'\beta \sin\alpha}{F_s} + \frac{u_w \beta \tan\phi' \sin\alpha}{F_s} + [D\sin\omega] + [D_r \sin\theta]}{m_\alpha} \quad \textbf{[6]}$$

3.3.4 Interslice Normal Force and Interslice Shear Force

The interslice normal force for each slice is obtained by summing forces horizontally on each slice in an integration manner progressing across the slope.

$$E_R = E_L + \{W - (X_R - X_L) + [D\sin\omega] + [D_r \sin\theta]\}\tan\alpha - \frac{S_m}{\cos\alpha} + kW - [D\cos\omega] - [D_r \cos\theta] \quad \textbf{[7]}$$

The interslice shear forces, *(X_R or X_L)*, are a function of the interslice normal forces. The interslice shear forces are computed from the interslice normal forces after each iteration, using the following equation. The calculation of the interslice shear forces is repeated after each iteration, until convergence is obtained for the overall factor of safety equations.

$$X_R = E_R \lambda \ f(x) \quad \textbf{[8]}$$

where:

$f(x)$ = mathematical equation describing the form of the interslice force function.

λ = percentage (in decimal form) of the function used.

Figure 4 shows a typical half-sine function. The upper curve is the specified function while the lower curve shows the percentage of the function used in satisfying force and moment equilibrium λ represents a ratio between the two curves.

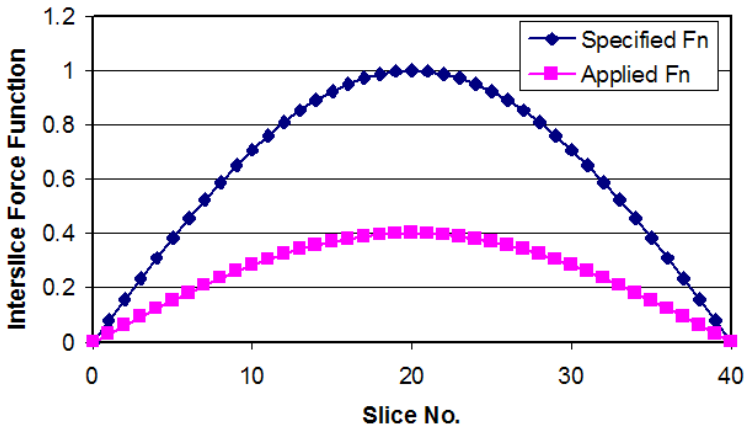

Figure 4 Half-sine interslice force function

3.3.5 The Relationship between General Limit Equilibrium Method and other Methods of Slices

The normal force at the base of a slice is dependent on the interslice shear forces, X_L and X_R, on either side of the slice. The interslice shear forces are determined from the interslice normal force and the interslice force function. Different methods of slices have been proposed based on different assumptions related to the interslice force functions.

In the Bishop Simplified method (1955) the interslice shear forces are set equal to zero. In other words, the interslice normal forces are assumed to be horizontal. Applying these conditions to the interslice force equations, gives the following conditions that must be met:

$$\frac{X}{E} = \frac{0}{E} = \lambda \quad f(x) = 0 \qquad \textbf{[9]}$$

where, f(x) cannot be equal to zero. The function f*(x)* should be a positive function, preferably extending between 0 and 1.

The Bishop Simplified method becomes a special case of the GLE method by setting lambda, λ equal to zero and setting the arbitrary function, *f(x)*, to any value and satisfying only the moment equilibrium equation.

In the Janbu's Simplified method (1954), the interslice shear force is also assumed to be equal to zero or the λ value can be set equal to zero. Janbu's Simplified method satisfies the force equilibrium equation.

In the Spencer method (1967), the direction of the interslice forces is assumed to have a constant direction throughout the sliding mass. This condition is simulated by setting λ equal to the tangent of the selected angle for the interslice forces. That is,

- *f(x)* is equal to 1.0, and
- λ is equal to [tan θ], where θ is the slope of the interslice forces.

Substituting these conditions into the general interslice force equation gives,

$$\frac{X}{E} = \tan\ \theta = \lambda\ \ f(x) \qquad \textbf{[10]}$$

The interslice force function can be viewed as a constant for the Spencer method. When *f(x*) is set as a constant, the GLE method solves the Spencer method. The Spencer method satisfies both moment and force equilibrium conditions.

The Corps of Engineers method internally computes the interslice force function based on the "average slope" of the geometry and sets λ equal to 1.0. Only the force equilibrium equation is solved. There are two interpretations of "average slope" in the Corps of Engineers method.

The Lowe-Karafiath method internally computes the interslice force function based on the average slope between the ground surface and the slip surface. λ is set to 1.0 and only the force equilibrium equation is solved.

Morgenstern-Price method is essentially the same as the GLE method in terms of the interslice force used in the analysis assumptions and the equations of static equilibrium solved. A slight difference between the two methods will be discussed later.

The GLE method can be specialized to all other methods of slices regardless of slip surface shape. The GLE method in the software utilizes a wide range of interslice force functions such as:

- Constant function
- Half-sine function
- Clipped-sine function
- Trapezoid function
- Specified function
- Wilson-Fredlund (1983) function

The GLE method satisfies both force and moment equilibrium by finding the intersection point of the moment and force equilibrium factors of safety (i.e., F_m and F_s), curves plotted versus lambda, λ.

3.4 ORDINARY OR FELLENIUS METHOD

The Ordinary or Fellenius method (sometimes known as Swedish or Conventional method of slices) was the first slope stability method based on dividing the sliding mass into slices. This method gives rise to a linear factor of safety equation and was subsequently used because of its simplicity. This method can readily be implemented using hand calculations.

This method assumes that the interslice shear and normal forces can be set to zero. Two equations of static equilibrium are used to solve for the factor of safety.

$\sum M_0 = 0$: Moment equilibrium equation is applied to the overall slope about the center of rotation and is the basis for calculating the factor of safety, F_S, and

$\sum F_\perp = 0$: Force equilibrium equation sums forces perpendicular to the base of each slice, and defines the normal force on the base of each slice, N, in terms of the weight of the slice, W.

There is a fundamental theoretical limitation associated with the Swedish method or the Ordinary method and it can be explained as follows. First, it is assumed that the inter-slice forces cancel between slices. The normal force on the base of each slice is then calculated by summing forces perpendicular to the base of the slice. This means that the interslice forces must be parallel to the base of the slice to NOT appear in the statics equation.

However, when moving to the next slice, the direction for summing forces at the base of the slice must change. Now, the inter-slice forces need to be in a slightly different direction to put two slices together. Consequently, the methodology has done something fundamentally wrong from a statics standpoint.

Consequently, the Swedish (Ordinary) method should not be considered as an acceptable methodology because of the fundamental statics flaw. In other words, it is unacceptable Newtonian static equilibrium. The Ordinary method is only implemented in the software to provide a reasonable transition from the earliest methods to subsequent methods. The use of the Ordinary method in geotechnical engineering practice is not recommended.

3.4.1 Factor of Safety for a Circular Slip Surface

Figure 5 defines the variables associated with a circular slip surface. The simplest form of the Ordinary method factor of safety when considering pore-water pressures is as follows.

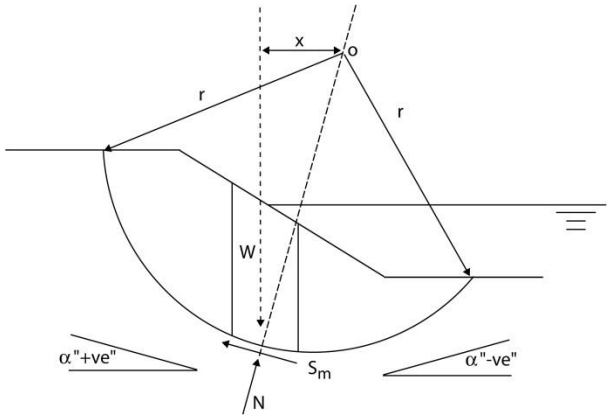

Figure 5 Forces associated with the Ordinary method using a circular slip surface

Applying the moment equilibrium equation, $\Sigma M_o = 0$, gives:

$$\sum Wr\sin\alpha - \sum S_m R = 0 \qquad \textbf{[11]}$$

where:

$$S_m = \frac{\beta}{F_s}\left[c' + (\sigma_n - u_w)\tan\phi'\right] \qquad \textbf{[12]}$$

$$\sigma_n = \frac{W\cos\alpha}{\beta} \qquad \textbf{[13]}$$

where:

c' = effective cohesion,

ϕ' = effective angle of internal friction,

u_W = pore-water pressure,

β = length along the base of a slice,

F_S = overall factor of safety,

W = self-weight of each slice,

S_m = shear force mobilized on the base of a slice,

α = angle of slice base,

r = radius (or moment arm) associated with the mobilized shear force, S_m, and

$\sigma\eta$ = normal stress on the base of a slice.

Substituting the shear force mobilized, S_m, into Equation [11] gives:

$$F_s = \frac{\sum \left[c' \beta + (W \cos \alpha - u_w \beta) \tan \phi' \right]}{\sum W \sin \alpha} \quad \textbf{[14]}$$

3.4.2 Factor of Safety for a Composite Slip Surface

A composite slip surface is shown in Figure 6. In the analysis of a composite slip surface, the radius associated with the shear force mobilized, S_m, does not cancel. Therefore, the radius, r, remains as a variable in the factor of safety equation. In addition, the normal force at the base of the slice, N, produces a moment about the center of rotation (or center of moments).

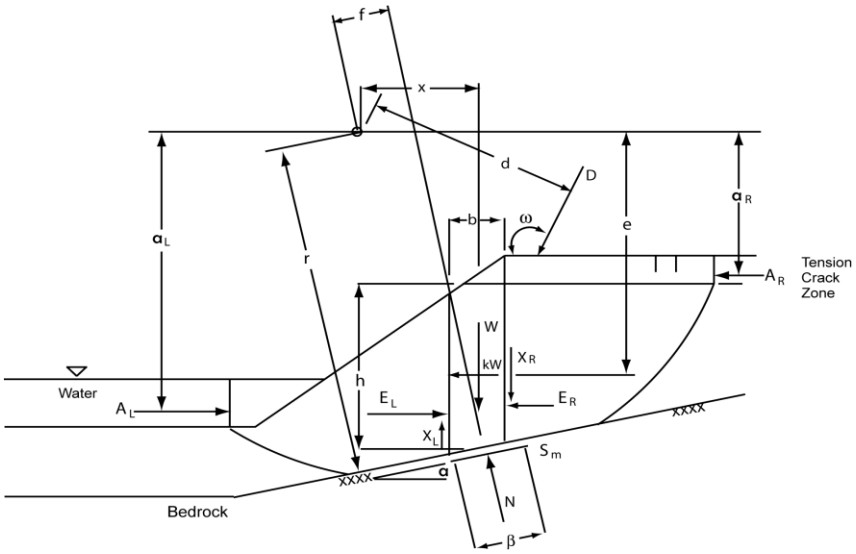

Figure 6 Forces acting on a composite slip surface

The following equations need to be solved for the more general case of a non-circular slip surface and complex loading conditions involving a line load, distributed load, and reinforcement load.

The moment equilibrium equation for a composite slip surfaces, $\Sigma M_o = 0$, can be written,

$$\sum W r \sin \alpha - \sum N f - \sum S_m r = 0 \quad \textbf{[15]}$$

Substituting the shear force mobilized S_m, into Equation [15] and solving for F_s gives:

$$F_s = \frac{\sum \left[c' \beta + (N - u_w \beta) \tan \phi' \right] r}{\sum W r \sin \alpha - \sum N f} \quad \textbf{[16]}$$

The normal force, N, can be substituted into Equation [16] to give,

$$F_s = \frac{\sum \left[c' \beta + (W \cos \alpha - u_w \beta) \tan \phi' \right] r}{\sum W r \sin \alpha - \sum W f \cos \alpha} \quad \textbf{[17]}$$

The effect of partial submergence of the slope by a fluid can also be added to the above equation. The normal force remains the same; however, additional moment terms are added to the denominator to account for the moments resulting from the left and right resultant water force about the center of rotation (or center of moments). The factor of safety equation then becomes,

$$F_s = \frac{\sum\left[c'\beta r + \left(W\cos\alpha - u_w\beta\right)r\tan\phi'\right]}{-A_L a_L + A_R a_R + \sum W r\sin\alpha - \sum Wf\cos\alpha} \qquad \textbf{[18]}$$

The effect of external line loads, *D*, changes the calculation of the normal forces on the base of a slice, for the slice on which the load is acting. Summing forces perpendicular to the base of the slice, $\Sigma F_{\perp} = 0$, gives,

$$N = W\cos\alpha + \left[D\cos\left(\omega + a - 90°\right)\right] \qquad \textbf{[19]}$$

A distributed load can also be converted to an equivalent line load on a slice. If the distributed load is due to gravity, it will act in a vertical direction and can be input as an equivalent material layer with a unit weight. The load due to gravity can either have associated shear strength parameters or no shear strength parameters. The use of a distributed load is discussed later.

The effect of a reinforcement load, D_r, changes the calculation of the normal force in a manner like that of a line load. However, the effect of reinforcement can be assumed to act immediately or to develop with strain. Each assumption will lead to different expressions for the factor of safety. Further details are presented in Chapter 7.

The effect of earthquake loading also affects the normal force calculated for the base of each slice. The horizontal earthquake force can be written as follows:

$$F_e = kW = \frac{\alpha}{g}W \qquad \textbf{[20]}$$

where:

F_e = horizontal earthquake force,

k = *a/g*, seismic coefficient,

a = horizontal acceleration caused by the earthquake, and

g = acceleration caused by gravity, 9.81 m/s^2.

The normal force, *N,* can be rewritten as:

$$N = W\cos\alpha - kW\sin\alpha + \left[D\cos\left(\omega + a - 90°\right)\right] \qquad \textbf{[21]}$$

Substituting the expanded normal force equation into the factor of safety Equation [18] and including the effect of positive and negative moment terms due to external line loads and earthquake loads gives,

$$F_s = \frac{\sum\left[c'\beta r + \left(W\cos\alpha - kW\sin\alpha + \left[D\cos(\omega + \alpha - 90^o\right] - u\beta\right)r\tan\phi'\right]}{\pm\left[Dd\right] \pm Aa + \sum Wx - \sum Nf + \sum kWe} \qquad \textbf{[22]}$$

The user should note that the Ordinary method is generally only used to provide an approximate starting value for calculating other factors of safety. In the software, the Ordinary method is used to provide an initial or starting value for the factor of safety since the factor of safety equation is linear in form. The Ordinary method is not extensively used in engineering practice due to its lack of accuracy.

The above equations for a composite slip surface satisfy static equilibrium but it should be noted that force equilibrium has not been satisfied in two orthogonal directions and the interslice force assumption is not reasonable. For further information on the effect of the axis for moment equilibrium, the user is referred to the paper by Fredlund et al. (1992).

3.5 BISHOP'S SIMPLIFIED METHOD

In 1956, Bishop derived a limit equilibrium method of slices based on the assumption that the interslice shear forces could be ignored while retaining the interslice normal forces. In other words, the resultant interslice forces act in a horizontal direction but overall horizontal force equilibrium is not satisfied.

The two static equilibrium equations used were:

$\sum M_o = 0$: Equation representing moment equilibrium about the center of rotation for an overall slope. This equation forms the basis for deriving the factor of safety, F_s, and

$\sum F_v = 0$: Equation representing vertical force equilibrium for each slice. This equation is used to obtain the normal force, *N,* at the base of each slice.

3.5.1 Factor of Safety for a Circular Slip Surface

The factor of safety equation with respect to the moment equilibrium about the center of rotation (or center of moments) is the same as that used for the Ordinary method and is shown in Figure 7. The force equilibrium equation is written in the vertical direction for each slice.

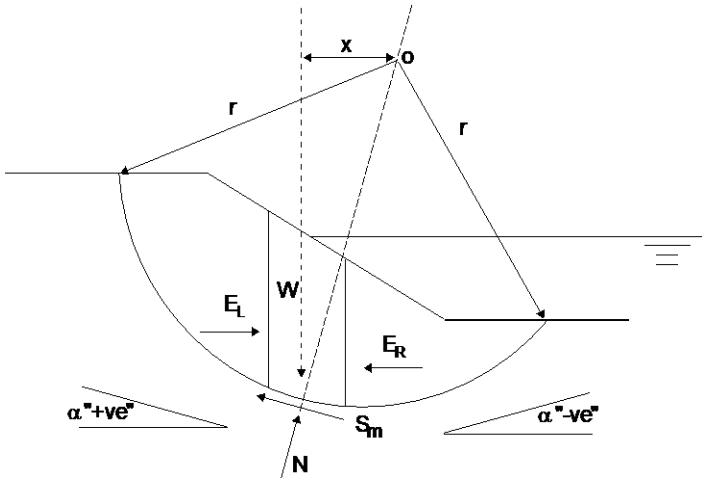

Figure 7 Forces associated with Bishop's Simplified method of slices

The moment equilibrium equation, $\Sigma M_n = 0$, can be written as follows:

$$\sum Wr \sin\alpha - \sum S_m\, r = 0 \qquad \textbf{[23]}$$

Where the shear force mobilized equation can be written as:

$$S_m = \frac{c'\beta + \left(N - u_w\beta\right)\tan\phi'}{F_s} \qquad \textbf{[24]}$$

Substituting the shear force mobilized Equation [24] into Equation [23] gives the factor of safety equation:

$$F_s = \frac{\sum\left[c'\beta + \left(N - u_w\beta\right)\tan\phi'\right]}{\sum W \sin\alpha} \qquad \textbf{[25]}$$

The normal force at the base of a slice can be obtained by substituting the shear force mobilized, S_m, into the vertical force equilibrium equation, $\Sigma F_v = 0$.

$$N\cos\alpha - W + \frac{\left[c'\beta + (N - u_w\beta)\tan\phi'\right]\sin\alpha}{F_s} = 0 \qquad \textbf{[26]}$$

Rearranging, the normal force can be written as,

$$N = \frac{W - \dfrac{c'\beta\sin\alpha}{F_s} + \dfrac{u_w\beta\tan\phi'\sin\alpha}{F_s}}{m_\alpha} \qquad \textbf{[27]}$$

where:

$$m_\alpha = \cos\alpha + \frac{\sin\alpha \tan\phi'}{F_s} \quad \textbf{[28]}$$

Substituting the normal force, *N*, into the factor of safety equation and rearranging the equation gives the following equation for a circular slip surface.

$$F_s = \frac{\sum \left[c'\beta\cos\alpha + (W - u_w\beta\cos\alpha)\tan\phi'\right]/m_\alpha}{\sum W\sin\alpha} \quad \textbf{[29]}$$

Since m_α involves the factor of safety, F_s, variable, Equation [29] is nonlinear. Therefore, an iterative technique is required when solving for the factor of safety, F_s. The proposed iterative technique is discussed in Section 2.5.3.

3.5.2 Factor of Safety for Bishop's Simplified Method for Composite Slip Surface

The *Bishop's Simplified Method* has been extended to a composite slip surface in a manner like that shown for the Ordinary method. The derivation of the factor of safety equation is shown for the case including external loads, earthquake loads and water submergence.

The moment equilibrium equation about an axis approximating the center for the slip surface, $\Sigma M_o = 0$, can be written as follows:

$$\sum Wx - \sum Nf - \sum S_m r + \sum kWe \pm [Dd] \pm [Aa] = 0 \quad \textbf{[30]}$$

Vertical forces equilibrium on each slice, $\Sigma F_V = 0$, can be written,

$$W - N\cos\alpha - S_m\sin\alpha + [D\sin\omega] = 0 \quad \textbf{[31]}$$

Substituting the mobilized shear force at the base of a slice, S_m, into Equation [31] gives the normal force, *N*,

$$N = \frac{W - \frac{c'\beta\sin\alpha}{F_s} + \frac{u_w\beta\tan\phi'\sin\alpha}{F_s} + [D\sin\omega]}{m_a} \quad \textbf{[32]}$$

Substituting the normal force, *N*, (Equation [32] into the moment equilibrium Equation [30] gives the factor of safety, F_s, equation for a composite slip surface.

$$F_s = \frac{\sum \left[c'\beta r\cos\alpha + (W + [D\sin\omega] - u_w\beta\cos\alpha)r\tan\phi'\right]/m_\alpha}{\pm[Dd] \pm Aa + \sum Wx - \sum Nf + \sum kWe} \quad \textbf{[33]}$$

3.5.3 Iterative Procedure Used in Solving Bishop's Simplified Method

The *iterative procedure* used in the software to solve for the factor of safety for Bishop Simplified method is as follows:

1. Assume an initial factor of safety F_s = 1.0, or use the factor of safety computed by the Ordinary method multiplied by 1.17,
2. Calculate m_α using the initial factor of safety and solve the factor of safety equation for a new factor of safety, F_s, corresponding to the first iteration,
3. The newly computed factor of safety, F_s, can now be used to compute new m_α values,
4. Compute a new factor of safety, F_s, using the new m_α values,
5. Repeat Steps 3) and 4) until the difference between consecutive factor of safety computations is less than the designated tolerance (i.e., generally about 0.001).

3.6 JANBU'S SIMPLIFIED METHOD

The equilibrium equations used for *Janbu's Simplified Method* are like those used for Janbu's Generalized method. Janbu's Simplified method assumes that the resultant interslice forces are horizontal. Therefore, the interslice shear forces are removed from the factor of safety equations.

The factor of safety equation can be written as follows:

$$F_s = \frac{\sum\left[c'\beta + \left(\frac{W + [D\sin\omega]}{\cos\alpha} - u\beta\right)\tan\phi'\right]/m_\alpha}{\sum\{W + [D\sin\omega]\}\tan\alpha + \sum kW - [D\cos\omega] \pm A} \qquad \textbf{[34]}$$

An iterative procedure is required when solving the factor of safety Equation [34]. The iterative technique is like that used when solving Bishop's Simplified method.

In the original publication of the Janbu Simplified Method, the computed factor of safety was multiplied by a correction factor. The correction factor was always slightly greater than 1.0 and depended on the depth of the slip surface. The basis for the correction factor has been somewhat contested and therefore it has not been included in the software code. Consequently, Janbu's Simplified method satisfies horizontal force equilibrium when using the designated assumptions.

3.7 SPENCER METHOD

The *Spencer Method* assumes that the ratio of the interslice shear force to the interslice normal force is constant throughout the sliding mass. This method independently satisfies horizontal force and moment equilibriums giving rise to force equilibrium factor of safety, F_f, and a moment equilibrium factor of safety, F_m.

The interslice force assumption can be written as follows:

$$X = E\tan\theta \qquad \textbf{[35]}$$

where:

X = interslice shear force,

E = interslice normal force, and

θ = angle of the resultant interslice force from the horizontal.

This relationship between the interslice shear force, *X,* and interslice normal force, *E*, can be considered as a specific case of the General Limit Equilibrium, GLE method. In the GLE method, the interslice forces are related using the empirical equation proposed by Morgenstern-Price (1965):

$$X = E\lambda\, f(x) \qquad \textbf{[36]}$$

The Spencer method corresponds to the case where lambda, λ, is equal to 1.0 and the function, *f(x)* is a constant equal to (tan θ) in the GLE method.

3.8 MORGENSTERN-PRICE METHOD

The *Morgenstern-Price Method* (M-P method) is like the GLE method in terms of the assumptions made and the static equilibrium equations solved. The M-P method satisfies both moment equilibrium and horizontal force equilibrium equations when computing the factor of safety. There are a variety of assumptions that can be made with respect to the interslice force functions that can be used. Several functions were suggested by Morgenstern and Price (1965) and Wilson and Fredlund (1983) suggested the use of an empirical interslice force function based on finite element stress analysis are:

- Constant function
- Half-sine function
- Clipped-sine function
- Trapezoid function
- Specified function
- Wilson-Fredlund (1983) function

The original Morgenstern-Price (1965) method used an integration type solution with a modified Newton-Raphson solver. The solution method used in the software is a summation approach that is like that used for other methods of slices.

A Rapid solver is used in the software for computing the factor of safety corresponding to the *M-P* method. The Rapid Solver procedure can be described as follows:

1. Set an initial value for λ = 2/3 'cord slope' where the 'cord slope' is defined as shown in Figure 8,
2. Obtain the initial factor of safety using the Ordinary method and increase the computed value by 17%. The estimated value for F_s, is used as the initial F_s, for solving the *M-P* method,
3. Compute a set of $(F_s)_m$ and $(F_s)_f$ (i.e., moment and force equilibrium factors of safety)$_f$ using the initial, λ,
4. Compare the two factors of safety and select a second λ value,

$$\begin{aligned} &if\ (F_s)_m > (F_s)_f,\ then\ \lambda = \lambda + 0.1 \\ &if\ (F_s)_m < (F_s)_f,\ then\ \lambda = \lambda - 0.1 \end{aligned} \qquad \textbf{[37]}$$

5. Compute a new set of factors of safety (i.e., (Fs)m and (Fs)f using the newly estimated lambda value, λ, and compare the difference in the two factors of safety to the tolerance. If the tolerance criterion is satisfied then the computations can be stopped,
6. If the tolerance criterion is not satisfied, repeat Step 3 using a new λ value estimated from the two previous sets of factor of safety and λ calculations.

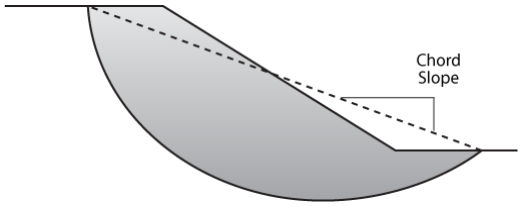

Figure 8 Definition of the chord slope

3.9 CORPS OF ENGINEERS METHOD

The U.S. Army *Corps of Engineers Method* satisfies overall horizontal force equilibrium in calculating the factor of safety, F_s. Moment equilibrium is not satisfied. The assumption regarding the direction of the resultant interslice forces has led to two interpretations of the Corps of Engineers method: namely, Corps of Engineers 1 and Corps of Engineers 2.

- Assumption #1 for Corps of Engineers: the direction of resultant interslice forces is assumed to be equal to the average slope between the extreme entrance and exit of the slip surface and the ground surface.
- Assumption #2 for Corps of Engineers: the direction of resultant interslice forces is assumed to be equal to the slope at the ground surface at the top of each slice.

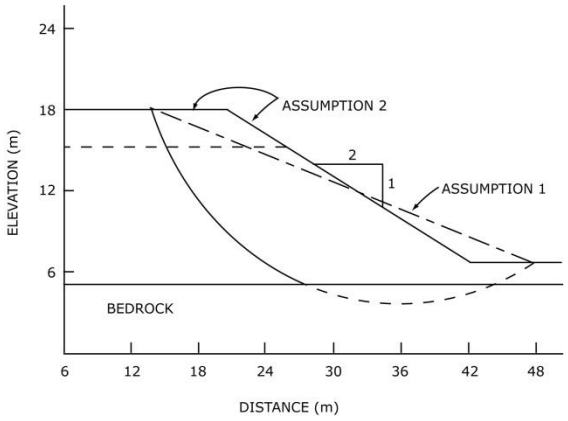

Figure 9 Assumptions regarding the interslice force direction for the Corps of Engineers method

3.10 LOWE-KARAFIATH METHOD

The *Lowe-Karafiath Method* is like the Corps of Engineers method and only differs in terms of the assumption regarding the direction of the resultant interslice forces. The Lowe-Karafiath assumption regarding the interslice force direction can be described as follows. The direction of the resultant interslice forces is assumed to be equal to the average of the ground surface slope and slip surface slope (Figure 10).

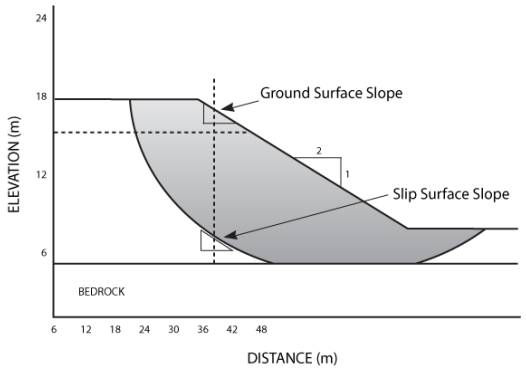

Figure 10 Lowe-Karafiath interslice force direction assumption.

3.11 SARMA METHOD (1973)

Sarma et al. (1973) proposed a limit equilibrium method of slices that calculated the "Critical Acceleration" required to force the factor of safety to become 1.0. Sarma et al. (1979) also made some additional comments related to calculating the internal stresses within the sliding mass by using non-vertical slices or general blocks. However, only vertical slices are used in the current implementation of the Sarma method in the software.

Another difference between the Sarma method and the other general methods defined by the GLE formulation is related to the relationship between the interslice shear and normal forces. The following equation was used to evaluate the interslice shear forces,

$$X = c'h + (E - u_w)\tan\phi' \qquad \textbf{[38]}$$

where:

c' = effective cohesion,

ϕ' = effective angle of internal friction,

h = height of the slice,

E = interslice normal force, and

u_W = pore-water pressure.

Calculating the "Critical Acceleration" for a factor of safety of 1.0 can be accomplished by using the GLE Method and using several trial horizontal acceleration values. A plot of Factor of Safety versus the "Assumed Acceleration" reveals the "Critical Acceleration" for a factor of safety of 1.0.

In the original Sarma method (1973), the average of the material properties was used to compute the interslice shear forces. In The software, the material properties and pore-water pressure at the 1/3 point upward from the base of each slice are used to compute the interslice shear forces.

3.12 SARMA NON-VERTICAL SLICES METHOD (1979)

Sarma (1979) developed an extended wedge approach of the limited equilibrium method. In this method, the mass contained within the slip surface and the free ground surface is divided into *n* slices like in vertical slice methods, but the slices need not be vertical or even parallel as shown in Figure 11(*a*). The forces acting on the *i*th slice are shown in Figure 11(*b*). It assumes that under the influence of the force, KW_i, the factor of safety on the slip surface is equal to one in which case *K* is the critical acceleration factor, k_c. The critical horizontal acceleration factor k_c can be calculated in a closed form. The solution obtained in the form of k_c can be used to determine the factor of safety, and the angle of each slice is found as part of the solution. The effect of the shear strength on the internal shear surfaces can be considered as well.

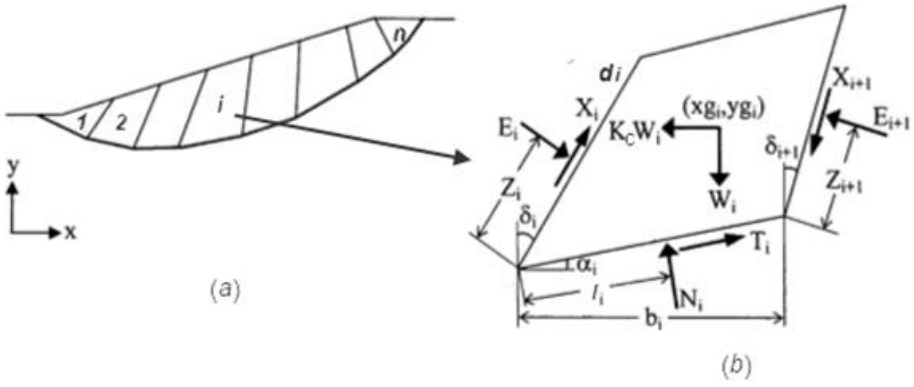

Figure 11 Forces acting on individual non-vertical slice.

From the vertical equilibrium of the slice,

$$N_i \cos\alpha_i + T_i \sin\alpha_i = W_i + X_{i+1}\cos\delta_{i+1} - X_i \cos\delta_i - E_{i+1}\sin\delta_{i+1} + E_i \sin\delta_i \quad \textbf{[39]}$$

From the horizontal equilibrium of the slice,

$$T_i \cos\alpha_i - N_i \sin\alpha_i = K_c W_i + X_{i+1}\sin\delta_{i+1} - X_i \sin\delta_i + E_{i+1}\cos\delta_{i+1} - E_i \cos\delta_i \quad \textbf{[40]}$$

Mohr Coulomb failure criterion gives,

$$T_i = (N_i - U_i)\tan\emptyset_i' + C_i' \sec\alpha_i \quad \textbf{[41]}$$

Mohr Coulomb failure criterion gives,

$$T_i = (N_i - U_i)\tan\emptyset_i' + C_i' \sec\alpha_i \quad \textbf{[42]}$$

When the sliding mass is in a state of limiting equilibrium, the mass will not be able to move unless shear surfaces are formed within the body. It is assumed that the normal body force *E* and shear body force *X* on the slicing boundaries are such that they are also in a state of limiting equilibrium, so that,

$$X_i = (E_i - PW_i)\tan\bar{\emptyset}_i' + \bar{C}_i' d_i \quad \textbf{[43]}$$

$$X_{i+1} = (E_{i+1} - PW_{i+1})\tan\bar{\emptyset}_{i+1}' + \bar{C}_{i+1}' d_{i+1} \quad \textbf{[44]}$$

Where

$\bar{\emptyset}'$ is the average friction angle along the inclined plane;
$\bar{C}'$ is the average cohesion along the same plane;
d is the length of the inclined plane; and
PW is the water pressure force on that plane.

From the above equations, we can get a closed form solution of k_c,

$$k_c = \frac{a_n + a_{n-1}e_n + a_{n-2}e_n e_{n-1} + \cdots + a_1 e_n e_{n-1} \ldots e_3 e_2}{p_n + p_{n-1}e_n + p_{n-2}e_n e_{n-1} + \cdots + p_1 e_n e_{n-1} \ldots e_3 e_2} \quad \textbf{[45]}$$

In which,

$$a_i = \frac{W_i \sin(\emptyset_i' - a_i) + R_i \cos \emptyset_i' + S_{i+1} \sin(\emptyset_i' - a_i - \delta_{i+1}) - S_i \sin(\emptyset_i' - a_i}{\cos(\emptyset_i' - a_i + \overline{\emptyset}_{i+1}' - \delta_{i+1}) \sec \overline{\emptyset}_{i+1}'} \quad \textbf{[46]}$$

$$p_i = \frac{W_i \cos(\emptyset_i' - a_i)}{\cos(\emptyset_i' - a_i + \overline{\emptyset}_{i+1}' - \delta_{i+1}) \sec \overline{\emptyset}_{i+1}'} \quad \textbf{[47]}$$

$$e_i = \frac{\cos(\emptyset_i' - a_i + \overline{\emptyset}_i' - \delta_i) \sec \overline{\emptyset}_i'}{\cos(\emptyset_i' - a_i + \overline{\emptyset}_{i+1}' - \delta_{i+1}) \sec \overline{\emptyset}_{i+1}'} \quad \textbf{[48]}$$

$$R_i = C_i' b_i \sec \alpha_i - U_i \tan \emptyset_i' \quad \textbf{[49]}$$

$$R_i = C_i' b_i \sec \alpha_i - U_i \tan \emptyset_i' \quad \textbf{[50]}$$

α - the angle of the base of the slice (relative to the horizontal axis);
δ - the angle of the side of the slice (relative to the vertical axis);
W - the weight of the slice;
U - the water pressure force on the base of slice.

The stability analysis solution obtained in the form of the acceleration factor k_c is straightforward and easy. Factor k_c itself can be used as a measure of the stability. After k_c is obtained, the factor of safety (FOS) is calculated through an iterative process where the shear strength parameters are reduced until the k_c is equal to zero.

$$C' = \frac{C}{F} \quad \textbf{[51]}$$

$$tan\emptyset' = \frac{tan\emptyset}{F} \quad \textbf{[52]}$$

The relationship between FOS and Acceleration Factor *K* is shown in Figure 2.

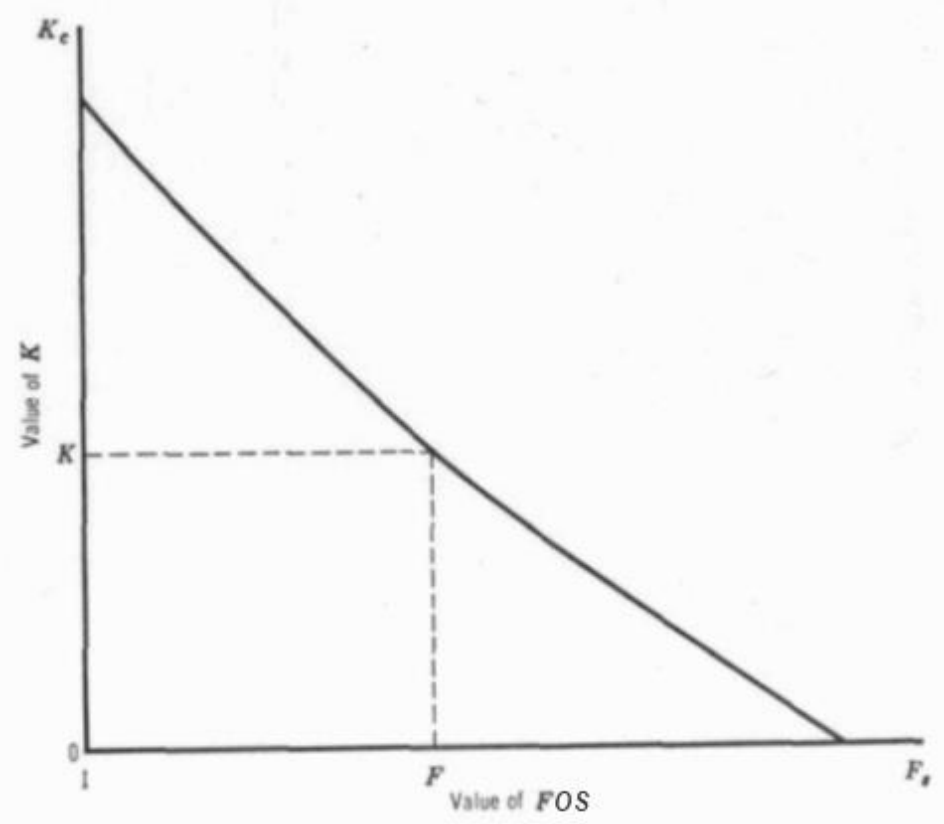

Figure 12 Relationship between FOS and acceleration factor, K.

4 STRESS-BASED METHODS

The following sections outline methods which use a finite element method of calculating the appropriate stresses along the slip surface.

4.1 ENHANCED LIMIT METHOD (KULHAWY METHOD)

The *Enhanced Limit Method* utilizes the finite element method for the calculation of the stress states in the material mass. The fundamental conditions associated with limit equilibrium methods of analysis are retained in the Enhanced Limited Method. The method uses a finite element analysis to compute the stresses in the material mass and then computes the factor of safety, F_s, along a prescribed slip surface. The minimum factor of safety is obtained through a series of trial slip surfaces.

4.1.1 Definition of Factor of Safety

There are several definitions that have been proposed for the factor of the safety based on the finite element stress analysis method. For example, Kulhawy (1969) proposed an equation for the factor of safety in term of the material strength. Zienkiewicz et al (1975) derived a factor of safety, based on stress level. Adikari and Commins (1985) published a factor of safety based on both material strength and stress level. The definition of safety factor proposed by Kulhawy (1969) appears to be the most reasonable and has been most widely adopted in geotechnical engineering practice. The Kulhawy (1969) Enhanced Limit method has been implemented in the software.

The equation for the factor of safety for a saturated material can be rewritten as:

$$F_s = \frac{\sum S_r}{\sum S_m} = \frac{\sum [c' + (\sigma_n - u_w)\tan\phi']\beta}{\sum \tau_m \beta} \qquad \textbf{[53]}$$

where:

τ_m = mobilized shear stress along the base of a slice,

S_r = resisting shear force,

S_m = mobilized shear forces, and

β = length across the base of the slice.

The factor of safety equation can be extended to accommodate unsaturated soils where matric suction is considered:

$$F_s = \frac{\sum S_r}{\sum S_m} = \frac{\sum \left[c' + (\sigma_n - u_a)\tan\phi' + (u_a - u_w)\tan\phi^b\right]\beta}{\sum \tau_m \beta} \qquad \textbf{[54]}$$

where:

u_a = pore-air pressure,

u_w = pore-water pressure, (negative) and

ϕ^b = angle defining the increase in strength due to matric suction, (u_a - u_w).

Equation [54] has also been extended to accommodate the situation where shear strength with respect to matric suction is nonlinear (i.e., nonlinear ϕ^b). Details related to the use of a nonlinear unsaturated shear strength envelope are presented in section 8.20.2.

4.1.2 Stress Transfer from the Finite Element Analysis to the Center of the Base of a Slice

The stresses computed in a finite element analysis generally correspond to the Gauss points. These stresses need to be transferred to the nodes of each finite element.

To compute the stresses at the center of the base of a slice, a search must first be undertaken to locate the element within which the center of a slice is located based in terms of global coordinates.

After the element encircling the center of the base of a slice has been located, the following steps are taken to compute the stresses at any arbitrary point. (Note that the following steps are applicable to for a triangular finite element).

Compute the areas of three sub-divided parts of the finite element as well as the entire area of the triangular element. The stresses at point, *P*, (i.e., $\sigma_{xp}, \sigma_{yp}, and\, \tau_{xyp}$), can be obtained from the node point stresses based on the weighted area method reflected by the following equations:

$$\sigma_{xp} = \frac{S_1\sigma_{xp1} + S_2\sigma_{xp2} + S_3\sigma_{xp3}}{S} \quad \textbf{[55]}$$

$$\sigma_{yp} = \frac{S_1\sigma_{yp1} + S_2\sigma_{yp2} + S_3\sigma_{yp3}}{S} \quad \textbf{[56]}$$

$$\tau_{xyp} = \frac{S_1\tau_{xyp1} + S_2\tau_{xyp2} + S_3\tau_{xyp3}}{S} \quad \textbf{[57]}$$

where:

σ_{xp}, σ_{xp}, σ_{xp} = stresses at point *P* within a triangular element, and

σ_{xpi},σ_{xpi}, σ_{xpi} = stresses at each node point (i = 1, 2, 3).

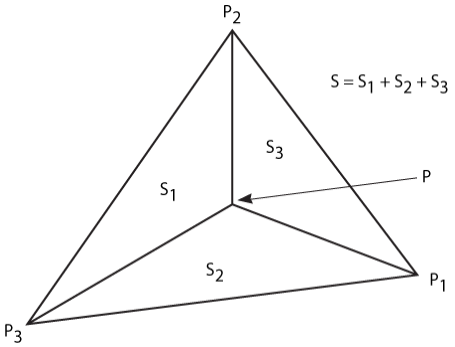

Figure 13 Designation of point, P, (i.e., center of the base of a slice) within a triangular finite element

4.1.3 The Normal and Shear Stresses at the Center of the Base of a Slice

Once the stress, σ_x, σ_y, σ_{xy}, are known at the center of the base of each slice, the normal stress, σ_n, and mobilized shear stress, τ_m, can be calculated using Equations [58] and [59].

$$\sigma_n = \frac{\sigma_x + \sigma_y}{2} + \frac{\sigma_x - \sigma_y}{2}\cos 2\theta + \tau_{xy}\sin 2\theta \quad \textbf{[58]}$$

$$\tau_m = \tau_{xy}\cos 2\theta - \frac{\sigma_x - \sigma_y}{2}\sin 2\theta \quad \textbf{[59]}$$

where:

σ_x = normal stress in the *x*-direction at the center of the base of a slice,

σ_y = normal stress in the *y*-direction at the center of the base of a slice,

τ_{xy} = shear stress in the *x*- and *y*-direction at the center of the base of a slice,

θ = angle measured from the positive *x*-direction to the line of application of the normal stress,

σ_n = normal stress perpendicular to the base of a slice, and

τ_m = shear stress parallel to the base of a slice.

The normal stress, σ_n, and the shear stress, τ_m, can be used in the calculation of the factor of safety when using Equations [53] or [54].

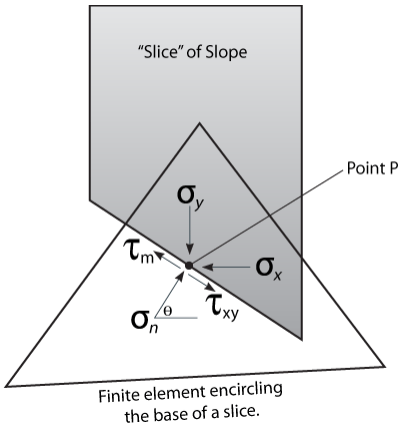

Figure 14 The relationship between the finite element stresses and stresses at the center of the base of a slice

4.2 SAFE-DP METHOD

The *SAFE-DP Method* utilizes the finite element method for the calculation of the stress states in the material mass. The method uses a finite element analysis to compute the stresses in the material mass and then search for the critical slip surfaces using Dynamic Programming Search method.

4.2.1 Definition of the Factor of Safety

For an arbitrary slip surface *AB*, as shown in Figure 15, the equation for the factor of safety can be defined as:

$$F_s = \frac{\int_A^B \tau_f \, dL}{\int_A^B \tau \, dL} \qquad \textbf{[60]}$$

where:

τ = mobilized shear stress along the slip surface,

τ_f = shear strength of the material, and

dL = an increment of length along the slip surface.

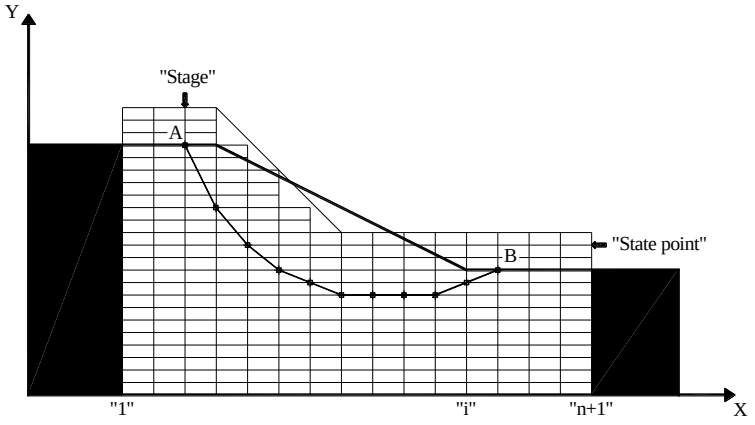

Figure 15 An arbitrary slip surface AB in a discretized form

It is assumed that the critical slip surface can be approximated by an assemblage of linear segments. Each linear segment connects two *state* points located in two successive *stages*. The *stage-state* system forms a grid consisting of rectangular elements called the *search grid*. The rectangular elements formed by the search grid are called grid elements. In this discretized form, the overall factor of safety for the slip surface *AB* is defined as follows:

$$F_s = \frac{\sum_{i=1}^{n} \tau_{f_i} \Delta L_i}{\sum_{i=1}^{n} \tau_i \Delta L_i} \quad \textbf{[61]}$$

where:

n = number of discrete segments,

τ_i = shear stress actuated,

τ_{fi} = shear strength, and

ΔL_i = length of the i^{th} segment.

4.2.2 Stress Transfer from the Finite Element Analysis to the Grid Point

The calculation of the stresses is the like the procedure used in the *Enhanced Limit Method.* The most significant difference is that the:

- *Enhanced Limit Method* calculates the stress at each base center point, and the
- *SAFE-DP method* calculates the stress at each Grid Point.

4.2.3 The Normal and Shear Stresses on a Segment

The normal and shear stresses acting on a segment can be computed from the results of a stress analysis as follows:

$$\sigma_n = \sigma_x \sin^2\theta + \sigma_y \cos^2\theta - \tau_{xy} \sin 2\theta \quad \textbf{[62]}$$

$$\tau_n = \tau_{xy}(\sin^2\theta - \cos^2\theta) - \frac{(\sigma_y - \sigma_x)}{2} \sin 2\theta \quad \textbf{[63]}$$

where:

σ_n = normal stress acting on a segment,

τ_n = shear stress acting on a segment,

θ = inclined angle of the segment with the horizontal direction,

σ_x = normal stresses acting in the *x*- coordinate direction,

σ_y = normal stresses acting in the *y*- coordinate direction, and

τ_{xy} = shear stresses acting in the *x*- and *y*-coordinate directions.

5 SEISMIC METHODS

Methods developed to date to calculate the stability or performance of slopes under earthquake loading fall into three general categories (Jibson R. W. 2011):

1. Pseudo-static analysis, i.e. Calculate the Yield Coefficient (Ky) for all slip surfaces,
2. Permanent-displacement analysis (Newmark method),
3. Stress-deformation analysis (finite-element method).

The Calculate the Yield Coefficient for All Slip Surfaces method and the Newmark Permanent Displacement method are outlined here. If an advanced seismic analysis method is selected in the software, then the regular horizontal seismic load options will be unavailable.

5.1 CALCULATE THE YIELD COEFFICIENT FOR ALL SLIP SURFACES SEISMIC ANALYSIS

Pseudo-static analysis models the seismic shaking as a permanent body force added to each slice/column in limit equilibrium analysis; normally, only the horizontal component of earthquake shaking is modeled because the effects of vertical forces tend to average out to near zero (Jibson R. W. 2011).

To calculate the yield coefficient, Ky, for all slip surfaces is to compute the critical pseudo-static horizontal seismic coefficient for each slip surface. In other words, the method will calculate the horizontal pseudo-static seismic coefficient required to lower the trial slip surface Factor of Safety (FOS) to the Target FOS. By default, the Target FOS = 1, but the user can enter a different value. This analysis is performed for all trial slip surfaces and the slip surface with the lowest value of Ky found to reach the Target FOS is the critical slip surface, and the Ky is the critical seismic coefficient. Note: If all trial slip surfaces have an initial FOS less than the Target FOS, then all the Ky values will be zero.

The output will be in terms of Ky values rather than FOS.

5.2 NEWMARK PERMANENT DISPLACEMENT SEISMIC ANALYSIS

Newmark (1965) introduced a method to assess the performance of slopes during earthquakes that fills the gap between over-simplistic pseudo-static analysis and over-complex stress-deformation analysis. In recent years, the Newmark analysis is becoming more popular in standard engineering practice. In simple pseudo-static seismic slope stability methods, the seismic force is considered as a permanent (static) body force, and the assumption is made that the slope will fail if the peak ground acceleration exceeds the critical acceleration. In reality the analysis shows that slopes with significantly lower critical acceleration can survive higher earthquake acceleration without significant damage. The reason for this is that seismic ground accelerations are a transient phenomenon and that some permanent deformation of the slope may precede any damage of practical significance (Newmark 1965). Therefore, the Newmark analysis is less conservative than the pseudo-static analysis (Wilson & Keefer, 1983).

Newmark's method models a slip surface as a rigid block under seismic loading, the steps are

Step 1. Calculate the critical seismic coefficient ky for each trial slip surface

Step 2. A seismic acceleration record of Acceleration vs. Time is selected. The record can be loaded from Dynamics analysis result output or inputted directly by the user from historic records, etc.

Step 3. Integrate the accelerations that exceed the ky to obtain the velocity vs. time as shown in Figure 16 (A and B).

Step 4. Integrate the velocity vs. time history to obtain the cumulative displacement as shown in Figure 16 C.

We can see that in the Newmark analysis two sets of data are combined: 1. A critical acceleration ky, i.e., the value of horizontal ground acceleration coefficient at which the slope would reach its ultimate strength, and 2. A seismogram which records acceleration vs. time history.

The seismogram can be input by the user. Newmark permanent displacement will be calculated for all trial slip surfaces, the slip surface with the maximum displacement is the critical slip surface.

The output will be in terms of permanent displacement rather than FOS.

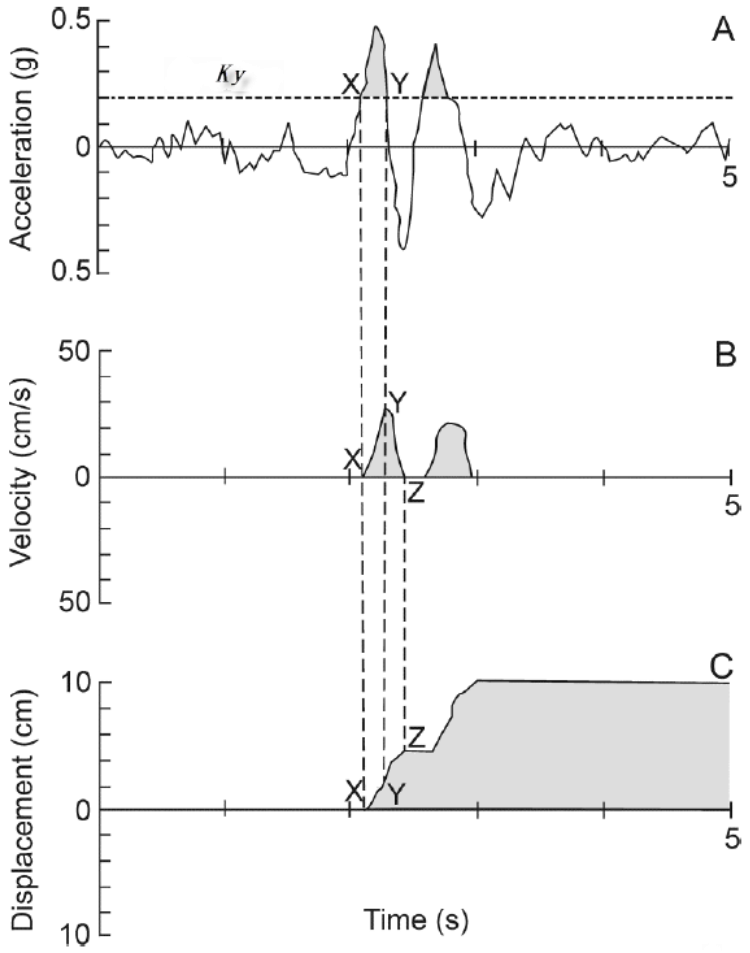

Figure 16 Illustration of the Newmark integrations algorithm (Jibson, R.W., 2011)

5.3 DYNAMICS - TECHNICAL PREVIEW

Refer to the Appendix of this document for theory related to the dynamic seismic functionality by the finite element method (FEM), currently in technical preview.

6 TENSION CRACKS

Tension cracks can be defined in the software in one of two ways. One way is to specify a tension crack zone and the other way is to define a tension crack angle.

6.1 TENSION CRACK LINE

A tension crack zone is defined by specifying a line defining the bottom of the tension cracks. The slip surface goes vertically upward to the ground surface as shown in Figure 17. In other words, slices above the slip surface, in the tension crack zone, will be ignored.

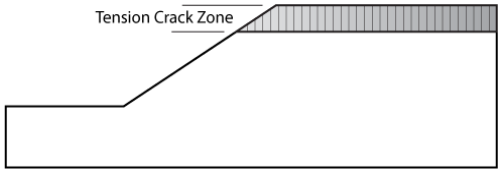

Figure 17 Tension crack line at the bottom of the cracks

The tension crack line cannot be set above the ground surface or within a material that is represented as having zero shear strength (i.e., c = 0 and ϕ = 0). The material is assumed to be a fluid when the shear strength parameters are zero.

6.2 TENSION CRACK ANGLE

Tension cracks can be considered when the angle of slip surface is steeper than a specified limiting tension crack angle. Therefore, a tension crack angle must be specified to designate the use of the tension crack zone. In other words, the tension crack zone is implemented when the angle of the slip surface is steeper than the specified limiting tension crack angle.

The depth of the tension crack zone is difficult to predict and is usually established on a somewhat empirical basis. For example, it might be decided that the steepest slip surface angle should be 45 degrees to be horizontal and therefore an angle can be used to designate the tension crack zone.

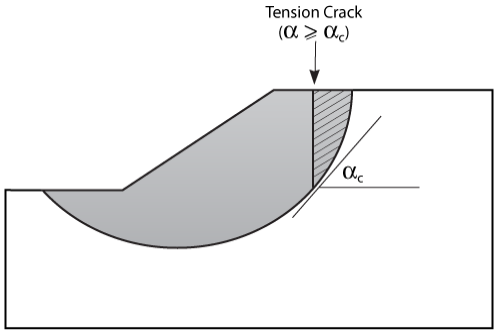

Figure 18 Definition of the limiting angle for tension cracks, α_c

6.3 HYDROSTATIC HORIZONTAL FORCE IN TENSION CRACK

If a tension crack is filled with water, there will be a hydrostatic horizontal force that needs to be taken into consideration in the slope stability analysis. The magnitude of the hydrostatic force is defined as follows:

$$F_w = \frac{\gamma_w [rH]^2}{2} \quad \textbf{[64]}$$

where:

γw = unit weight of the fluid in the tension crack (e.g., water)

H = depth of the tension crack from ground surface, and

r = percentage of the crack filled with water from the bottom of the crack.

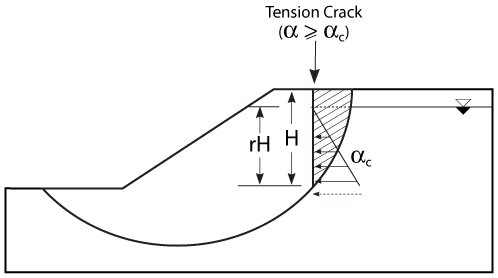

Figure 19 Diagram showing the horizontal water force generated in the tension crack

7 SLIP SURFACES

A factor of safety can be computed for every slip surface that is defined. The overall factor of safety of a slope is the minimum factor of safety of all the trial slip surfaces and is called the critical slip surface. In other words, each factor of safety is tied to a specific slip surface. It is necessary to specify the assumed shape of the slip surface before the factor of safety is calculated.

There are numerous procedures that can be used to define the slip surfaces. The types of slip surfaces can be classified as:

1. circular slip surfaces,
2. composite slip surfaces and,
3. non-circular slip surfaces.

Circular slip surfaces have been most commonly associated with earlier limit equilibrium formulations (e.g., Ordinary method or Bishop Simplified method). Composite slip surfaces are the combination of circular slip surfaces and linear line slip surfaces and were introduced by Fredlund and Krahn (1977). The non-circular slip surfaces consist of a series of linear line segments.

Details pertaining to the three types of slip surface shapes are discussed in the following sections.

7.1 CIRCULAR SLIP SURFACES

This section describes the theory behind some of the circular slip surfaces. All the Circular Slip Surface and Composite Slip Surface search methods involve finding trial circles with a circle center and circle radius. For example, for the Grid & Tangent search, Grid & Point search, and Grid & Line search, the circle center will be located on the Grid points, the circle radius will be the distance between the grid points and tangent points.

7.1.1 Slope Search

Slope Search method is one of the search methods for locating the Global Minimum safety factor for CIRCULAR slip surfaces.

1) Parameters

1. Number of Surfaces

   This is the total number of valid surfaces generated by the slope Search. The invalid surfaces generated by the Slope Search are discarded and are not included in this number.

   Invalid slip surfaces include:

   - The Entry or Exit point is outside the slope limits,
   - Incorrect Initial Angle at Toe
2. Initial Angle at Toe

   The Initial Angle at Toe is the orientation of the line tangential to the circular surface at toe. The initial angle is calculated by the following equation:

   Initial Angle = Lower Angle+ (Upper Angle-Lower Angle) *Random

where:

Lower Angle: if the Lower angle is checked then the Lower angle input by user is used,
Otherwise, the Lower Angle = -90 deg.

Upper Angle: if the Upper angle is checked then the Upper angle input by user is used,
Otherwise, Upper Angle = the angle of the slope segment at the initiation point of the slip surface

Random: a random value between 0 and 1.

2) The procedure for the Generation of a slip surface

1. Generate the first point.

   The first point is randomly generated based on the Slope Limits.
2. Generate the second point

   The second point is randomly generated based on the first point and slope limits or the second set of limits if selected:

   - When the second set of limits is selected, the second point is randomly generated within the second set of limits.
   - When the second set of limits is not selected, the second point is randomly generated between the first point and the right point of the first set of the limits.

3. Generate the center point

   The center point is generated using the Initial Angle at Toe and the generated two points.

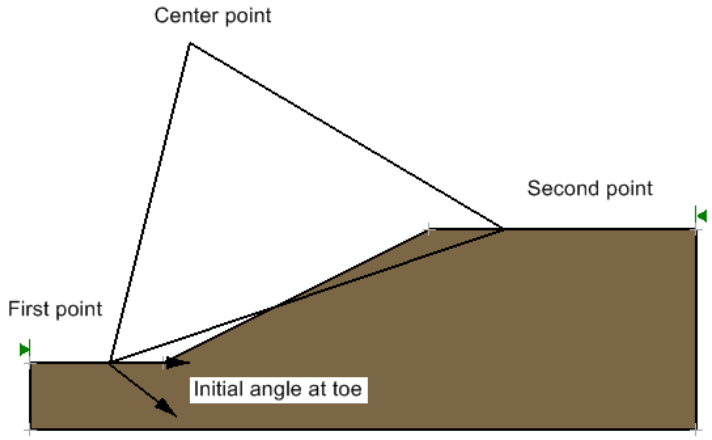

Figure 20 Single Slope Limit for Slope Search

Auto Refine Search

Auto Refine Search is one of the search methods for locating the Global Minimum factor of safety for CIRCULAR slip surfaces.

1) Parameters

1. Division Along Slope.

   The Division Along Slope is the number of divisions into which the slope surface is divided for Each Iteration of the Search.

   i. In the initial iteration, the length of slope surface is defined by the Slope Limits.

   ii. In each subsequent iteration, the length of the slope surface to be analyzed is defined by the value of Division to Use in Next iteration.

NOTE:
The length of the slope surface is always measured along the slope polyline. They are not measured horizontally. This means the length of the slope surface is independent of the angle of the slope segments.

2. Radius per Division

   This number shows how many slip circles are generated for each pair of divisions along the slope. The procedure is:

   i. For each pair of division along the slope, a straight line joining the mid-points (e.g., A and B) of the two divisions is generated.

   ii. The angle of this line is considered as a Minimum angle.

   iii. Vertical angle (i.e., 90 degrees) is considered as a Maximum angle.

   iv. The angular range between the Minimum angle and the Maximum angle is then divided equally with the number of Circles Per Division.

NOTE:
To generate the valid slip surfaces, a small offset is applied to the Minimum and Maximum angles, respectively.

   v. A set of slip surfaces is then generated with the two points (e.g., A and B and a set of the initial angles generated in iv).

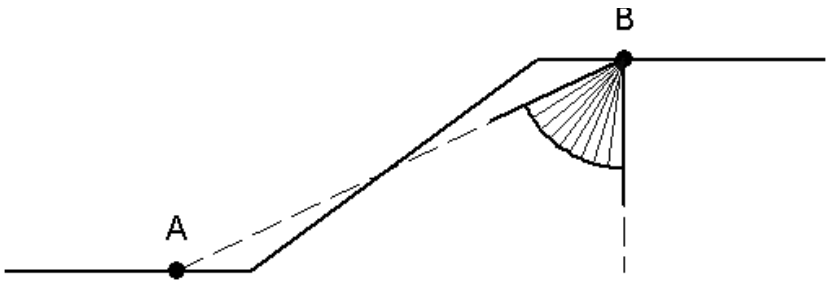

Figure 21 Radii Per Division

Iterations.

The Number of Iterations used for the Auto Refine Search is not for convergent purpose. The analysis is always carried out for the specified Number of Iterations.

3. Divisions to Use in Next Iteration.

   The number of divisions along the slope, with the lowest factor of safety is used as the basis for the next iteration in the Auto Refine Search.

   For example,

   Divisions Along Slope = 10

   Divisions to Use in Next Iteration = 50%

   5 divisions with the lowest factors of safety will be used to divide by 10 in the next iteration.

4. Total number of surfaces.

   Total number of surfaces is not an input parameter. It is calculated from the input parameters described above.

   Number of circles generated Per Iteration = yx(x-1)/2

   Total number of surfaces = z[yx(x-1)/2]

where:

x = Division Along Slope

y = Radius per Division

z = Iterations.

2) Procedure for Generation of Slip Surfaces

1. The slope surface is divided into several divisions according to the value of the Divisions Along the Slope,

NOTE:
If the second set of limits is selected, the segments within the two limits will be used.

2. Slip Circles are generated between Each Pair of Divisions according to value of Radius per division,
3. The factors of safety are calculated for these slip circles. The average factor of safety associated with Each Division along the slope is recorded,
4. This constitutes one iteration of the Auto Refine Search,
5. In the subsequent iteration, the percentage of Divisions to Use In Next Iteration is used. For example:
   - The Division Along Slope = 10
   - Divisions To Use In Next Iteration = 50%
   - 5 divisions (10*50% = 5) with the lowest average factors of safety will be used and another 5 divisions with higher average factors of safety will be discarded.
6. The selected divisions in step 5) are used to form a new slope polyline and repeat Step 1) to Step 4) until the Number of Iterations is satisfied.

7.2 COMPOSITE CIRCULAR SLIP SURFACE

Circular slip surfaces are quite realistic for most homogeneous or slightly non-homogeneous material slopes. The circular slip surface cannot, however, satisfy cases where there are adjacent materials with highly contrasting shear strength parameters. Figure 22 shows a bedrock layer with high shear strength parameters. The slip surface will pass along the top of the bedrock through a softened zone. Accordingly, some portion of the slip will be circular, and another portion of the slip will tend to be linear. The combination of circular and linear lines is called a "composite" slip surface.

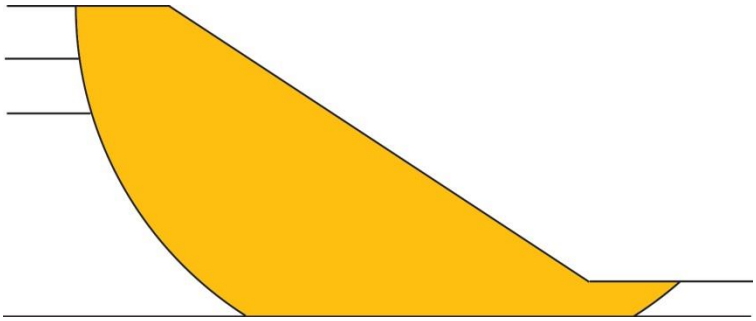

Figure 22 "Composite" slip surface formed as a result of a bedrock layer

The *"composite"* slip surfaces procedure is quite effective for slopes with a low shear strength material layer immediately overlying the top of the bedrock as shown in Figure 23.

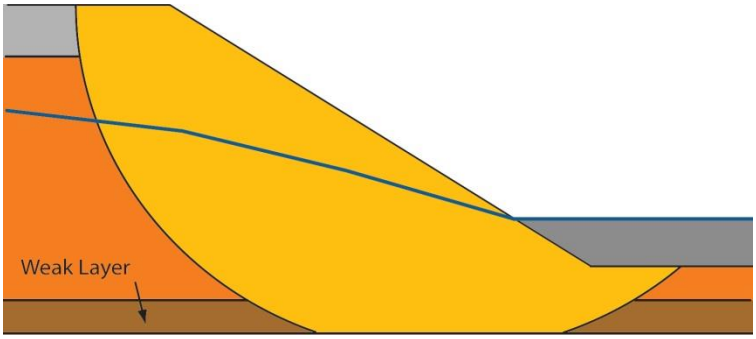

Figure 23 "Composite" slip surface within a weak layer

"Composite" slip surfaces are created in a manner similar to the creation of circular slip surfaces. The differences are as follows:

1. When the slip surfaces pass into the bedrock layer, the slip surface will force the positioned immediately above the bedrock layer.
2. The shear strength properties at the bottom (or composite portion) of the slip surface are taken from the layer of material just above the bedrock layer.

NOTE:
That the defined bedrock layer does not always means a bedrock material. Rather, a material layer with high shear strength can simply be specified as "Bedrock" layer to force the slip surface into a composite mode.

7.3 NON-CIRCULAR SLIP SURFACES

Non-circular slip surfaces are designated in quite a different manner from circular or composite slip surfaces. The differences are as follows:

1. Non-circular slip surfaces use a common rotation center referred to as the Axis point. This point is used as the center for moment equilibrium (Circular slip surfaces use the center of rotation for the center of moment equilibrium).
2. Non-circular slip surfaces are specified using a series of points (Circular slip surfaces are specified using a set of rotation points and a set of radii).

In the software, non-circular slip surfaces can be specified using one of two procedures; namely, fully specified and block specified.

7.3.1 Block Search

A block search is one of the powerful non-circular slip surface search methods available in 2D. For example, it is especially useful to perform non-circular analysis along a thin weak layer. To define a non-circular slip surface with a block search, one or more block search objects must be defined. There are four block search objects available:

1. Block
2. Point
3. Line
4. Polyline

7.3.1.1 Block Search – Block

A Block Search – Block is an arbitrary four-sided convex polygon as shown in Figure 24 where two Blocks are drawn. The software in 2D randomly generates ONE slip surface vertex inside each Block Search – Block for each slip surface.

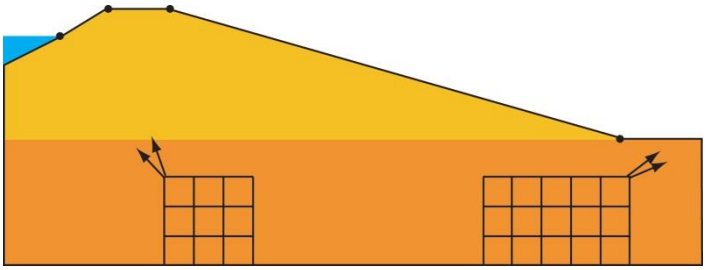

Figure 24 The grids generated in the Block specified method

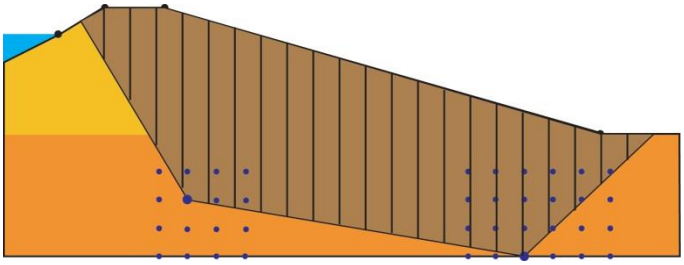

Figure 25 Slip surface designation using the Block specified method

7.3.1.2 Block Search – Point

A Block Search – Point is a single point, each slip surface generated by a Block Search must pass through this point. This block search object is very useful to force the slip surface pass through the toe of a slope, or the bottom of a tension crack, etc.

7.3.1.3 Block Search – Line

A Block Search – Line is a line segment defined by two end points. The software randomly generates ONE slip surface vertex along each Block Search – Line for each slip surface.

7.3.1.4 Block Search - Polyline

A Block Search - Polyline consists of one or more line segments. The software randomly generates TWO slip surface vertexes along the polyline. The polyline points will be part of the slip surface points between these two generated slip surface vertexes. Block Search - Polyline is useful to define slip surfaces that pass through complex thin weak material layer.

7.3.2 Fully Specified (Segments)

Fully specified slip surfaces can be designated using a set of points. This allows for considerable flexibly in specifying the location and the shape of the slip surfaces.

Fully specified slip surfaces are useful for situations when the slip surface can be predetermined to some extent such as in the case of a retaining wall (Figure 26).

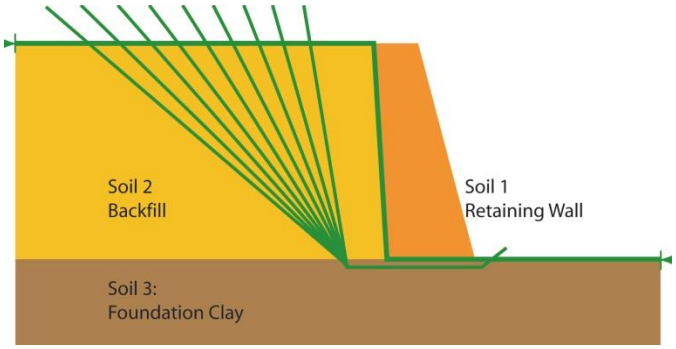

Figure 26 Fully specified slip surfaces

It should be noted that the specified slip surface starts and ends outside the geometry. The entry point and exit point are then automatically computed. This procedure avoids difficulties associated with placing points directly on the ground surface.

7.3.3 Path Search

A Path Search is one of the Search Methods that can be used for locating the Global Minimum factor of safety for NON-CIRCULAR slip surfaces.

1) Parameters

1. Number of Surfaces.

   This is the total number of valid surfaces generated by the Path Search. Invalid surfaces are NOT included in this number.

   The invalid surfaces may occur when either of the following factors is involved.

   - Initial Angle at Toe is incorrect.
   - The endpoint does not intersect the slope within the slope Limits.

2. Initial Angle at Toe

   The Initial Angle at Toe is the orientation of the FIRST line segment of a slip surface generated by the Path Search.

   Note: that the slip surfaces for the Path Search are generated from the toe of the slope to the crest of the slope regardless of the slip direction (Left to Right or Right to Left).

   Initial Angle = Lower Angle + (Upper Angle-Lower Angle) *Random

   where:

   Lower Angle: if the Lower angle is checked then the Lower angle input by user is used,
   Otherwise, Lower Angle = -90 degrees.

   Upper Angle: if the Upper angle is checked then the Upper angle input by user is used,
   Otherwise, Upper Angle = the angle of the slope segment at the initiation point of the slip surface

   Random: a random value between 0 and 1.

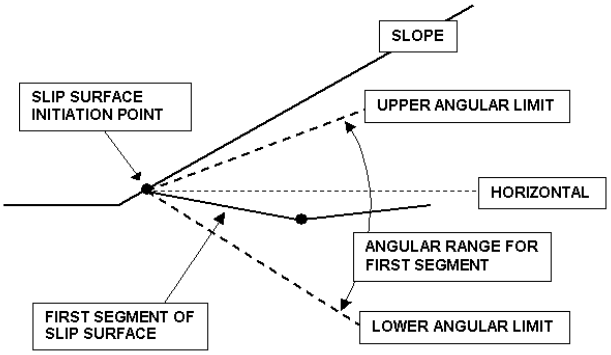

Figure 27 Path Search

The user can define angular limits through selecting the Upper Angle and/or Lower Angle. The Angle measurement is from –90 degrees to 90 degrees:

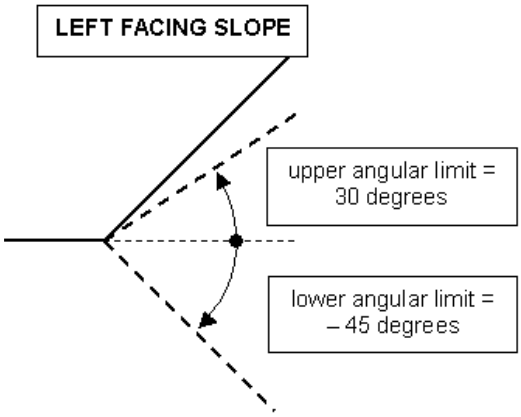

Figure 28 Angular limit (Left Facing Slope)

3. Segment Length.

   Segment length is used for each segment of a non-circular surface generated by using the Path Search.

   Note that:

   By default, the segment length is automatically calculated based on the geometry boundaries.

   Segment length = 0.3H

   H = Maximum height of the slope.

   The user can specify a segment length by selecting the Use Segment Length Checkbox and entering a value into the editable box. Improper segment length (e.g., too small, or too large) will lead irrational results.

4. Random Number Generation

   For the Path Search, random numbers are used to generate:

   - slip surface initiation points based on the Slope Limits.
   - angle of the first slip surface segment based on Upper Angle and/or Lower Angle.
   - angle of all subsequent slip surface segments.

2) Procedure for Generation of Slip Surfaces

1. A starting point is randomly generated on the slope surface based on the Slope Limits. If the second set of limits is selected, the right range will be used for Left-to-Right slip direction and the left range will be used for Right-to-Left slip direction.

Possible Range of Path Search Initial Points

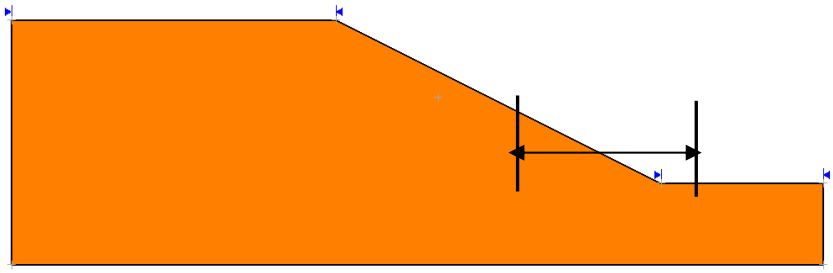

Figure 29 Possible Range of Path Search Initial points (Right Facing Slope)

2. Starting from the first point, the first segment is randomly generated according to the Initial Angle at Toe and the Segment Length specified.
3. The subsequent segments are randomly generated according to the segment length, and the previous segment angle. A restriction is to generate concave surfaces.
4. Calculations will continue until the segment intersects the ground surface. If the intersect point (i.e., endpoint) is within Slope Limits then this surface is valid, otherwise, invalid.
5. Repeat Steps 1 to 4, until the number of valid slip surfaces generated is equal to the Number of Surfaces specified.

7.3.4 Greco Method

There are several Optimization methods that have been proposed in the research literature. The optimization methods remove the necessity for assuming the shape and location of the critical slip surface. The assumptions related to shape and location of the slip surface become part of the solution.

7.3.4.1 Definition of the Geometry

The Monte Carlo technique proposed by Greco (1996) is one of the Optimization methods used in the software for locating the critical slip surface. The critical slip surface is defined using a series of straight lines segments. The concepts of the method are described as follows:

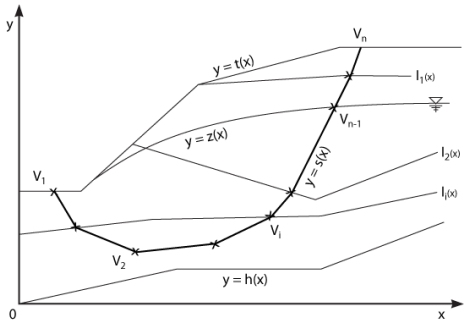

Figure 30 Typical cross-section of a slope used in the Greco Optimization method (Greco 1996)

The following variables used in Figure 30 are defined as follows:

$y = t(x)$: a function describing the topographic profile of the material,

$y = s(x)$: a function describing the slip surface,

$y = z(x)$: a function describing the water table, and

$y = I_j(x)$: a function describing a discontinuity surface in a layered material system.

The following practical constraints can be introduced.

$$x_{min} \le x \le x_{max} \quad \textbf{[65]}$$

$$h(x) \le s(x) \le t(x); \text{ for all the x when } x_{min} \le x \le x_{max} \quad \textbf{[66]}$$

7.3.4.2 Objective Function of the Problem

A potential slip surface is approximated by a series of line segments with *n* vertices: V_1, V_2, V_3, V_n, whose coordinates (x_1, y_1), (x_2, y_2), (x_n, yn) are unknowns in the problem, but can be used for locating the critical slip surface. These coordinates can be considered as components of a two-dimensional array:

$$S = \{V_1, V_2, \cdots\cdots\cdots, V_n\} \quad \textbf{[67]}$$

or

$$S = \{x_1, y_1, x_2, y_2, \cdots\cdots\cdots, x_n, y_n\} \quad \textbf{[68]}$$

The critical slip surface can be found by minimizing the objective function for the factor of safety, F_s, with respect to the array of coordinates, *S*:

$$\min\{F_s(S)\} \quad \textbf{[69]}$$

7.3.4.3 Solution of the Greco (1996) Formulation

Searching for the minimum factor of safety, F_s, requires a nonlinear programming procedure. The factor of safety is calculated by starting with an initial assumed slip surface location and proceeding towards the minimized location through use of an iterative procedure. Consequently, a sequence of feasible slip surfaces, S_1, S_2, …., *Sk*, S_{k+1}, are generated along with the corresponding factors of safety in a decreasing sequence.

$$F(S_0) > F(S_1) > \cdots\cdots > F(S_k) > F(S_{k+1}) > \cdots\cdots \quad \textbf{[70]}$$

where:

$$S_k = \{x_1^k, y_1^k, x_2^k, y_2^k, \cdots\cdots, x_n^k, y_n^k\} \quad \textbf{[71]}$$

$$S_{k+1} = \{x_1^{k+1}, y_1^{k+1}, x_2^{k+1}, y_2^{k+1}, \cdots\cdots, x_n^{k+1}, y_n^{k+1}\} \quad \textbf{[72]}$$

where:

(x_i^k, y_i^k) = coordinates of vertex *i* at stage *k* of the minimization procedure, and

$\left(x_i^{k+1}, y_i^{k+1}\right)$ = coordinates of same vertex i at next stage k+1.

There are two stages involved in generating a new slip surface, S_{k+1^i} from S_k in the current Greco (1996) method. The two steps are referred to as the "Exploration" stage and the "Extrapolation" stage.

During the "Exploration" stage, each slip surface vertex is shifted to a new position using a random technique. If the factor of safety of the modified slip surface is smaller than the factor of safety for the previous location, then the vertex is fixed at the new position. If the opposite is true, its position is returned to the previous position.

In the "Extrapolation" stage, the total displacement obtained in the "Exploration" stage is repeated, and the slip surface is updated if the corresponding factor of safety is smaller than that obtained at the end of the "Exploration" stage.

- **"Exploration" Stage**

  Vertex *i* is randomly moved from point (x_i^k, y_i^k) to point (x_i^{k+1}, y_i^{k+1}). To attempt to reduce the factor of safety, vertex *i* can be expressed as:

$$x_i^{k+1} = x_i^k + \varepsilon_i^k \quad \textbf{[73]}$$

$$y_i^{k+1} = t(x_i^{k+1}) \quad \text{for } i = 1 \text{ and } i = n \quad \textbf{[74]}$$

$$y_i^{k+1} = y_i^k + \eta_i^k \quad \text{for } i = 2 \text{ to } n\text{-}2 \quad \textbf{[75]}$$

where:

ε_i^k = random displacement of vertex *i* in the *x*-direction, and

η_i^k = random displacement of vertex *i* in the *y*-direction.

The displacements are given as follows:

$$\varepsilon_i^k = N_x R_x Dx_i^k \quad \textbf{[76]}$$

$$\eta_i^k = N_y R_y Dy_i^k \quad \textbf{[77]}$$

where:

R_x = random number in the range [-0.5, 0.5],

R_y = random number in the range [-0.5, 0.5],

Dx_i^k = width of the search steps in *x*-direction for vertex *i* at stage *k*,

Dy_i^k = width of the search steps in *y*-direction for vertex *i* at stage *k*,

N_x = defined number, and

N_y = defined number.

The combination of N_x, N_y provides various movements of vertex *i* for the same pair of random numbers R_x and R_y. The following eight combinations are given for parameters N_x and N_y:

$$N_x = 1 \quad N_y = 1$$

$$N_x = -1 \quad N_y = -1$$

$$N_x = 1 \quad N_y = -1$$

$$N_x = -1 \quad N_y = 1$$

$$N_x = 0 \quad N_y = 1$$

$$N_x = 0 \quad N_y = -1$$

$$N_x = 1 \quad N_y = 0$$

$$N_x = -1 \quad N_y = 0$$

Eight random displacements are tested for every vertex of the slip surface (see Figure 31). Effective directions for the displacements also depend on the sign of R_x and R_y.

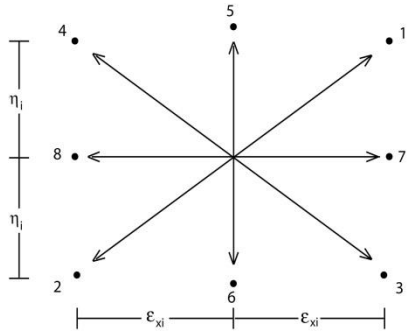

Figure 31 The moving directions of vertex *i*

If one of the trials is successful, no further trials are made for a particular vertex, and the width of the search is increased as follows:

$$Dx_i^{k+1} = Dx_i^k + \left| x_i^{k+1} - x_i^k \right| \quad \textbf{[78]}$$

$$Dy_i^{k+1} = Dy_i^k + \left| y_i^{k+1} - y_i^k \right| \quad \textbf{[79]}$$

If no trial is successful for vertex *i*, then the width of the search step for the successive step, *k+1*, is reduced as follows:

$$Dx_i^{k+1} = Dx_i^k (1-\varepsilon) \quad \textbf{[80]}$$

$$Dy_i^{k+1} = Dy_i^k (1-\varepsilon) \quad \textbf{[81]}$$

where:

ε = a number [0,1], a value of 0.5 is recommended.

The initial width of the search steps, Dx_i^o and Dy_i^o are fixed as:

$$Dx_i^0 = \frac{x_n - x_1}{2(n-1)} \quad \textbf{[82]}$$

$$Dy_i^0 = \frac{y_{\max} - y_{\min}}{n} \quad \textbf{[83]}$$

where:

y_{max} = maximum value of the vertex ordinates of the slip surface, and

y_{min} = minimum value of the vertex ordinates of the slip surface.

- **Extrapolation Stage**

$$x_i^e = 2x_i^{k+1} - x_i^k \quad \text{for } i = 1 \text{ and } i = n \quad \textbf{[84]}$$

$$y_i^e = 2y_i^{k+1} - y_i^k \quad \text{for } i = 2 \text{ to } i = n\text{-}1 \quad \textbf{[85]}$$

$$y_i^e = t(x_i^e) \quad \text{for } i = 1 \text{ and i} = n \quad \textbf{[86]}$$

The boundary conditions for Equation [84] are checked against the computed slip surface and then modified if required. If the factor of safety of the computed slip surface is less than the previous minimum factor of safety value, then the current slip surface is updated to the computed slip surface as follows:

$$x_i^{k+1} = x_i^e \quad \text{for } i = 1 \text{ to } i = n \quad \textbf{[87]}$$

$$y_i^{k+1} = y_i^e \qquad \text{for } i = 1 \text{ to } i = n \qquad \textbf{[88]}$$

Otherwise, the new "Exploration" stage begins by starting with the slip surface obtained at the end of the previous trial.

- **Criterion for searching when using the iterative process**

The iterative procedure involved the "Exploration" and "Extrapolation" stages is stopped if the following conditions are satisfied:

$$Dx_i^{k+1} < \Delta \qquad \text{for } i = 1 \text{ to } i = n \qquad \textbf{[89]}$$

$$Dy_i^{k+1} < \Delta \qquad \text{for } i = 1 \text{ to } i = n \qquad \textbf{[90]}$$

$$\left|F(S^K) - F(S^{K+1})\right| < \delta \qquad \textbf{[91]}$$

where:

Δ = specified width for search range, and

δ = tolerance between subsequent values of factor of safety.

The tolerance parameter δ varies from 0.001 to 0.00001. The search range parameter, Δ, is determined in terms of the size of sliding mass and the number of vertices, *n*, by using the following equation:

$$\Delta = \frac{x_n - x_1}{4(n-1)} \qquad \textbf{[92]}$$

7.3.4.4 Implementation of Greco (1996) Method

To avoid too many vertices along the slip surface, Greco (1996) suggested adopting a 3-step procedure when searching for the critical slip surface. The Greco recommendation has been implemented in the software.

- **Step 1**

Randomly generate a 4-vertices slip surface as follows:

a. The abscissas of vertices 1 and 4 are randomly generated within the range [x_{min}, x_{max}]

$$x_1 = x_{\min} + R_1\left(x_{\max} - x_{\min}\right)/4 \qquad \textbf{[93]}$$

$$x_4 = x_{\max} - R_4\left(x_{\max} - x_{\min}\right)/4$$

b. The ordinates of vertices 1 and 4 are given by,

$$y_1 = t(x_1) \qquad y_4 = t(x_4) \qquad \textbf{[94]}$$

c. The inclinations of the first and the last segments of the slip surface are randomly generated as,

$$\alpha_1 = 45^\circ - 15^\circ R_5 \qquad \alpha_3 = 45^\circ + 15^\circ R_6 \qquad \textbf{[95]}$$

d. Point P with coordinates, (xp, yp), is determined as an intersection between the line passing through vertex 1 at an inclined angle of α_1, and the line through vertex 4 and at an inclined angle of α_3.

e. Vertices 2 and 3 are then generated as,

$$x_2 = x_1 + R_2\left(x_p - x_1\right) \qquad \textbf{[96]}$$

$$y_2 = y_1 + \left(x_2 - x_1\right)\tan\alpha_1 \qquad \textbf{[97]}$$

$$x_3 = x_4 - R_3\left(x_4 - x_p\right) \quad \textbf{[98]}$$

$$y_3 = y_4 + \left(x_3 - x_4\right)\tan\alpha_3 \quad \textbf{[99]}$$

- **Step 2**
  In this step, a 7-vertex slip surface is generated in which 4 vertices are those obtained at the end of Step 1 and the other 3 vertices are introduced at the midpoint of the straight line jointing adjacent vertices. Then the two-phase procedure is used to search for the critical slip surface with a minimum factor of safety.

- **Step 3**
  In the same way, a 13-vertex slip surface is generated and the two-phase procedure is used to obtain the critical slip surface. Slip surfaces with seven vertices are relatively smooth and satisfactory for most engineering studies.

7.3.5 Dynamic Programming Method

A conventional slope stability analysis involving limit equilibrium methods of slices consists of the calculation of the factor of safety for a specified slip surface of predetermined shape, and the determination of the location of the critical slip surface with the lowest factor of safety through a trial-and-error analysis. To render the inherently indeterminate analysis determinate, conventional limit equilibrium methods generally make use of assumptions regarding the relationship between the interslice forces. These assumptions become disadvantages to limit equilibrium methods since the actual stresses acting along the slip surface are quite approximate, and the location of the critical slip surface depends on the shape assumed by the analyst.

The assumptions related to the interslice force function in limit equilibrium methods are unnecessary when a finite element stress analysis is used to obtain the normal and shear stresses acting at the base of slices (Fredlund and Scoular, 1999). A stress analysis can provide the normal and shear stresses through use of finite element numerical method with a "switch on" of the gravity body forces. Subsequently, the normal stress at the base of a slice is known and the equation for the factor of safety becomes linear. Assumptions regarding shape of the critical slip surface can be by-passed when an appropriate optimization technique is introduced into the analysis.

Optimization techniques have been developed by several researchers for over two decades and have provided a variety of approaches to determine the shape and the location of the critical slip surface (Celestino and Duncan, 1981; Nguyen, 1985; Chen and Shao, 1988; Greco, 1996). Each approach has its own advantages and shortcomings. The main shortcoming associated with these approaches is that the actual stresses within a slope may be quite approximate. However, it would appear that these stresses should be more accurate than those computed by the methods of slices.

In 1957, Bellman introduced a mathematical method called the "dynamic programming" method. One of the objectives of the dynamic programming method was to maximize or minimize a function. The dynamic programming method has been widely used in various fields other than geotechnical engineering. Baker (1980) appears to be the first to apply the optimization technique to the analysis of the stability of slopes.

In 1980, Baker introduced an optimization procedure that utilized the dynamic programming algorithm to determine the critical slip surface. In this approach, the associated factors of safety were calculated using the Spencer (1967), method of slices. Yamagami and Ueta (1988), enhanced Baker's (1980) approach by combining the dynamic programming method with a finite element stress analysis to more accurately calculate the factor of safety (Figure 32). The critical slip surface was assumed to be a chain of linear segments connecting two "state" points located in two successive "stages". Figure 32 shows that "stages" defined points under consideration in the *x*-direction while "stages" defined points in the *y*-direction. Straight line segments were used to join possible "stage" and "state" points.

The resisting and the actuating forces used to calculate an auxiliary function were determined from stresses interpolated from Gaussian points within the domain of the problem. Yamagami and Ueta (1988) analyzed two example problems to illustrate the proposed procedure.

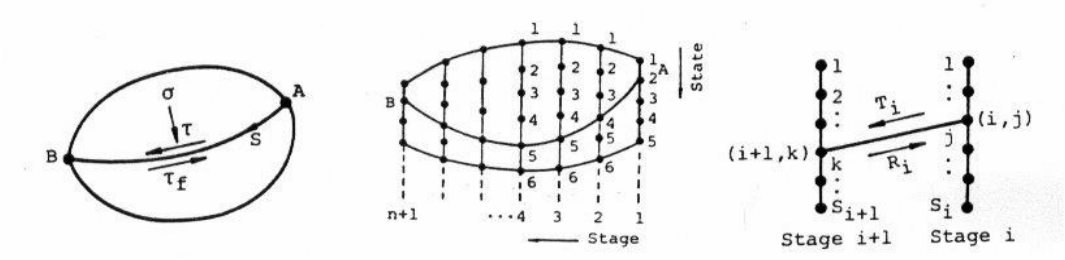

Figure 32 Search for the critical slip surface based on the dynamic programming method

(After Yamagami and Ueta, 1988)

In 1995, Zou et al. proposed an improved dynamic programming technique that used essentially the same method as introduced by Yamagami and Ueta (1988). The modification made by Zou et al. (loc. cit.) was that the critical slip surface might contain a segment connecting two "state" points located in the same "stage". The stability of a trial dam in Nong Ngu Hao, Bangkok, Thailand, was analyzed as part of the study verifying the proposed procedure.

The dynamic programming method can be combined with a finite element stress analysis to provide a more complete solution for the analysis of slope stability because the technique overcomes the primary difficulties associated with limit equilibrium methods. However, the disadvantage of the dynamic programming approach is that there are more variables to specify for the analysis; namely, the Poisson's ratio and the elastic moduli associated with the stress analysis. Fortunately, the computed stresses associated with the "switch-on" of gravity are quite insensitive to the elastic parameters of the soil.

The minimum factor of safety and critical slip surface are obtained by combining the dynamic programming method and the stress fields obtained from a finite element analysis. The stress fields input into the software can be generated by the finite-element method (FEM). The dynamic programming method is mainly based on the research of Yamagami and Ueta (1988) and Ha Pham (1999). Numerous example problems have been solved using the dynamic programming method. Examples include homogenous slopes, layered slopes as well as case histories. The results obtained from the analyses have been compared with results from several well-known limit equilibrium methods of slices (Fredlund and Krahn, 1977). While the factor of safety computations are quite similar by both methodologies for circular slip surfaces, the dynamic programming technique opens the way for solving more complex problems.

7.3.5.1 General

In 1957, Bellman introduced a mathematical theory involving multi-stage decision process. The *"decision process"* was defined as a system whose state at any time *t* is specified by a vector *P* that undergoes transformations in the course of time. The transformation of the variable *P* is equivalent to a decision. If a single decision is made, the process is called a single-stage decision process. On the other hand, the system is defined as a multistage decision process if there are sequences of decisions to be made.

The originality of the terminology *"dynamic programming"* is derived from the nature of the solution. The problem treated is a *"programming"* problem and the adjective *"dynamic"* indicates the significant involvement of time. However, the essential feature of the approach is the re-interpretation of many static processes as dynamic processes in which time can be artificially introduced.

Features of the dynamic programming theory can be summarized as follows:

1. The purpose of the dynamic programming method is to maximize or minimize a function,
2. The function can be described as a system containing "stages". The system is characterized at any "stage" by a set of parameters called "state" variables,
3. At each "stage" of the process, there is a number of decisions to be made,
4. The effect of a decision is a transformation of the "state" variables, and
5. The past history of the system is not of importance in determining future actions.

At this point, it is of interest to quote classic *"principle of optimality"*, introduced by Bellman (1957).

Principle of optimality: An optimal policy has the property that whatever the initial state and initial decision are the remaining decision must constitute an optimal policy regarding the state resulting from the first decision.

The mathematical transliteration of this principle yields all the functional equations that will be encountered throughout the theory of the dynamic programming method.

7.3.5.2 Definition of the Factor of Safety

For an arbitrary slip surface *AB*, as shown in Figure 33, the equation for the factor of safety can be defined as:

$$F_s = \frac{\int_A^B \tau_f \, dL}{\int_A^B \tau \, dL} \qquad \textbf{[100]}$$

where:

τ = mobilized shear stress along the slip surface,

τ_f = shear strength of the material, and

dL = an increment of length along the slip surface.

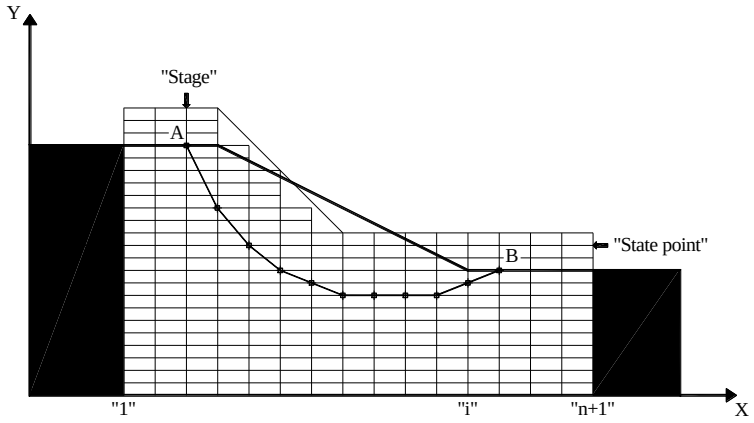

Figure 33 An arbitrary slip surface AB in a discretized form

It is assumed that the critical slip surface can be approximated by an assemblage of linear segments. Each linear segment connects two *state* points located in two successive *stages*. The *stage-state* system forms a grid consisting of rectangular elements called the *search grid*. The rectangular elements formed by the search grid are called grid elements. In this discretized form, the overall factor of safety for the slip surface *AB* is defined as follows:

$$F_s = \frac{\sum_{i=1}^{n} \tau_{f_i} \Delta L_i}{\sum_{i=1}^{n} \tau_i \Delta L_i} \quad \textbf{[101]}$$

where:

n = number of discrete segments,

τ_i = shear stress actuated,

τ_{fi} = shear strength, and

ΔL_i = length of the i^{th} segment.

7.3.5.3 Formulation of the Dynamic Programming Method

A minimization is necessary to determine the value of the factor of safety, F_s, in Equation [101]. Baker (1980) showed that the minimization of the factor of safety in Equation [101] may be found by using an *auxiliary function, G*. The auxiliary function is also known as the return function and can be defined as follows (Figure 34):

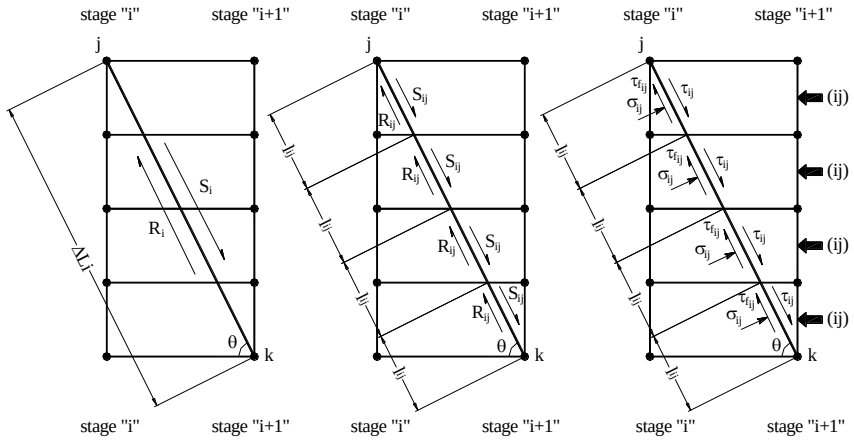

Figure 34 Actuating and resisting forces acting on the *i*th segment.

$$G = \sum_{i=1}^{n} (R_i - F_s S_i) \quad \textbf{[102]}$$

where:

S_i = actuating forces acting on the *i*th segment of the slip surface,

R_i = resisting forces acting on the *i*th segment of the slip surface, and

n = total number of discrete segments comprising the slip surface.

The minimum value of the auxiliary function, G_{min} is defined as:

$$G_{\min} = \min \sum_{i=1}^{n} (R_i - F_s S_i) \quad \textbf{[103]}$$

Along the line segment, the shear strength for a saturated-unsaturated soil can be calculated using the following equation (Fredlund and Rahardjo, 1993):

$$\tau_{f_i} = c' + (\sigma_n - u_a)\tan\phi' + (u_a - u_w)\tan\phi^b \quad \textbf{[104]}$$

where:

c′ = effective cohesion of the material at the base of a slice,

ϕ' = effective angle of internal friction of the material at the base of a slice,

ϕ^b = angle defining the increase in shear strength due to matric suction (or negative pore-water pressure),

$(\sigma_n - u_a)$ = net normal stress acting on the *i*th segment, and

$(u_a - u_w)$ = matric suction on the *i*th segment.

The normal and shear stresses acting on the *i*th segment can be computed from the results of a stress analysis as follows:

$$\sigma_n = \sigma_x \sin^2\theta + \sigma_y \cos^2\theta - \tau_{xy} \sin 2\theta \quad \textbf{[105]}$$

$$\tau_n = \tau_{xy}(\sin^2\theta - \cos^2\theta) - \frac{(\sigma_y - \sigma_x)}{2}\sin 2\theta \quad \textbf{[106]}$$

where:

σ_n = normal stress acting on the *i*th segment,

τ_n = shear stress acting on the i^{th} segment,

θ = Inclined angle of the i^{th} segment with the horizontal direction,

σ_x = normal stresses acting in the *X*- coordinate direction,

σ_y = normal stresses acting in the *y*- coordinate direction, and

τ_{xy} = shear stresses acting in the *x*- and *y*-coordinate directions.

These stresses can be determined from a finite element stress analysis that uses any particular material behavior model. If the density of the search grid is sufficiently fine, it can be assumed that stresses are constant within a small grid element. These constant stresses are signified as stresses at the center points of the grid element. Consequently, the resisting and actuating forces acting on the i^{th} segment of a slip surface can be calculated as follows (Figure 34):

$$R_i = \sum_{ij=1}^{ne} R_{ij} = \sum_{ij=1}^{ne} \tau_{f_{ij}} l_{ij} \qquad \textbf{[107]}$$

$$R_i = \sum_{ij=1}^{ne} \{c'_{ij} + (\sigma_n^{ij} - u_a)\tan\phi'_{ij} + (u_a - u_w)\tan\phi^b_{ij}\} l_{ij}$$

$$S_i = \sum_{ij=1}^{ne} S_{ij} = \sum_{ij=1}^{ne} \tau_{ij} l_{ij} \qquad \textbf{[108]}$$

where:

(ij) = a grid element traversed by the segment,

τ_{fij} = shear strength actuated at the center point of (*ij*),

τ_{ij} = shear stress actuated at the center point of (*ij*),

c'_{ij} = effective cohesion of the material within (*ij*),

ϕ'_{ij} = effective angle of internal friction of the material within (*ij*),

ϕ^b_{ij} = angle defining the increase in shear strength due to matric suction (or negative pore-water pressure) within (*ij*),

ne = number of (*ij*), and

l_{ij} = length of the i^{th} segment limited by the boundary of (*ij*).

An optimal function*, $H_i(j)$,* obtained at state point {*j*} located in stage [*i*] is introduced. The optimal function, $H_i(j)$, is defined as the minimum of the *return function, G*, calculated from a state point for the initial stage to state point {*j*} located in stage [*i*]. According to *the* principle of optimality (Bellman, 1957), the optimal function, $H_{i+1}(j)$, obtained at state point {*k*} located in stage [*i+1*] is defined as:

$$H_{i+1}(k) = H_i(j) + G_i(\overline{j,k}) \qquad \textbf{[109]}$$

where:

$G_i(\overline{j,k})$ = the *return function* calculated from state point {*j*} of stage [*i*] to state point {*k*} of stage [*i*+1].

At the initial stage, the value of the optimal function, $H_i(j)$, is equal to zero. That is:

$$H_1(j) = 0 \qquad j = 1...NP_1 \qquad \textbf{[110]}$$

where:

$NP1$ = number of state points in the initial stage.

At the final stage (i.e., $i = n+1$), the optimal function, $H_{n+1}(k)$, must be equal to the minimum value of the return function, G^{min}, that is:

$$H_{n+1}(j) = G_{\min} = \min \sum_{i=1}^{n} (R_i - F_s S_i) \qquad j = 1 \ldots NP_{n+1} \qquad \textbf{[111]}$$

where:

NP_{n+1} = number of state points in the final stage.

The optimal point in the final stage is defined as the state point at which the calculated optimal function is a minimum. From the optimal state point {*k*} found in the final stage, the optimal state point {*j*} located in the previous stage is also determined. The optimal *path* defined by connecting optimal state points located in every stage is eventually found by tracing back from the final stage to the initial stage. This optimal path defines the *critical slip surface*.

The value of the overall factor of safety, F_s, in Equation [89] has not been defined in advance and therefore an initial value must be assumed. The trial value for the factor of safety is updated using the value of F_s evaluated after each trial of the search. The optimization process will stop when a pre-defined convergence is reached.

7.3.5.4 Procedure of the Dynamic Programming Search

The analytical scheme of the dynamic programming method for performing a slope stability analysis is illustrated in Figure 35.

In Figure 35, stages lie in the horizontal direction and each stage contains a number of state points located in the vertical direction. Since the dynamic programming optimization search works on the stage-state point system, the output grid can also be called the *"search grid"*. The boundary of the search grid is called the *"search boundary"* and this boundary should be defined by the analyst as input data to the analysis.

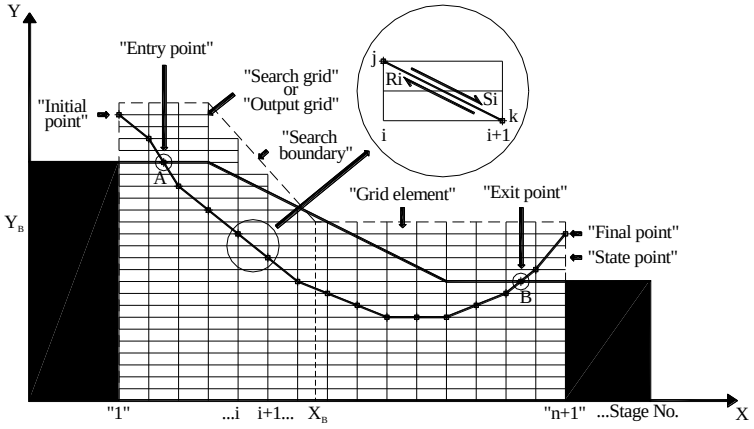

Figure 35 The analytical scheme of the dynamic programming method in slope stability analyses.

The search grid, which is essentially the same as the output grid, is designed such that it encloses most of the parts of the slope but contains one point located well within the physical boundary of the slope to prevent the search from choosing the optimal path outside the slope (i.e., point $\{X_B, Y_B\}$ in Figure 35). The search boundary should be defined as input data for the optimization search. The actual "*entry*" point, A, and the actual "*exit*" point, *B*, of the critical slip surface are eventually found at the intersections of the optimal path with the physical boundary of the slope.
It is important to note that the value of the factor of safety, F_s, in Equation [98] has not been defined in advance. Therefore, a trial value of F_s must be assumed prior to the first performance of the dynamic programming search. The trial value of F_s is updated using the value of F_s evaluated after each trial of the optimization search. The dynamic programming search, therefore, is a nonlinear analysis. The search procedure will stop only after the convergence criteria defined by the analyst is reached. In other words, while the factor of safety equation is linear, the search procedure for the critical slip surface is nonlinear.

Let us suppose that the initially assumed value of the factor of safety is F^i_s (i.e., F^i_s=1). Using this assumed value of the factor of safety when performing the initial optimization search, the initial optimal path (i.e., the critical slip surface) is obtained. The factor of safety of the initial critical slip surface is re-evaluated using Equation [98]. This newly evaluated factor of safety is called F^e_s.

If the convergence defined by the analyst is l then the following condition must be checked:

$$\left| F_s^e - F_s^i \right| \le \lambda \qquad \textbf{[112]}$$

If the condition presented by Equation [98] is satisfied, then F^{e}_{s} is the minimum factor of safety and the corresponding slip surface is the critical slip surface. Otherwise, the new value of the factor of safety used in the next iteration, F^{n}_{s}, is calculated as follows:

$$F_s^n = \frac{F_s^i + F_s^e}{2} \quad \textbf{[113]}$$

The same routine is repeated until the condition shown in Equation [98] is satisfied. The final slip surface determined is the critical slip surface and the corresponding factor of safety is the minimum factor of safety.

The dynamic programming method to solve a slope stability problem using the following steps:

1. Input the geometry data and material properties of the problem,
2. Import the output grid with corresponding nodal stresses,
3. Define a search boundary using the output grid imported as the search grid,
4. Interpolate stresses at the center point of each grid element from nodal stresses,
5. Assume an initial factor of safety, F_s (e.g., F_s=1.0),
6. Launch the search from all state points located in the initial stage,
7. Generate the first trial segment of the slip surface by connecting all state points of the initial stage to all state points located in the second stage,
8. Calculate the values of the optimal function obtained at all state points of the second stage using Equations [96], [97] and the assumed factor of safety. The number of optimal functions to be calculated at one state point of the second stage is equal to the number of state points located in the initial stage,
9. Determine the minimum value of the optimal function at each state point in the second stage. The corresponding state point in the previous stage (i.e., the initial stage for the first segment) is identified,
10. Proceed to the next stage with the same routine until the final stage is reached,
11. Compare the values of the optimal functions obtained at all state points of the final stage and determine the state point at which the corresponding value of the optimal function is a minimum. The determined state point will be the first optimal point of the optimal path,
12. Trace back to the previous stage to find the corresponding state point with the first optimal point. This corresponding state point will be the second optimal point of the optimal path,
13. Keep tracing back to the initial stage to determine the entire optimal path,
14. Evaluate the actual factor of safety corresponding to the optimal path obtained from step 13 using Equation [87]. A new value for the factor of safety is calculated based on the initially assumed and the actual factors of safety,
15. Repeat the procedure until the difference between the assumed and the actual factor of safety is within the convergence criterion, *d*, defined prior to the performance of the optimization process, and
16. Define the actual critical slip surface by determining the entry and exit points of the critical slip surface. These points are found at the intersections of the optimal path with the physical boundary of the slope.

7.3.5.5 Research Applied to the Shape of the Critical Slip Surface

The shape of the critical slip surface must be kinematically admissible. Baker (1980) assumed that the critical slip surface must be concave. Therefore, that was the condition applied to the shape of the critical slip surface proposed by Baker (1980).

The first derivative calculated from the crest to the toe of the curve that represents the critical slip surface had to be greater than or equal to zero. Kinematic restriction conditions were not mentioned in Yamagami and Ueta (1988). Zou et al. (1995) stated that a check must be made to assure that the critical slip surface is kinematically admissible. However, there was no further comment regarding how this "check" should be applied.

In general, kinematical restrictions play an important role in the applicability of the dynamic programming method in slope stability analysis. Using appropriate kinematical restrictions prevents the shape of the critical slip surface from being unreasonable.

Theoretically, when failure takes place the resisting force and the actuating force along the slip surface must be in contrary directions. The resisting force must always act in the direction opposite to the mass movement. At the same time, the actuating force must be in the same direction as the movement (Figure 36). The kinematical restriction applied to the shape of the critical slip surface in the dynamic programming method in the software is that if the actuating force calculated is in a contrary direction

to the anticipated direction of mass movement, then the entire trial segment in which the actuating force is being calculated will be eliminated from the search.

In other words, a trial segment will be eliminated from the optimization search if the actuating and resisting forces are found having the same sign. Applying this condition to the optimization procedure will eliminate all trial segments that constitute "*kinky*" shaped slip surfaces.

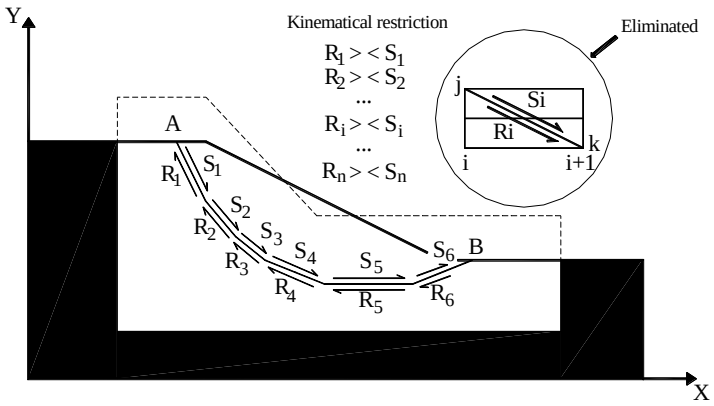

Figure 36 Kinematical restrictions applied to the shape of the critical slip surface

7.3.6 Cuckoo Search

Cuckoo Search (CS) is one of the latest nature-inspired metaheuristic optimization algorithms, developed by Xin-She Yang in Cambridge University and Suash Deb in C. V. Raman College of Engineering in 2009 (Yang and Deb, 2009). CS is based on the brood parasitic behavior of some cuckoo species. In addition, this algorithm is enhanced by the so-called Lévy Flights random walk. Recent studies show that CS is potentially far more efficient than Genetic Algorithms (GA) and Particle Swarm Optimization (PSO) (Yang, 2010).

Description of Critical Slip Surface Search Problem

1. For any 2D non-circular slip surface, it can be expressed as a polyline with *n* points, the factor of safety along this slip surface is described as a function of these points as F(***P***), where ***P*** is the coordinates of the points (x_0, y_0), (x_1, y_1), …., (x_{n-1}, y_{n-1}).
2. For any 2D circular slip surface, the factor of safety along a circular slip surface is described as a function of F(***P***), where ***P*** is the coordinate of the center point of the circle (x_0, y_0) and the radius of the circle *r*.
3. For 3D Ellipsoid slip surface search, the factor of safety along an Ellipsoid slip surface is described as a function of F(***P***), where ***P*** is the coordinate of the center point of the ellipsoid (x_0, y_0, z_0) and the radius of the Ellipsoid (r_x, r_y, r_z).

The task of slope stability analysis is to locate the critical slip surface (to get the critical set of ***P***) and calculate its FOS. The algorithm to locate the critical slip surface is a global minimization issue. i.e., to minimize objective function F(***P***) with valid points ***P***. A good global optimization search technique should avoid local minima, while satisfying geometric and kinematic constraints and conditions. Since the slope stability calculation function F(***P***) is highly discontinuous and multimodal, it is always challenging to find an efficient global optimization technique. The recent stochastic algorithm Cuckoo Search shows great promise, it can find the best set of admissible points to achieve the optimum objective function while escape from local minima. It is claimed as one of the most efficient nature-inspired metaheuristic search algorithms (Yang, 2010).

7.4 OPTIMIZE SURFACES

The optimize slip surfaces function is used to find lower factor of safety starting from some initial slip surfaces. The initial slip surface can be defined by fully specified slip surfaces or the critical slip surface generated by non-circular slip surface search or circular slip surface search. The optimization is based on "Random walk" Monte Carlo technique (Greco, 1996; Malkawi, Hassan and Sarma, 2001).

The basic steps to optimize a slip surface are:

1. The factor of safety for the initial slip surface is calculated and saved.
2. If the initial slip surface is circular, the slip surface is divided into a number of straight line segments.

3. Each vertex of the slip surface is randomly walked/modified for different directions and magnitudes, a new trial slip surface is formed with new vertex location.
4. The factor of safety is calculated for the new trial slip surface. If the factor of safety is lower than the factor of safety of initial slip surface, the new trial slip surface will replace the initial slip surface and repeat step 1
5. If the factor of safety is higher than factor of safety of initial slip surface, then repeats step 3 to generate new random walks or loop through next vertex.
6. After the random walks are finished for all the vertex in current slip surface and does not meet the STOP process criteria. A new point will be inserted into the middle of the longest slip surface line segment and repeat from step 1
7. This process STOPS if the difference in the computed factors of safety is less than the user specified factor of safety tolerance or until the number of optimization trials reaches the user specified maximum number.

Like other optimization techniques, it is not always guaranteed a correct global minimum factor of safety is obtained. For example, this random walking technique may only find a localized minimum factor of safety, or the critical slip surface found may not be physically admissible. The user must validate the optimized results by checking both the factor of safety value and the shape of critical slip surface.

8 MATERIAL STRENGTH

There are numerous procedures that can be used to describe the shear strength of a material. Procedures implemented in the software are described below.

There are several shear strength models that can be used for representing a soil or rock. Several models are described in this section, but it is likely that more models will be added with time.

8.1 MOHR-COULOMB STRENGTH

The most used shear strength designation for saturated soils encountered in geotechnical engineering is the Mohr-Coulomb equation:

$$\tau = c' + (\sigma_n - u_w)\tan\phi' \quad \textbf{[114]}$$

where:

- τ = effective shear strength,
- c' = effective cohesion,
- σ_n = normal stress on the shear plane,
- u_w = pore-water pressure, and
- ϕ' = effective angle of internal friction.

The shear strength parameters are often determined from triaxial tests or direct shear tests and the Mohr-Coulomb failure envelope will be of the form shown in Figure 37.

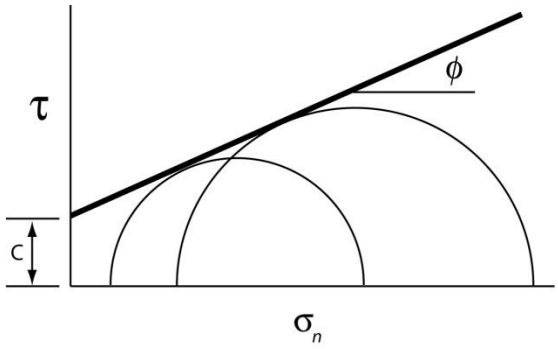

Figure 37 Mohr-Coulomb failure envelope written in terms of effective stresses

The Mohr-Coulomb equation can also be written in terms of total stress conditions (Figure 38). For a total stress analysis, the pore-water pressures are not considered, and the cohesion and friction angle are defined in terms of total stress conditions. The Mohr-Coulomb equation can be written:

$$\tau = c + \sigma_n \tan\phi \quad \textbf{[115]}$$

where:

τ = total shear strength,

c = total cohesion,

σn = normal stress on shear plane, and

ϕ = total angle of internal friction.

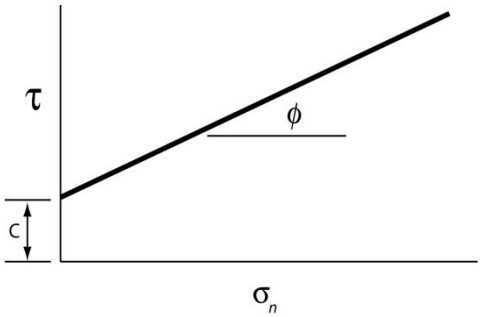

Figure 38 The relationship between shear strength and total normal stress

8.2 CURVED-SURFACE ENVELOPE MOHR-COULOMB

The curved-surface envelope extended Mohr Coulomb shear strength model was introduced by Md. Noor and Anderson (2006). The purpose of the curvilinear type of shear strength envelope is to replicate the unique shear strength behavior at low stress levels and improve the slope stability analysis for shallow rainfall induced failure. When in the low range of net stress, a drastic steep reduction in shear strength is observed. The shear strength of soil cannot be extrapolated from a traditional Mohr-Coulomb model but needs to follow an exact curve equation as shown in the following Figure 39. Using conventional types of shear strength models would over-estimate the soil strength near the ground surface. The advantage of the model is that it can exhibit both the steep non-linear drop in shear when suction and depth approach zero.

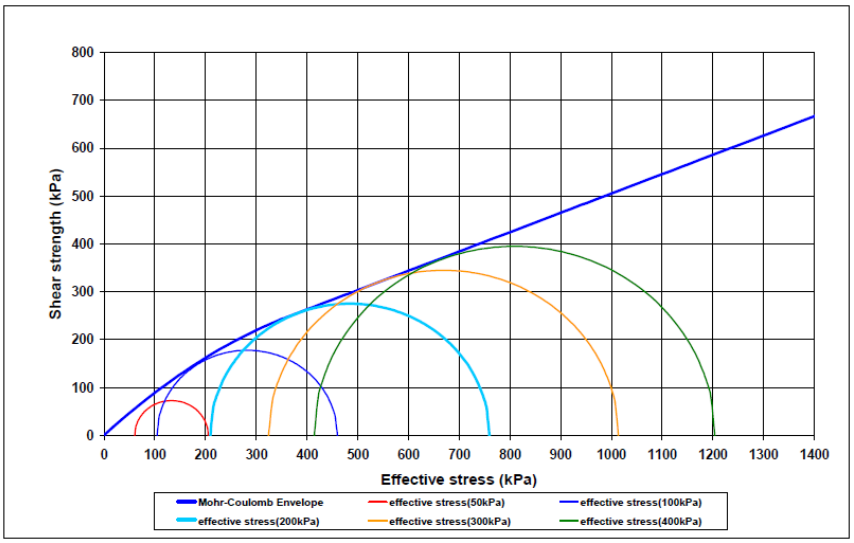

Figure 39 Curvilinear shear strength envelope of granitic residual soil grade VI from Rawang, Malaysia

The curved-surface envelope is shown in Figure 40. It has seven shear strength parameters. The curved-surface envelope shear strength model can represent the shear strength behavior of many soils if the right shear strength parameters are selected. There are four zones in the curved-surface envelope. The shear strength equation representing each zone can be obtained by adding the saturated and the partially saturated equations that represent the area. Users can refer to the reference for the detailed information about the model and its parameters.

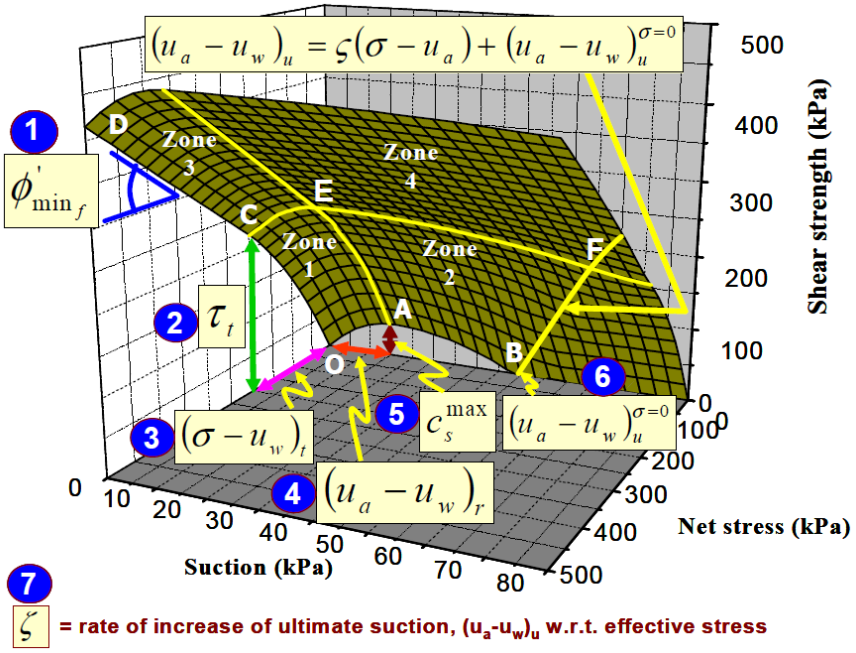

Figure 40 Curved-surface envelope Mohr-Coulomb model and the seven shear strength parameters

where:

ϕ'_{min_f}	= minimum friction angle at failure,
τ_t	= transition shear strength,
$(\sigma - u_w)_t$	= transition effective stress,
$(u_a - u_w)_r$	= residual suction,
$(u_a - u_w)_u^{\sigma'=0}$	= ultimate suction when the net stress is zero,
C_s^{max}	= maximum apparent cohesion, and
ς	= the rate of change of ultimate suction with respect to net stress.

8.3 UNDRAINED SHEAR STRENGTH

The undrained strength of a material forms a special total stress case of the Mohr-Coulomb shear strength envelope. For the undrained material model, the friction angle ϕ is set to zero and the shear strength of the material is specified using the cohesion intercept, *c*. Pore-water pressures are assumed to have no effect apart from the effect observed when measuring the shear strength of the material. An undrained strength envelope is shown in Figure 41.

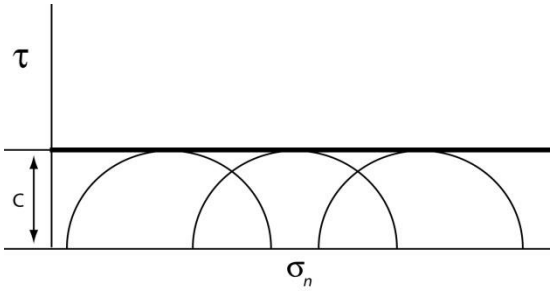

Figure 41 Undrained shear strength envelope

There are three sub-options available for defining the undrained shear strength (i.e., undrained cohesion):

1. Constant: cohesion is assumed to be constant throughout the material.
2. Depth dependent strength from the top of a material layer: cohesion is a function of depth where depth is measured from the top of the material layer to the center of the base of a slice. With this option, it is necessary to specify the

undrained shear strength, *c*, at the top of the layer and to specify a rate of increase in shear strength with depth. It is also possible to specify a maximum cohesion in this option. The concept of this model is shown in Figure 42.

The top of the material layer is automatically searched for each slice in the software. The top of the material layer does not need to be a straight line; rather, it can also be a folded line.

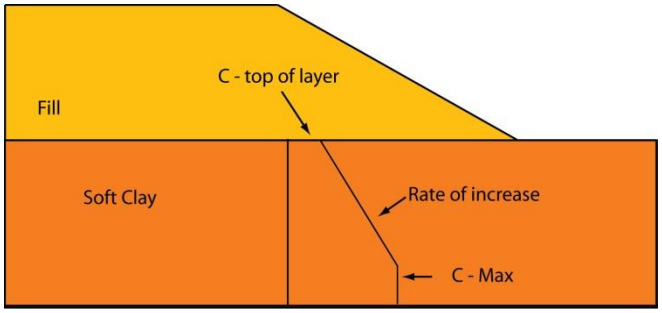

Figure 42 - Depth-dependent strength from top of a layer

3. Depth dependent strength from top of an arbitrarily specified Datum: cohesion is a function of depth, where depth is measured from a specified Datum to the center of a slice base. The datum is specified as an elevation (i.e., y-coordinate). This option is illustrated in Figure 43.

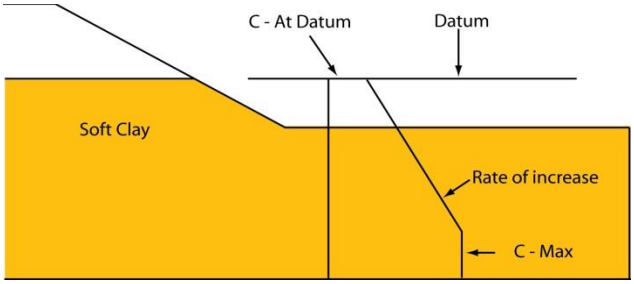

Figure 43 - Depth-dependent strength from specified Datum

8.4 NO-STRENGTH

The ″No-Strength″ option can be used to model water and any other material that will not contribute shear strength. A "No-Strength" material contributes weight and hydraulic force (i.e., hydrostatic force) to the model. The "No-Strength" option means that *c* and ϕ are both zero (i.e., shear strength parameters are disabled).

8.5 BEDROCK

Bedrock is considered to be a hard impenetrable material through which the slip surface cannot enter. Bedrock in the software is not really a strength model but rather represents an internal flag that represents special treatment of the slip surface. Slip surfaces are not allowed to enter the Bedrock layer. No shear strength parameters need to be input for the Bedrock model.

8.6 ANISOTROPIC STRENGTH

Anisotropic shear strength utilizes the following equations to represent anisotropy of the material strength:

$$c = c_1 \cos^2 \alpha + c_2 \sin^2 \alpha \quad \textbf{[116]}$$

$$\phi = \phi_1 \cos^2 \alpha + \phi_2 \sin^2 \alpha \quad \textbf{[117]}$$

where:

C_1 = cohesion in 1-direction,

C_2 = cohesion in 2-direction,

$\phi 1$ = angle of internal friction in 1-direction,

$\phi 2$ = angle of internal friction in 2-direction,

α = angle of the base of a slice with 1-direction,

c = cohesion at the base of a slice, and

ϕ = angle of internal friction at the base of each slice.

Angle = angle from positive x-axis to 1-direction, ccw is positive.

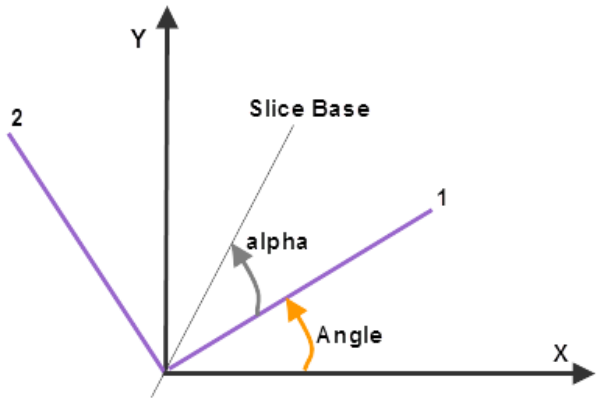

Figure 44 Definition of Axes and Angle for Anisotropic Strength model

8.7 ANISOTROPIC FUNCTION

The Anisotropic Strength Function is another material strength model that allows the user to define anisotropic shear strength. The user can define ranges of slice base angles with corresponding material cohesion and friction angle. The example in Figure 41 shows three slice base angle ranges of strength properties.

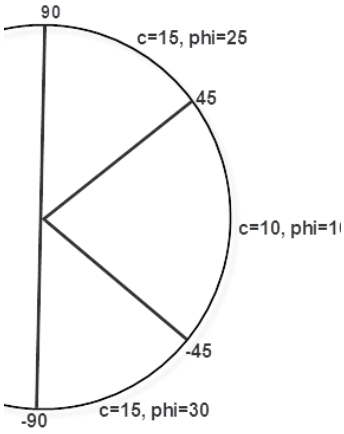

– 90 to –45 degrees, with c = 15 and phi = 30
– 45 to 45 degrees, with c = 10 and phi = 10
45 to 90 degrees, with c = 15 and phi = 25

Figure 45 Definition of Axes and Angle for Anisotropic Strength model

8.8 ANISTROPIC LINEAR MODEL (ALM1)

ALM is a constitutive model that describes the shear strength of an anisotropic rock mass in relation to the change of Angle of Anisotropic (AoA). The AoA is defined as the angle between the orientations of the plane of shear and the plane of weakness. This model was originally developed by Snowden Mining Industry Consultants in Perth, Australia in 2005. The theory outlined in this manual is based on Mercer (2013) and Mercer (2017).

There are four generations of the model are now available. The first generation (ALM1) is based on the Mohr-Coulomb criterion.

The bedding and rock mass shear strengths for ALM1 are defined in terms of the Mohr-Coulomb parameters of cohesion and friction angle. In this model, a rock material is defined with the following anisotropic strength parameters:

- The weakness plane (usually the bedding plane) cohesion and friction angle (c1, phi1), corresponds to the minimum shear strength
- Rock mass cohesion and friction angle (c2, phi2), corresponds to the maximum shear strength

- Angle of bedding plane orientation (theta) from horizontal
- Parameters A and B define a linear transition from bedding plane strength to rock mass strength, with respect to shear plane orientation

ALM1 defines the shear strength relationship to the AoA, rock mass strength, and bedding shear strength. The parameters A and B allow the user to define a linear transition from bedding plane strength to rock mass strength, with respect to shear plane.

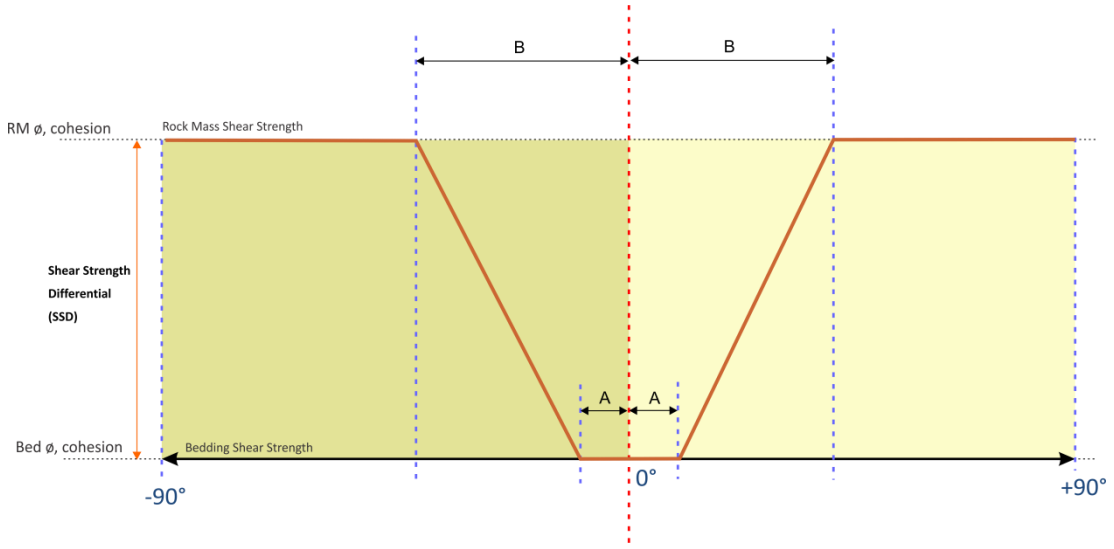

Figure 46 Anisotropic Linear Model 1 (ALM1)

ALM is available in 3D analysis as well. In 3D, the weakness plane dip angle is converted into an apparent dip angle along the mass sliding direction (not per-column) using the standard apparent dip equation. The apparent dip angle decreases as the difference between the weakness plane dip direction and the mass sliding direction increases, approaching 0 when the sliding direction follows the strike of the weakness plane.

8.8.1 Computation of Anisotropic Shear Strength

Assuming the angle of anisotropic (AoA) is α (i.e., the angle between the orientation of an individual slice base and orientation of bedding plane); the Mohr-Coulomb cohesion and friction angle of the shear plane are calculated as follows for the ALM1.

First, a dimensionless parameter is computed.

$$\delta = \frac{\|\alpha\| - A}{B - A} \qquad \textbf{[118]}$$

where:

A = ALM1 parameter (Figure 46),

B = ALM1 parameter (Figure 46),

$\|\alpha\|$ = absolute value of the angle α.

Depending on the value ofδ, the cohesion, *c* and friction angle, *phi* of the shear plane are computed using the following equations:

$$\begin{array}{lll} \delta \le 0 & c = c_1 & \tan\phi = \tan\phi_1 \\ \delta \ge 1 & c = c_2 & \tan\phi = \tan\phi_2 \\ 0 < \delta < 1 & c = c_1(1-\delta) + c_2\delta & \tan\phi = \tan\phi_1(1-\delta) + \tan\phi_2\delta \end{array} \qquad \textbf{[119]}$$

8.9 MODIFIED ANISTROPIC LINEAR MODEL 2 (ALM2)

Since 2009, Snowden has been undertaking further research and development of the ALM1 method. In the second generation of ALM, the Modified Anisotropic Linear model (ALM2), Snowden recognizes that cohesion, *c* and friction angle, *phi* for a typical

rock mass and bedding plane are a function of the stress state within the rock mass and along the bedding plane. As a result, the model requires either a shear stress versus normal stress function or a function relating cohesion and friction angle to normal stress.

In ALM2, as shown in Figure 47, with the parameters "A1", "A2", "B1" and "B2", the non-symmetrical shape of the shear strength transition can be modeled. The rate and shape of the transition depends on the bedding to rock mass strength ratio as well as the normal stress. Both the rock mass and bedding shear strengths are now modeled non-linearly in terms of the normal stress.

The formula to calculate the shear strength of the ALM2 model is:

$$\alpha \le 0 \qquad \delta = \frac{\|\alpha\| - A_1}{B_1 - A_1} \qquad \textbf{[120]}$$

$$\alpha > 0 \qquad \delta = \frac{\|\alpha\| - A_2}{B_2 - A_2}$$

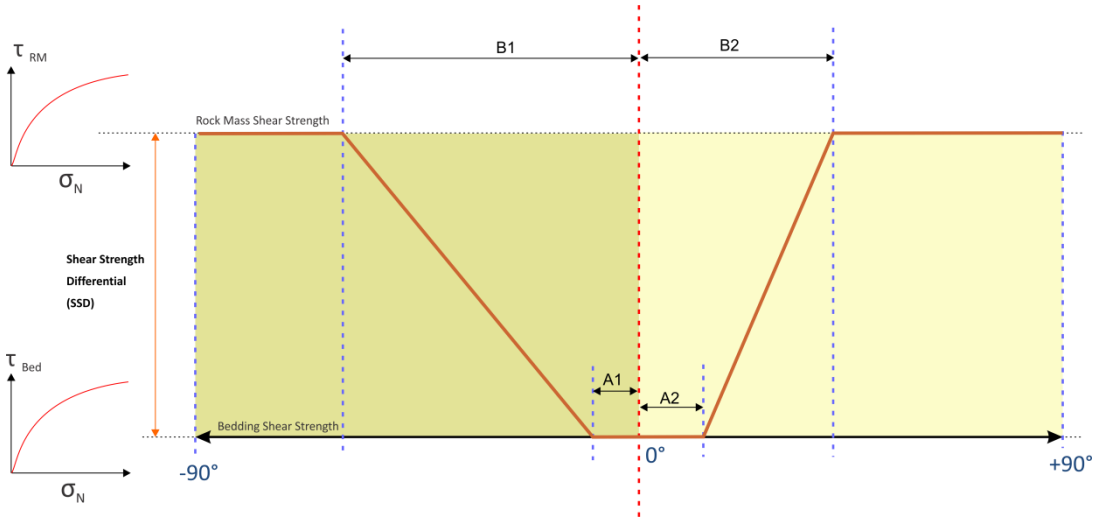

Figure 47 Modified Anisotropic Linear Model 2 (ALM2)

8.10 MODIFIED ANISOTROPIC LINEAR MODEL 3 (ALM3)

ALM3 further extended ALM2 on the upslope side (positive AoA). The downward shear strength side (negative AoA) of the model between 0 to -90 degrees remains unchanged from ALM2. It is developed to specifically address the concern regarding the overestimation of the shear strength as a result of the upslope shear strength reduction which can occur between an AoA of +40 to 90 degrees.

The parameters used in the model are defined as follows:

σ_N:	Normal stress
A1, A2, D:	Modelling parameters as discussed below
B1, B2:	Transition angles for negative and positive AoA
τ_{Bed}:	Bedding shear strength for all AoA
$\tau_{RM\text{-}UP}$:	Rock mass shear strength for positive AoA's as a linear or non-linear function of σ_N
$\tau_{RM\text{-}DWN}$:	Rock mass shear strength for negative AoA's as a linear or non-linear function of σ_N
DSSD:	Downward shear strength differential = $\tau_{RM\text{-}DN}$ - τ_{Bed}
USSD:	Upward shear strength differential= $\tau_{RM\text{-}UP}$ - τ_{Bed}
C1:	AoA reflecting the start of the USSD
C2:	AoA at which the local USSD minimum occurs
C3:	AoA reflecting the transition of the USSD into $\tau_{RM\text{-}UP}$
λ:	Percentage reduction in USSD to achieve minimum USSD

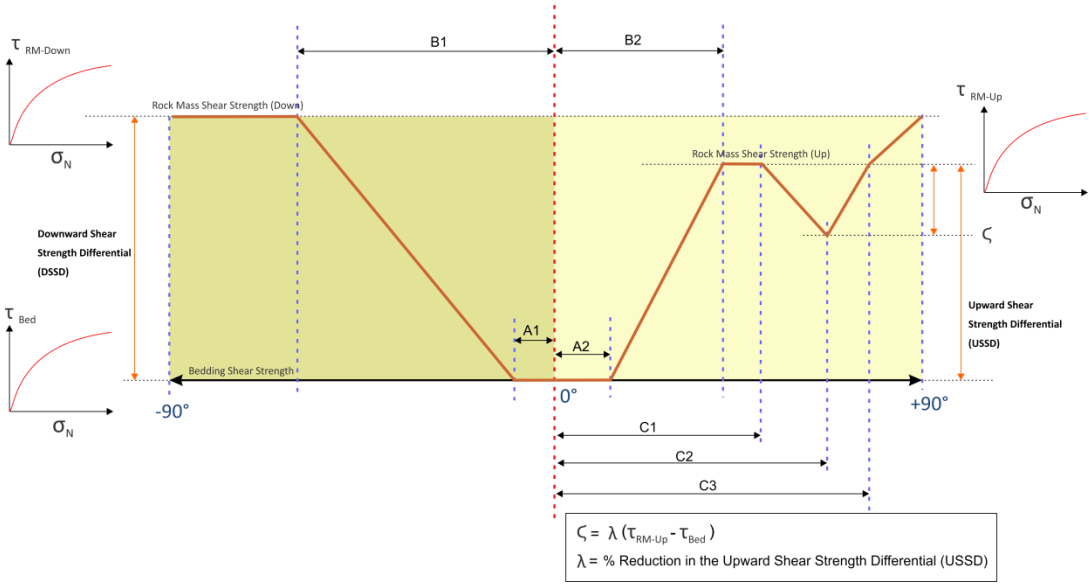

Figure 48 Modified Anisotropic Linear Model 3 (ALM3)

8.11 MODIFIED ANISOTROPIC LINEAR MODEL 4 (ALM4)

ALM4 further extended ALM3 on the relationship between AoA and shear strength. Now custom definitions of the relationship (equations) between AoA and shear strength can be described.

The parameters used in the model are defined as follows:

τ_{Bed}:	Bedding shear strength for all AoA
τ_{RM-UP}:	Rock mass shear strength for positive AoA's as a linear or non-linear function of σ_N
τ_{RM-DWN}:	Rock mass shear strength for negative AoA's as a linear or non-linear function of σ_N
DSSD:	Downward shear strength differential = $\tau_{RM-DN} - \tau_{Bed}$
USSD:	Upward shear strength differential= $\tau_{RM-UP} - \tau_{Bed}$
λ:	Percentage of shear strength differential. $\tau_{Rock} = \tau_{Bed} + \lambda*(\tau_{RM} - \tau_{Bed})$
LU:	Defines the upslope shear strength relationship between AoA vs. λ. $\tau_{Rock} = \tau_{Bed} + \lambda_{LU}*USSD$
LD:	Defines the downslope shear strength relationship between AoA vs. λ. $\tau_{Rock} = \tau_{Bed} + \lambda_{LD}*DSSD$

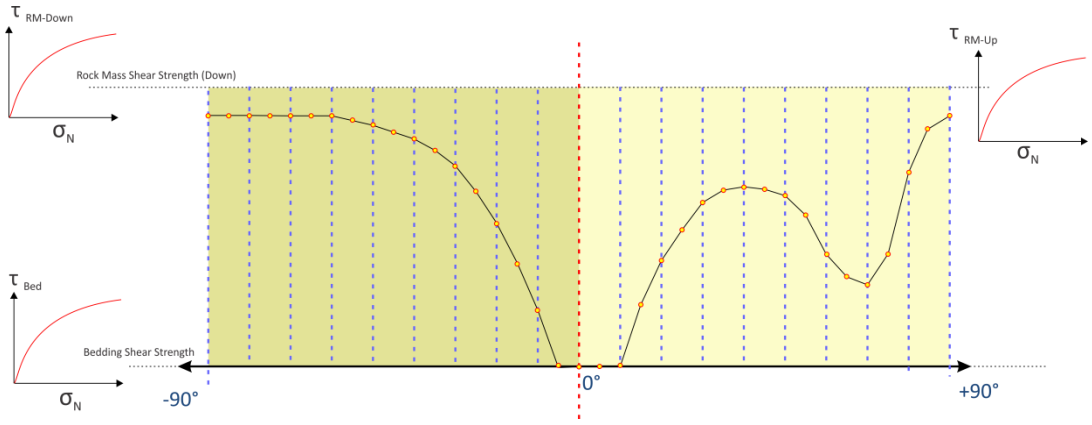

Figure 49 Modified Anisotropic Linear Model 4 (ALM4)

8.12 BILINEAR MODEL

The failure shear strength envelope can be described as having a Bilinear form (Figure 50). In this case, a cohesion value, two angles of internal friction, ϕ, and a normal stress at which the angles of internal friction change, must be specified.

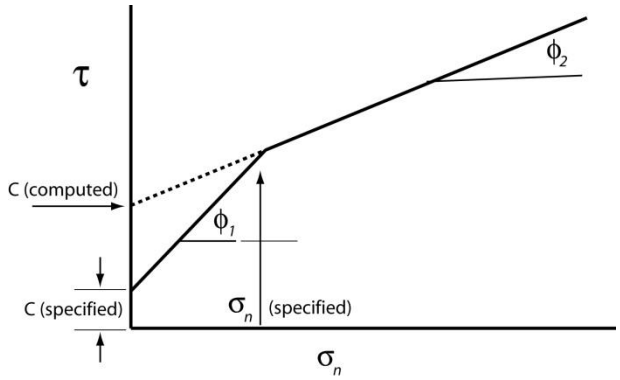

Figure 50 Bilinear shear strength model

When the normal stress at the base of a slice is greater than the specified normal stress, the software computes the line corresponding to the ϕ_2 material back to the shear strength axis and computes an inferred cohesion value for the material when the normal stress exceeds the specified normal stress for a change in the angle of internal friction. The Bilinear model acts as a two Mohr-Coulomb model that can be used to accommodate a nonlinear shear strength envelope.

8.13 POWER CURVE 1

The Power Curve 1 soil strength model uses the power equation:

$$\tau = c + a\sigma_n^b \quad \textbf{[121]}$$

where:

σ_n = normal stress on shear plane,

c = soil cohesion,

a = power curve parameter,

b = power curve parameter, and

τ = shear strength.

8.14 POWER CURVE 2

The Power Curve 2 soil strength model uses the power equation:

$$\tau = c + a(\sigma_n + d)^d \quad \textbf{[122]}$$

Where:

σ_n = normal stress on shear plane,

c = soil cohesion,

a = power curve parameter,

b = power curve parameter,

d = power curve parameter, and

τ = shear strength.

8.15 UNDRAINED STRENGTH RATIO

The undrained strength stress ratio assumes that the shear strength is a constant ratio (or percentage) of the vertical effective stress. The vertical effective stress is computed from the total weight of each slice and the pore-water pressure acting at the center of the base of each slice. The shear strength can be computed using the following equation:

$$\tau = K\sigma'_v \quad \textbf{[123]}$$

where:

K = undrained strength stress ratio,

σ'_V = effective vertical stress, and

τ = shear strength.

8.16 COMBINED FRICTIONAL-UNDRAINED MODEL

The combined frictional-undrained model is designed for materials that demonstrate cohesion versus angle of internal friction relationship up to some maximum undrained shear strength value as illustrated in Figure 51.

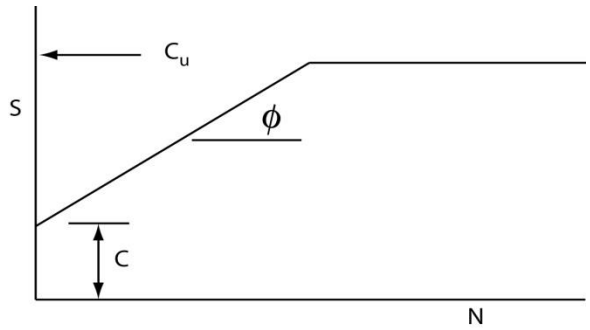

Figure 51 Combined frictional-undrained strength model

8.17 SHEAR-NORMAL STRESS FUNCTION

The Shear-Normal Stress Function model is used for defining a curved shear strength envelope for a material with an empirical shear-normal relationship (Figure 52).

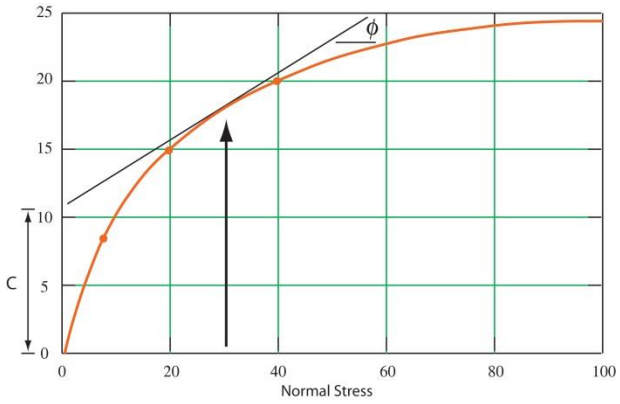

Figure 52 Shear-Normal stress function

8.18 GENERALIZED HOEK-BROWN MODEL

The Generalized Hoek-Brown Model is a nonlinear shear strength model commonly used for rock. The Generalized Hoek-Brown model in the software refers to the Generalized Hoek-Brown shear strength criterion (Hoek, Carranza-Torres and Corkum, 2002).

The Generalized Hoek-Brown shear strength criterion is described using the following equation:

$$\sigma_1' = \sigma_3' + \sigma_{ci}' \left(m_b \frac{\sigma_3'}{\sigma_{ci}'} + s \right)^a \quad \textbf{[124]}$$

where:

$\sigma'ci$ = uniaxial compressive strength of the intact rock,

m_b = reduced value for the rock mass of the material constant,

s = constant that depends on the characteristics of the rock mass,

a = constant that depends on the characteristics of the rock mass,

$\sigma'1$ = major principal stress, and

$\sigma'3$ = minor principal stress.

The parameters in the generalized Hoek-Brown shear strength equation can be determined from triaxial shear tests on rock materials. In most cases, however, it is difficult to carry out the necessary tests. Therefore, Hoek et al. (2002) have proposed empirical equations to determine the necessary parameters. There are four input parameters in the Generalized Hoek-Brown model that are required to compute the shear strength versus normal stress curve. The four parameters are:

σci = uniaxial compressive strength of the intact rock,

m_i = a property of the intact rock,

GSI = Geological Strength Index (0-100), and

D = rock mass disturbance factor (0-1).

The D, GSI, and m_i properties can be used to compute m_b as follows:

$$m_b = m_i \exp\left(\frac{GSI - 100}{28 - 14D} \right) \quad \textbf{[125]}$$

The two curve parameters a and s are defined as:

$$a = \frac{1}{2} + \frac{1}{6}\left(e^{-GSI/15} - e^{-20/3} \right) \quad \textbf{[126]}$$

$$s = \exp\left(\frac{GSI - 100}{9 - 3D} \right) \quad \textbf{[127]}$$

8.19 HOEK-BROWN MODEL

Hoek Brown failure criterion was developed for the design of underground excavation (Hoek E. & Brown E.T. 1980). The original Hoek-Brown equation is identical to the one used for describing the failure of concrete in 1936. Hoek and Brown, however, made a significant contribution to linking the equation to geological observations in the form of Bieniawski's Rock Mass Rating and later the geological Strength Index (GSI).

The equation for the Hoek-Brown Failure Criterion used in the software is the one published in the Rankine Lecture (1983). Also, this criterion became more popular because of the development of the relationship between Hoek-Brown criterion, with the non-linear parameters m and s and the Mohr-Coulomb criterion with the parameters c and ϕ, which allows the software to deal with this criterion like most commonly used Mohr-Coulomb criterion.

The Hoek-Brown shear strength criterion is described using the following equation:

$$\sigma_1' = \sigma_3' + \sigma_{ci}' \sqrt{m_b \frac{\sigma_3'}{\sigma_{ci}'} + s} \quad \textbf{[128]}$$

where:

$\sigma'ci$ = uniaxial compressive strength of the intact rock,

m_b = reduced value for the rock mass of the material constant,

s = constant that depends on the characteristics of the rock mass (=1 for intact rock),

σ'_1 = major effective principal stress at failure, and

σ'_3 = minor effective principal stress at failure.

The relationship between the constant parameters in Equation [128] and the Mohr-Coulomb shear strength parameter c and ϕ can be described as:

$$h = 1 + \frac{16\left(m\sigma'_n + s\sigma_{ci}\right)}{3m^2\sigma_{ci}} \quad \textbf{[129]}$$

$$\theta = \frac{90 + \arctan\left(\frac{1}{\sqrt{h^3 - 1}}\right)}{3} \quad \textbf{[130]}$$

$$\phi'_i = \arctan\left(\frac{1}{\sqrt{4h\cos^2\theta - 1}}\right) \quad \textbf{[131]}$$

$$\tau = \frac{m\sigma'_{ci}\left(\cot\phi'_i - \cos\phi'_i\right)}{8} \quad \textbf{[132]}$$

$$c' = \tau - \sigma'_n \tan\phi'_i \quad \textbf{[133]}$$

σ'_n = effective normal stress at centre of the base of each slice,

$\phi'i$ = equivalent friction angle at base of each slice,

τ = equivalent Shear strength, and

c' = equivalent cohesion.

8.20 UNSATURATED SOIL MODELS

The most common trigger for slope stability failures world-wide is rainfall events. Such events destroy the negative water pressures (suctions) in the upper zone of the soil and cause failures. As such, it is important that slope stability software be able to accommodate this type of failure mechanism. The software implements many types of unsaturated soil strength models to provide increased capabilities to the user. In addition, the software may import steady-state or transient pore-water pressure distributions from FEM Groundwater software.

The following sections define the theoretical aspects of several unsaturated shear strength models, which the software uses.

8.20.1 Linear Model (Phi-b)

Matric suction (or negative pore-water pressures) in an unsaturated soil affects the shear strength. The negative pore-water pressure increases the shear strength of an unsaturated soil. The shear strength of unsaturated soil has been shown to be nonlinear in form when matric suction is varied over a considerable range. Consequently, there are nonlinear forms for the unsaturated shear strength equation as well as a linear approximation of the unsaturated shear strength. The linear approximation of the unsaturated soil shear strength equation can be written as follows:

$$\tau = c' + \left(\sigma_n - u_a\right)\tan\phi' + \left(u_a - u_w\right)\tan\phi^b \quad \textbf{[134]}$$

where:

c' = effective cohesion,

ϕ' = effective angle of internal friction,

ϕ^b = angle defining the increase in shear strength due to matric suction (or negative pore-water pressure),

σ_n = total normal stress,

u_a = pore-air pressure, and

u_w = pore-water pressure.

The term (u_a - u_w) is called matric suction and is a positive representation of the negative pore-water pressure. The angle, ϕ^b, is a material property. The angle, ϕ^b, can range from zero to the ϕ' value depending on the material type and the magnitude of matric suction. The default value for ϕ^b is set to $\phi'/2$.

In The software, the effect of negative pore-water pressures is ignored when ϕ^b is not specified (i.e., zero). For other values of ϕ^b, an increase in shear strength due to matric suction (u_a - u_w) will be included in accordance with the above equation.

8.20.2 Nonlinear Models

The shear strength envelope can generally be assumed to be linear with respect to the (σ_n - u_a) stress state variable. However, the shear strength envelope with respect to matric suction, (u_a - u_w), tends to be nonlinear when the complete range of soil suction values are considered. The nonlinearity commences when matric suction approaches the air entry value of the soil. The shear strength envelope takes on a gradual curvature with increasing matric suction until the residual soil suction is reached. At this point the shear strength envelope is assumed to become horizontal (i.e., no further increase in shear strength), for most materials. Sand materials may even experience a decrease in shear strength after the residual suction is exceeded. The nonlinear shear strength equation can be related to the soil-water characteristic curve and written in one or more forms.

8.20.2.1 Fredlund Unsaturated Shear Strength Equation

One of the nonlinear shear strength equations for an unsaturated material can be written as follows (Fredlund et al., 1996):

$$\tau = c' + (\sigma_n - u_a)\tan\phi' + (u_a - u_w)\Theta_d^{\kappa}\tan\phi' \qquad \textbf{[135]}$$

where:

Θ_d = θ (u_a - u_w) / θ_s; water content with θ (u_a - u_w) = volumetric water content at any suction; θ_s = saturated volumetric water content, and

κ = Fitting material parameter that has a value near 1.0 for sands, increasing to 2 to 3 for materials of medium to high plasticity (Figure 53).

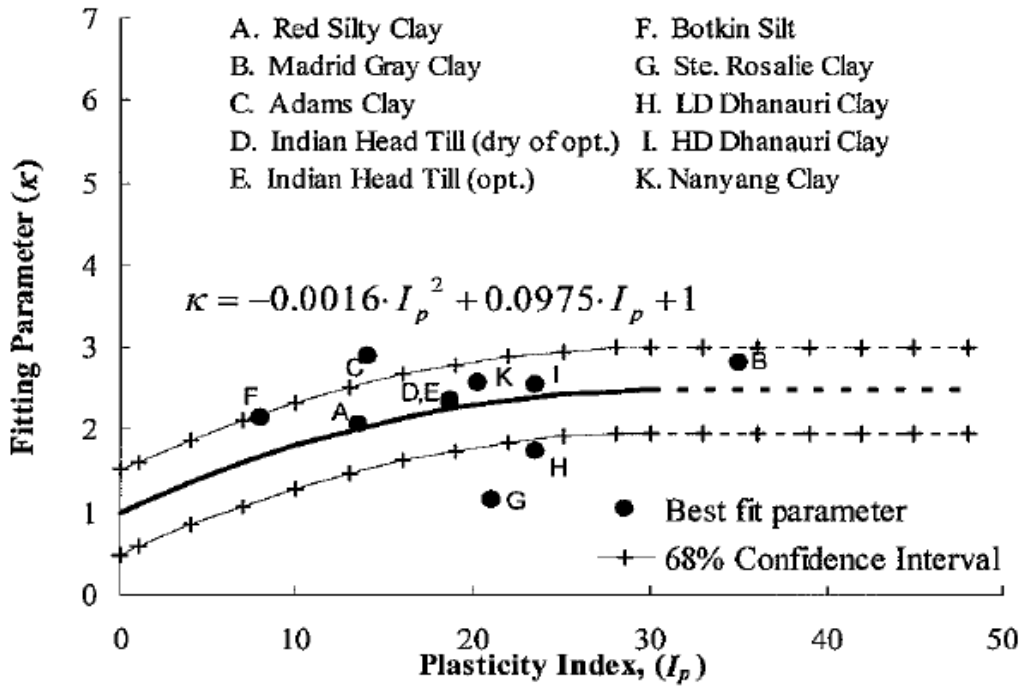

Figure 53 Approximate variation in Kappa with the plasticity of the material (Vanapalli et al., 1994)

The Fredlund and Xing (1994) equation for the soil-water characteristic curve can be used when defining the soil-water characteristic curve.

$$\theta(u_a - u_w) = C(u_a - u_w) \frac{\theta_s}{\left\{ \ln\left[e + \left(\frac{(u_a - u_w)}{a_f} \right)^{n_f} \right] \right\}^{m_f}} \qquad \textbf{[136]}$$

where:

a_f = material parameters which is primarily a function of the air entry value of the material,

n_f = material parameter which is primarily a function of the rate that water can be extracted from the material once the entry value is exceeded,

m_f = material parameter, which is primarily a function of residual water content, and

$C(u_a - u_w)$ = Correction which ensures that the soil-water characteristic curve passes Through 1,000,000 kPa of suction at zero water content.

$$c(u_a - u_w) = 1 - \frac{\ln\left(1 + \frac{(u_a - u_w)}{(u_a - u_w)_r} \right)}{\ln\left(1 + \frac{(1{,}000{,}000)}{(u_a - u_w)_r} \right)} \qquad \textbf{[137]}$$

where:

$(u_a - u_w)_r$ = soil suction at residual conditions.

The soil-water characteristic curve can either be measured in the laboratory or estimated using one of several procedures (Fredlund, 2006). Once the soil-water characteristic curve data is known, the SoilVision Soils knowledge-based software can be used to best-fit the data and obtain the a_f, n_f, and m_f material parameters.

8.20.2.2 Vanapalli Unsaturated Shear Strength Equation

A second nonlinear shear strength equation that can also be used for an unsaturated soil (Vanapalli et al., 1996).

$$\tau = c' + (\sigma_n - u_a)\tan\phi' + (u_a - u_w)\Theta_n \tan\phi' \qquad \textbf{[138]}$$

where:

Θ_n = normalized water content, $\frac{\theta(u_a - u_w) - \theta_r}{\theta_s - \theta_r}$;

(i.e., water content is normalized between the saturated water content and residual water content)

$\theta(u_a - u_w)$ = volumetric water content at any suction,

θ_r = volumetric water content at residual suction conditions, and

θ_s = volumetric water content at saturation.

The above-mentioned dimensionless water content, Θ_d, and normalized water content, Θ_n, can also be written in terms of gravimetric water contents, *w*, or degree of saturation, *S*. All these representations give essentially the same results when volume changes under changing soil suction are small.

The selection of the shear strength equation for the unsaturated soil can be made in the SVSOILS knowledge-based software and the shear strength versus suction can be imported to the software in a tabular form.

8.20.2.3 Vilar Unsaturated Shear Strength Equation

Vilar (1987) proposed method to predict the shear strength of unsaturated soils. The method uses an empirical hyperbolic function that has been used to fit experimental data. The parameters of this function are obtained considering effective shear strength parameters from a saturated soil along with the test results from air-dried samples tested without suction control.

Air dried samples can be, alternatively, replaced by test results of samples tested at suction larger than the maximum suction expected in the problem under consideration. The hyperbolic equation is given as follows:

$$c = c' + \frac{\Psi}{a + b\Psi} \quad \textbf{[139]}$$

where:

c = the total cohesion of the soil,

c' = the effective cohesion of the saturated soil,

a = fitting parameters,

b = fitting parameters, and

Ψ = suction, u_a-u_w,

The fitting parameters (a, b) can be obtained as follows:

$$\left.\frac{dc}{d\Psi}\right|_{\Psi \to 0} = \frac{1}{a} = \tan\phi' \quad \textbf{[140]}$$

$$\lim_{\Psi \to \infty} c = c_{ult} = c' + \frac{1}{b} \quad \textbf{[141]}$$

where:

c_{ult} = ultimate shear strength of the air-dried soil.

8.20.2.4 Khalili Unsaturated Shear Strength Equation

Khalili and Khabbaz (1998) assumed that the soil behaved as a saturated soil as long as the matric suction was less than the air-entry value of the soil.

$$\tau = c' + (\sigma_n - u_a)\tan\phi' + (u_a - u_w)\tan\phi' \quad \textbf{[142]}$$

Once the air-entry value was exceeded, the suction component of shear strength was reduced by multiplying soil suction by the variable λ', and the shear strength equation was written as follows.

$$\tau = c' + (\sigma - u_a)\tan\phi' + (u_a - u_w)[\lambda']\tan\phi' \quad \textbf{[143]}$$

The parameter λ′ was defined as follows:

$$\lambda' = \left\{ \frac{(u_a - u_w)}{(u_a - u_w)_b} \right\}^{-0.55} \quad \textbf{[144]}$$

8.20.2.5 Bao Unsaturated Shear Strength Equation

Bao et al., (1998) assumed that the soil behaved as a saturated soil as long as the matric suction was less than the air-entry value of the soil.

$$\tau = c' + (\sigma_n - u_a)\tan\phi' + (u_a - u_w)\tan\phi' \quad \textbf{[145]}$$

Once the air-entry value was exceeded, the suction component of shear strength was reduced by multiplying soil suction by the variable, ζ, as shown in the following equation.

$$\tau = c' + (\sigma - u_a)\tan\phi' + (u_a - u_w)[\zeta]\tan\phi' \quad \textbf{[146]}$$

The parameter ζ. was defined by the following equation:

$$\zeta = \left[\frac{\log(u_a - u_w)_r - \log(u_a - u_w)}{\log(u_a - u_w)_r - \log(u_a - u_w)_b} \right] \quad \textbf{[147]}$$

8.21 BARTON-BANDIS STRENGTH MODEL

Barton and Choubey (1977) developed the non-linear strength criterion for rock joints. The Barton-Bandis strength model could be written as:

$$\tau = \sigma_n tan\left(\phi_r + JRC log_{10}\left(\frac{JCS}{\sigma_n}\right)\right) \quad \textbf{[148]}$$

where:

Φ_r = the residual friction angle of the failure surface,

JRC = the joint roughness coefficient,

JCS = the joint wall compressive strength,

σ_n = effective normal stress.

Detailed discussion on how to get the model parameters can be found in the reference Barton and Choubey (1977).

8.22 SHANSEP STRENGTH MODEL

Ladd and Foote (1974) developed the SHANSEP (Stress History and Normalized Soil Engineering Properties) to model undrained shear strength of clay soils. The shear strength function for the model can be written as:

$$\tau = C_{min} + k\,\sigma_v'(OCR)^m$$

where:

τ - Undrained Shear Strength

C_{min} - Minimum Undrained Shear Strength

K – Normally Consolidated Ratio

σ_v' - Vertical Effective Stress

OCR – Over Consolidated Ratio

m – Exponent, typically value is between 0.75 and 1

Detailed discussion on how to get the model parameters can be found in the reference Ladd and Foote (1974).

9 INITIAL CONDITIONS

This section provides detail on the use of pore-water pressures and stresses in the software.

9.1 PORE-WATER PRESSURE (PWP)

Pore-water pressures may be specified through a variety of different methods in the software including:

- Water Surfaces (Water Table and Piezometric Lines)
- Ru Coefficients (per material)
- Discrete points
- Groundwater file

Note that to represent a water table above the ground surface, which applies a hydrostatic load, all methods except piezometric lines can be used. Each of the above methods is described theoretically in the following sections.

In addition, B-bar parameters can be set to consider excess pore-water pressure.

9.1.1 Water Surfaces

Water surfaces may be defined as either:

- Water tables
- Piezometric lines

The specific application of each of these methods is described in the following sections.

9.1.1.1 Water Table

1) Submerged Slope defined by a Water table

An important feature of the water table is the automatic creation of the submerged slope (or also known as ponded slope) if the Water table is drawn above the ground surface. The region of submerged water is automatically filled with a blue hatch pattern as illustrated as shown in Figure 54.

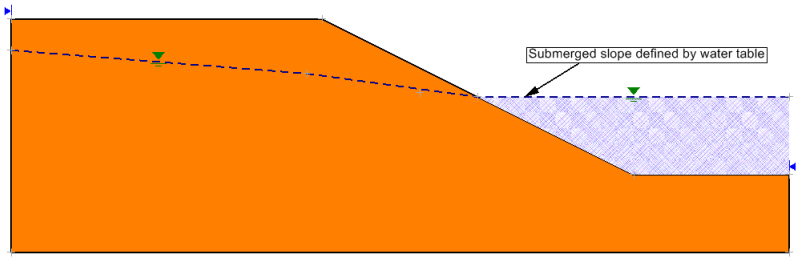

Figure 54 Submerged slope automatically created by Water Table

In this particular case where the water table daylights above the ground surface then it should be noted that the water acts like a distributed load on the ground surface. The loading of the water on the ground surface is AUTOMATICALLY handled in the software solver calculations and does not require further actions from the model designer. For example, an extra distributed load does NOT need to be added to the upper ground surface.

The weight of water slices above slip surface slices is automatically added to the calculations. This concept can be seen in the visual presentation of the results when a water table is included in an analysis (Figure 55).

It is worth noting that piezometric surfaces are NOT considered in this manner.

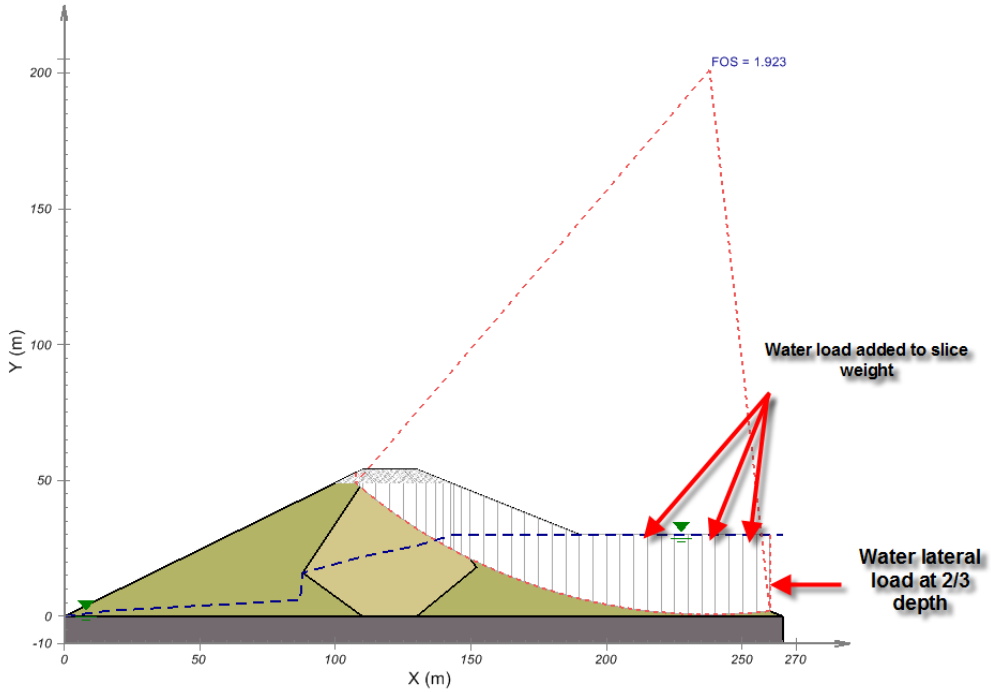

Figure 55 Illustration of calculation properties with daylighting water tables

Other slope stability software programs apply a distributed pressure along the upper boundary of the ground. This alternative approach to this problem has been historically shown to produce identical results. It should be noted that the software method of adding water calculations into slice weights is more robust and generally applicable for complex geometries than any other methods.

2) Unit Weight above and below the Water Table
If Water Table is selected to define the pore-water pressures, then the User can define different unit weight for the material above and below the Water Table.

In other cases, only a single unit weight can be defined for one material.

3) Comparison between Water Table and Piezometric Line
The method of pore pressure calculation is the same for a water table or a piezometric line. The significant differences between the two procedures are as follows:

a. A water table can be used to define submerged slope when the water table is above the ground surface while a piezometric cannot be used for this purpose.
b. A water table can be used to define different unit weight for a material above and below the water table while this cannot be done when using a piezometric line.
c. Only one water table is allowed for a model but multiple piezometric lines can be defined for a model with the User assigning a piezometric line to each material.

9.1.1.2 Piezometric line

One of the common historical procedures for defining pore-water pressures is through the use of piezometric lines. The pore-water pressure at the base of a slice is then evaluated by multiplying the vertical distance from the center of the base of a slice to the piezometric line by the unit weight of the water as shown in Figure 56. For increased accuracy in the designation of pore-water pressures, it is recommended that other procedures be used for the computation of pore-water pressures (e.g., designation of a grid of pore-water pressure values). It must be understood that a piezometric line procedure is approximate due to the fundamental difference between a piezometric line and a phreatic line.

The phreatic line is generally input as a piezometric line. However, the true piezometric line changes for every slip surface analyzed. However, it is easy to simply use the phreatic line as an approximate piezometric line for all slip surfaces analyzed. Consequently, this is often done in slope stability analysis.

The difference between a piezometric line and the water table was described in the previous section.

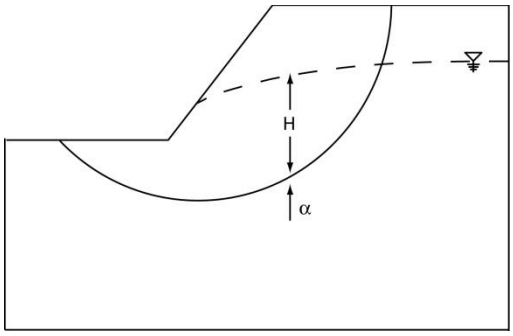

Figure 56 Pore-water pressure from a piezometric line

9.1.2 Ru Coefficient

The pore pressure coefficient, r_u, is the ratio between the pore-water pressure and the overburden vertical stress. The pore pressure coefficient, r_u, is defined as:

$$r_u = \frac{u_w}{\gamma_t h} \quad \textbf{[149]}$$

where:

u_w = pore-water pressure,

γ_t = total unit weight (γh is the total overburden pressure), and

h = distance from the base of the slip surface to the ground surface.

There may be one or more soil layers that induce pore-water pressure which may be applied at the base of the slice. If there are several soil layers, then the unit weights from each soil layer will be summed as in the following equation:

$$r_u = \frac{u_w}{\sum(\gamma_t h)} \quad \textbf{[150]}$$

The pore-water pressure can be computed as follows once the pore pressure coefficient is known.

$$u_w = r_u \gamma_t h \quad \textbf{[151]}$$

The pore-water pressure computed when using r_u is based on the entire weight of the overburden materials.

9.1.3 Discrete Points

Pore-water pressures can be measured from field observations such as piezometric measurements or computed using an independent analysis from a saturated-unsaturated seepage program such as FEM Groundwater. A discrete distribution of pore-water pressure values can be input as shown in Figure 57.

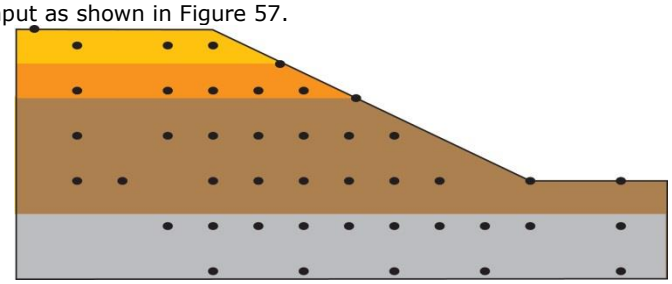

Figure 57 Pore-water pressures designated at discrete points

Based on the discrete points where pore-water pressures, u_w, (or pore-water heads) can be designated as pore-water pressures (heads) arbitrary points within the slope. These pore-water pressures can be determined using an independent numerical method. The software makes use of a spline interpretation technique (see Appendix 18.1.1) to calculate the pore-water pressure at a particular point.

The number of data points used for the Spline interpretation technique needs not be excessively large and the data points can be quite sparsely spread across the slope. It should be noted that the pore-water pressures need to be computed only at the

base of slices along the slip surface. Therefore, the data points should be located around the zone of the potential slip surfaces. A further refinement of the use of pore-water pressures on a designated grid is presented in Section 6.7.

In this case where the water table daylights above the ground surface then it should be noted that the water acts like a distributed load on the ground surface, as described in the Water Surfaces section above.

9.1.3.1 Discrete Point Types

There are four types of Discrete Points available in the software:

1. Discrete (Pore Pressure) Points,
2. Discrete (Pressure Head) Points,
3. Discrete (Total Head) Points, and
4. Discrete (Suction) Points.

9.1.3.2 Discrete Points Interpolation Method

The Spline function method is available in the current version of the software. The details of Spline Method are described in Appendix 18.1.1.

9.1.4 Groundwater File

When the Groundwater File Option is selected for the pore-water pressure method, a Groundwater pore-water pressure file must be defined. The format for the PWP file is PLAXIS LE DAT (.dat), which is an output file from the PLAXIS LE - Groundwater software.

The pore-water pressures can be calculated from a specified file using the interpolation technique as described in Appendix 18.2.

9.1.5 Stress File

When the Stress File Option is selected, a Stress file must be defined. The format of the Stress file is PLAXIS LE DAT (.dat), which is an output file from the Stress software.

The initial stresses can be calculated from a specified transfer File using the interpolation technique as described in Appendix 18.2.

9.1.6 Allow Per Material Ru Coefficients to Override Selected PWP Method

When defining properties for a specific material the Ru Coefficient is available only when the "Pore Water Pressure Method" is selected as Ru Coefficient or "Allow Per Material Ru Coefficients to Override Selected PWP Method" checkbox in the PWP Tab of Initial Conditions Dialog is selected.

9.1.7 B-Bar Coefficient

If the Allow Application of B-bar for Excess Pore-Water Pressure checkbox is selected, the incremental / excess pore water pressure calculated using the B-Bar coefficient will be added into the initial pore-water pressure value calculated when using the main pore-water pressure method for a total value of pore-water pressure.

The B-Bar pore pressure coefficient, $\overline{B}$, is the ratio between the pore-water pressure and the major principal stress. The B-Bar pore pressure coefficient, $\overline{B}$, is defined as:

$$\overline{B} = \frac{\Delta u_w}{\Delta \sigma_1} \qquad \textbf{[152]}$$

or

$$\Delta u_w = \overline{B} \Delta \sigma_1 \qquad \textbf{[153]}$$

where:

Δu_w = incremental pore-water pressure, and

$\Delta \sigma 1$ = incremental principal stress.

The software assumes that the vertical stress is the principal stress. However, this assumption may not be sufficiently accurate. The incremental major principal stress used for pore-water pressure calculations is only used for the sum of the material layers where the B-Bar option is checked. In other words, the weight of material layers is not included when the B-Bar option is not

checked. This characteristic allows for a differentiation between the use of the B-Bar coefficient and the r_u coefficient (Figure 58).

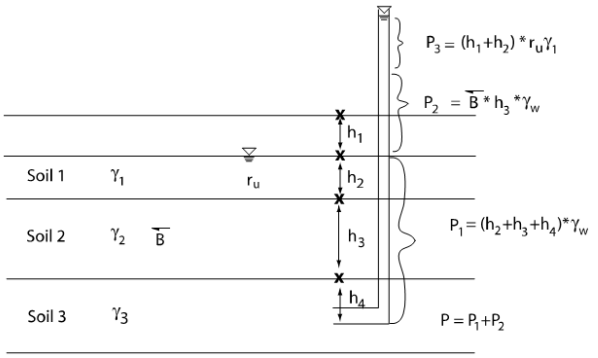

Figure 58 Combination of r_u/B-Bar with piezometric pore-water pressure.

9.2 SUCTION AND NEGATIVE PORE-WATER PRESSURE

Matric suctions, (u_a- u_w), in an unsaturated soil (i.e., above the water table), increases the shear strength of the material. In most cases, the unsaturated soil zone is assumed to be open to the atmosphere and, therefore, the pore-air pressure is set equal to zero. The pore-water pressure is negative relative to atmosphere conditions.

The effect of matric suction on the shear strength of the material is taken into consideration through the use of the angle, ϕ^b, in the case where the shear strength is assumed to be linear with respect to change in matric suction. The angle, ϕ^b, can also be nonlinear and in this case the shear strength of the unsaturated soil is written in terms of the soil-water characteristic curve.

Negative pore-water pressures can be computed in the software in terms of the vertical distance between the slice base and piezometric line. This procedure is like the computation for positive pore-water pressures, where the distance is below the water table. The pore-water pressure is a negative value when the slice base is above the piezometric line. Negative pore-water pressures can also be computed through the use of an interpolation technique on a grid of designated values. For example, the pore-water pressures can have been computed using Groundwater software and imported to the software.

9.2.1 Water Table Suction

When the water table suction is selected as the pore-water pressure method, three suction options are available as described as follows:

1. No Maximum Value.

   In this option, the suction ($u_a - u_w$), can be computed from a water table.

$$u_w = \rho * (y - y_0) \quad \textbf{[154]}$$

where:

u_a = pore-air pressure *(F/L²)*

u_w = pore-water pressure *(F/L²)*

ρ = unit weight of water *(F/L³)*

y = *y*-coordination at the point to be calculated *(L)*

y_0 =*y*-coordinate with zero pore-water pressure *(L)*

2. Constant Above Maximum.

   If the suction exceeds the maximum value specified by the user, the suction will keep a constant specified value.

3. Zero Above Maximum.

   If the suction exceeds the maximum value specified by user, the suction will be set at a constant specified value of zero.

9.3 STRESSES FROM STRESS

If the Stress-Based Limit Equilibrium methods such as Kulhawy method or SAFE-DP method is used a stress file in the PLAXIS LE DAT File format (.dat) is necessary.

9.3.1 Gridlines for Dynamic Programming Method

If the Dynamic Programming Search Method is used. The Gridlines in *x* and *y* direction are specified for the final purpose. The default value is 30 in *x*-direction and 120 in *y* direction.

NOTE:

For better performance, it is recommended that the Gridline number in *y*-direction be 4 times of that in *x*-direction (e.g., 30/120). However, it should also be noted that this recommendation is not applicable to all cases.

10 SPECTRAL PSEUDO-STATIC LOADING

The conventional pseudo-static method is considered the simplest approach to evaluate the stability of earth-slopes against seismic loading by using constant seismic coefficient(s). However, it has some deficiencies: it ignores the earthquake effect on shear strength and, in addition, masks the dynamic aspect of the problem (site effect, degradation of the modulus, synchronization of the movement, etc.) (Ghobrial et al. 2015). The spectral pseudo-static method is a more effective analysis method that maintains the benefits of the pseudo-static method and replaces the conventional constant seismic coefficient with a variable coefficient. The spectral pseudo-static approach is a function of the geometry of the slope and the thickness of the soil deposit as well as the seismic characteristics and the soil properties. The magnitude of horizontal seismic loading coefficient $K_h(z)$ can be expressed as:

$$k_h(z) = k_{ho}[1 + a(z / H_t)^b] \quad \textbf{[155]}$$

where:

k_{ho} = seismic coefficient at the bedrock (initial value),

H_t = total height of the slope and the thickness of the deposit,

a = spectral pseudo-static coefficient,

b = spectral pseudo-static coefficient, and

z = the variation of the height measured from the presumed bedrock.

11 SUPPORTS

This section outlines the theoretical basis for utilizing supports in a slope stability analysis. The details of the support implementation may be found in the User Manual. The sections immediately following cover the theory of each of the types of supports which may be specified.

Support objects apply a force to slices at the point of intersection with a particular slice. The orientation of the applied force for each type of support is summarized in Table 1.

Table 1 Orientation of forces with various applied supports

Support	***Force Orientation***
End Anchored	Parallel to support
Geotextile	Parallel to support
	Tangent to slip surface
	Bisector of parallel and tangent
	User-defined angle
Grouted Tieback	Parallel to support
Grouted Tieback with Friction	Parallel to support
Micro-Pile	Tangent to slip surface
Soil Nail	Parallel to support
Soil Nail - Hong Kong Practice	Parallel to support
User-Defined	Parallel to support
	Tangent to slip surface
	Bisector of parallel and tangent
	User-defined angle

11.1 END ANCHORED

The End Anchored support type is applied to simple end anchored support systems e.g., end anchored rock bolts or anchors.

The force of an End Anchored support is constant regardless of where a slip surface intersects the body of the support. The applied force is given as follows:

$$F = \frac{C}{S} \qquad \textbf{[156]}$$

where:

F = Applied force (per unit width of slope),

C = Tensile capacity, and

S = Out-of-Plane spacing.

The force diagram is a horizontal line as shown in Figure 59.

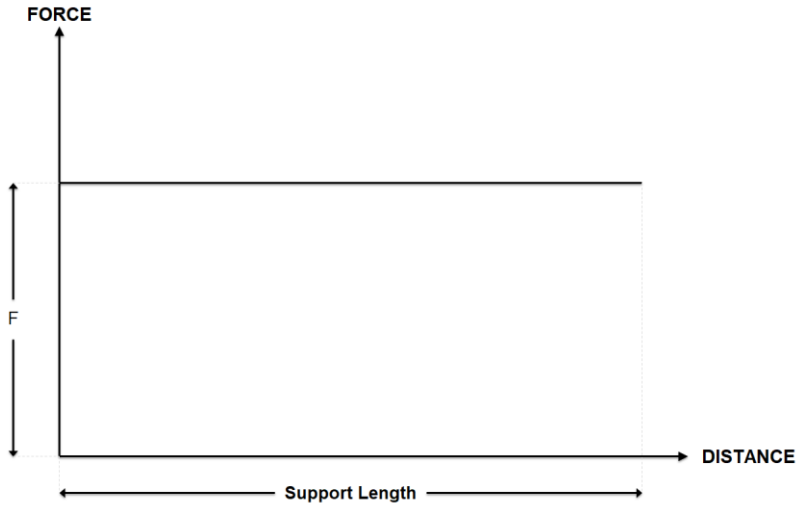

Figure 59 Force diagram for End Anchored support

11.2 GEOTEXTILE

The *Geotextile* support type can be used to simulate all forms of flexible planar reinforcement such as textile, fabrics, meshes, grids, strips, membranes, synthetics steel strip, etc.

The *Strip Coverage* refers to the spacing of the strips in the Out-of-Plane direction (i.e., along the slope). As shown in the following figure:

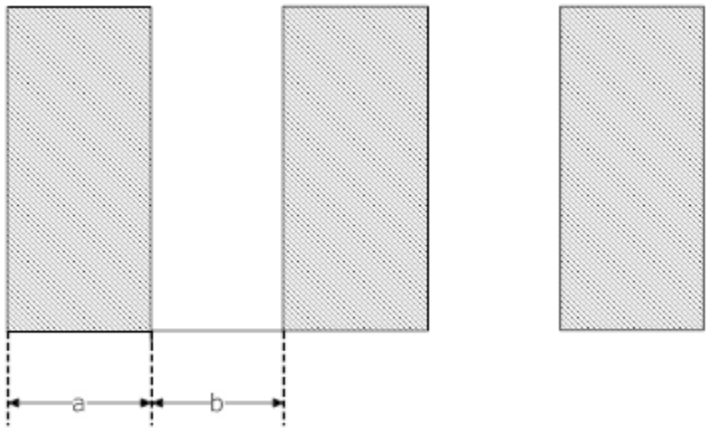

Figure 60 Plan view of geotextile placement

The Strip Coverage can be evaluated as follows:

$$Strip\ \text{cov}erage = \left[\frac{a}{a+b}\right] \times 100 \qquad \textbf{[157]}$$

where:

a = the width of the geotextile,

b = the spacing between geotextiles.

11.2.1 Shear Strength Models

A variety of shear strength soil models may be specified for geomembranes. The Linear and Hyperbolic models are supported for the software and are described below.

Linear Shear Strength

Linear shear strength is determined from the Mohr-Coulomb relationship and can be expressed as follows:

$$\tau = a + \sigma_n \tan\phi \quad \textbf{[158]}$$

where:

a = interface adhesion,

ϕ = interface friction angle, and

σ_n = effective normal stress.

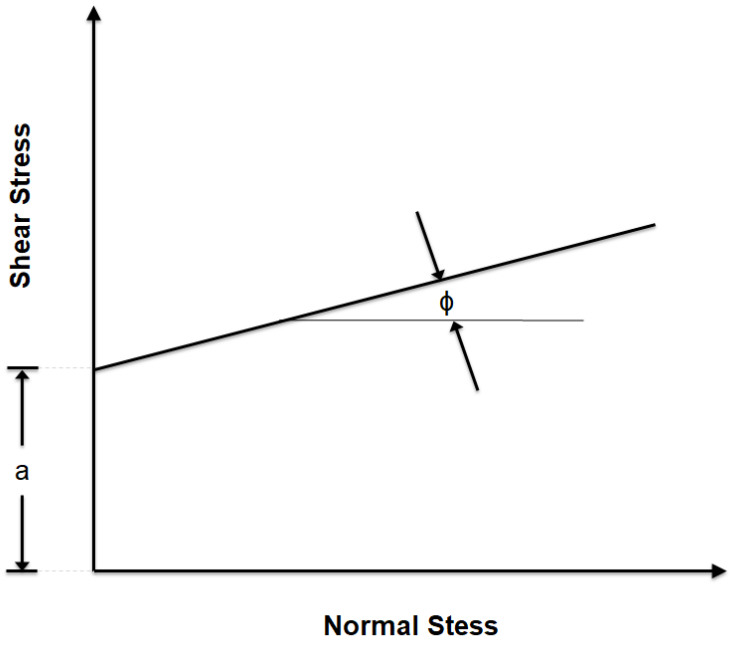

Figure 61 Linear Mohr-Coulomb shear strength envelope

Hyperbolic Shear Strength

Hyperbolic Shear Strength is determined by the following equation:

$$\tau = \frac{a_\infty \sigma_n \tan\phi_0}{a_\infty + \sigma_n \tan\phi_0} \quad \textbf{[159]}$$

where:

a_∞ = Adhesion, or the shear strength when $\sigma_n=\infty$,

ϕ_0 = Friction angle when $\sigma_n=0$,

σ_n = effective normal stress.

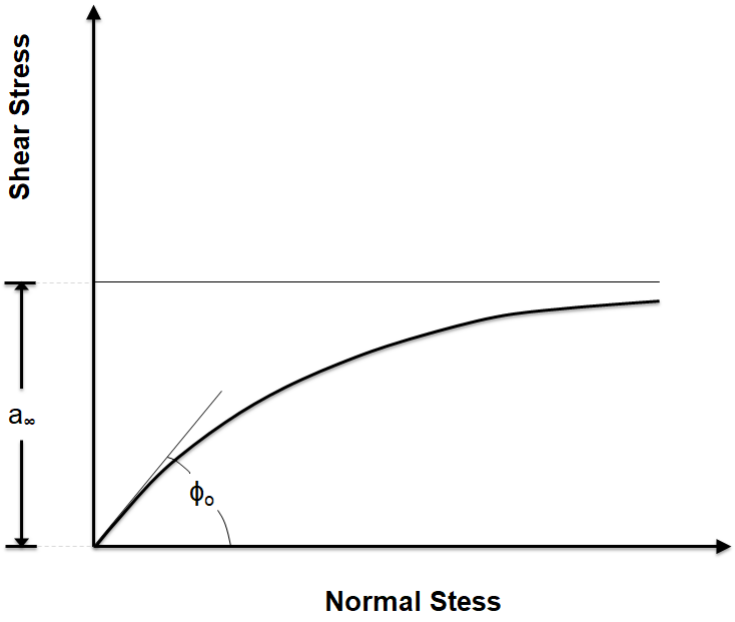

Figure 62 Hyperbolic shear strength envelope

Normal Stress

1. The normal stress used in shear strength Equations [158] and [159] varies along the length of a Geotextile.
2. When pore ware pressure is involved, the normal stress is then the effective normal stress.
3. In most cases, geotextiles are placed horizontally; therefore, the normal stress is equal to the vertical stress. In cases where geotextiles are not placed horizontally, hydrostatic stress is assumed, so again, the normal stress is equal to the vertical stress.
4. Since the normal stress varies along the length of a Geotextile, the vertical stress is calculated as follows:
   - Each Geotextile support element is first subdivided into 50 equal segments.
   - For each subdivision along the geotextile, the vertical stress is calculated from the overburden load, as well as any vertical component of external loading, which acts on the slope above the geotextile.

11.2.2 Geotextile Support Theory

The Geotextile properties are used to determine a Force Diagram for a Geotextile, as described as follows.
Consider a Geotextile, which intersects a slip surface as shown below.

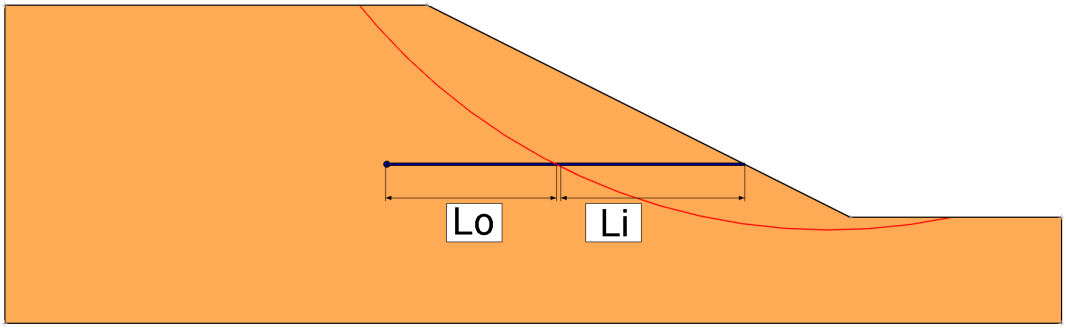

Figure 63 Geotextile

where:

Li = length of geotextile within sliding mass,

Lo = length of geotextile embedded behind slip surface.

Geotextile parameters

A = Strip Coverage (%),

ϕ = Interface Friction Angle (deg),

T = Tensile Strength (force / width).

Three failure modes are possible for Geotextile support depending on the Anchorage option selected.

1. Tensile (always possible, for all Anchorage settings),
2. Pullout (only if Anchorage is None or Slope Face), and
3. Stripping (only if Anchorage is None or Embedded End).

Tensile Force
Tensile failure of a geotextile is always a possible failure mode, regardless of the Anchorage type. If the Anchorage option is set to Both Ends, then tensile failure will be the only failure for the geotextile. The mobilized maximum tensile load (per unit width of slope) at any point along the geotextile is expressed as:

$$F1 = \frac{TA}{100} \qquad \textbf{[160]}$$

Pullout
For a geotextile, pullout can only occur if the embedded end is **not** anchored (i.e., Anchorage = Slope Face or Anchorage = None). The mobilized maximum pullout force (per unit width of slope) is given by:

$$F2 = \frac{2LoA\tau}{100} \qquad \textbf{[161]}$$

where:

τ is given by Equation [158] when the strength model is Linear or Equation [159]] when the strength model is Hyperbolic.

The factor "2" in the equation means both sides of the Geotextile are contributing to the calculation of the shear strength of Geotextile/Soil interface.

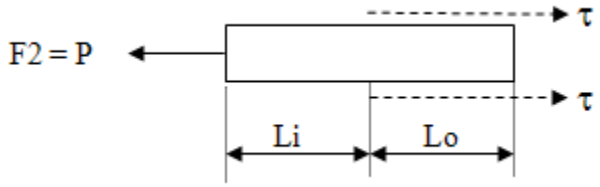

Figure 64 Pullout force in Geotextile

NOTE:

a. Equation [160] is applicable to those support types with a 100% contact area with the soil such as geo-textiles, geo-fabrics, metal strips, etc. In other words, there are no "holes" in the material and the interface between Geotextile and soil is continuous.

b. The "apparent" or "equivalent" shear strength parameters (Adhesion and Friction Angle) should be calculated when Equation [161] is used for Geogrids in which there are "holes".

Stripping
Stripping failure means that the support remains embedded in the slope while the sliding mass strips off the support. Stripping failure is possible only if the geotextile is not anchored to the slope face (i.e., Anchorage = None, Embedded End). The force required for the sliding mass to "strip" off the support, is given by:

$$F3 = \frac{2LiA\tau}{100} \qquad \textbf{[162]}$$

where:

τ is given by Equation [158] when strength model is Linear or Equation [159] when strength model is Hyperbolic.

Force Diagram
At any point along the length of a geotextile, the magnitude of the force, which will be applied to a slip surface that intersects the Geotextile, is given by the minimum of the Tensile, Pullout (if applicable), and Stripping (if applicable) forces. Different Anchorages use different formula:

Anchorage	Applied Force
None	MIN (F1, F2, F3)
Slope Face	MIN (F1, F2)
Embedded End	MIN (F1, F3)
Both Ends	F1

11.3 GROUTED TIEBACK

The Grouted Tieback support type can be used to model grouted tieback supports and ground anchors which may have a variable grouted length.

The Grouted Tieback is different from The Grouted Tieback with Friction only in that the Grouted Tieback support type does not consider stress dependent (i.e., frictional) strength of the soil / grout interface while the later does.

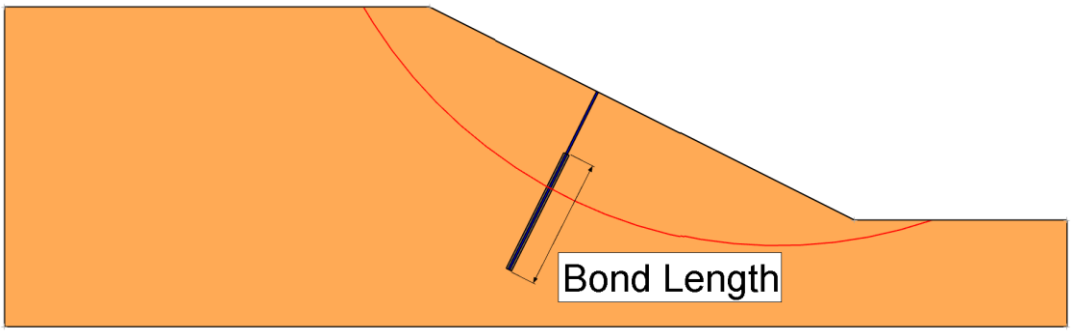

Figure 65 Bond Length of Grouted Tieback

The Grouted Tieback properties are used to determine a Force Diagram for a Grouted Tieback, as described as follows. Consider a Grouted Tieback which intersects a slip surface as shown in Figure 66.

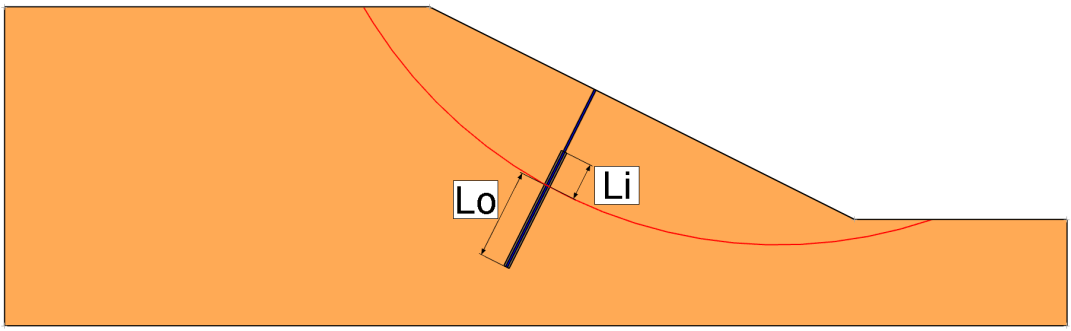

Figure 66 Grouted Tieback

where:

Li = bonded length of tieback within the sliding mass, and

Lo = bonded length of tieback embedded behind slip surface.

Tieback Parameters:

B = Bond Strength (force / unit length of bond),

S = Out-of-Plane Spacing,

T = Tensile Capacity (force), and

P = Plate Capacity (force).

For a Grouted Tieback, at any point along the length of the tieback, there are 3 potential failures:

1. Pullout (Slope failure occurs, and tieback is pulled out of the slope),
2. Tensile Failure (Axial force exceed maximum axial capacity of the tieback), and
3. Stripping (Slope failure occurs, but tieback remains embedded in the slope).

The mobilized maximum force (per unit width of slope) for each potential failure is given by the following equations:

Tensile Force

$$F1 = \frac{T}{S} \quad \textbf{[163]}$$

Pullout Force

$$F2 = \frac{BLo}{S} \quad \textbf{[164]}$$

Stripping Force

$$F3 = \frac{P + BLi}{S} \quad \textbf{[165]}$$

Force Diagram

At any point along the length of a Tieback, the magnitude of the force, which will be applied to a slip surface that intersects the Tieback, is given by the minimum of the Tensile, Pullout (if applicable), and Stripping (if applicable) forces. That is,

$$Applied \quad Force = MIN(F1, F2, F3) \quad \textbf{[166]}$$

A Force diagram for a Grouted Tieback, which includes all three failures, is shown in Figure 67.

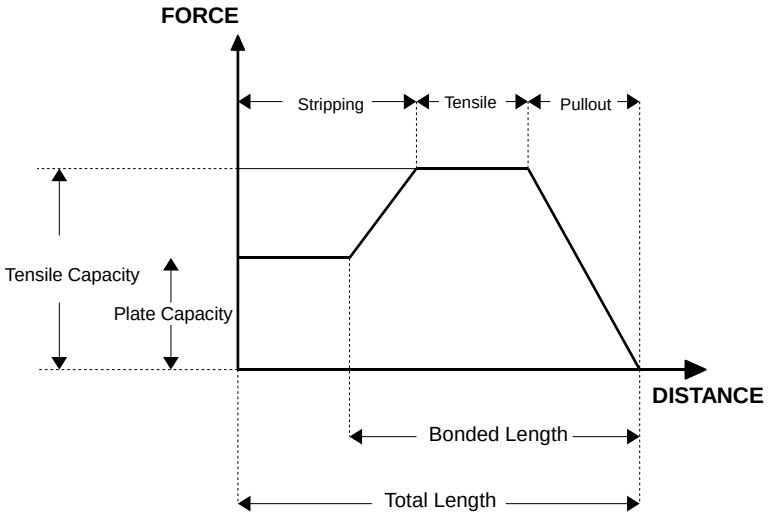

Figure 67 A typical force diagram including three types of failure

It should be noted that:

- Stripping failure will occur only when the Plate Capacity exceeds the Tensile Capacity.

- If the tieback Bond Strength is specified as Material Dependent, then the Pullout Force and Stripping Force are determined by the bond strength of each segment of the bonded length, which passes through different materials.

11.4 GROUTED TIEBACK WITH FRICTION

The Grouted Tieback with Friction is different from Grouted Tieback only in that the Grouted Tieback with Friction support allows the user to consider the frictional strength (stress dependent) of the soil / grout interface.

The Grouted Tieback with Friction properties are used to determine a Force Diagram for a Grouted Tieback with Friction, as described as follows.

Consider a Grouted Tieback with Friction, which intersects a slip surface as shown in Figure 68.

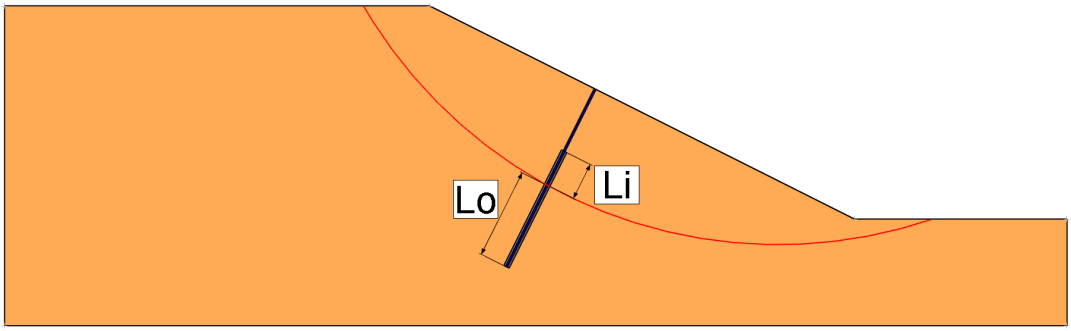

Figure 68 Grouted Tieback with Friction

where:

Li = bonded length of tieback within sliding mass, and

Lo = bonded length of tieback embedded behind slip surface.

Tieback with Friction Parameters:

S = Out-of-Plane Spacing,

T = Tensile Capacity (force),

P = Plate Capacity (force),

a = Interface Adhesion (force / area),

ϕ = Interface Friction Angle (deg), and

D = Grout Diameter.

For a Grouted Tieback with Friction, at any point along the length of the tieback, there are 3 potential failures:

1. Pullout (Slope failure occurs, and tieback is pulled out of the slope),
2. Tensile Failure (Axial force exceed maximum axial capacity of the tieback), and
3. Stripping (Slope failure occurs, but tieback remains embedded in slope).

The mobilized maximum force (per unit width of slope) for each potential failure is given by the following equations:

Tensile Force:

$$F1 = \frac{T}{S} \quad \textbf{[167]}$$

Pullout Force:

$$F2 = \frac{\pi D Lo \tau}{S} \quad \textbf{[168]}$$

Stripping Force:

$$F3 = \frac{P + \pi DLi\tau}{S} \quad \textbf{[169]}$$

The shear strength along the grouted length is calculated from the Adhesion, Friction Angle and Shear Strength Model.

For Linear Shear Strength Model

$$\tau = a + \sigma_n \tan\phi \quad \textbf{[170]}$$

For Hyperbolic Shear Strength Model

$$\tau = \frac{a_\infty \sigma_n \tan\phi_o}{a_\infty + \sigma_n \tan\phi_o} \quad \textbf{[171]}$$

For detailed description of the two equations, see the Geotextile Support type.

Force Diagram
At any point along the length of a Tieback, the magnitude of the force, which will be applied to a slip surface that intersects the Tieback, is given by the minimum of the Tensile, Pullout (if applicable), and Stripping (if applicable) forces. That is:

$$Applied\ Force = MIN(F1, F2, F3) \quad \textbf{[172]}$$

A Force diagram for a Grouted Tieback, which includes all three failures, is shown as follows:

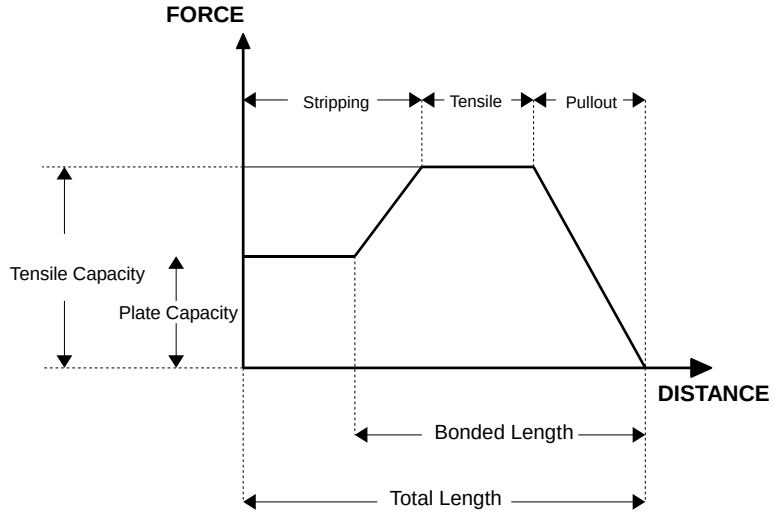

Figure 69 A typical force diagram including three types of failure

It should be noted that:

1. The stripping failure will occur only when the Plate Capacity exceeds the Tensile Capacity.

2. If the tieback Bond Strength is specified as Material Dependent, then the Pullout Force and Stripping Force are determined by the bond strength of each segment of the bonded length, which passes through different materials.

11.5 MICRO-PILE

The Micro-Pile support can be used to simulate a micro pile or pile type of support. The Micro-Pile support is different from other types of support. The characteristics of the Micro-Pile support are:

1. Resistance is assumed to be transverse to the support direction, rather than parallel to the support direction. Therefore, only shear failure happens transversely through the pile.

2. Tensile, pullout or stripping failure are potential failure mechanisms for the Micro-Pile support type.

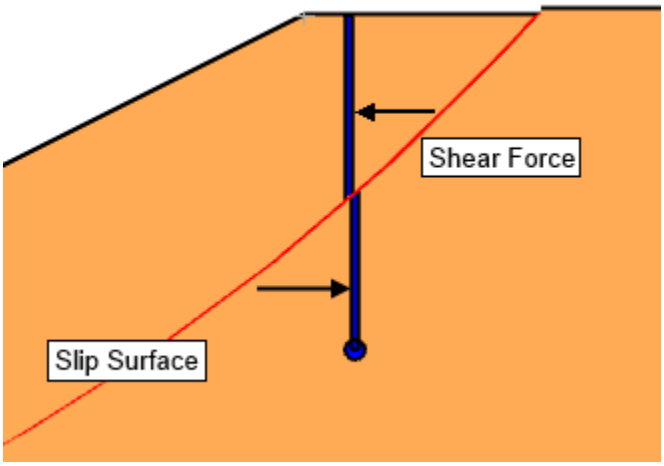

Figure 70 A typical failure pattern of Micro-pile

.

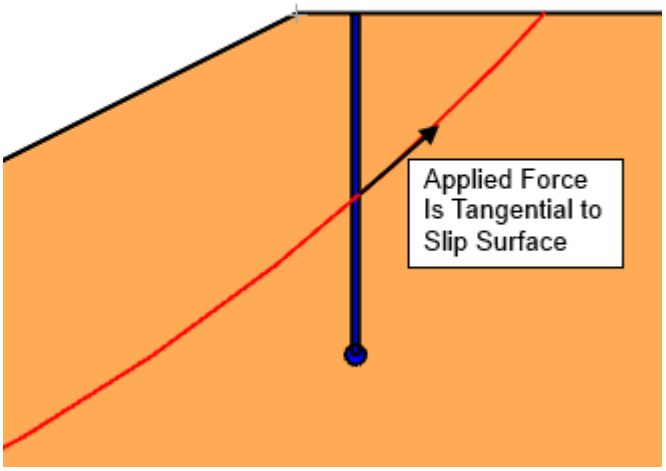

Figure 71 Applied Force Orientation for Micro-Pile support type

Applied Load
The applied load is obtained as follows:

$$F = \frac{P}{S} \quad \textbf{[173]}$$

where:

F = Applied load (per unit width of slope),

P = Pile Shear Strength (force),

S = Out-of-Plane Spacing (Length).

Force Diagram
The Force Diagram for a Micro-Pile support type is a horizontal line regardless of where a slip surface intersects the pile.

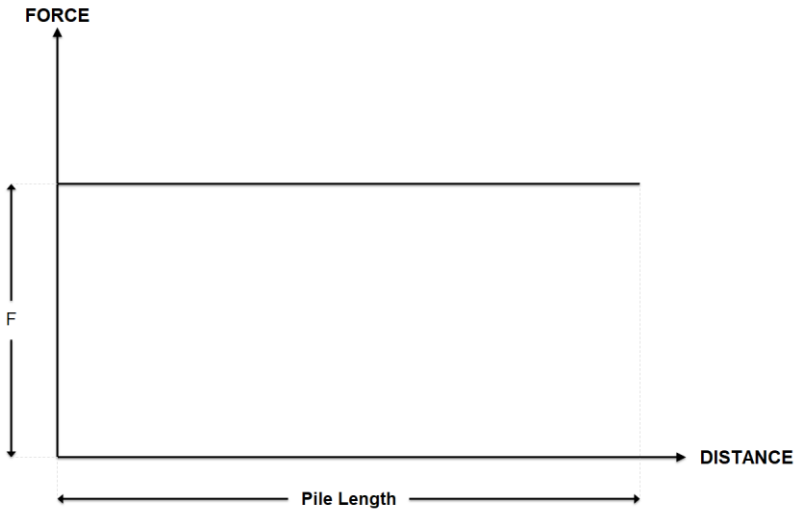

Figure 72 Force Diagram of Micro-Pile

11.6 SOIL NAIL

The Soil Nail is a special case of the Grouted Tieback support type with a Bond Length set to the entire support. Therefore, a Grouted Tieback with Bond Length = 100% would behave exactly the same as a Soil Nail, all other parameters being equal.

The Soil Nail properties are used to determine a Force Diagram for a Soil Nail, as described as follows. Consider a Soil Nail, which intersects a slip surface as shown in Figure 73.

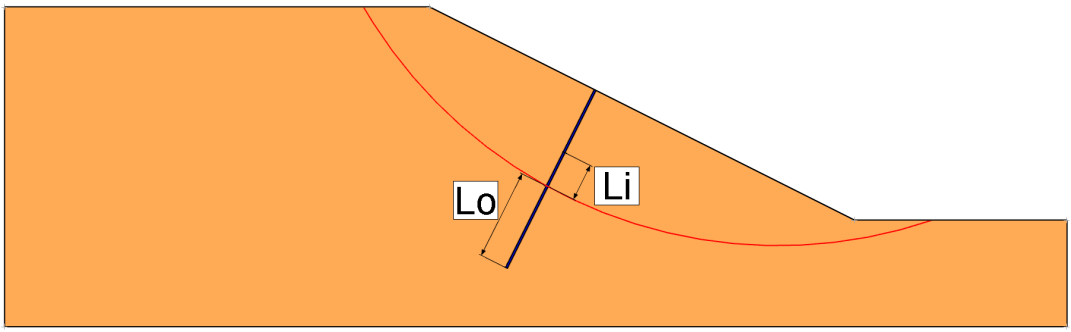

Figure 73 Soil Nail

where:

Li = bonded length of within sliding mass,

Lo = bonded length of tieback embedded behind slip surface.

Tieback Parameters:

B = Bond Strength (force / unit length of bond),

S = Out-of-Plane Spacing,

T = Tensile Capacity (force),

P = Plate Capacity (force).

For a Soil Nail, at any point along the length of the tieback, there are 3 potential failures:

a. Tensile Failure (Axial force exceed maximum axial capacity of the soil nail)
b. Pullout (Slope failure occurs, and soil nail is pulled out of the slope)
c. Stripping (Slope failure occurs, but soil nail remains embedded in slope)

The mobilized maximum force (per unit width of slope) for each potential failure is given by the following equations:

Tensile Force:

$$F1 = \frac{T}{S} \quad \textbf{[174]}$$

Pullout Force:

$$F2 = \frac{BLo}{S} \quad \textbf{[175]}$$

Stripping Force:

$$F3 = \frac{P + BLi}{S} \quad \textbf{[176]}$$

Force Diagram

At any point along the length of a Soil Nail, the magnitude of the force, which will be applied to a slip surface, which intersects the Soil Nail, is given by the minimum of the Tensile, Pullout, and Stripping forces. That is

$$AppliedForce = Min(F1, F2, F3) \quad \textbf{[177]}$$

A Force diagram for a Soil Nail, which includes all three failures, is shown as follows:

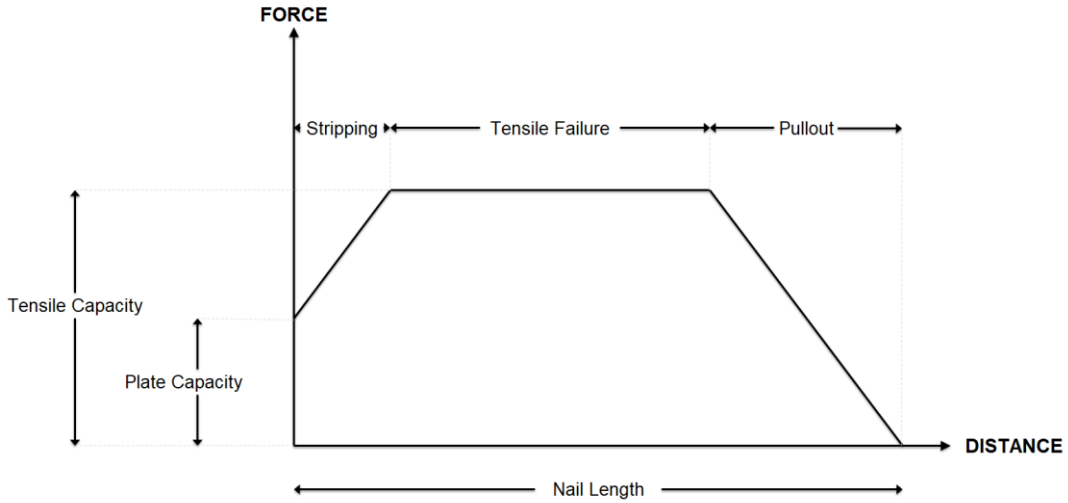

Figure 74 A typical Force Diagram for Soil Nail including three types of failure

It should be noted that:

1. The stripping failure will occur only when the Plate Capacity exceeds the Tensile Capacity,
2. If the tieback Bond Strength is specified as Material Dependent, then the Pullout Force and Stripping Force are determined by the bond strength of each segment of the bonded length, which passes through different materials.

11.7 SOIL NAIL - HONG KONG PRACTICE

Soil Nail-Hong Kong Practice is a special type of Soil Nail. The significant differences are:

1. Plate capacity is not considered in Soil Nail-Hong Kong Practice. In other words, the stripping failure is not considered, or the Plate Capacity is assumed to be higher than Tensile Capacity,
2. The pullout resistance determined by Hong Kong practice is as follows:

$$F1 = \frac{Lo(\pi Dc' + 2D\sigma_v' \tan\phi')}{Fs} \quad \textbf{[178]}$$

where:

$F1$ = Pullout resistance,

Lo = Bonded length of tieback embedded behind slip surface,

D = Bond diameter,

Fs = Factor of safety for Bond,

c' = the effective cohesion (force/area) of the soil through which the Soil Nail passes,

σ_v' = vertical effective stress in the soil calculated at mid-depth of the soil-nail reinforcement in the passive zone, with a maximum value of 300kPa (6266psf),

ϕ' = the effective internal friction angle of the soil through which the Soil Nail passes.

3. The minimum of the allowable tensile capacity and the pullout resistance is used as the effective nail load.

$$AppliedLoad = Min(F1, F2) \quad \textbf{[179]}$$

where:

$F2$ = the allowable tensile capacity.

Force Diagram for Soil Nail-Hong Kong Practice

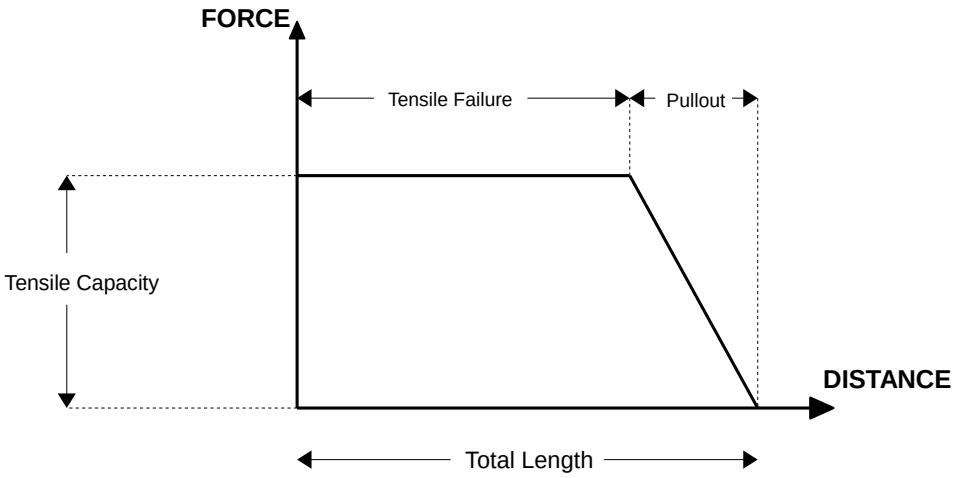

Figure 75 A typical Force Diagram for Soil Nail-Hong Kong Practice

11.8 USER DEFINED

Details of the user-defined support may be found in the User's Manual.

12 RAPID DRAW-DOWN (3-STAGE METHOD)

This section describes the implementation of the 3-stage method (Duncan, 1990) based on the original USACE method. The following section describes the generalized theory of the method.

12.1 GENERAL

Rapid drawdown takes place when water level outside a slope drops so quickly that impermeable soils within the slope do not have sufficient time to dissipate. Due to the removal of stabilizing effect of the water outside the slope, the shear stresses for equilibrium increase. This is a severe condition that can cause failure of slopes that are stable before drawdown.

Usually, the undrained shear strength is applied to those zones with low permeability and drained shear strength is used for the soils with higher permeability.

12.2 EFFECTIVE STRESS METHODS AND TOTAL STRESS METHODS

Slope stability analyses are usually classified into effective stress methods and total stress methods. The significant difference between the two methods is using different shear strength parameters.

The advantage of effective stress analyses is that it is relatively easy to evaluate the required shear strength parameters. The disadvantage of effective stress analysis, however, is that it is difficult to estimate the pore water pressures that will exist within the lower-permeability soils during draw-down.

On the other hand, the total stress method is based on undrained shear strengths in low-permeability zones. The undrained shear strengths are estimated based on the effective stress that exist in the slope prior to drawdown.

It should be noted that the calculation of Pore Water Pressure in low-permeability soils is different from the commonly used method since the water table draws down rapidly and there is not enough time for water to dissipate.

12.3 THREE-STAGE TOTAL STRESS METHOD

Several total stress analysis methods have been proposed for rapid draw-down analysis. These methods include U.S. Army Corps of Engineers (1970) method (USACE method), Lowe-Karafiath (1959) method (L-K method) and Duncan et al. (1990) method.

Duncan et al. (1990) proposed a three-stage total stress method combining the best features of both USACE method and L-K method. The three-stage method accounts for the effect of drainage and the fact that the drained strength may be less than undrained strength. It differs from the USACE method in the way that the undrained strength is evaluated and the way that the drained strength is taken into account. Following L-K's suggestion, the three-stage method is account for the effects of anisotropic consolidation, which result in significant increase of undrained shear strength.

For those materials with high-permeability, effective stresses are used for all the three stages with different pore water pressures based on water levels and seepage conditions. There are no changes for effective shear strength during the calculation.

For those with low permeability, the effective stresses and drained strengths are used for the first stage before drawdown and the total stress and undrained strengths are used for the second stage after drawdown. For the third stage the lower of the drained strengths and undrained strengths is used.

12.3.1 Three-stage procedure

The following sections outline the specific procedure for the 3-stage method.

12.3.1.1 First-stage

The purpose of the first-stage computation is to estimate the effective stresses along the slip surface prior to drawdown. It should be noted that the factor of the safety is not of interest in this stage.

The first-stage computation is used to obtain the shear stress and effective normal stress on the slip surface as follows:

$$\sigma_{fc} = \frac{N}{\Delta\ell} - \mu \qquad \textbf{[180]}$$

where:

N = Normal force acting on the slice,

μ = Pore-water pressure

The corresponding shear stress is obtained as:

$$\tau_{fc} = \frac{1}{F}\left(c^1 + \sigma^1 \tan\phi^1\right) \quad \textbf{[181]}$$

12.3.1.2 Second stage

In the second stage, undrained shear strengths and total stress analysis are applied to low-permeability zones. Undrained shear strengths are estimated for second-stage using the effective stresses calculated from the first-stage. The undrained shear strength is expressed as

$$\tau_{ff} = \frac{\sigma_{1f} - \sigma_{3f}}{2}\cos\phi^1 \quad \textbf{[182]}$$

The undrained shear strength envelope used for second-stage is a bi-linear envelope.

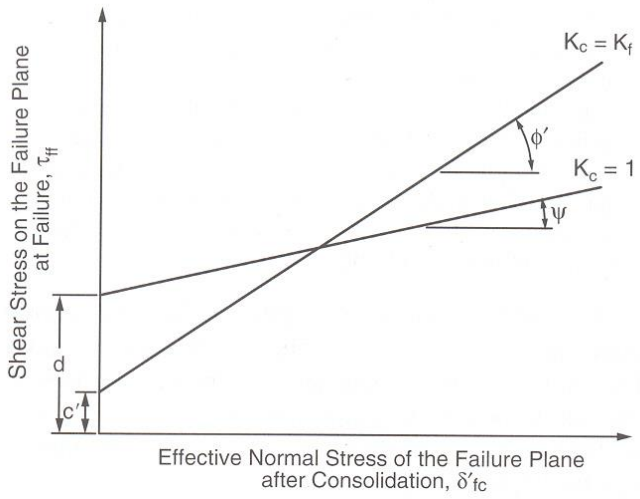

Figure 76 Shear strength envelopes used to define the undrained shear strengths for the second stage of a three-stage analysis (Duncan and Wright, 2005)

where:

c' = effective cohesion

ϕ' = effective friction angle

d = cohesion corresponding to total stress

ϕ^t = friction angle corresponding to total stress

Undrained shear strength then is calculated using Equation [183]:

$$\tau_{ff} = \frac{\left(K_j - K_1\right)\tau_H\left(K_{c=1}\right) + \left(K_1 - 1\right)\tau_H\left(K_c = K_f\right)}{K_f - 1} \quad \textbf{[183]}$$

and $\tau_H\left(K_c = K_f\right)$

$\tau_{ff}\left(K_c = 1\right)$

Undrained strength from two shear strength envelopes is shown in Figure 76.

where:

$$K_c = \frac{\sigma^1 + \tau\left[\left(Sin\phi^1 + 1\right)/\cos\phi^1\right]}{\sigma^1 + \tau\left[\left(\sin\phi^1 - 1\right)/\cos\phi^1\right]} \quad \textbf{[184]}$$

$$K_f = \frac{\left(\sigma^1 + c^1\cos\phi^1\right)\left(1 + \sin\phi^1\right)}{\left(\sigma^1 - c^1\cos\phi^1\right)\left(1 - \sin\phi^1\right)} \quad \textbf{[185]}$$

If a significant effective cohesion (c') exists, the effective minor stress σ'3 implicit in equation [184] and [185] may become negative. Negative effective stresses can be detected by calculating the effective minor principal stresses after consolidation using equations [186] and [187].

$$\sigma_{3c^1} = \sigma_{fc^1} + \tau_{fc}\frac{\sin\phi^1 - 1}{\cos\phi^1} \quad \textbf{[186]}$$

$$\sigma_{3f^1} = \left(\sigma_{fc^1} - c^1\cos\phi^1\right)\frac{1 - \sin\phi^1}{\cos^2\phi^1} \quad \textbf{[187]}$$

Equation [186] is the effective minor principal stress corresponding to the K_c=1 envelope; equation [187] corresponding to the K_c=K_f envelope. If either value from equation [186] and equation [187] is negative, no interpolation in equation [183] is performed and the lower of the K_c=1 and K_c=K_f strength is used for the undrained shear strength in the second-stage stability computations.

12.3.1.3 Third stage

The factor of the safety calculated in the second stage assumes that all the low-permeability materials are undrained during rapid drawdown. The Third-stage calculation is performed to check if the drained shear strength might be lower than the undrained shear strength and thus the factor of safety would be lower if these low-permeability materials where drained rather than undrained.

For the third stage the undrained shear strength used for the second stage computation are compared with the drained strengths for each point along the slip surface. If at any point on the slip surface the drained shear strength is lower than the undrained shear strength, an additional slope stability analysis is performed. If, however, the estimated drained strengths are all higher than the undrained shear strength used for second stage calculation, no additional computations are performed and the FOS from second-stage is the final FOS for rapid drawdown.

13 PROBABILISTIC

The software employs an efficient probabilistic methodology for reliability-based slope analysis and sensitivity analysis. Probabilities are considered using the Alternative Point Estimate Method and the comprehensive analysis framework that were proposed by Gitirana Jr. (2005).

Uncertainties associated with input variables, such as shear strength and hydraulic properties, results in uncertainty in the factor of safety, F_s. A superior assessment of slope stability is possible if the uncertainties involved are taken into account in an explicit, quantitative manner. The application of probabilistic approaches to slope stability has been widely advocated during the past three decades (Ang and Tang, 1975, Vanmarcke, 1977, Whitman, 1983, Harr, 1987, Christian et al., 1992, Becker, 1996a and 1996b, Whitman, 2000, Duncan, 2000, among many others).

The uncertainty in F_s can be assessed through the analysis of different "case scenarios" or using a measure of safety that takes into account the uncertainty in F_s, such as the probability of failure. The probability of failure, *Pf*, is generally defined as the probability of the factor of safety being less than 1 (shaded areas in Figure 77).

The two probability density functions (p.d.f.) presented in Figure 77 make the case for incorporating uncertainty into the assessment of embankment stability. From a traditional deterministic standpoint, a slope with an expected factor of safety E[F_s] = 1.5 is safer than a slope with E[F_s] = 1.2. The expected or mean values of F_s correspond to a certain extent to the stability measure used in deterministic analyses. The two scenarios presented in Figure 77 show that the p.d.f. with higher E [F_s] has a higher probability of failure. Therefore, E[F_s] alone may provide incomplete or even misleading information about the stability of an embankment.

Foundation design codes have been rewritten to accommodate probabilistic concepts (Becker, 1996b). Becker (1996a) presents a review of reliability-based foundation design approaches and describes the motivations for the use of probabilistic methods. The approach taken by some foundation design codes is evidence that a formal probabilistic framework based on the analysis of "case scenarios" provides a protocol that is appropriate for geotechnical engineering practice.

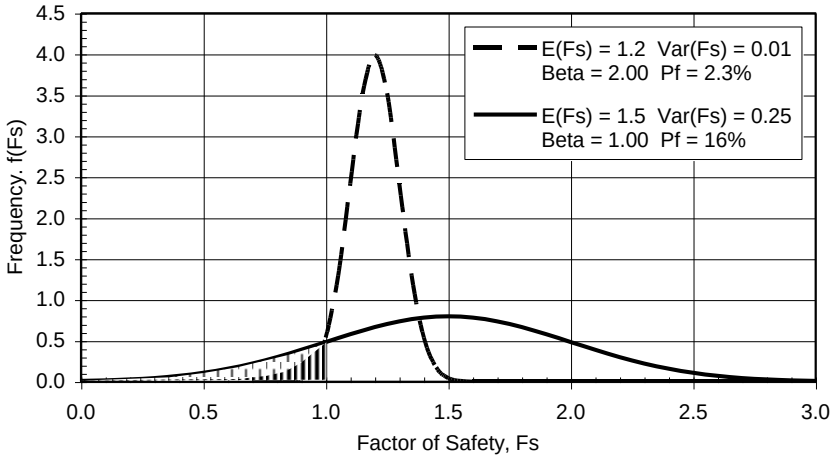

Figure 77 Probability density function of Factor of Safety, F_s, and probability of failure, P_f.

Probabilistic approaches in geotechnical engineering require:

- establishment of methods of characterization of soil property variability,
- development of a method of reliability analysis, and
- establishment of acceptable risks.

Soil property variability can be quantified using conventional statistical tools. Acceptable risk levels can be established by decision makers, based on the historic frequency of disasters, or based on calibration approaches using previous successful designs (Becker, 1996a). Several reliability analysis methods are available in the literature. Reliability analysis methods must be selected based on their accuracy and computation requirements.

13.1 MONTE CARLO METHOD

According to Harr (1987), the Monte Carlo method was first developed by Hammersley and Handscomb (1964). Several sets of values of *n* input random variables *X = (x1, x2,…, xn)* must be randomly generated. The sets of random input variables *X* are obtained using random number generators that produce the selected probability density function. Each randomly generated set must be used to calculate a realization of $F_s(X)$. The realizations of F_s(X) are then used to define the probability density function of $F_s(X)$.

It is important to note that unbiased random number generators are required to perform an unbiased Monte Carlo simulation. Hahn and Shapiro (1967) present a summary of random number generators for a series of probability density functions. A detailed discussion about equations for the generation of random numbers can be found in Rubinstein (1981).

The Monte Carlo simulation method requires a large number of trials (i.e., evaluations of F_s). Theoretically, the larger the number of trials in the simulation, the more precise will be the final answer. Harr (1987) presents the following equation for the number of Monte Carlo simulations required to achieve a given accuracy:

$$N = \left[\frac{d^2}{4\varepsilon^2} \right]^m \quad \textbf{[188]}$$

where:

N = number of Monte Carlo trials required;

d = confidence coefficient for normal distribution;

ε = maximum allowable system error, equal to the complement of the confidence level;

m = number of random input variables.

Hahn and Shapiro (1967) point out that the Monte Carlo method has a more intuitive appeal than the other available methods. Another advantage is the fact that the method precision can be calculated using. In addition, the Monte Carlos method is flexible, and can accommodate different probability density functions and correlated variables. Unfortunately, the large number of trials required limits the applicability of the Monte Carlo method. For instance, a Monte Carlo simulation with 99% of confidence requires 16,641 trials if the problem has one variable (Harr, 1987). If the problem has *m* variables, the number of trials increases geometrically, according to the power *m*.

13.2 LATIN HYPERCUBE METHOD

The Latin Hypercube method is based on "stratified" sampling technique with random selection within each stratum. This method provides a smoother sampling of the probability distributions and gives comparable results to the Monte Carlo Method with few fewer samples. Typically, an analysis using 1000 samples obtained by the Latin Hypercube method will produce comparable results to an analysis of 5000 samples using the Monte Carlo method.

13.2.1 Sampling

Latin hypercube sampling (LHS) is a form of stratified sampling that can be applied to multiple variables. The method commonly used to reduce the number or runs necessary for a Monte Carlo simulation to achieve a reasonably accurate random distribution. LHS can be incorporated into an existing Monte Carlo model fairly easily, and work with variables following any analytical probability distribution.

To perform the stratified sampling, the cumulative probability (100%) is divided into segments, one for each iteration of the Monte Carlo simulation. A probability is randomly picked within each segment using a uniform distribution, and then mapped to the correct representative value in of the variable's actual distribution.

A simulation with 500 iterations would split the probability into 500 segments, each representing 0.2% of the total distribution. For the first segment, a number would be chosen between 0.0% and 0.2%. For the second segment, a number would be chosen between 0.2% and 0.4%. This number would be used to calculate the actual variable value based upon its distribution.

P(X <= x) = n is solved for x, where n is the random point in the segment. How this is done is different for every distribution, but it's generally just a matter of reversing the process of the probability function.

13.2.2 Grouping

Once each variable has been sampled using this method, a random grouping of variables is selected for each Monte Carlo calculation. Independent uniform selection is done on each of the variable's generated values. Each value must only be used once.

13.2.3 Example

An illustrative example with three variables and 10 samples is described as follows. For simplicity, all the three variables are assumed to be normal distributed and have the same Mean value (=30) and Standard Deviation (=3.16). The cumulative curve can be shown in the following Figure 78.

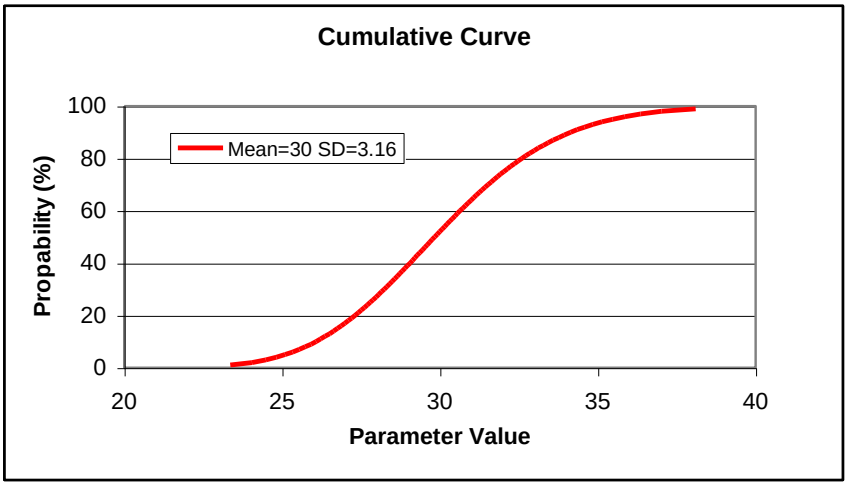

Figure 78 Cumulative curve of a parameter (Normal Distributed Function)

The sampling process can be summarized as follows:

1. Divided the cumulative probability (100%) into 10 segments (Column Segment in Table 2).
2. Calculate each segment point for each variable (Column Segment Point in Table 2).
   Segment Point=SegmentMin+(SegmentMax-SegmentMin)*Random
   where
   Random means a randomly generated decimal value between 0 to 1
3. Calculate each parameter value for each variable from cumulative curve (Figure 78).
4. Pick three parameters as a set randomly. This will be done 10 times (=Total Samples).

NOTE:
To make the procedure more efficient, the first set will be picked among 10 samples, remove the chosen values. The second set will be picked among remained 9 samples and removed again and so on.

Table 2 Illustrative example for Latin hypercube sampling

Sample	Segment		Segment Point			Parameter Value*		
	Min (%)	Max (%)	Variable 1 (%)	Variable 2 (%)	Variable 3 (%)	Variable 1	Variable 2	Variable 3
0	0	10	2.25	9.92	5.64	24.16	26.06	25.25
1	10	20	15.91	10.99	13.06	26.86	26.22	26.51
2	20	30	24.34	25.00	26.69	27.73	27.79	27.95
3	30	40	32.89	31.92	35.70	28.48	28.40	28.71
4	40	50	47.23	48.06	41.00	29.62	29.68	29.13
5	50	60	53.69	52.11	50.27	30.13	30.00	29.86
6	60	70	65.53	64.70	65.25	31.12	31.04	31.09
7	70	80	73.57	77.24	70.56	31.88	32.27	31.58
8	80	90	87.05	82.20	87.30	33.59	32.87	33.64
9	90	100	95.15	99.81	93.15	35.52	40.47	34.88

13.3 ALTERNATIVE POINT ESTIMATE METHOD (APEM)

13.3.1 Point Estimated Method

The term, Point Estimate Method (PEM) refers to the category of probabilistic methods for calculating the moments of a function of random variables that are based on the calculation of $F_s(X)$ at pre-determined values of X. The pre-determined values of X are combined with corresponding "weights" or discrete probabilities. Most PEM approaches are based on two-point estimates (i.e., two values for each x_i), but references to third- and higher-order point estimates can be found in the literature (Harr, 1987).

Evans (1967, 1972) proposed an early PEM for independent random variables. However, the first popular PEM approach is generally credited to Rosenblueth (1975, 1981). Rosenblueth (1975) proposed a two-point PEM for correlated variables in which the joint probability density function of X was assumed to be concentrated at points in the $2n$ hyperquadrants of the space defined by X. A univariated formulation was presented as the basis of the more general, multivariate equations. The moments of the set of two estimate points were matched to the three first central moments of the input variables.

Rosenblueth (1981) pointed out that a univariated two-point approximation of $E[F_s(x)]$ based on three moments has an accuracy that is equivalent to that of a third order Taylor series approximation (i.e., errors equivalent to the fourth order term). Rosenblueth (1975) also introduced the n-point estimate for univariated functions. Analytical equations for a three-point estimate of a symmetrical function $F_s(x)$ were provided. It was pointed out that the larger the number of estimate points, the more accurate is the procedure.

Rosenblueth (1975 and 1981) presented a generalization of the univariated procedure, for a multivariate analysis, using two-point estimates. Rosenblueth (1981) proposed the use of a superabundant number of estimate points and the procedure used the assumption of symmetric p.d.f.

Equations 2.55 to 2.61 have permutation elements that can be extended easily for any number of n variables. The number of evaluations of $F_s(X)$ is $2n$. This number may become excessive if a large number of random variables are being considered and if each evaluation of $F_s(X)$ involves time consuming computations (e.g., when finite element numerical analyses are involved). Nevertheless, the number of evaluations of $F_s(X)$ may be significantly lower than the number required by a Monte Carlo simulation.

Other authors have proposed different versions of the point estimate method, to address different issues, such as skewness of multivariate functions, correlations, accuracy, and the number of realizations required. Some examples of different point estimate approaches found in the literature are Lind (1983), Harr (1989), Li (1991, 1992), and Panchalingam and Harr (1994).

13.3.2 The Alternative Point Estimate Method

The probabilistic assessment of factors of safety can be performed based on the first few moments of the probability distribution of the factor of safety, F_s. Among the numerous probabilistic measures available, the reliability index, b, and the probability of failure, P_f, seem to be the most widely accepted and have been adopted in the software.

The reliability index corresponds to the number of standard deviation of F_s, $_+[F_s]$, separating the computed mean value of F_s, $E[F_s]$, and the value of F_s that represents imminent failure (i.e., F_s equals 1). The reliability index can be determined according to the following equation:

$$\beta = \frac{E[F_s]-1}{\sigma[F_s]} \qquad \textbf{[189]}$$

where:

$E[F_s]$ = expected value of the factor of safety; and

$\sigma[F_s]$ = standard deviation of the factor of safety.

The probability of failure, P_f, is a more complete measure, based on the first few statistical moments of F_s (or on the entire probability density function of F_s when available) and corresponds to the probability of the event "$F_s < 1$":

$$P_f = P(F_s < 1) \quad \textbf{[190]}$$

The reliability index requires the computation of the expected value and standard deviation of F_s. When using an approximate method, the probability of failure requires these two measures and an assumption regarding the shape of the probability density function of F_s.

The lognormal distribution is adopted by the software as the probability distribution function of F_s, based on the recommendation of Becker (1996a), among others. Once a probability density function is assumed, the probability of failure can be obtained from the integral of the assumed probability distribution function.

13.3.3 Development of the Alternative Point Estimate Method

Exact closed-form solutions for the first few statistical moments of F_s are rarely available. Therefore, approximate solutions are often used. Probabilistic models are generally based on the analyses of the deterministic factor of safety for several case scenarios.

A probabilistic method for the factor of safety needs to be able to accommodate a multivariate function of numerous correlated non-symmetric random variables. The method employed by the software has these capabilities and is based on the combination of the Taylor series approach and the univariated point estimate method proposed by Rosenblueth (1975, 1981).

To combine the Taylor series approximation and the two-point estimation method, the factor of safety, F_s, must first be expanded using a Taylor series about the mean values of the input random variables. The following equation uses terms up to the second order:

$$F_s(X) = F_s(E[X]) + \sum_{i=1}^{n} \left.\frac{\partial F_s}{\partial x_i}\right|_{E[X]} (x_i - E[x_i]) + \frac{1}{2}\sum_{i=1}^{n} \left.\frac{\partial^2 F_s}{\partial x_i^2}\right|_{E[X]} (x_i - E[x_i])^2 + \sum_{\substack{i \\ j>i}} \sum_{j} \left.\frac{\partial^2 F_s}{\partial x_i \partial x_j}\right|_{E[X]} (x_i - E[x_i])(x_j - E[x_j]) \quad \textbf{[191]}$$

where:

F_s = factor of safety,

X = set of n input random variables, x_1, x_2, …, x_n,

$E[\ ]$ = expected value, and

$F_s(E[X])$ = $F_s(E[x_1], E[x_2], ..., E[x_n])$.

The derivatives must be obtained at the mean values, $E[X]$, as indicated. The expected value of F_s, $E[F_s(X)]$, can be obtained by taking the expected value of both sides of the above equation, as follows:

$$E[F_s(X)] = F_s(E[X]) + \frac{1}{2}\sum_{i=1}^{n} \left.\frac{\partial^2 F_s}{\partial x_i^2}\right|_{E[X]} Var[x_i] + \sum_{\substack{i \\ i<j}} \sum_{j} \left.\frac{\partial^2 F_s}{\partial x_i \partial x_j}\right|_{E[X]} Cov[x_i, x_j] \quad \textbf{[192]}$$

where:

$Var[x_i]$ = is the variance of x_i,

$Cov[x_i, x_j]$ = is the covariance between x_i and x_j.

Moments of F_s of order m, $\mu_m[F_s]$, can be obtained based on the definition: $\mu_m[F_s] = E[(F_s - E[F_s])^m]$. For instance, the variance of F_s can be calculated using the equation $Var[F_s] = E[(F_s - E[F_s])^2]$. Any other higher order statistical moment of F_s can be obtained using the above equation and replacing F_s by $(F_s - E[F_s])^m$.

The required derivatives are not readily available, leaving the equation of little use. The univariated two-point estimation method proposed by Rosenblueth (1975, 1981) can be employed in order to obtain the derivatives.

In order to do so, let us first define $F_s(x_i) = F_s(E[x_1],...,E[x_{i-1}], x_i, E[x_{i+1}],...,E[x_n])$. According to the method proposed by Rosenblueth (1981), the following univariated two-point estimate of $E[F_s(x_i)]$ can be written:

$$E[F_s(x_i)] = p_i^+ F_s(x_i^+) + p_i^- F_s(x_i^-) \quad \textbf{[193]}$$

where:

$F_s(x_i)$ = $F_s(E[x_1],..., E[x_{i-1}], x_i, E[x_{i+1}],..., E[x_n])$,

$F_s(x_i^\pm)$ = $F_s(E[x_1],..., E[x_{i-1}], x_i^\pm, E[x_{i+1}],..., E[x_n])$,

$x_i^\pm$ = $E[x_i] + \xi^\pm[x_i]\sigma[x_i]$,

$\xi^\pm[x_i]$ = $\gamma_1[x_i]/2 \pm \sqrt{1+(\gamma_1[x_i]/2)^2}$,

$\gamma_1[x_i]$ = $\mu_3[x_i]/\{\sigma[x_i]\}^3$ is the skewness of x_i,

$\mu_3[x_i]$ = is the third statistical moment of x_i,

$\sigma[F_s]$ = the standard deviation of x_i,

$x_i^\pm$ = $\frac{1}{2}\left[1 \mp \sqrt{1-\frac{1}{1+[\gamma_1[x_i]/2]^2}}\right]$.

The univariated two-point estimate presented above is based on the moment-matching equations up to the third statistical moment. Note that:

$$x_i^\pm = E[x_i] \pm \sigma[x_i] \text{ and } p_i^\pm = 1/2 \quad \textbf{[194]}$$

when xi is assumed as symmetrically distributed (i.e., $\gamma_1[x_i] = 0$).

An alternative equation for $E[F_s(x_i)]$ can be obtained using a univariated Taylor series expansion of $F_s(x_i)$ about the mean values of the input variables. The following equation is obtained by keeping the terms up to the second order and applying the expectancy operator:

$$E[F_s(x_i)] = F_s(E[X]) + \frac{1}{2}\left.\frac{\partial^2 F_s}{\partial x_i^2}\right|_{E[X]} Var[x_i] \quad \textbf{[195]}$$

The following equation can be obtained after equalizing the two previous equations, summing the equation obtained for all *n* input variables, and rearranging:

$$F_s(E[X]) + \frac{1}{2}\sum_{i=1}^{n}\left.\frac{\partial^2 F_s}{\partial x_i^2}\right|_{E[X]} Var[x_i] \quad \textbf{[196]}$$

$$= F_s(E[X]) + \sum_{i=1}^{n}\left[p_i^+ F_s(x_i^+) + p_i^- F_s(x_i^-) - F_s(E[X])\right]$$

This equation provides the two first terms of the right-hand side of the Taylor Series approximation for $E[F_s]$. The last term of the Taylor Series approximation can be determined if the second order derivative.

$\partial^2 F_s / \partial x_i \partial x_j$ is obtained. In order to do so, let us define:

$$F_s(x_i^+, x_j^+) = F_s(E[x_1],...,E[x_{i-1}], x_i^+, E[x_{i+1}],...,E[x_{j-1}], x_j^+, E[x_{j+1}],...,E[x_n]) \quad \textbf{[197]}$$

One manner for obtaining $\partial^2 F_s / \partial x_i \partial x_j$ is to use the Taylor series expansion of $F_s(x_i^+, x_j^+)$ about the mean values of the input variables. Such Taylor series expansion can be written as follows:

$$\begin{aligned} F_s(x_i^+, x_j^+) = F_s(E[X]) &+ \left.\frac{\partial F_s}{\partial x_i}\right|_{E[X]} (x_i^+ - E[x_i]) + \left.\frac{\partial F_s}{\partial x_j}\right|_{E[X]} (x_j^+ - E[x_j]) \\ &+ \frac{1}{2}\left.\frac{\partial^2 F_s}{\partial x_i^2}\right|_{E[X]} (x_i^+ - E[x_i])^2 + \frac{1}{2}\left.\frac{\partial^2 F_s}{\partial x_j^2}\right|_{E[X]} (x_j^+ - E[x_j])^2 \\ &+ \left.\frac{\partial^2 F_s}{\partial x_i \partial x_j}\right|_{E[X]} (x_i^+ - E[x_i])(x_j^+ - E[x_j]) \end{aligned} \quad \textbf{[198]}$$

Noting that:

$$\partial F_s / \partial x_i \big|_{E[X]} (x_i^+ - E[x_i]) + (1/2)(\partial^2 F_s / \partial x_i^2 \big|_{E[X]})(x_i^+ - E[x_i])^2 = F_s(x_i^+) - F_s(E[X])$$

The above equation can be rearranged as follows:

$$\left.\frac{\partial^2 F_s}{\partial x_i \partial x_j}\right|_{E[X]} = \frac{F_s(x_i^+, x_j^+) - F_s(x_i^+) - F_s(x_j^+) + F_s(E[X])}{\xi^+[x_i]\sigma[x_i]\xi^+[x_j]\sigma[x_j]}$$

This equation provides the last term required in order to define all terms for the Taylor Series approximation of $E[F_s]$. The following equation is obtained:

$$\begin{aligned} E[F_s(X)] = F_s(E[X]) &+ \sum_{i=1}^{n} \left[p_i^+ F_s(x_i^+) + p_i^- F_s(x_i^-) - F_s(E[X])\right] \\ &+ \sum_{\substack{i \\ i<j}} \sum_{j} \left[F_s(x_i^+, x_j^+) - F_s(x_i^+) - F_s(x_j^+) + F_s(E[X])\right] \frac{\rho[x_i, x_j]}{\xi^+[x_i]\xi^+[x_j]} \end{aligned} \quad \textbf{[199]}$$

where:

$F_s(E[X]) = F_s(E[x_1], E[x_2], ..., E[x_n])$,

$F_s(x_i^{\pm}) = F_s(E[x_1], E[x_2], ... E[x_{i-1}], x_i^{\pm}, E[x_{i+1}], ..., E[x_n])$,

$x_i^{\pm} = E[x_i] + \xi^{\pm}[x_i]\sigma[x_i]$,

$\xi^{\pm}[x_i] = \gamma_1[x_i]/2 \pm \sqrt{1 + (\gamma_1[x_i]/2)^2}$,

$p_i^{\pm} = \frac{1}{2}\left[1 \mp \sqrt{1 - \frac{1}{1 + [\gamma_1[x_i]/2]^2}}\right]$,

$F_s(x_i^+, x_j^+) = F_s(E[x_1], ..., E[x_{i-1}], x_i^+, E[x_{i+1}], ... , ..., E[x_{j-1}], x_j^+, E[x_{j+1}], ..., E[x_n])$,

$\rho[x_i, x_j]$ = the correlation coefficient between x_i and x_j,

$\rho[x_i, x_j] = \frac{Cov[x_i, x_j]}{\sigma[x_i]\sigma[x_j]}$.

This is the final equation for the computation of the expected value of F_s. Any moment of F_s of order m can be obtained based on the definition, $\mu_m[F_s] = E[(F_s - E[F_s])^m]$, as mentioned previously. In other words, the higher order statistical moments of F_s can be obtained using the above equation and replacing F_s by $\{F_s(X) - E[F_s]\}^m$:

$$\mu_m[F_s(X)] = E[\{F_s(X) - E[F_s(X)]\}^m]$$
$$= \{F_s(E[X]) - E[F_s(X)]\}^m$$
$$+ \sum_{i=1}^{n} \begin{bmatrix} p_i^+ \{F_s(x_i^+) - E[F_s(X)]\}^m + p_i^- \{F_s(x_i^-) - E[F_s(X)]\}^m \\ - \{F_s(E[X]) - E[F_s(X)]\}^m \end{bmatrix} \quad \textbf{[200]}$$
$$+ \sum_{\substack{i \\ i<j}} \sum_{j} \begin{bmatrix} \{F_s(x_i^+, x_j^+) - E[F_s(X)]\}^m - \{F_s(x_i^+) - E[F_s(X)]\}^m \\ - \{F_s(x_j^+) - E[F_s(X)]\}^m + \{F_s(E[X]) - E[F_s(X)]\}^m \end{bmatrix} \frac{\rho[x_i, x_j]}{\xi^+[x_i]\xi^+[x_j]}$$

where:

$\mu_m[F_s(X)]$ = statistical moment of F_s of order m,

$E[F_s(X)]$ = is computed using the first the first APEM equation.

The two APEM equations can be used in the computation of the first few statistical moments of F_s. The moments of F_s are used by the software in the computation of the reliability index and the probability of failure. The input requirements for each input variable are:

- mean,
- standard deviation (or coefficient of variation),
- skewness, and
- correlation matrix.

The accuracy of the equations presented herein is the same as that of the Rosenblueth (1975, 1981) method, since the same moment-matching estimate points were adopted (Gitirana Jr., 2005).

13.3.4 Efficiency of the Alternative Point Estimate Point

The combination of the univariated two-point estimation equation proposed by Rosenblueth (1975, 1981) and the univariated and multivariated Taylor series expansions of F_s produces a theoretically sound equation with a significantly higher efficiency when compared with conventional point estimate methods.

The Figure 79 presents a comparison of the number of evaluations required by different probabilistic approaches. The APEM equations require ($n2 + 3n + 2$)/2 evaluations of F_s if all variables are correlated and $2n + 1$ evaluations of F_s if all variables are independent. The PEM proposed by Rosenblueth (1975) requires $2n$ evaluations of F_s for the 2-point approximation and $3n$ evaluations of F_s for the 3-point approximation.

Routine geotechnical problems often involve soil profiles comprised of several layers and numerous parameters. For instance, a slope comprised of 4 layers involved 12 parameters if cohesion, friction angle and unsaturated shear strength are considered uncertain. It becomes apparent that the Rosenblueth (1975) are unfeasible if numerical simulations of seepage, for instance, are used. The Taylor series approximation requires $n + 1$ evaluations of F_s if the derivatives are obtained using a simple discrete approach. However, such an approach would not be theoretically sound since the function involved may be nonlinear.

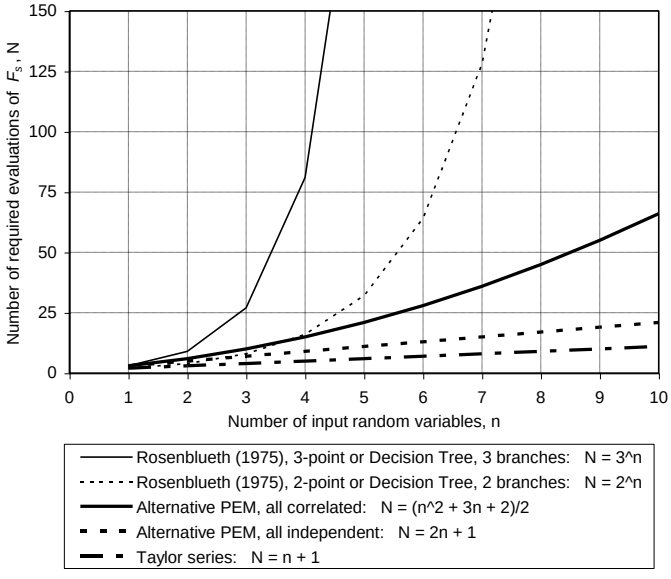

Figure 79 Number of evaluations of F_s required by several probabilistic methods

13.3.5 Tornado Diagram

The software employs a formal framework for sensitivity analysis, based on fundamental Decision Analysis concepts. The most fundamental objective of sensitivity analysis is to aid in the decision and to determine what input variables have significant influence in the decision at hand (Clemen, 1996).
One and two-way sensitivity analysis, tornado diagrams, and spider plots are some of the most straightforward approaches for studying the sensitivity of the input variables in a decision problem (Eschenbach, 1992, Clemen, 1996). One and two-way sensitivity analyses are performed for one and two input variables at a time, respectively. The input variables are varied along a range of possible values, and the remaining input variables must be kept at the base value.

One-way sensitivity analyses of several input variable can be compared using tornado diagrams (Figure 80). These diagrams indicate which variables require close consideration and which variables can be considered as certain values. The term tornado diagram refers to the typical appearance of these plots.

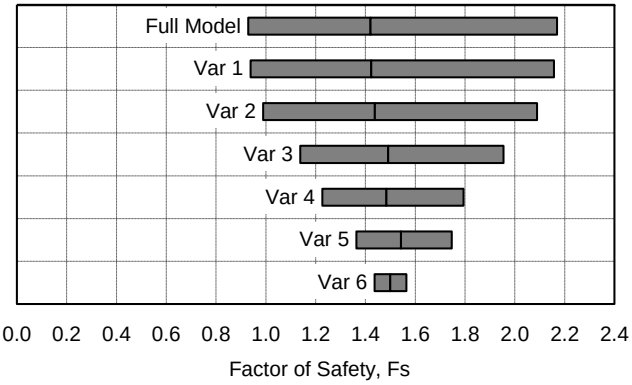

Summary of data

Variable	$E[F_s]_k$	$Var[F_s]_k$	10^{th} percentile	50^{th} percentile	90^{th} percentile
Full Model	1.500	0.260	0.930	1.420	2.170
Var 1	1.500	0.250	0.939	1.423	2.157
Var 2	1.500	0.200	0.989	1.437	2.089
Var 3	1.525	0.106	1.138	1.492	1.954
Var 4	1.500	0.050	1.227	1.484	1.794
Var 5	1.550	0.023	1.363	1.543	1.746
Var 6	1.500	0.003	1.436	1.499	1.565

Figure 80 Probabilistic Event Tornado diagram for the W-GHA model.

Tornado diagrams can be used in the software to show and compare how much each input variable's uncertainty is transformed into uncertainty in the factor of safety. Two types of tornado diagrams may be used for the same purpose: namely, deterministic, and probabilistic event tornado diagrams. These diagrams are based on rigorous construction rules and can benefit from detailed statistical information about the input random variables.

In a deterministic event tornado diagram, all but one source of uncertainty in the model are removed at a time. Therefore, correlations are not considered. In a probabilistic event tornado diagram, one source of uncertainty in the model is removed at a time and all the remaining probabilistic information is kept, including any existing correlations.

Probabilistic Event Tornado Diagram

Figure 80 presents an illustrative, hypothetical probabilistic event tornado diagram. The values used for the construction of this illustrative tornado diagram are also presented. The tornado diagram shows how much each input variable's uncertainty contributes to the uncertainty in the factor of safety. Probabilistic event tornado diagrams receive this name because this is the type of tornado diagram that is capable of retaining the most uncertainty in a model. The following steps are taken by the software for the construction of probabilistic event tornado diagrams:

1. The uncertainty of one input variable is removed and the first and second moments of the factor of safety are calculated using equations based on the alternative point estimate method presented in the previous sections. To remove the uncertainty of one variable (the k^{th} variable), as follows:

$$E[F_s(X)]_k = F_s(E[X]) + \sum_{\substack{i=1 \\ i \neq k}}^{n} \left[p_i^+ F_s(x_i^+) + p_i^- F_s(x_i^-) - F_s(E[X]) \right] \quad \textbf{[201]}$$
$$+ \sum_{i<j \text{ and } i \neq k} \sum_{j} \left[F_s(x_i^+, x_j^+) - F_s(x_i^+) - F_s(x_j^+) + F_s(E[X]) \right] \frac{\rho[x_i, x_j]}{\xi^+[x_i]\xi^+[x_j]}$$

$$Var[F_s(X)]_k = \left\{ F_s(E[X]) - E[F_s(X)]_k \right\}^2$$
$$+ \sum_{\substack{i=1 \\ i \neq k}}^{n} \begin{bmatrix} p_i^+ \left\{ F_s(x_i^+) - E[F_s(X)]_k \right\}^2 + p_i^- \left\{ F_s(x_i^-) - E[F_s(X)]_k \right\}^2 \\ - \left\{ F_s(E[X]) - E[F_s(X)]_k \right\}^2 \end{bmatrix}$$
$$+ \sum_{i<j \text{ and } i \neq k} \sum_{j} \begin{bmatrix} \left\{ F_s(x_i^+, x_j^+) - E[F_s(X)]_k \right\}^2 - \left\{ F_s(x_i^+) - E[F_s(X)]_k \right\}^2 \\ - \left\{ F_s(x_j^+) - E[F_s(X)]_k \right\}^2 + \left\{ F_s(E[X]) - E[F_s(X)]_k \right\}^2 \end{bmatrix} \frac{\rho[x_i, x_j]}{\xi^+[x_i]\xi^+[x_j]}$$

where:

$E[F_s(X)]_k$ = the first statistical moment of F_s calculated when the uncertainty of the input variable *k* is removed;

$Var[F_s(X)]_k$ = the second statistical moment of F_s calculated when the uncertainty of the input variable *k* is removed.

2. The first and second statistical moments obtained for the factor of safety using the above equations are used to compute the 10th, 50th, and 90th percentiles. A lognormal distribution is assumed for the factor of safety to compute the percentiles. Other extreme percentiles can be adopted, such as 5th and 95th, and so on,
3. The procedure depicted in steps "*i*" and "*ii*" is repeated for all random input variables,
4. A bar is created on the tornado diagram for each run performed following steps "*i*" to *"iii".* Each bar corresponds to the input random variable whose uncertainty was removed from the model. The ends of the bars correspond to the extreme percentiles of F_s. A line located near or at the middle of the bar indicates the 50th percentile,
5. The procedure described in steps "*i*" to "*iv"* is repeated for the "full model" (i.e., without removing any input variable uncertainty) and a "full model" bar is created, and
6. Finally, the bars are sorted from widest to narrowest, resulting in the tornado-shaped appearance. Sorting the bars helps identifying the input variables with greatest impacts.

The size of each bar is directly proportional to the spread of the factor of safety probability distribution function is. Therefore, the size of each bar can be related to the uncertainty that was transferred from the input variables into the factor of safety. The closer the size of a bar is to that of the "full model" bar, the less sensitive is F_s to the corresponding input variable. Smaller bars correspond to the most significant parameters.

For instance, in Equation [162] Variables 4, 5, and 6 have impacts considerably higher than Variables 1 and 2. Variables 1 and 2 could be considered certain variables, and this simplification would not affect the analysis results considerably. Variable 3 appears to have an intermediate impact in F_s.

An experimental campaign for determining "Parameter 6" with greater certainty would greatly reduce the uncertainty associated with the factor of safety. Tornado Diagrams are powerful tools that can be used in a wide variety of Geotechnical Design problems.

It becomes apparent from examining the above equations that any existing correlations between input variables are fully considered. It is also important to point out that the computations of factor of safety required by the "full model" bar are sufficient to construct the other bars of a probabilistic event tornado diagram. Therefore, a probabilistic event tornado diagram can always be constructed whenever probabilistic analysis is used in the software. No additional computations of factor of safety are required.

Deterministic Event Tornado Diagram

The deterministic event tornado diagram also shows how much each input variable's uncertainty contributes to the uncertainty in the factor of safety. The following steps are taken by the software for the construction of probabilistic event tornado diagrams:

1. The uncertainty of all input variables is removed except for one and the first and second moments of the factor of safety are calculated using equations based on the alternative point estimate method presented in the previous sections. To use the uncertainty of one variable (the kth variable) the following equations are used:

$$E[F_s(X)]_k = F_s(E[X]) + p_k^+ F_s(x_k^+) + p_k^- F_s(x_k^-) - F_s(E[X]) \quad \textbf{[202]}$$

$$\begin{aligned} Var[F_s(X)]_k = & \left\{F_s(E[X]) - E[F_s(X)]_k\right\}^2 \\ & + p_k^+ \left\{F_s(x_k^+) - E[F_s(X)]_k\right\}^2 + p_k^- \left\{F_s(x_k^-) - E[F_s(X)]_k\right\}^2 \\ & - \left\{F_s(E[X]) - E[F_s(X)]_k\right\}^2 \end{aligned}$$

2. The first and second statistical moments obtained for the factor of safety using the above equations are used to compute the 10th, 50th, and 90th percentiles. A lognormal distribution is assumed for the factor of safety to compute the percentiles. Other extreme percentiles can be adopted, such as 5th and 95th, and so on,
3. The procedure depicted in steps "i" and "ii" is repeated for all random input variables,
4. A bar is created on the tornado diagram for each run performed following steps *"i"* to *"iii".* Each bar corresponds to the input random variable whose uncertainty was removed from the model. The ends of the bars correspond to the extreme percentiles of F_s. A line located near or at the middle of the bar indicates the 50th percentile, and
5. The bars are sorted from widest to narrowest, resulting in the tornado-shaped appearance.

The smaller a bar is, the less sensitive is F_s to the corresponding input variable. Deterministic event tornado diagrams often result in more pleasing shapes and are useful in addressing the relative importance of each input variable. However, the variability presented in each individual bar is considerably smaller than the total variability that would result from the full model. In other words: the relative size of the bars can be used when analyzing a problem, but the absolute size of each bar must be seen with caution.

13.3.6 Implementation of the Alternative Point Estimate Method

The alternative point estimate theory implemented in the software requires the following input data:

1. The expected value of each input variable, *E[X],*
2. The coefficient of variation of each input variable, *CV[X],*
3. The probability density function assumed for each variable, and
4. The correlation matrix if any of the input variables are correlated.

Two probability density functions are available: namely, the normal distribution and the lognormal distribution. Based on the expected value, the coefficient of variation, and on the probability density function chosen, the software automatically selects the appropriate equations to calculate the skewness and kurtosis of the probability density function of each input variable. The variance and standard deviation of each input variable are calculated based on the expected values and coefficients of variations.

Next, the software calculates the estimate points, *x*+ and *x*–, and the discrete probabilities or "weights", *p*+ and *p*–. The estimation points for the normally distributed variable are symmetrical with respect to the expected value. Non-symmetric estimation points are presented for the log normally distributed variable.

Once the univariated estimate points and concentrated discrete probabilities are determined, the software lays out the sets of variable values required for the multivariate analysis. The sets of values are organized in four groups. The first set corresponds to the expected values. The second group corresponds to the sets using upper estimate points, *x*+. The third group corresponds to the sets using lower estimate points, *x*–. The fourth group corresponds to the estimate points required by correlated variables. The total number of sets required is a function of the number of input variables. Five evaluation sets are required for two uncorrelated variables, and six evaluation sets are required for two correlated variables.

13.4 NUMBER OF SAMPLES

The *Number of Samples* is specified for each random variable. If *Number of Samples* = 1000, then 1000 sets of random variables will be generated and 1000 Factor of Safety will be calculated for each calculation method (e.g., Bishop etc.). Theoretically, the more Samples used in an analysis, the more accurate the solution will be.

How many samples are enough for a probabilistic slope stability analysis? It has been known that the number of Sample is dependent on the desired level of confidence in the solution, as well as the number of variables to be considered. The following equation is recommended for the calculation of *Number of Samples* in the software.

$$NoS = \left[\frac{d^2}{4(1-\varepsilon)^2}\right]^m \quad \textbf{[203]}$$

where:

NoS = number of samples,

d = the normal standard deviate corresponding to the level of confidence,

ε = the desired level of confidence (0-100%) expressed in decimal form (0-1.0),

m = number of variables to be considered.

13.5 CRITICAL SLIP SURFACE LOCATION

In the probabilistic analysis, the slip surface location may affect the results. The differences are described as follows:

13.5.1 Fixed

1. The most critical slip surface of all the trial slip surfaces is determined using deterministic slope stability analysis,
2. The probabilistic analysis is then carried out on the most critical slip surface for each set of random variables. In other words, the calculation of Factor of Safety will be repeated until the Number of Samples is satisfied on the same slip surface obtained from deterministic analysis,
3. Different calculation methods (e.g., Ordinary, Bishop, etc.) can provide different critical slip surfaces. The probabilistic analysis is implemented independently on each critical slip surface obtained from each calculation method, and
4. NOTE: the critical slip surface obtained from deterministic analysis is based on the deterministic input parameters. Theoretically, this critical slip surface will vary with the set of subsequent probabilistic parameters. The floating critical slip surface option is used for this purpose.

13.5.2 Floating

The most critical slip surface of all the trial slip surfaces is obtained for each set of probabilistic parameters. The only difference compared to *Fixed* Option is that the critical slip surface varies for each set of probabilistic parameters in *Floating* Option, while the critical slip surface is fixed in *Fixed* Option.

14 SPATIAL VARIABILITY

It is well known that soils are spatially variable or non-homogeneous. To investigate how spatial variability affects geotechnical behavior, soils can be modeled as one dimensional (1D), two dimensional (2D) or multi-dimensional (3D) randomly varying processes. The software implements 1D and 2D Spatial Variation, respectively.

14.1 NONE

The *None* option represents a single value for each trial for each distinct region for the property to be considered as shown in Figure 81.

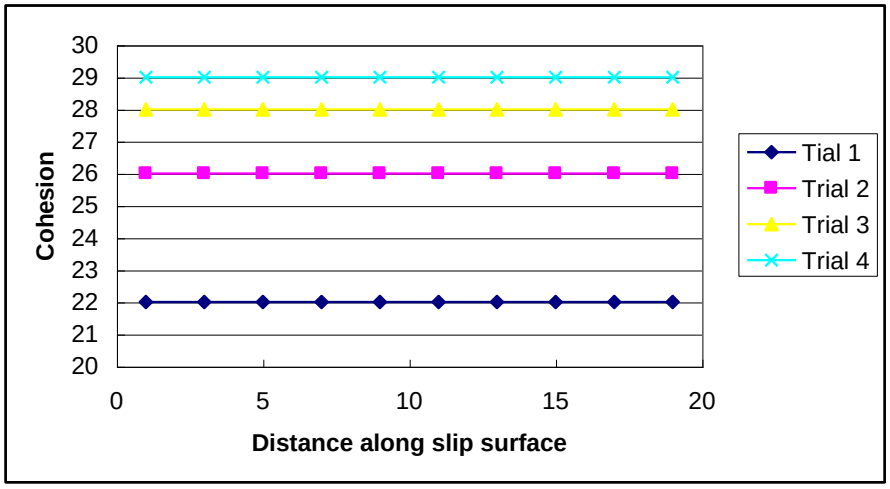

Figure 81 Illustrative example for 1D Spatial Variability (None)

14.2 1D SPATIAL VARIABILITY

1D Spatial Variation option is used for Probability analysis in the software. When a potential slip surface has a significant length within one material, Spatial Variability can become an important issue.

The software has three options for considering the spatial variability along the slip surface. The options determine the number of times for the samplings of the soil properties along the slip surface.

1. Sample the properties only once for each soil for the whole slip surface (Default),
2. Sample the properties for each slice along the slip surface, and
3. Sample the properties at a specified distance along the slip surface.

The three options can be illustrated using a simple model shown in Figure 82. A significant portion of the slip surface is in *Soil 2* and it is also assumed that there is some statistical variability in Soil 2 along the slip surface. The length of the slip surface in *Soil 2* is around 21 m and the horizontal distance is 20 m.

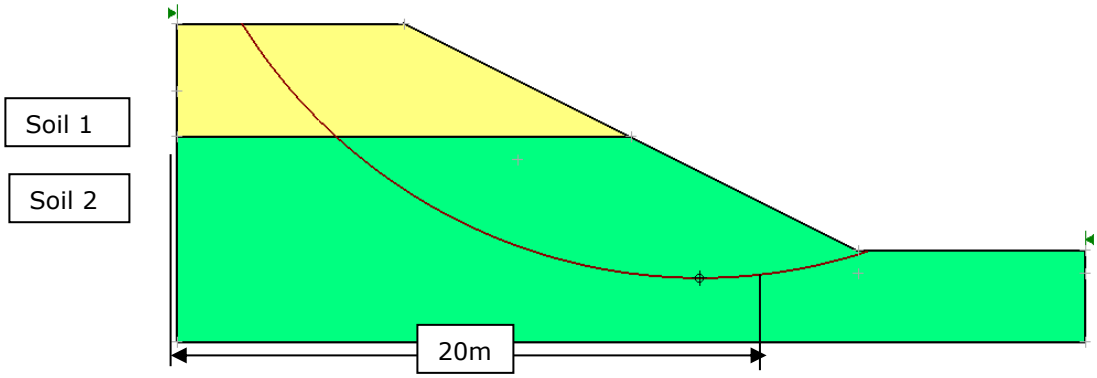

Figure 82 Illustrative example for 1D Spatial Variability

The statistic values for cohesion of Soil 2 are: mean=10 kPa, SD = 2kPa. The three options have different presentations as described as follows:

14.2.1 Each Slice

Each Slice Option is to sample the soil strength for each slice. The variation along the slip surface then could be illustrated as shown in Figure 83 for two trial runs. If there are 10 slices in Soil 2, as a result, there will be 10 different strengths along the slip surface.

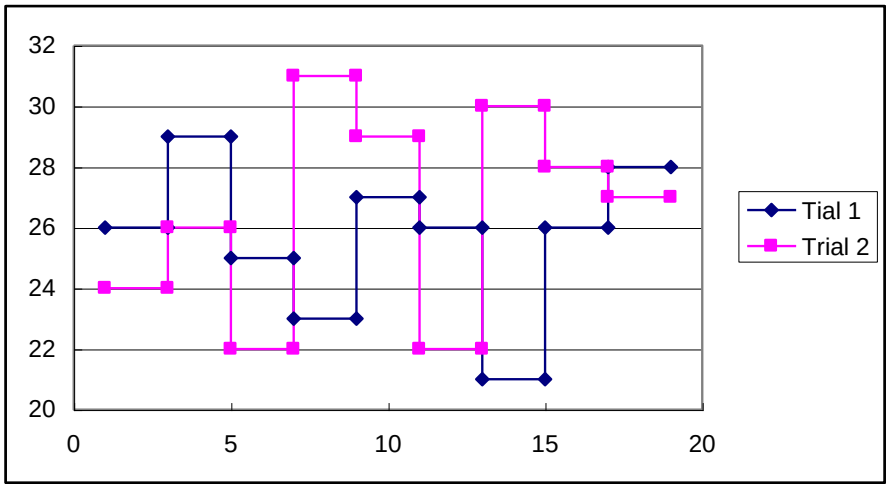

Figure 83 Illustrative example for 1D Spatial Variability (Each Slice)

NOTE:

As shown in Figure 83, the strength between each slice may fluctuate with a large range along the slip surface. It seems an irrational situation even though this is statistically possible. Users should pay enough attention to this option.

14.2.2 Distance

Distance Option is to sample the soil's properties at a specified distance. For example, if the sampling distance is 8m, then the strength variation along the slip surface for two trials can be shown in Figure 84. The distance specified is set back to zero at the intersection point with each new region.

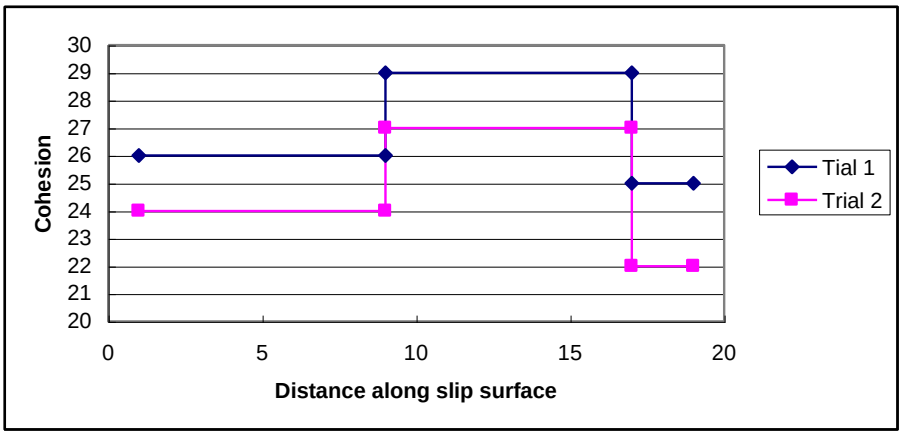

Figure 84 Illustrative example for 1D Spatial Variability (Distance)

At this sampling distance, there are three different strengths along the slip surface. There are two complete 8m sampling distance and a third partial sampling distance (20-8*2=4m). A partial sampling distance is regarded as to be correlated with the immediately preceding sampling distance. The coefficient of correlation between two soil segments can be computed with the equation as proposed by Vanmarcke (1983):

$$\rho(\Delta Z,\Delta Z') = \frac{Z_0^2\Gamma(Z_0) - Z_1^2\Gamma(Z_1) + Z_2^2\Gamma(Z_2) - Z_3^2\Gamma(Z_3)}{2\Delta Z\Delta Z'[\Gamma(\Delta Z)\Gamma(\Delta Z')]^{0.5}} \qquad \textbf{[204]}$$

where:

ΔZ, $\Delta Z'$ = the length between two segments, respectively,

Z_0 = the distance between the two segments,

Z_1 = $\Delta Z + Z_0$,

Z_2 = $\Delta Z + Z_0 + \Delta Z'$,

Z_3 = $\Delta Z' + Z_0$,

Γ = a dimensionless variance function.
$\Gamma(Z)$=1.0 when $Z \leq \delta$;
$\Gamma(Z)$= δ/Z when $Z > \delta$.
δ = the scale of fluctuation. It is about twice the autocorrelation distance.

NOTE:
The shorter the partial distance is, the strong the correlation is. The correlation is weak when the partial distance approaches the specified sampling distance.

14.3 2D SPATIAL VARIABILITY

2-D Spatial Variability Option is used to generate a 2-D random field for soil's properties using the Random Field Theory proposed by Fenton and Vanmarke (1990) as described in Appendix 18.3.

14.3.1 General

The software uses Random Field Theory to generate a 2-D discrete random field which signifies the averages of a homogeneous random function. The averages are calculated using incremental domains formed by different levels and the functions are defined by their mean and covariance function (Fenton and Vanmarcke, 1990).

The use of this theory to represent random properties as averages is beneficial because the properties are usually not properly defined when represented by a point and they show significant scale effects. Also, with this approach, it is easier to incorporate known data and change resolution in different sub-regions. This is illustrated using the Ornstein-Uhlenbeck and fractional Gaussian noise processes (Fenton and Vanmarcke, 1990).

14.3.2 Covariance Function

There are five covariance functions (dlavx2, dlsep2, dlspx2, dlafr2, dlsfr2) that are available for 2-D random field generation. They are described below:

1. dlavx2:2-D exponentially decaying (Markov) model

This function returns the covariance between two points in a 2-D Markov random field, separated by lag vector {X,Y}. The covariance function for this process is given by:

$$B(x,y) = \text{var}^* \exp\left(-\sqrt{(2\times x/dthx)^2 + (2^* y/dthy)^2}\right) \qquad \textbf{[205]}$$

where:

$B(x,y)$ = covariance function,

var = the point variance,

$dthx$ = the scales of fluctuation in the x-direction,

$dthy$ = the scales of fluctuation in the y-direction,

x = component of the lag vector between the points (or the dimensions of the averaging area, if var < 0), and

y = component of the lag vector between the points (or the dimensions of the averaging area, if var < 0).

If var < 0, then this function returns the variance of a local average of the process, |var|*V(X,Y), averaged over the domain X x Y. This variance is obtained by 16-pt Gauss quadrature integration of the covariance function. The 4-fold integral is reduced to a 2-fold integration by taking advantage of the quadrant symmetry of the covariance function.

NOTE:
When the element is non-square, extremely small scales of fluctuation tend to yield inaccurate local average variances (either directly here using var < 0, or through dcvaa2). More Gauss points are needed in the integration.

2. dlsep2: 2-D separable (1D x 1D) Markov model

This function returns the covariance between two points, separated by lag vector {X,Y}, in a 2-D random field having separable Markovian covariance function. The covariance function for this field is given by:

$$B(x,y) = \text{var}^* \exp\left(-(2|x|/dthx)\right)^* \exp\left(-(2|y|/dthy)\right) \quad \textbf{[206]}$$

where:

$B(x,y)$	= covariance function,
var	= the point variance,
$dthx$	= the scales of fluctuation in the x-direction,
$dthy$	= the scales of fluctuation in the y-direction,
x	= component of the lag vector between the points (or the dimensions of the averaging area, if var < 0), and
y	= component of the lag vector between the points (or the dimensions of the averaging area, if var < 0).

NOTE:
This function is NOT isotropic even if dthx = dthy.

If var < 0, then this function returns the variance of a local average of the process, |var|*V(*X,Y),* averaged over the domain *X* x *Y.* For a separable covariance function, the variance function is also separable and can be written as the product of two 1-D variance functions corresponding to the exponential correlation function

$$V(X,Y) = V(X)^* V(Y) \quad \textbf{[207]}$$

where:

$V(X,Y)$	= covariance function,
$V(X),V(Y)$	= individual functions are based on the 1-D analytical model

$$V(X) = 2^* \frac{dthx^2}{4^* X^2} * \left[\left(2^* |X|/dthx\right) + \exp\left(-2^* |X|/dthx\right) - 1\right] \quad \textbf{[208]}$$

$$V(Y) = 2^* \frac{dthy^2}{4^* Y^2} * \left[\left(2^* |Y|/dthy\right) + \exp\left(-2^* |Y|/dthy\right) - 1\right] \quad \textbf{[209]}$$

The variance of the local average is then given by var*V(X,Y).

3. dlspx2: 2-D separable Gaussian decaying model

This function returns the covariance between two points, separated by lag vector {X, Y}, in a 2-D random field having separable (and mean-square differentiable) covariance function.

$$B(x,y) = \text{var}^* \exp\left(-\pi^* (|x|/dthx)^2\right)^* \exp\left(-\pi^* (|y|/dthy)^2\right) \quad \textbf{[210]}$$

where:

$B(x,y)$	= covariance function,
var	= the point variance,
$dthx$	= the scales of fluctuation in the *x*-direction,
$dthy$	= the scales of fluctuation in the *y*-direction,
x	= component of the lag vector between the points (or the dimensions of the averaging area, if var < 0), and
y	= component of the lag vector between the points (or the dimensions of the averaging area, if var < 0).

4. dlafr2: 2-D isotropic fractional Gaussian noise model

This function computes and returns the covariance between two points, separated by the distance T, in a 2-D fractional Gaussian noise (fGn) process. The radial covariance function of the fractional noise process is given by:

$$B(s) = \frac{\text{var}}{2*(pb)^{2H}}\left[|s+pb|^{2H} - 2|s|^{2H} + |s-pb|^{2H}\right] \quad \textbf{[211]}$$

where:

$B(s)$ = radial covariance function,

var = point variance of the fGn process,

pb = length over which the fractional Brownian motion is averaged in order to make this, the derivative process, exist, normally `pb' is selected to be quite small (of the order of the size of the discretization interval),

s = Euclidean length of the lag vector {X,Y}, s = sqrt(X^2+Y^2),

H = Hurst exponent. In this implementation, 0.5 < H < 1; values of H near 1 yield a correlation structure which remains very high (and thus a covariance matrix which may be nearly singular). Values of H near 0.5 yield a band-limited white noise process.

If var < 0, then this function returns the variance of a local average of the process, |var|*V(D), averaged over the domain `D' (see below). The variance function which yields a close approximation to the above radial covariance function is given by

$$V(D) = \frac{|D+pb|^r - 2\left(|D|^r + |pb|^r\right) + |D-pb|^r}{D^2*(2H+1)*(2H+2)*pb^{2H}} \quad \textbf{[212]}$$

where:

r = (2H+2),

D = |X| + |Y|, the 1-norm of {*X, Y*},

pb = length over which the fractional Brownian motion is averaged in order to make this, the derivative process, exist, normally `*pb*' is selected to be quite small (of the order of the size of the discretization interval).

NOTE:

The actual covariance function corresponding to [172] is equal to [171] along the coordinate axes and remains close to [171 for H > 0.8. For H < 0.7, the covariance in the diagonal direction is too high, but since the covariance in such fields dies off very rapidly, the error is believed negligible.

5. dlsfr2: 2-D separable fractional Gaussian noise model

This function computes and returns the covariance between two points, separated by the lag vector {*X, Y*}, in a random field, which is a separable 2-D fractional Gaussian noise. The covariance function for such a field is separable, and given by:

$$B(X,Y) = \text{var}* r(X) * r(Y) \quad \textbf{[213]}$$

For two points separated by distance {*X, Y*}, where *r(X)* and *r(Y)* are the directional correlation functions,

$$r(X) = \frac{1}{2*pb^{2H}}\left[|X+pb|^{2H} - 2|X|^{2H} + |X-pb|^{2H}\right] \quad \textbf{[214]}$$

$$r(Y) = \frac{1}{2*pb^{2G}}\left[|Y+pb|^{2G} - 2|Y|^{2G} + |Y-pb|^{2G}\right] \quad \textbf{[215]}$$

where:

pb = the length over which the fractional Brownian motion is averaged to make this, the derivative process, exist, normally `*pb*' is selected to be quite small (of the order of the size of the discretization interval)

H = self-similar parameter, the Hurst exponent governing the process in the *X* direction. In this implementation, 0.5 < H < 1; values of H near 1 yield a correlation structure which remains very high (and thus a covariance matrix which may be nearly singular). Values of H near 0.5 yield a band-

limited white noise process.

G = self-similar parameter, the Hurst exponent governing the process in the *Y* direction. In this implementation, 0.5 < G < 1; values of G near 1 yield a correlation structure which remains very high (and thus a covariance matrix which may be nearly singular). Values of G near 0.5 yield a band- limited white noise process.

If var < 0, then this function returns the variance of a local average of the process, |var|*V(*X,Y*), averaged over the domain *X x Y*. If the covariance function is separable, then so too is the variance function.

$$V(X,Y) = V(X) * V(Y) \quad \textbf{[216]}$$

where:

X,Y = dimensions of the averaging region,

$V(X),V(Y)$ = 1-D variance functions.

$$V(X) = \frac{|X + pb|^r - 2\left(|X|^r + |pb|^r\right) + |X - pb|^r}{X^2 * (2H+1) * (2H+2) * pb^{2H}} \quad \textbf{[217]}$$

$$V(Y) = \frac{|Y + pb|^r - 2\left(|Y|^r + |pb|^r\right) + |Y - pb|^r}{Y^2 * (2G+1) * (2G+2) * pb^{2G}} \quad \textbf{[218]}$$

where:

r =28H+2,

NOTE:
As X goes to zero V(X) or V(Y) becomes 0/0, but its limiting value is 1.0.

14.3.3 Parameters

To generate a random field, users can determine Distribution Type, Mean Value, Standard Deviation, Correlation Length and Number of Grid for each soil's property as described as follows:

1. Distribution
   The software simulates up to 3 soil property fields (cohesion, friction angle, unit weight). Individual fields are generated as standard Gaussian random fields using the 2-D Local Average Subdivision (LAS) algorithm. These fields are then combined to produce correlated standard Gaussian fields using the Covariance Matrix Decomposition approach. Finally, the individual fields are transformed so that they have the desired marginal distributions. These transformations are as follows.

   a. Normal

$$P(x,y) = \mu + \sigma * G(x,y) \quad \textbf{[219]}$$

   b. Lognormal

$$P(x,y) = \exp\left[\mu_{\ln} + \sigma_{\ln} * G(x,y)\right] \quad \textbf{[220]}$$

$$\sigma_{\ln}^2 = \ln\left(1 + \frac{\sigma^2}{\mu^2}\right) \quad \textbf{[221]}$$

$$\mu_{\ln} = \ln(\mu) - \frac{1}{2}\sigma_{\ln}^2 \quad \textbf{[222]}$$

   c. Bounded

$$P(x,y) = a + 0.5 * (b-a) * \{1 + \tanh[(\mu + \sigma * G(x,y)) / 2 * \pi]\} \quad \textbf{[223]}$$

where:

$P(x,y)$ = the desired random field (one of the soil properties),

$G(x,y)$ = the standard correlated Gaussian field,

μ = mean value,

σ = standard Deviation,

μ_{ln} = mean value of a lognormal distribution,

σ_{ln} = standard Deviation of a lognormal distribution,

a = lower Bound for Bounded distribution,

b = upper Bound for Bounded distribution,

m = location parameter for Bounded distribution, and

s = scale parameter for Bounded distribution.

2. Correlation Length
Correlation lengths give the scale of fluctuation in x-direction and y-direction. Correlation lengths govern the decay rate of correlation between points in the random field as a function of the distance between them. Loosely speaking, the scale of fluctuation can be thought of as the distance over which points on the random field show substantial correlation.

   The effect of Correlation Length can be summarized as follows:

   a. When correlation length is small, random fields tend to be rough,
   b. As correlation length is close to zero, all points in the field become uncorrelated with one another and field becomes infinitely rough. This is called white noise and physically unrealizable,
   c. As correlation length increases, the field becomes smoother,
   d. As correlation length is close to ∞, all points in the fields become completely correlated for finite-scale correlation functions. If the field is stationary, this means that the random field becomes completely uniform like a traditional soil model.

3. Number of Grid
Number of grid gives the number of divisions for a soil mass in *x*-direction and *y*-direction.

14.3.4 Random Field

Figure 85 shows a random field for c in a simple slope.

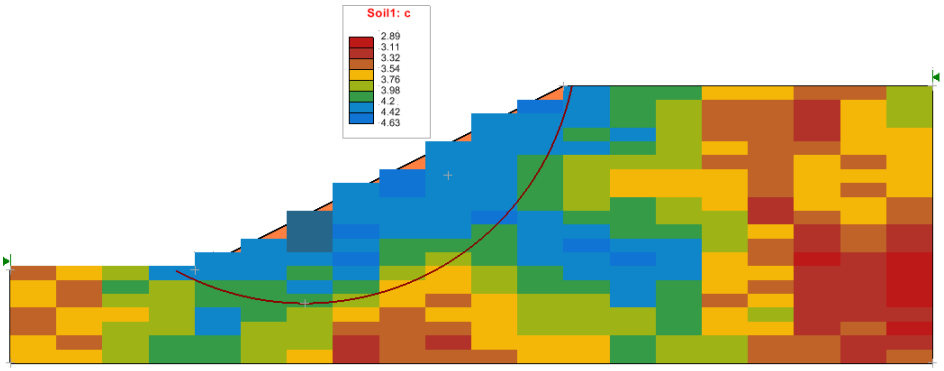

Figure 85 2-D Random Field Distribution (Mean = 3, SD = 1, normal)

(Correlation Length *x* = 100m, *y* =100m)

15 SENSITIVITY ANALYSIS

15.1 GENERAL

Sensitivity analysis is implemented to explore the effect of variability in the values of input parameters. Sensitivity analysis helps users to identify the parameters that have the most effect on the stability of a slope. The software introduces two sensitivity analysis procedures that are one-way sensitivity analysis and two-way sensitivity analysis as described in the following sections.

15.2 PARAMETERS

The software simulates soil properties in sensitivity analysis with four input parameters (Mean, Min, Max, and Increments/2).

EXAMPLE:
Mean = 10, Min = 5, Max = 20, Increments/2 = 3
Increments/2 = 3 means there are totally 7 values; there are 3 divisions between Min (= 5) and Mean (= 10) and three divisions between Mean (= 10) and Max (= 20). A Run-List consists of 7 values which are 5 (Min), 6.667, 8.333,10 (Mean), 13.333, 16.667,20 (Max), respectively.

15.3 ONE-WAY SENSITIVITY ANALYSIS

One-way sensitivity analysis is a commonly used sensitivity analysis in which model parameters selected by the user, are varied across a range of values as described in the section above and the effect on computed factors of safety observed. The procedure of one-way sensitivity is:

1. Four parameters are involved into the calculation. Only three of them (i.e., Min, Max, and Increments/2) are input by the user as sensitivity input, while the mean value is obtained from the *material properties* entered,
2. A Run-List for each variable will be generated automatically based on the input parameters, and
3. The safety factor of the critical slip surface will be re-computed, for each of the values in the Run-List, and

NOTE:
The critical slip surface may be the one obtained from a deterministic analysis if the user selected the *Fixed* option, otherwise one among all the trial slip surfaces based on the new set of values including the one in Run-List for the *Floating* option.

4. This process is repeated for EACH variable selected for the Sensitivity analysis, and

NOTE:
When the Sensitivity Analysis is being performed on a variable, All Other Variables are kept constant at their mean (i.e., Deterministic) values. Sensitivity Analysis is only carried out on one variable at a time, even if multiple variables have been selected for the analysis.

5. A graph representing the relation between safety factor and the variable will be plotted. When multiple variables are selected to display, the values of Horizontal axis represent a normalized value from 0-1. 0 stands for Min and 1 stands for Max, respectively.

15.4 TWO-WAY SENSITIVITY ANALYSIS

Two-way sensitivity analysis is significant feature used to identify the relationship of the factor of safety between two variables. The general procedure for a two-way sensitivity is:

1. *Two-Way Pairs*: define each pair of the parameter to be considered,
2. The safety factor of the critical slip surface will be re-computed, for each pair of variables,

NOTE:
There are two options for Critical Slip Surface Location (i.e., *Fixed* or *Floating)*.

3. A graph of contours of Factor of Safety is plotted with the horizontal axis Variable 1 and the vertical axis Variable 2.

15.5 CRITICAL SLIP SURFACE LOCATION

In the sensitivity analysis, the slip surface location may affect the results like the probabilistic analysis. The details are described in previous section.

16 THEORY FOR 3D ANALYSIS

In this chapter the general theory for the 3D general limit equilibrium method is developed. Each section provides a definition of different aspects of the developed theory.

There are two categories of existing 3D LEM slope stability analysis methods:

1) Based on one directional (sliding direction) force and/or moment equilibrium equations in the assumed sliding direction, i.e., one directional methods (Baligh and Azzouz 1975; Chen et al. 2003; Hovland 1977; Hungr 1987; Hungr et al. 1989; Lam and Fredlund 1993; Xing 1988). The one directional method implemented in the software is based on Hungr (2010)

2) Based on two directional (sliding direction and transverse direction) force and/or moment equilibrium equations, i.e., two directional methods (Cheng and Yip 2007; Huang and Tsai 2000; Huang et al. 2002; Kalatehjari et al. 2014; Wan et al. 2016). The two directional method implemented in the software is based on Cheng & Yip (2007).

16.1 ONE-DIRECTIONAL 3D GENERAL LIMIT EQUILIBRIUM METHOD

The methods of columns are utilized in the software in 3D which represent basically an extension of the methods of slices in a 2D analysis. Visualization of the forces on a particular 3D column is illustrated in Figure 86. This figure forms the basis for subsequent derivations.

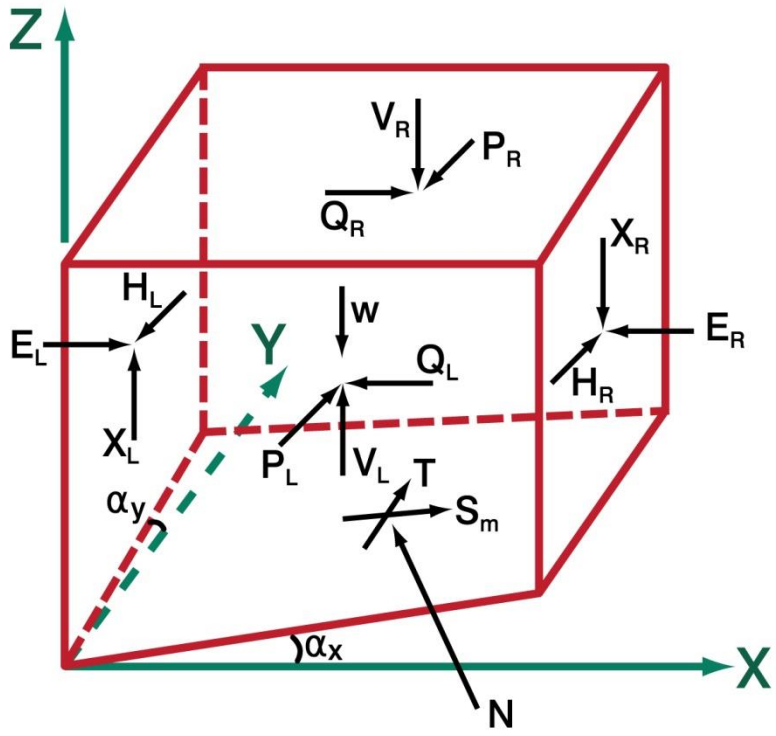

Figure 86 Free body diagram of a single column (sliding direction: from right to left)

Symbols used in the derivations:

N	= Normal force at the base of each column
Sm	= Shear force mobilized at the base of each column
T	= Shear force in Y direction at the base of each column
E_L, E_R	= Intercolumn normal force on YZ plane

X_L, X_R = Intercolumn vertical shear force on YZ plane

H_L, H_R = Intercolumn horizontal shear force on YZ plane

P_L, P_R = Intercolumn normal force on XZ plane

V_L, V_R = Intercolumn vertical shear force on XZ plane

Q_L, Q_R = Intercolumn horizontal shear force on XZ plane

W = Weight of the column

$\propto_x$ = Inclination of the column in the X direction

$\propto_y$ = Inclination of the column in the Y direction

Y_x, Y_y, Y_z = Direction angles of the normal force N at the column base

D_z = Total vertical point load and reinforcement force of the column

D_x = Total horizontal point load and reinforcement force of the column in X direction

K_v = Vertical earthquake acceleration

K_h = Horizontal earthquake acceleration

A = The true area of the column base

c = cohesion of the material

φ = Friction angle of the material

λ = The percentage of the intercolumn force function

$f(x)$ = Intercolumn force function

Assumptions:

1. Based on Lam and Fredlund (1993), H_L, H_R and T can be assumed as zero.
2. The intercolumn shear force X_L, X_R on the YZ plane can be related to its respective normal force E_L, E_R by intercolumn force function, *i.e.*

$$\frac{X}{E} = \lambda f(x) \qquad \textbf{[224]}$$

3. The resultant of the shear forces V and Q on the XZ plane is parallel to the base of the column, i.e.

$$\frac{V_R - V_L}{Q_R - Q_L} = \frac{\Delta V}{\Delta Q} = \tan \alpha_x \qquad \textbf{[225]}$$

4. Horizontal shear force Q in the XZ plane is in proportion to the weight of all the columns in each row

Based on the vertical Z direction force equilibrium of the column, we can get:

$$W * (1 + k_v) + (X_L - X_R) + (V_L - V_R) - N * \cos \gamma_z - S_m * \sin \alpha_x \pm D_z = 0 \qquad \textbf{[226]}$$

where:

$$\cos \gamma_z = 1 \Big/ \sqrt{\tan^2 \alpha_x + \tan^2 \alpha_y + 1} \qquad \textbf{[227]}$$

Based on the horizontal X direction force equilibrium of the column, we can get:

$$W * K_h + (E_L - E_R) + (Q_L - Q_R) + N * \cos \gamma_x - S_m * \cos \alpha_x \pm D_x = 0 \qquad \textbf{[228]}$$

Based on the Mohr-Coulomb strength criterion, we can get:

$$S_m = \{c \cdot A + (N - uA)\tan\phi\} / F \quad \textbf{[229]}$$

Where, $A = dx\,dy\,\frac{\sqrt{1-\sin^2\alpha_x \sin^2\alpha_y}}{\cos\alpha_x \cos\alpha_y}$, and dx and dy are the column width and length.

Based on assumption 2:

$$X = E \cdot \lambda \cdot f(x) \quad \textbf{[230]}$$

Based on assumption 3:

$$\Delta V / \Delta Q = \tan\alpha_x \quad \textbf{[231]}$$

Substitute, [229], [230], [231] into [228]

$$W*(1+Kv)+(E_L-E_R)*\lambda*f(x)+(Q_L-Q_R)*\tan\alpha_x - N\cos\gamma_z - \{cA+(N-uA)\tan\phi\}/F*\sin\alpha_x + D_z = 0 \quad \textbf{[232]}$$

Solve for *N*:

$$N = \frac{W*(1+kv) \pm D_z + (E_L - E_R)*\lambda*f(x) + (Q_L - Q_R)\tan\alpha_x + (uA\tan\phi - cA)/F*\sin\alpha_x}{\cos\gamma_x + \frac{\tan\phi\sin\alpha_x}{F}} \quad \textbf{[233]}$$

Substitute [229], [230], [231], into [228]:

$$W*K_h + (E_L - E_R) + (Q_L - Q_R) + N\cos\gamma_x \pm D_x - \frac{cA\cos\alpha_x}{F} - (N - uA)\frac{\tan\phi\cos\alpha_x}{F} = 0 \quad \textbf{[234]}$$

Solve for *N*:

$$N = \frac{\pm D_x - Wk_h - (E_L - E_R) - (Q_L - Q_R) + \frac{cA\cos\alpha_x}{F} - uA\frac{\tan\phi\cos\alpha_x}{F}}{\cos\gamma_x - \frac{\tan\phi\cos\alpha_x}{F}} \quad \textbf{[235]}$$

Let:

$$m_\alpha = \cos\gamma_z + \frac{\tan\phi\sin\alpha_x}{F} \quad \textbf{[236]}$$

$$m_\beta = \cos\gamma_x - \frac{\tan\phi\cos\alpha_x}{F} \quad \textbf{[237]}$$

Eliminate *N* by equating [233] and [235]:

$$\frac{[\pm D_x - Wk_h - (E_L - E_R) - (Q_L - Q_R) + \frac{cA\cos\alpha_x}{F} - uA\frac{\tan\phi\cos\alpha_x}{F}]}{m_\beta} = \frac{[\pm D_z + W*(1+kv) + (E_L - E_R)\lambda f(x) + (Q_L - Q_R)\tan\alpha_x - \frac{cA}{F}\sin\alpha_x + \frac{uA\tan\phi\sin\alpha_x}{F}]}{m_\alpha} \quad \textbf{[238]}$$

Collect terms on the above equation, we can get:

$$WS_1 + (E_L - E_R)S_2 + (Q_L - Q_R)S_3 + (u\tan\phi - c)*\frac{A}{F}S_4 \pm \frac{D_z}{M_\alpha} \pm \frac{D_x}{M_\beta} = 0 \quad \textbf{[239]}$$

where:

$$S_1 = \frac{1+k_v}{m_\alpha} + \frac{k_h}{m_\beta} \quad \textbf{[240]}$$

$$S_2 = \frac{1}{m_\beta} + \frac{\lambda f(x)}{m_\alpha} \quad \textbf{[241]}$$

$$S_3 = \frac{\tan\alpha_x}{m_\alpha} + \frac{1}{m_\beta} \quad \textbf{[242]}$$

$$S_4 = \frac{\sin\alpha_x}{m_\alpha} + \frac{\cos\alpha_x}{m_\beta} \quad \textbf{[243]}$$

Based on assumption 4:

$$Q_L - Q_R = a_c W \quad \textbf{[244]}$$

Where a_c is constant for any given row of columns.

Then [239] is changed into:

$$WS_1 + (E_L - E_R)S_2 + a_c WS_3 + (u\tan\phi - c)*\frac{A}{F}S_4 \pm \frac{D_z}{m_\alpha} \pm \frac{D_x}{m_\beta} = 0 \quad \textbf{[245]}$$

From [245], we can get:

$$E_L = E_R - W\frac{S_1}{S_2} - a_c W\frac{S_3}{S_2} - (u\tan\phi - c)*\frac{A}{F}\frac{S_4}{S_2} \pm \frac{D_z}{m_\alpha S_2} \pm \frac{D_x}{m_\beta S_2} \quad \textbf{[246]}$$

By summing all the columns' horizontal forces in one row with toe submergence external force *H*; we can get based on [247]:

$$\sum[W\frac{S_1}{S_2} + a_c W\frac{S_3}{S_2} + (u\tan\phi - c)*\frac{A}{F}\frac{S_4}{S_2} \pm \frac{D_z}{m_\alpha S_2} \pm \frac{D_x}{m_\beta S_2}] = H \quad \textbf{[247]}$$

With [247] we can solve for a_c for each row:

$$a_c = \frac{H - \sum W \frac{S_1}{S_2} + \sum [(c - u\tan\phi)\frac{A}{F}\frac{S_4}{S_2} \pm \frac{D_z}{m_\alpha S_2} \pm \frac{D_x}{m_\beta S_2}]}{\sum W \frac{S_3}{S_2}} \qquad \textbf{[248]}$$

After a_c is obtained, N for each column can be obtained from equation [233] or equation [235]. The factor of safety for 3D can then be obtained from moment equilibrium and force equilibrium with the same iteration scheme used in 2D.

The factor of safety regarding moment equilibrium is derived by summing the moments of all the forces over the entire sliding mass column assembly. The moment equilibrium is taken with respect to a common axis of rotation over the entire failure mass. For a rotational slip surface, the reference axis is also the axis of rotation. The rotation center will be obtained as suggested by Fredlund and Krahn (1977) as for 2D analysis for composite slip surfaces or non-rotational slip surfaces.

Since all the internal inter-column normal and shear forces will cancel when summing the moment over the entire sliding mass, the total moment of sliding mass can be expressed as:

$$\sum M_f = \sum Wx - \sum Nf\cos\gamma_z / \cos\alpha_x + \sum Wk_h \cdot e \pm Dd \pm Pa - \sum S/F_m * R = 0 \qquad \textbf{[249]}$$

where:

x = Moment arm of column weight

f = Moment arm of normal force

R = Moment arm of resisting force

e = Moment arm of the horizontal seismic load

D = External point load

d = Moment arm of the external point load

P = Resultant external water force

a = Moment arm of the external water force.

Based on [249], the factor of safety equation F_m with respect to moments can be express as:

$$F_m = \frac{\sum [cA + (N - uA)\tan\phi]R}{\sum Wx - \sum Nf\cos\gamma_z / \cos\alpha_x + \sum Wk_h \cdot e \pm Dd \pm Pa} \qquad \textbf{[250]}$$

The factor of safety with respect to force equilibrium can be derived by summing forces in the X direction over the entire sliding mass column assembly. Since all the internal inter-column normal and shear forces can cancel, based on [203], we can get:

$$\sum F_x = \sum [W * K_h + N * \cos\gamma_x - S/F_f * \cos\alpha_x \pm D_x] \pm P = 0 \qquad \textbf{[251]}$$

Then the factor of safety with respect to force equilibrium in 3D is

$$F_f = \frac{\sum [cA + (N - uA)\tan\phi]\cos\alpha_x}{\sum N\cos\gamma_x + \sum Wk_h \pm \sum D_x \pm P} \qquad \textbf{[252]}$$

Where N is from equation [235]. Both the equations for F_m and F_f are non-linear since the normal force N in the equations is also a function of the factor of safety. To solve the equations, an iterating procedure as used in 2D should be applied.

16.2 TWO-DIRECTIONAL 3D GENERAL LIMIT EQUILIBRIUM METHOD

The two-directional method when referring to two directions means the sliding direction and the transverse direction. Both directions are considered for force and/or moment equilibrium. The methods of columns are utilized in the software in 3D which represent basically an extension of the methods of slices in a 2D analysis. The two directional method implemented in the software is based on Cheng & Yip (2007).

As shown in Figure 88, the forces acting a typical soil column in two directional method are:

W	= weight of the column
P	= vertical external loading
N, *U*	= effective normal force and pore pressure force on column base
S	= mobilized shear force on column base
E	= intercolumn normal forces
X	= intercolumn vertical shear forces
H	= intercolumn horizontal shear forces
a	= sliding direction angle
ax, *ay*	= column base inclination angles along x- and y- directions

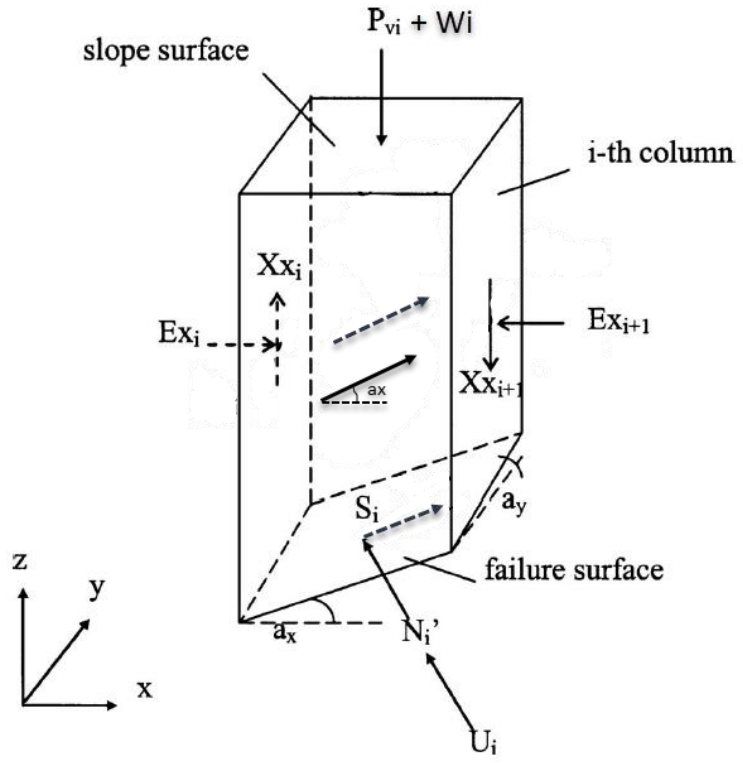

Figure 87 The force diagram on a typical soil column in the One Directional Method

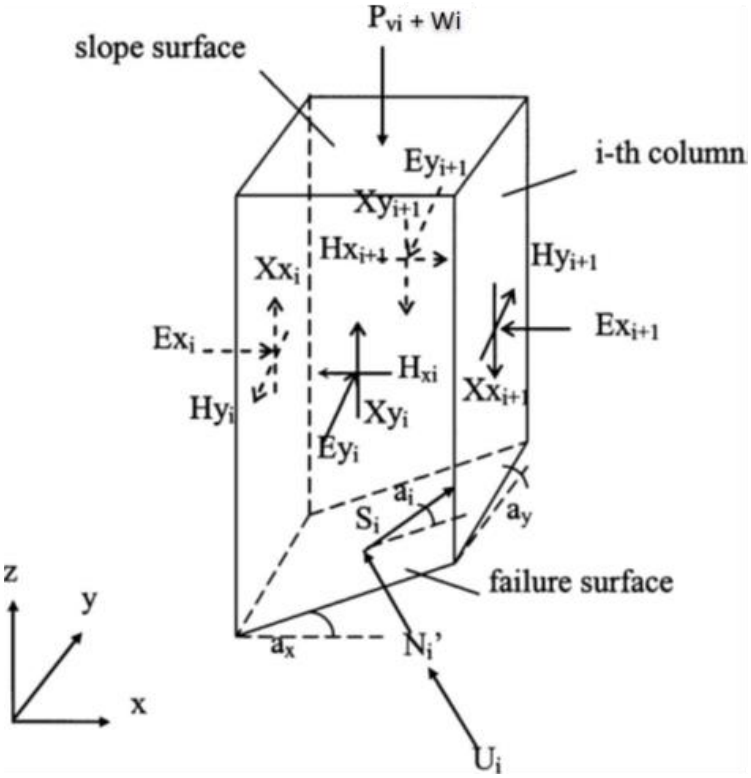

Figure 88 The force diagram on a typical soil column in the Two Directional Method

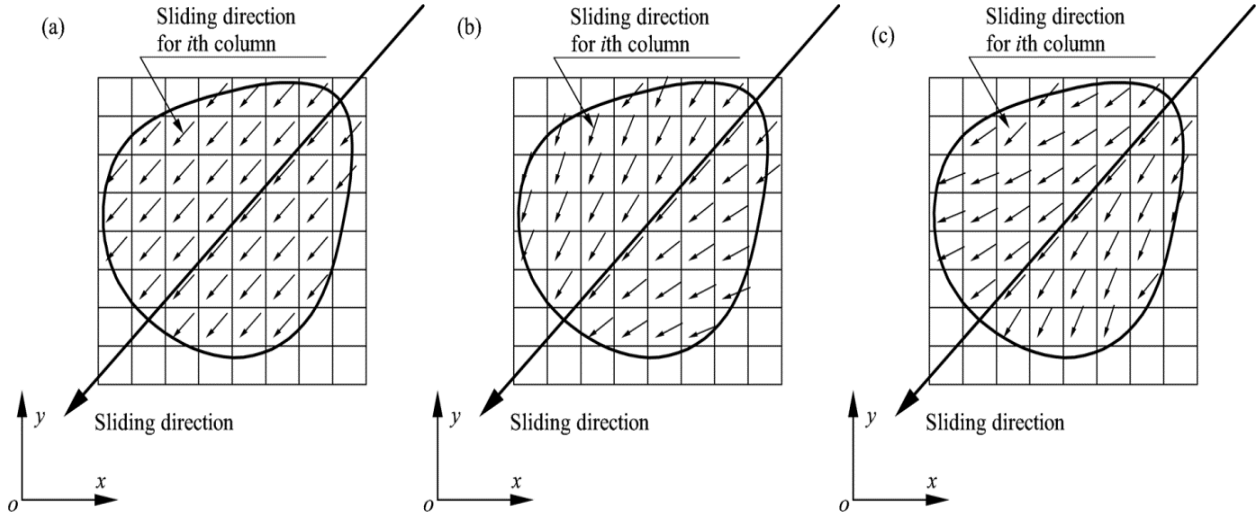

Figure 89 Different assumptions of the column sliding direction

There are three assumptions for the sliding direction (Cheng and Yip 2007) as shown in Figure 89.

1. Soil columns move in the same order and have a unique sliding direction (a)
2. Soil columns move towards each other (b)
3. Soil columns move away from each other (c)

The first assumption that the sliding directions are unique for all columns is adopted in Cheng and Yip (2007) as well as by many other researchers since the soil mass can be considered as a rigid body, and it is implemented in the software.

The key equations used in deriving the two-directional method are summarized below, see Cheng and Yip (2007) for details.

The assumptions required in the present 3D formulation are:

- Mohr–Coulomb failure criterion is valid.
- The factors of safety with respect to force and moment are equal for Spencer, MP, GLE and Sarma, etc.
- Sliding direction is the same for all soil columns as discussed above.

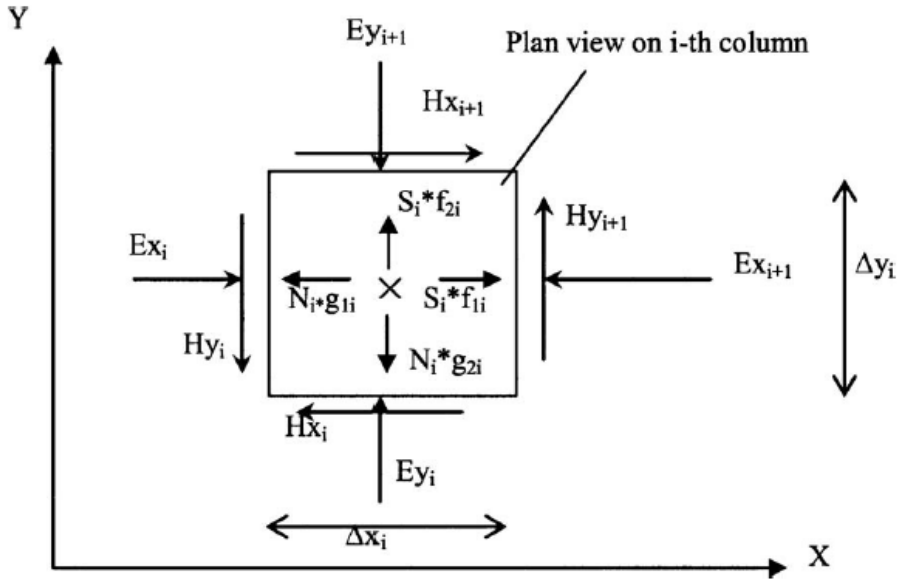

Figure 90 Force equilibrium in the x-y plane

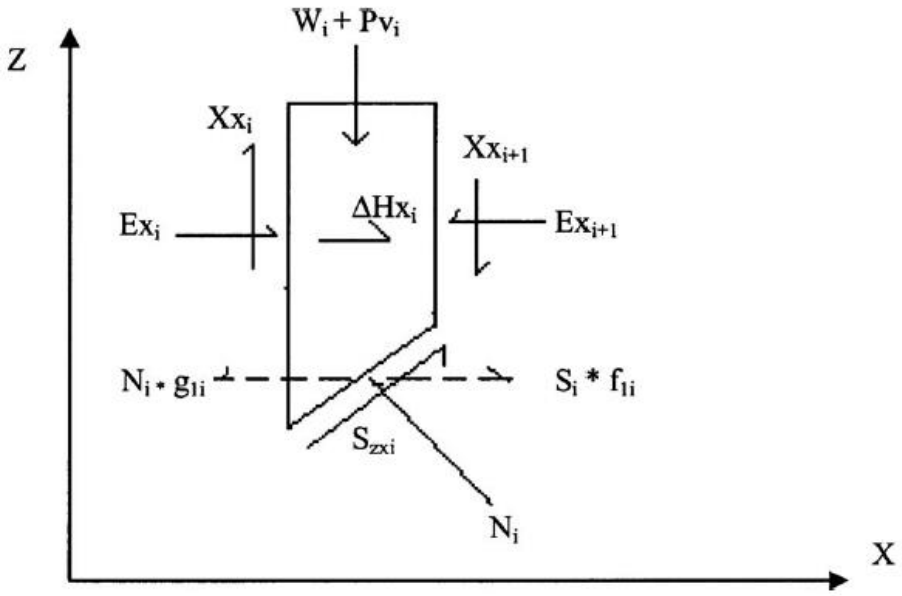

Figure 91 Horizontal force equilibrium in the x-direction in the x-z plane

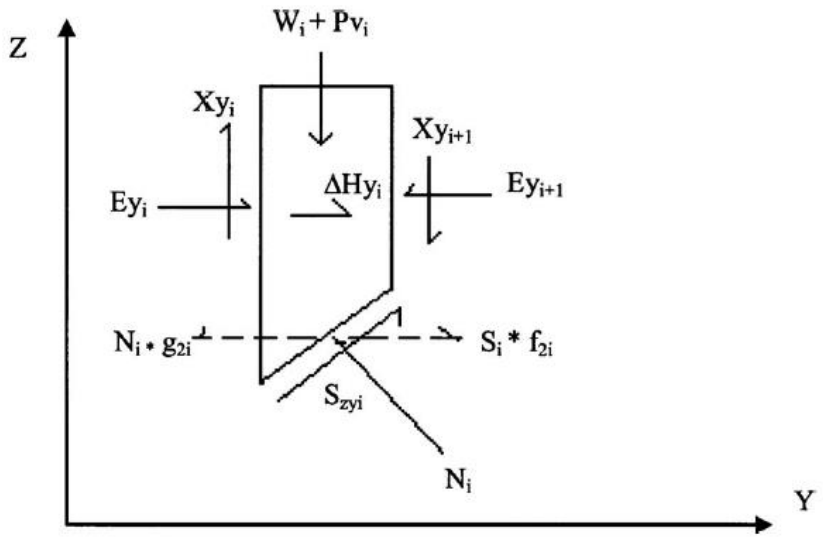

Figure 92 Horizontal force equilibrium in y-direction in y-z plane

The *f1*, *f2*, *f3* and *g1*, *g2*, *g3* used in the following equations are unit vectors in the direction of *Si* and *Ni* respectively.

By the Mohr–Coulomb criteria, the global factor of safety, *F*, is defined as

$$F = \frac{S_{fi}}{S_i} = \frac{C_i + N_i' \tan \phi_i'}{S_i} \quad \textbf{[253]}$$

The base shear force *Si* and base normal force *Ni* are expressed as the components of forces with respect to *X*-, *Y*-, and *Z*-directions for column *I,* by Huang and Tsai (2000)

$$S_{xi} = f_1 S_i; \quad S_{yi} = f_2 S_i; \quad S_{zi} = f_3 S_i$$
$$N_{xi} = g_1 N_i; \quad N_{yi} = g_2 N_i; \quad N_{zi} = g_3 N_i \quad \textbf{[254]}$$

Considering the vertical force equilibrium for the *i*th column

$$\sum F_z = 0 \rightarrow N_i g_{3i} + S_i f_{3i} - (W_i + P_{vi}) = (Xx_{i+1} - Xx_i) + (Xy_{i+1} - Xy_i) \quad \textbf{[255]}$$

Based on Equations (1), (2), and (3), the base normal and shear forces can be expressed as

$$N_i = A_i + B_i S_i; \quad S_i = \frac{C_i + (A_i - U_i)\tan \phi_i}{F\left[1 - (B_i \tan \phi_i / F)\right]} \quad \textbf{[256]}$$

In which,

$$A_i = \frac{W_i + P_{vi} + \Delta Ex_i \lambda_x + \Delta Ey_i \lambda_y}{g_{3i}}; \quad B_i = -\frac{f_{3i}}{g_{3i}} \quad \textbf{[257]}$$

Overall Force and Moment Equilibrium in the *X*- and *Y*-Directions:

Considering the overall force equilibrium in *X*-direction

$$-\sum Hx_i + \sum N_i g_{1i} - \sum S_i f_{1i} = 0 \quad \textbf{[258]}$$

From overall moment equilibrium in the *X*-direction

$$\sum (W_i + P_{vi} - N_i g_{3i} - S_i f_{3i}) RX + \sum (N_i g_{1i} - S_i f_{1i}) RZ = 0 \quad \textbf{[259]}$$

Considering overall force equilibrium in the *Y*-direction

$$-\sum Hy_i + \sum N_i g_{2i} - \sum S_i \cdot f_{2i} = 0 \quad \textbf{[260]}$$

Overall moment equilibrium in the *Y*-direction

$$\sum (W_i + P_{vi} - N_i g_{3i} - S_i f_{3i}) RY + \sum (N_i g_{2i} - S_i f_{2i}) RZ = 0 \quad \textbf{[261]}$$

Based on a trial sliding angle, λ_x is consistently changing until the calculated force factor of safety *Fx* from [258] satisfies the overall moment equilibrium factor of safety *Fmx* from equation (7) in the *X*-direction, i.e., *Fx* = *Fmx*. A similar procedure is applied to λ_y until the calculated force factor of safety *Fy* also satisfies the overall moment equilibrium factor of safety *Fmy* in the *Y*-direction, i.e., *Fy* = *Fmy*. If *Fx* is not equal to *Fy*, the sliding angle will be varied until *Fx*=*Fy* and then force as well as moment equilibrium will be achieved. As all the equilibrium equations have been used in the formulation, there is no equation to determine λ_{xy} unless additional assumptions are specified, in the software, the λ_{xy} can be specified.

16.3 DISCUSSION OF ONE-DIRECTIONAL AND TWO-DIRECTIONAL 3D METHODS

Differences between the One-Directional and the Two-Directional limit equilibrium methods:

- One-directional methods do not include the sliding direction calculation explicitly in their formulation and transverse sliding direction force and moment balance equations are neglected (Figure 87). The factor of safety and sliding direction are determined from axes and geometry rotation procedures as implemented in the software. (Jiang and Yamagami 1999, Yamagami and Jiang 1997)

- For two-directional methods, the direction of sliding is included in the formulation, can calculate both the factor of safety and the possible sliding direction of 3D asymmetrical slopes in the formulation (Figure 88).

- Cheng and Yip (2007), Wan etc. (2019) have demonstrated that the results calculated by the one-directional methods with geometry rotation or with some extension on sliding angle calculation are equivalent to the two-directional methods on asymmetrical problems.

The two-directional method developed by Cheng and Yip (2007) is implemented in the software. The improvements over the one the one-directional methods are:

- Two directional (sliding direction and traverse direction) force and moment are in equilibrium.
- The unique sliding direction is included in the LEM equations, so it can be solved without rotating the geometry to find the sliding direction.
- Better suited for non-symmetrical models.

16.4 DERIVATION OF 3D ENHANCED LIMIT METHOD (KULHAWY METHOD)

The Enhanced Limit Method uses a finite element analysis to compute the stresses at the column base center in a sliding mass and then compute the factor of safety. The definition of the factor of safety for the Enhanced Limit Equilibrium method is the same as that for 2D. The Kulhawy (1969) Enhanced Limit Method is implemented in the software in 3D.

The equation for the factor of safety for a saturated material can be written as:

$$F_s = \frac{\sum S_r}{\sum S_m} = \frac{\sum [c' A + (N - uA) \tan \phi]}{\sum \tau_m A} \quad \textbf{[262]}$$

where:

τ_m - mobilized shear stress along the base of a column,

S_r - resisting shear force,

S_m - mobilized shear forces,

A - True column base area
N - Normal Force at the column base

To calculate the normal and shear stresses at the center of a column base, a search must first be undertaken to locate the finite element within which the center of the column base is included. After the element encircling the center of the base of a column has been located, the stresses σ_{ij} at the base center can be calculated by using interpretation.

Once the stress σ_x, σ_y, σ_z, τ_{xy}, τ_{xz}, τ_{yz} are known at the base center of each column, the normal stress σ_n, and the mobilized shear stress τ_m can be calculated as follows:

The column base center point's unit vector normal is:

$$\vec{n} = \cos\gamma_x \vec{\imath} + \cos\gamma_y \vec{\varnothing} + \cos_z \vec{k} \quad \textbf{[263]}$$

The components of the traction $T^{(n)}$ at the column base center are:

$$T_i^{(n)} = \sigma_{ij} n_j \quad \textbf{[264]}$$

The normal stress σ_n can be calculated by the dot production of the traction $T^{(n)}$ and the unit normal vector $\vec{n}$.

$$\sigma_n = T^n \cdot \vec{n} \quad \textbf{[265]}$$

The mobilized shear stress τ_m for 3D is:

$$\tau_m = \sqrt{\left|T^{(n)}\right|^2 - \left|\sigma_n\right|^2} \quad \textbf{[266]}$$

16.5 SLIDING SURFACES FOR 3D MODELS

Sliding surfaces represented by a line in a 2D model now become a surface in a 3D numerical model. This section outlines the theory associated with the representation of trial slip surfaces in a 3D numerical model.

16.5.1 Ellipsoidal Sliding Surface

The equation for an ellipsoidal slip surface is:

$$\frac{(x - x_0)^2}{r_x^2} + \frac{(y - y_0)^2}{r_y^2} + \frac{(z - z_0)^2}{r_z^2} = 1 \quad \textbf{[267]}$$

An ellipsoidal sliding surface is a rotational sliding surface. It is symmetrical around the horizontal axis of rotation ($r_x = r_z$) and perpendicular to the direction of sliding. It is specified with its center point (x_0, y_0, z_0), the elevation of a horizontal tangent plane (r_z can be determined) and an aspect ratio γ.

$$\gamma = \frac{r_x}{r_y} \qquad [268]$$

which is defined as the ratio between ellipsoid semi-axes perpendicular and parallel with the direction of sliding.

It should also be noted that:

If $y = 1$, then the sliding surface is a spherical surface.
If y = a very large number, such as 1000, the sliding surface can be considered as a cylinder.

The ellipsoidal sliding surfaces can be set with the grid and tangent, slope search, cuckoo search, and entry and exit search methods, as well as, with the fully specified ellipsoid search method.

16.5.2 Multi-planar Wedges

Multi-planar wedges are non-rotational sliding surfaces. Each plane wedge is specified by dip, dip direction, and a position in space. The wedge can be used to model different orientations and surface properties such as joints, seams on faults. These discontinuities can be assigned with discontinuity properties to over-ride material properties. The discontinuity properties are entered as material properties. Each wedge plane can be assigned with the discontinuity properties.

For the fully specified multi-planar wedge sliding surface, the sliding surface is formed by choosing the highest situated plane below ground surface at each column. This algorithm applies to other composite sliding surfaces.

The user must ensure that the multi-planar wedge sliding surface's sliding direction is along the axis X and the movement of the wedges is kinematically feasible.

16.5.3 Moving Wedges

In a forward analysis the most likely location of a wedge failure may not be known. This is especially true in an area where rock fracture patterns may exist. To accommodate this type of analysis in the software the multi-planar wedge analysis has been extended to accommodate multiple potential failure planes on each side of the specified wedge. The multiple planes are defined by specifying a range of physical locations for each plane. Each resulting combination is analyzed.

16.5.4 Fully-specified General Sliding Surface

It is specified the same way as the 3D geometry surface in the software 3D. It can be used to model irregular surfaces of known geometries such as the known existing sliding failure surfaces.

16.5.5 Composite Sliding Surface

The Ellipsoids can be combined with other fully specified ellipsoids, wedges, and general surfaces, etc. Each resulting combination is analyzed.

16.6 BEDROCK

Bedrock is considered in the same manner in 3D as that in 2D. The 3D slip surface cannot pass through the Bedrock layer and therefore the slip surface is truncated by the bedrock. The bedrock layer is set by assigning a Bedrock material for the region/layer.

16.7 TENSION CRACKS

A tension crack in 3D is specified with a Tension Crack Surface which is like the tension crack line in 2D, another option is to add tension crack by Polyline on 3D ground surface, which specifies the tension crack location. The sliding surface will be truncated at the tension crack surface and tension crack polyline. The tension crack also can be filled with percentage of water as that in 2D.

16.8 DISCONTINUITIES

Discontinuities or weakness planes are those structural features which separate intact rock blocks within a rock mass and upon which movement can take place (Hoek and Bray, 1973). These can include faults, dykes, bedding planes, cleavage, tension joints and shear joints. In 3D, discontinuity properties are specified in the same way as material properties. While material properties are assigned to a region/layer combination in a 3D model, discontinuities are assigned to a wedge plane, etc., i.e., part of a sliding surface.

16.9 INITIAL CONDITIONS

The same initial conditions are implemented in 3D as those in 2D with the 2D settings converted into 3D settings. For example, the 2D pore water table line is converted into a 3D water surface. The 2D discrete pore-water pressure point is converted into a 3D discrete pore-water pressure point, etc.

16.10 POINT LOADS

The external loads in 3D are specified with Point Loads. Each point load is specified by its point of application (*x, y, z*) on the ground surface and its horizontal P_x and vertical P_z magnitude components. After the user enters the (x, y) value of the point, the program will calculate the *z* value on the ground surface automatically. Point load's *y* component is not considered in the equilibrium equations, since it is parallel to the rotation axis.

Note: Only the point loads located inside the sliding surface will be considered.

16.11 SUPPORTS

All the Support types implemented in 2D are also implemented in 3D. The main difference between the 2D and 3D implementation is that in 3D there is no need to consider the out-of-spacing value.

For example, for the End Anchored support Type, in 2D, we have the following applied force:

$$F = \frac{C}{S} \qquad \textbf{[269]}$$

where:

F = applied force of Per Unit Width of Slope,

C = tensile capacity, and

S = Out-of-Plane Spacing.

While in 3D, we have the applied force as:

$F = C$

16.12 MATERIAL STRENGTH MODELS

All the material strength models used in 2D are also supported in 3D.

16.13 VERTICAL SIDE SHEAR RESISTANCE

The shear resistance along the two vertical sides of the slide mass that parallel the direction of movement is included in calculating the 3D factor of safety to accurately simulate the 3D slide mass. The consideration of 3D end effects is important compared to 2D slope stability analysis. The method for incorporating the shear resistance along the vertical sides of a slide mass presented by Timothy D. Stark, etc. [1, 2] is coded in the software in 3D. Figure 93 is a simple 3D slope model showing shear resistance along vertical sides.

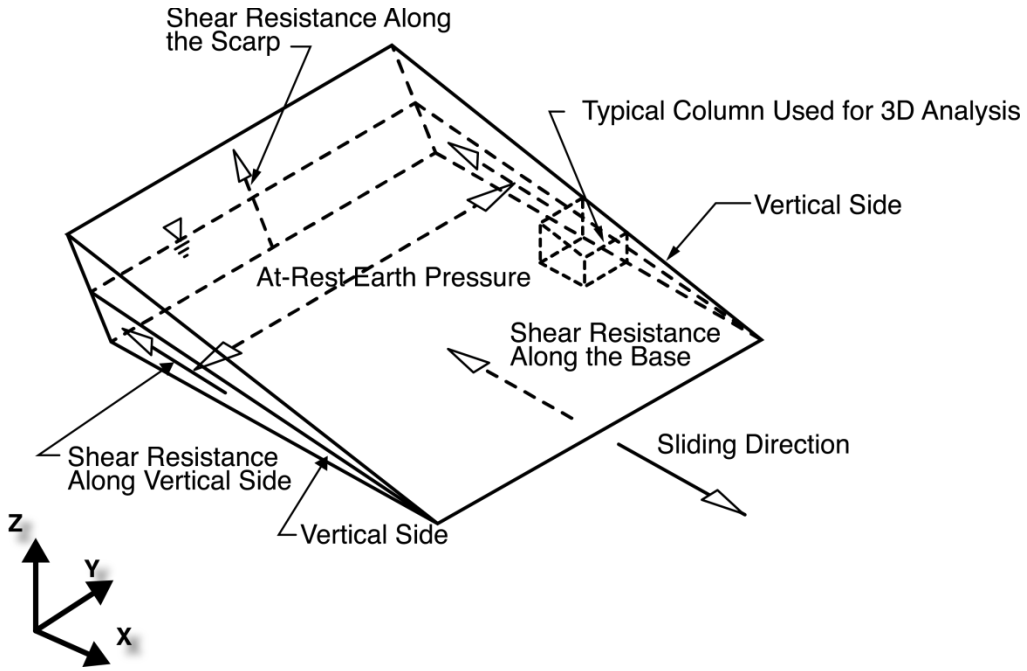

Figure 93 3D View of a simple Slope Model (based on Arellano, D. etc. [1])

To include this side resistance, an external horizontal and vertical side force equivalent to the shear resistance due to the at-rest earth pressure acting on the vertical side of each side column is added. From Figure 94, the at-rest earth pressure acting on the vertical side of the side column,σ_y', is estimated by multiplying the coefficient of earth pressure at rest,K_0, by the average vertical effective stress over the depth of side column,σ_z'. The coefficient of earth pressure at rest is determined from $K_0 = 1 - \sin\varphi'$, where φ' is the friction angle of the soil layer material of the side column.
The shear resistance due to the at-rest earth pressure action on the vertical side of the side column is estimated by the following equation:

$$S_i' = c' + K_0\sigma_z' \tan\varphi' \qquad \textbf{[270]}$$

The direction of the shear resistance S_i' is parallel to the base of each side column. The point of application is (1/3 * height of the side column) up from the side column base.

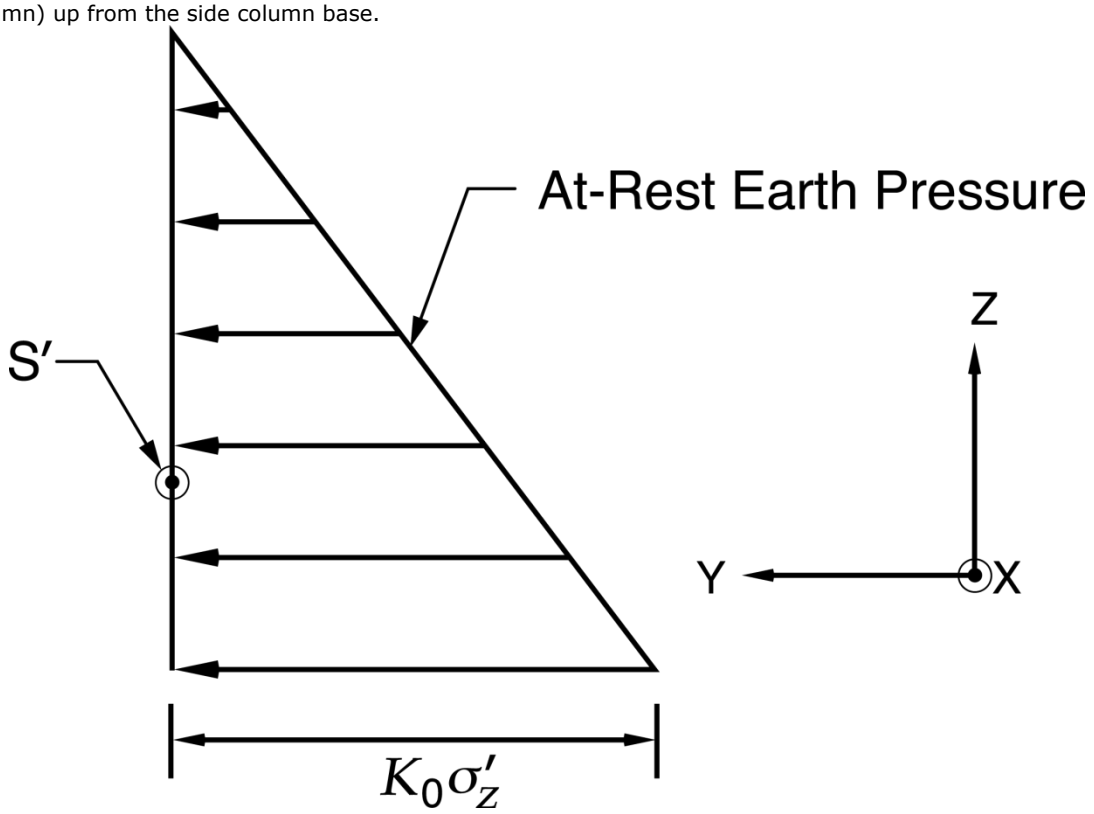

Figure 94 Shear Resistance Due to the At-Rest Earth Pressure Action on the Vertical Side of Each Side Column.

Note: Usually only translational slide mass with vertical side needs to consider the vertical side shear resistance, for rotational slide mass, no vertical side shear resistance needs to be considered with dense columns.

Generally, the calculation of the Factor of Safety can be expressed as the ratio of the resisting forces to the driving forces. Active Vertical Side Shear Resistance (VSSR) is included in the software as in following equation:

$$FOS = \text{Resisting Force} / (\text{Driving Force} - VSSR) \quad \textbf{[271]}$$

Passive Vertical Side Shear Resistance (VSSR) is included in the software as in following equation:

$$FOS = (\text{Resisting Force} + VSSR) / \text{Driving Force} \quad \textbf{[272]}$$

17 REFERENCES

Ang, A.H-S. and Tang, W.H. (1975). "Probability Concepts in Engineering Planning and Design". John Wiley and Sons. New York. 562p.

Arellano, D. and Stark, T. D. (2000), "Importance of Three-Dimensional Slope Stability Analysis in Practice," Proceedings of Sessions of Geo-Denver 2000, Slope Stability 2000, Sponsored by the Geo-Institute of the American Society of Civil Engineers. Aug. 5-8, 2000, Denver, Colorado. PP. 18-32.

Baker, R. (1980). "Determination of the critical slip surface in slope stability computations". International Journal for Numerical and Analytical Methods in Geomechanics, 4, pp. 333-359.

Bao, C., Gong, B., and Zhan, L. 1998. Properties of unsaturated soils and slope stability of expansive soils, *Proceedings of the Second International Conference on Unsaturated Soils (UNSAT 98)*, Beijing, China, Vol. 1, pp. 71-98

Barton, N. R. and Choubey, V. (1977). "The shear strength of rock joints in theory and practice". Rock Mechanics, 10(1-2): 1-54.

Becker, D. E. (1996a). "Eighteenth Canadian Geotechnical Colloquium: Limit states design for foundations. Part I. An overview of the foundation design process." Canadian Geotechnical Journal, 33: 956-983.

Becker, D. E. (1996b). "Eighteenth Canadian Geotechnical Colloquium: Limit states design for foundations. Part II. Development for the national building code of Canada." Canadian Geotechnical Journal, 33: 984-1007.

Bellman, R. (1957). "Dynamic programming". Princeton University press, Princeton, New Jersey, USA.

Bishop, A. W. (1955). "The use of the slip circle in the stability analysis of slopes". Geotechnique, 5, pp. 7-17.

Celestino, T. B., and Duncan, J. M. (1981). "Simplified search for non-circular slip surfaces". In Proceedings of the 10th International Conference on Soil Mechanics and Foundation Engineering, Stockholm, Vol. 3, pp. 391-394.

Chen, Z. -Y., and Shao, C. M. (1988). "Evaluation of minimum factor of safety in slope stability analysis". Canadian Geotechnical Journal, 25, pp. 735-748.

Cheng, Y.M., Yip, C.J., 2007. Three-Dimensional Asymmetrical Slope Stability Analysis Extension of Bishop's, Janbu's, and Morgenstern–Price's Techniques. Journal of Geotechnical and Geoenvironmental Engineering, Vol. 133, No. 12.

Ching, R. K. H., and Fredlund, D. G. (1984). "Quantitative comparison of limit equilibrium methods of slices". In Proceedings of the 4th International Symposium on Landslides, Sept. 16-21, Toronto, Canada, pp. 373-379.

Christian, J.T., Ladd, C.C., and Baecher, G.B. (1992). Reliability and probability in stability analysis. ASCE. Geotechnical Special Publication No 31. 1071-1111.

Clemen, R.T. (1996). "Making Hard Decisions." Duxbury Press, U.S. 664p.

Clough, R. W., and Woodward, R. J. (1967). "Analysis of embankment stresses and deformations". Journal of Soil Mechanics and Foundations Division, ASCE, 93(SM4), pp. 529-549.

Ditlevsen, O. (1981). "Uncertainty Modeling." McGraw Hill, New York.

Duncan, M. (2000). "Factors of safety and reliability in geotechnical engineering." Journal of Geotechnical and Geoenvironmental Engineering, ASCE, 126(4): 307-316.

Duncan, J.M., and Wright, S.G. (2005) "Soil Strength and Slope Stability." John Wiley and Sons, Inc, New Jersey.

Eschanbach, T.G. (1992). "Spiderplots versus Tornado diagrams for sensitivity analysis." Interfaces, 22(6): 40-46.

Evans, D. H. (1967). "An application of numerical techniques to statistical tolerancing." Technometrics, vol. 9.

Evans, D. H. (1972). "An application of numerical integration techniques to statistical tolerancing, general distributions." Technometrics, Vol. 14.

Fan, K., Fredlund, D. G., and Wilson, G. W. (1986). "An interslice force function for limit equilibrium slope stability analysis". Canadian Geotechnical Journal, 23, pp. 287-296.

Fenton, G. A., Griffiths, D. V. (2008). "Risk assessment in geotechnical engineering." John Wiley and Sons, Inc, New Jersey.

Fenton, G. A., Vanmarcke, E. H. (1990). "Simulation of random fields via local average subdivision". Journal of Engineering Mechanics, 116(8), pp. 1733-1749

FlexPDE 6 (2007). *Reference Manual*, PDE Solutions Inc., Spokane Valley, WA 99206.

FlexPDE 7 (2017). *Reference Manual*, PDE Solutions Inc., Spokane Valley, WA 99206.

Fredlund, D. G., and Krahn, J. (1977). "Comparison of slope stability methods of analysis". Canadian Geotechnical Journal, 14, pp. 429-439.

Fredlund, D. G., Krahn, J., and Pufahl, D.E. (1981). The relationship between limit equilibrium slope stability methods. Proceedings, International Conference on Soil Mechanics and Foundation Engineering, Stockholm, Sweden, Vol. 3, pp. 409-416.

Fredlund, D. G., Morgenstern, N.R. and Widger, R.A. (1978). Shear Strength of unsaturated soils. Canadian Geotechnical Journal, 15(3): 313-321.

Fredlund, D. G., and Rahardjo, H. (1993). "Soil mechanics for unsaturated soils". John Wiley & Sons, Inc, New York.

Fredlund, D. G., Zhang, Z.M., and Lam, L. (1992). Effect of the axis of moment equilibrium in slope stability analysis. Canadian Geotechnical Journal, 29:456-465.

Fredlund, D. G., and Scoular, R. E. G. (1999). "Using limit equilibrium in finite element slope stability analysis". Slope Stability Engineering, Balkema, Rotterdam, pp. 31-47.

Garven, E., and Vanapalli, S.K. (2006). Evaluation of empirical procedures for predicting the shear strength of unsaturated soils. Proceedings of the Fourth International Conference on Unsaturated Soils, Carefree, Arizona, American Society of Civil Engineers Geotechnical Special Publication No. 147, Vol. 2, pp. 2570-2581.

Gitirana Jr., G.F.N. (2005). "Weather-Related Geo-Hazard Assessment for Railway Embankment Stability". Ph.D. Thesis. University of Saskatchewan, Saskatoon, SK, Canada, 411p.

Ghobrial, F., Karray, M., Delisle, M-C. and Ledoux, C. (2015) Development of spectral pseudo-static method for dynamic clayey slope stability analysis. Proceedings of the 68th Canadian Geotechnical Conference and 7th Canadian Permafrost Conference: GeoQuébec 2015, Quebec City, QC. 8pgs.

Greco, V. R. (1996). "Efficient Monte-Carlo technique for locating critical slip surface". Journal of Geotechnical Engineering, ASCE, 122(7), pp. 517-525.

Hahn, G.J. and Shapiro, S.S. (1967). "Statistical Models in Engineering." John Wiley & Sons, New York.

Hammersley, J.M. and Handscomb, D. C. (1964). "Monte Carlo Method." John Wiley & Sons, New York.

Harr, M.E. (1987). "Reliability-Based Design in Civil Engineering." John Wiley and Sons. New York. 291p.

Harr, M.E. (1989). "Probabilistic estimates for multivariate analyses." Applied Mathematical Modelling, 13: 313-318.

Ho, D.Y.F., and Fredlund, D.G. (1982). The increase of shear strength due to soil suction for two Hong Kong soils. Proceedings, American Society of Civil Engineers, Canadian Geotechnical Conference on Engineering and Construction in Tropical and Residual Soils, Honolulu, Hawaii, January, pp. 263-295.

Hoek, E. (1983). 23rd Rankine lecture, Strength of jointed rock masses. Geotechnique, 33, No. 3, 187-223.

Huang, C. C., and Tsai, C. C. 2000. New method for 3D and asymmetrical slope stability analysis. Journal of Geotechnical and Geoenvironmental Engineering, Vol. 126, No. 10.

Huang, C. C., Tsai, C. C., and Chen, Y. H. 2002. "Generalized method for three-dimensional slope stability analysis." Journal of Geotechnical and Geoenvironmental Engineering, Vol. 128, No. 10.

Hungr, O. 2010, CLARA-W Slope stability analysis in two or three dimensions for microcomputers, O. Hungr Geotechnical Research Inc.

Jaky, J. (1944). "The coefficient of earth pressure at rest". Journal of Society of Hungarian Architects Engineering, 7, pp. 355-358.

Janbu, N. (1954). "Application of composite slip surfaces for stability analysis". Proceedings of the European Conference on Stability of Earth Slopes, Stockholm, 3, pp. 43-49.

Jiang, J. C., and Yamagami, T. 1999. Determination of the sliding direction in three-dimensional slope stability analysis. Proc., 44th Symp. on Geotechnical Engineering, 193–200.

Jibson, R.W., 2011, Methods for assessing the stability of slopes during earthquakes – A retrospective: Engineering Geology, v. 122, p. 43-50.

Khalili, N., and Khabbaz, M.H. 1998. A unique relationship for χ for the determination of the shear strength of unsaturated soils, *Geotechnique*, Vol. 48, No. 5, pp. 681-687.

Krahn, J. (2001). "The limits of limit equilibrium analysis". R.M. Hardy Lecture. Proceedings of the Canadian Geotechnical Conference, An Earth Odyssey, Calgary, Canada,

Ladd, C.C. and Foote, R. (1974). A new design procedure for stability of soft clays. Journal of the Geotechnical Engineering Division. ASCE, Vol. 100(GT7), 763-786

Li, K.S. (1991). "Point estimate methods in geotechnics." Computational Mechanics, Cheung, Lee, and Leung (eds), 827-832.

Li, K.S. (1992). "Point estimate method for calculating statistical moments." Journal of Engineering Mechanics, 118(7): 1506-1511.

Lind, N.C. (1983). "Modeling of uncertainty in discrete dynamical systems." Applied Mathematical Modeling, 7: 146-152.

Malkawi, A.I.H, Hassan, W.F. and Sarma, S.K. (2001). Global Search Method for Locating General Slip Surface Using Monte Carlo Technique. Journal of Geotechnical and Geoenvironmental Engineering, 127(8), 688-698.

Martins, J. B., Reis, E. B., and Matos, A. C. (1981). "New method of analysis for stability of slopes". In Proceedings of the 10th International Conference on Soil Mechanics and Foundation Engineering, Stockholm, pp. 463-467.

Matos, A. C. (1982). "The numerical influence of the Poisson's ratio on the safety factor". In Proceedings of the 4th International Conference on Numerical Methods in Geomechanics, pp. 207-211.

Mercer, K. G. (2013). "Ongoing research into anisotropic rock masses using numerical modelling", in PM Dight (ed.), *Proceedings of the 2013 International Symposium on Slope Stability in Open Pit Mining and Civil Engineering*, Australian Centre for Geomechanics, Perth, pp. 237-247.

Mercer, K. G. (2017). ALM4 Development, personal communication, October 2017.

Morgenstern, N. R., and Price, V. E. (1965). "The analysis of the stability of general slip surfaces". Geotechnique, 15, pp. 79-63.

Newmark, N.M., 1965. Effects of earthquakes on dams and embankments. Geotechnique 15, 139-159.

Nguyen, T. M. T. (1999). "Solution of saturated/unsaturated seepage problems using a general partial differential equation solver". M.Sc. thesis, University of Saskatchewan, Saskatoon, Canada.

Nguyen, V. U. (1985). "Determination of critical slope failure surfaces". Journal of Geotechnical Engineering, ASCE, 111(2), pp. 238-250.

Md. Noor, M J and Anderson, W F (2006) "A comprehensive shear strength model for saturated and unsaturated soils" Proc. 4th Int. Conf. on Unsaturated Soils, ASCE Geotechnical Special Publication No. 147, Carefree, Arizona, Vol. 2, pp 1992-2003 ISBN 0-7844-0802-5

Panchalingam, G. and Harr, M.E. (1994). "Modeling of many correlated and skewed random variables." Applied Mathematical Modeling, 18: 635-640.

Rosenblueth, E. (1975). "Point estimates for probability moments." Proc. National Academy of Sciences, 72(10): 3812-3814.

Rosenblueth, E. (1981). "Two-point estimates in probabilities." Applied Mathematical Modelling, 5: 329-335.

Rubinstein, A. (1981). "Simulation and the Monte Carlo Method." John Wiley and Sons, New York.

Sarma, S.K. (1979). "Stability Analysis of Embankments and Slopes". J. Geotech. Eng. Div. ASCE 105, No. 12, pp. 1511-1524.

Scoular, R. E. G. (1997). "Limit equilibrium slope stability analysis using a stress analysis". M.Sc. thesis, University of Saskatchewan, Saskatoon, SK. Canada.

Sevaldson, R. A. (1956). "The slide in Lodalen, October 6th, 1954". Geotechnique, 6, pp. 167-182.

Smith, J.E. (1993). "Moment methods for decision analysis." Management Science, The Institute of Management Science, 39(3): 340-358.

Spencer, E. (1967). "A method for analysis of the stability of embankments assuming parallel interslice forces". Geotechnique, 17(1), pp. 11-26.

Stark, T.D. and Eid, H.T. (1998), "Performance of Three-Dimensional Slope Stability Methods in Practice," Journal of Geotechnical and Geoenvironmental Engineering, ASCE, 124(1): 1049-1060.

Vanapalli, S.K., and Fredlund, D.G. (2000). Comparison of different procedures to predict the unsaturated soil shear strength of unsaturated soils, Geo-Denver 2000. American Society of Civil Engineers, Geotechnical Special Publication. No. 99, pp. 195-209.

Vanmarcke, E.H. (1974). "Decision analysis in dam safety monitoring." Proceedings Engineering Foundation Conf. on the Safety of Small Dams, (Henniker, N.H.), Aug.

Vanapalli, S.K., Fredlund, D.G., Pufahl, D.E., and Clifton, A.W. (1996). "Model for prediction of shear strength with respect to soil suction". Canadian Geotechnical Journal, 33, 379-392.

Whitman, R.V. (1984). "Evaluating calculated risk in geotechnical engineering." ASCE Geotechnical Engineer Journal. 110(2): 145-189.

Whitman, R.V. (2000). "Organizing and evaluating uncertainty in geotechnical engineering." Journal of Geotechnical and Geoenvironmental Engineering, ASCE, 126(7): 583-593.

Wilson, R.C., Keefer, D.K., 1983. Dynamic analysis of a slope failure from the 6 August 1979 Coyote Lake, California, earthquake. Bulletin of the Seismological Society of America 73, 863-877.

Yamagami, T., and Ueta, Y. (1988). "Search for noncircular slip surfaces by the Morgenstern-Price method". In Proceedings of the 6th International Conference on Numerical Methods in Geomechanics, Innsbruck, pp. 1335-1340.

Yamagami, T., and Jiang, J. C. 1997. A search for the critical slip surface in three-dimensional slope stability analysis. Soils Found., 37(3), 1–16.

X.-S. Yang, S. Deb, Cuckoo search via Levy flights, in: Proc. of World Congress on Nature \& Biologically Inspired Computing (NaBIC 2009), December 2009, India. IEEE Publications, USA, pp. 210-214 (2009).

Yang X-S, Deb S. Engineering optimisation by cuckoo search. PhD thesis. International Journal of Mathematical Modelling and Numerical Optimisation. 2010; 1:330–343.

Zou, J. Z., Williams, D. J., and Xiong, W. L. (1995). "Search for critical slip surfaces based on finite element method". Canadian Geotechnical Journal, 32, pp. 233-246.

18 APPENDIX A

18.1 DISCRETE POINTS INTERPOLATION METHODS

18.1.1 Spline Method

Spline method is an interpolation technique, which is used to determine the pore-pressure at a point (i.e., the center of slice base or a grid point) when the pore-pressures are defined as discrete points.

This method represents a fitting of a spline function to a series of spatially distributed points. The weighting coefficients are evaluated for the fitting of the spline function to the discrete points. The weighting coefficients can then be used to compute values for any other point in the region. It has been known that this method is not a good choice for a large problem because this method requires considerable computer storage. However, with the development of the computer techniques, the storage will not be a significant problem. In addition, it has also been found that a small number of designated points can provide reasonably accurate results.

In the following, the Spline Method is illustrated through a two-dimensional problem.

$$u(x,y) = P(x,y) + \sum_{i=1}^{N} \lambda_i K\left(h_m - h_i\right) \qquad \textbf{[273]}$$

where:

$u(x,y)$ = pore pressure at any point to be considered,

$P(x,y)$ = the chosen trend,

$K(h)$ = the chosen interpolation function,

h = the distance between two points, (e.g., $h=h_m-h_i$) and can be obtained from

$$(h_m - h_i) = \sqrt{(x_m - x_i)^2 + (y_m - y_i)^2}$$

λ_i = the computed weighting coefficients referred to as Kriging coefficients (i=1,2,3,…N),

P(x,y) and K(h) can be expressed as

$$P(x,y) = a + bx + cy \qquad \textbf{[274]}$$

$$K(h) = \delta(0) + h^2 \ln(h) \qquad \textbf{[275]}$$

where:

$\delta(0)$ = nugget effect, and

a,b,c = coefficients.

The weighting coefficients (a,b,c, λ_i, i=1,2,…,N) are the solution of the following set of linear equations:

$$\begin{bmatrix} K(0) \cdots K(h_1 - h_n) & 1 & x_1 & y_1 \\ \vdots & \vdots & \vdots & \vdots \\ & 1 & x_N & y_N \\ & 0 & 0 & 0 \\ & & 0 & 0 \end{bmatrix} \begin{bmatrix} \lambda_1 \\ \vdots \\ \lambda_N \\ a \\ b \\ c \end{bmatrix} = \begin{bmatrix} u_1 \\ \vdots \\ u_N \\ 0 \\ 0 \\ 0 \end{bmatrix} \qquad \textbf{[276]}$$

From the above equation set, the weight coefficients can be obtained. Then, the value of u(x,y) at any point can be computer using the equation:

$$u(x,y) = a + bx + cy + \sum_{i-1}^{N} \left[\lambda_i \left(h_m - h_i\right)^2 \times \ln(h_m - h_i)\right] \qquad \textbf{[277]}$$

18.2 CALCULATION BASED ON A DAT FILE

The PLAXIS LE suite of software packages utilizes the concept of regions in a consistent manner and, therefore, pore-pressures and stresses can be imported into the software from another finite element analysis such as:

- Groundwater
- Stress

For simplicity, the PLAXIS LE DAT File format (.dat) is used in the software. The values from a finite element analysis provide the node point information including *x-y* coordinates and the pore pressures, stresses and the element information including the node numbers as included in a transfer file.

The procedure for computing the values from finite element analysis is as follows:

1. Find the element encompassing the center of the base of a slice,
2. Compute the areas S_1, S_2, S_3 and S as shown in Figure 95,
3. The value at any required point P (e.g., a center of the base of a slice or a Grid Point) can be obtained from the nodal point information based on the area weight method,

$$u_p = \frac{S_1 u_{p1} + S_2 u_{p2} + S_3 u_{p3}}{S} \qquad \textbf{[278]}$$

4. Repeat Step 1) to Step 3) for the base of all slices.

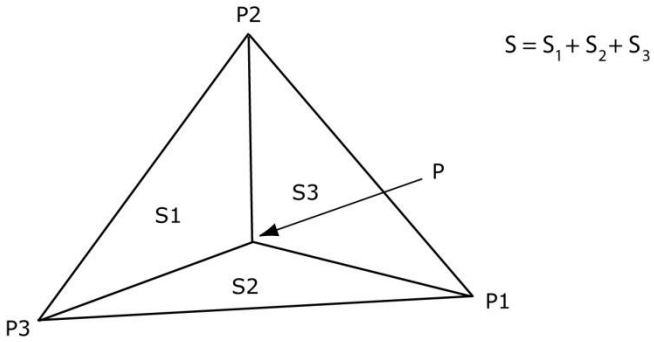

Figure 95 The area components for computing the value inside an element

18.3 LOCAL AVERAGE SUBDIVISION

18.3.1 General

The software uses Local Average Subdivision (LAS) approach to generate 2-D random fields (Fenton et al.). This approach is a fast and accurate method of generating a homogeneous Gaussian scalar random process in one, two, or three dimensions. The resulting discrete process represents local average of a homogeneous random function defined by its mean and covariance function; the averaging being performed over incremental domains formed by different levels of discretization of the field. The approach is motivated first by the need to represent engineering properties as local averages (since many properties are not well defined at a point and show significant scale effects), and second to be able to easily condition the field to incorporate known data or change resolution within sub-regions.

Although only two-dimensional fields are generated in the software, one-dimensional LAS theory is also introduced for the consistency of the approach.

18.3.2 One-Dimensional Local Average Subdivision

Local average processes which are made using Local Average Subdivision (LAS) follow a top-down recursive fashion (Figure 96). The first stage (Stage 0) contains the global average which is generated for the process. The next stage contains two subdivided regions. In the subsequent stages, each "parent cell" is subdivided and values are generated for the resulting regions while maintaining upwards averaging throughout the process. The average of each generated sub region is equivalent to the "parent" cell value; this maintains a constant average throughout the process (Fenton and Griffiths, 2008).

Such internal consistency allows for simple conditioning of the process. Specifically, the algorithm proceeds as explained in Fenton and Griffiths (2008) are as follows:

1. Generate a normally distributed global average (labeled Z_1^0 in Figure 96) with mean zero and variance obtained from local averaging theory,
2. Subdivide the field into two equal parts,
3. Generate two normally distributed values, Z_1^1, Z_2^1, whose means and variances are selected to satisfy three criteria:
    a. that they show the correct variance according to local averaging theory,
    b. that they are properly correlated with one another,
    c. that they average to the parent value,

$$\frac{1}{2}\left(Z_1^1 + Z_2^1\right) = Z_1^0 \qquad \textbf{[279]}$$

    That is, the distributions of Z_1^1 and Z_2^1 are considered on the value of Z_1^0,
4. Subdivide each cell in stage 1 into two equal parts,
5. Generate two normally distributed values, Z_1^2 and Z_2^2, whose means and variances are selected to satisfy four criteria:
    a. that they show the correct variance according to local averaging theory,
    b. that they are properly correlated with one another,
    c. that they average to the parent value,

$$\frac{1}{2}\left(Z_1^2 + Z_2^2\right) = Z_1^1 \qquad \textbf{[280]}$$

    d. that they are properly correlated with Z32, and Z42.

    The third criterion implies conditioning of the distributions of Z_1^2 and Z_2^2 on the values of Z_1^1. The fourth criteria will only be satisfied approximately by conditioning their distributions also on Z_2^1.

The process continues in this order. There are two main ways that are used to approximate in the algorithms. Adjacent cells are correlated across parent boundaries through the parent values. Secondly, the range of parent cells on which to condition the distribution will be limited to some neighborhood (Fenton and Griffiths, 2008).

The following section focuses on the determination of the conditional Gaussian and estimation of algorithmic errors. The terms 'parent cell' and 'within-cell' used in the explanations mean previous stage cell and region defined by the parent cell, respectively.

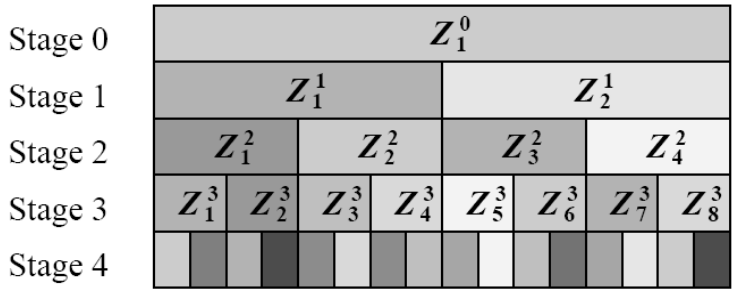

Figure 96 Top-down approach to the LAS construction of a random progress (Source: Fenton and Griffiths, 2008)

The mean and variance of the Stage 0 value, Z_1^0 is determined by considering first a continuous stationary scalar random function *Z(t)* in one dimension, a sample of which may appear as shown in Figure 97, and define a domain of interest (0, D] within which a realization is to be produced (Fenton and Griffiths, 2008).

This process is restricted to stationary processes which are described by their second-order statistics. Second-order statistics refer to their mean, variance and autocorrelation function or spectral density function. However, there is a broad class functions which can be used to model most natural phenomena. Also, the procedure used in the subdivision depends on the size of the

domain being defined. The dimensions of the domain over which the averaging will be performed must be known. The process 0 beyond the domain (0, D] is ignored. (Fenton and Griffiths, 2008).

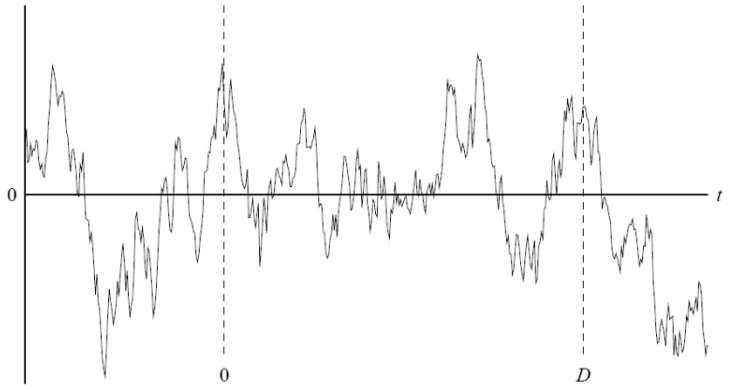

Figure 97 Sample function of an Ornstein-Uhlenbeck progress (Fenton and Griffiths, 2008)

The Average of *Z(t)* over the domain (0, D] is given by

$$Z_1^0 = \frac{1}{D}\int_0^D Z(\xi)d\xi \qquad \textbf{[281]}$$

where Z_1^0 is a random variable whose statistics

$$E\left[Z_1^0\right] = E[Z] \qquad \textbf{[282]}$$

$$E\left[\left(Z_1^0\right)^2\right] = \left(\frac{1}{D^2}\right)\iint_{0-D} E[Z(\xi)Z(\xi')]d\xi d\xi' = Z[Z]^2 + \left(\frac{2}{D^2}\right)\int_0^D (D-\tau)B(\tau)d\tau \qquad \textbf{[283]}$$

It can be found by making use of stationarity and the fact that $B(\tau)$, the covariance function of *Z(t)*, is an even function of lag τ, Without loss in generality, *E[Z]* will henceforth be taken as zero where *E[•]* is the expectation operator. If *Z(t)* is a Gaussian random function, [218] and [219] give sufficient information to generate a realization of Z_1^0 which becomes stage 0 in the LAS method. If *Z(t)* is not Gaussian, then the complete probability distribution function for Z_1^0 must be determined and a random field generated according to such a distribution. This is beyond the scope of the present approach and so we restrict our attention to Gaussian processes (Fenton and Griffiths, 2008).

Consider now the general case where stage *i* is known and stage *i+ 1* is to be generated. In the following the superscript *i* denotes the stage under consideration. Define

$$D^i = \frac{D}{2^i}, \qquad i = 0,1,2,....,L, \qquad \textbf{[284]}$$

where the desired number of intervals in the realization is $N=2^L$, and define Z_k^i to be the average of *Z(t)* over the interval $(k-1)D^i<t<=kD^i$

$$Z_k^i = \frac{1}{D^i}\int_{(k-1)D^i}^{kD^i} Z(\xi)d\xi \qquad \textbf{[285]}$$

Where $E[Z_k^i]=E[Z]=0$. The target covariance between local averages separated by lag mD^i between centers is

$$E\left[Z_k^i Z_{k+m}^i\right] = E\left[\left(\frac{1}{D^2}\right)\int_{(k-1)D^i}^{kD^i}\int_{(k+m-1)D^i}^{(k+m)D^i} Z(\xi)Z(\xi)d\xi d\xi'\right]$$

$$= \left(\frac{1}{D^i}\right)^2 \int_0^{2D^i}\int_{mD^i}^{(m+1)D^i} B(\xi-\xi')d\xi d\xi' \qquad \textbf{[286]}$$

$$= \left(\frac{1}{D^i}\right)^2 \int_{(m-1)D^i}^{mD^i}\left[\xi-(m-1)D^i\right]B(\xi)d\xi + \left(\frac{1}{D^i}\right)^2 \int_{mD^i}^{2(m+1)D^i}\left[(m+1)D^i-\xi\right]B(\xi)d\xi$$

A much simpler formulation is possible by introducing the concept of a variance function defined as follows (Vanmarcke, 1974)

$$\gamma\left(D^i\right) = \left(\frac{1}{\sigma D^i}\right)^2 \int_0^{2D^i}\int_0^{D^i} B(\xi-\xi')d\xi d\xi' = 2\left(\frac{1}{\sigma D^i}\right)^2 \int_0^{D^i}\left(\left|D^i\right|-|\tau|\right)B(\tau)d\tau \qquad \textbf{[287]}$$

where

$$\sigma^2 = B(0) \qquad \textbf{[288]}$$

Vanmarcke (1974) has determined this function for a variety of processes. In terms of the variance function, Equation [197] becomes for n≥ 0

$$E\left[Z_k^i Z_{k+n}^i\right] = \frac{\sigma^2}{2}\left[(n-1)^2\gamma\left((n-1)T^i\right) - 2n^2\gamma\left(nT^i\right) + (n+1)^2\gamma\left((n+1)T^i\right)\right] \qquad \textbf{[289]}$$

	j		$j+1$		
	$2j-1$	$2j$	$2j+1$	$2j+2$	

Figure 98 1D LAS indexing scheme for stage *i* (top) and stage *i+1* (bottom)

With reference to Figure 98, the construction of stage *i+1* values given stage *i* is obtained by estimating a mean for Z_{2j}^{i+1} and adding a zero mean discrete white noise $c^{i+1}W_j^{i+1}$ having variance $(c^{i+1})^2$,

$$Z_{2j}^{i+1} = M_{2j}^{i+1} + c^{i+1}W_j^{i+1} \qquad \textbf{[290]}$$

where:

Z =the algorithmic process which will approximate Z,

The best linear estimate for the mean M_{2j}^{i+1} can be determined by a linear combination of stage *i* values in some neighborhood *j-n,…,j+n*,

$$M_{2j}^{i+1} = \sum a_{k-j}^i Z_k^i \qquad \textbf{[291]}$$

Multiplying Equation [201] through by Z_m^i, taking expectations and using the fact that W_j^{i+1} is uncorrelated with the stage I values allows the determination of the coefficients a in terms of the desired covariance,

$$E\left[Z_{2j}^{i+1} Z_m^i\right] = \sum_{k=j-n}^{j+n} a_{k-j}^i E\left[Z_k^i Z_m^i\right] \qquad \textbf{[292]}$$

i.e., a system of equations ($m=j-n,\ldots,j+n$) from which the coefficients $a_l^i, l=-n,\ldots,n$ can be solved.

Note that the exact process Z is used when evaluating expectations. The covariance matrix multiplying the vector $\{a_l\}$ is both symmetric and Toeplitz (elements along each diagonal are equal). For $W_j^{i+1} \sim N(0,1)$, the variance of the noise term is $(c^{i+1})^2$ which can be verified by squaring Equation [275], taking expectations, and employing the results of Equation [277]

$$\left(c^{i+1}\right)^2 = E\left[\left(Z_{2j}^{i+1}\right)^2\right] - \sum a_{k-j}^{i} E\left[Z_{2j}^{i+1} Z_{k}^{j}\right] \quad \textbf{[293]}$$

The adjacent cell value, Z_{2j-1}^{i+1}, is determined by ensuring that upwards averaging is preserved that the average of each stage *i + 1* pair equals the value of the stage *i* parent,

$$Z_{2j-1}^{i+1} = 2Z_{j}^{i} - Z_{2j}^{i+1} \quad \textbf{[294]}$$

which incidentally gives a means of evaluating the cross-stage covariance

$$E\left[Z_{2j}^{i+1} Z_{m}^{i}\right] = \frac{1}{2} E\left[Z_{2j}^{i+1} Z_{2m-1}^{i+1}\right] + \frac{1}{2} E\left[Z_{2j}^{i+1} Z_{2m}^{i+1}\right] \quad \textbf{[295]}$$

All the expectations in Equations [277] to [280] are evaluated using [274] or [276] at the appropriate stage.

For stationary processes, the set of coefficients {*a*/}_g and ci are independent of position since the expectations in [293] and [295] are just dependent on lags. The generation procedure can be restated as follows:

1. for *i = 0,1,2,…,L* compute the coefficients {*a*/}, *l=-n,…,n* using [277] and the coefficients c^{i+1} using [293],
2. starting with *i* = 0, generate a realization for the global mean using [218] and [219],
3. subdivide the domain,
4. for each j = 1, 2,…,2i, generate realizations for Z2ji+1 and Z2j-1i+1 using [275] and [279],
5. increment *i* and, if not greater than *L*, return to step 3.

Because the LAS procedure is recursive, obtaining stage *i+1* values using the previous stage, it is relatively easy to condition the field simply by specifying the values of the local averages at a particular stage. So, for example, if the global mean of a process is known *a priori*, then the stage 0 value Z_1^0 can be set to this mean and the LAS procedure started at stage 1. Similarly, if the resolution is to be refined in a certain region, then the values in that region become the starting values and the subdivision resumed at the next stage.

Although the LAS method yields a local average process, when the discretization size becomes small enough it is virtually indistinguishable from the limiting continuous process. Thus, the method can be used to approximate continuous functions as well.

Finally, it should be noted that the calculation of the coefficients a and c need only be done once for a particular process. Subsequent realizations can then be produced extremely efficiently by starting at step 2 in the procedure listed above.

18.3.3 Multi-Dimensional Extensions

In two dimensions, a rectangular domain is defined and the subdivision proceeds by dividing rectangles into 4 equal areas at each stage. To preserve the exact 'within cell' covariance structure, three random noises are added to three of the cell quadrants and the fourth quadrant is determined such that upwards averaging is preserved. Figure 99 presents the 2D LAS scheme for the first 3 stages in which the center of each local average is marked with a different symbol for each stage. The generating relationships are,

$$Z_1^{i+1} = Z_{2j,2k}^{i+1} = c_{11}^{i+1} W_{1jk}^{i+1} + \sum_{\ell=1}^{n_{xy}} a_{\ell 1}^{i} Z_{m(\ell),n(\ell)}^{i} \quad \textbf{[296]}$$

$$Z_2^{i+1} = Z_{2j,2k-1}^{i+1} = c_{21}^{i+1} W_{1jk}^{i+1} + c_{22}^{i+1} W_{2jk}^{i+1} + \sum_{\ell=1}^{n_{xy}} a_{\ell 2}^{i} Z_{m(\ell),n(\ell)}^{i} \quad \textbf{[297]}$$

$$Z_3^{i+1} = Z_{2j-1,2k}^{i+1} = c_{31}^{i+1} W_{1jk}^{i+1} + c_{32}^{i+1} W_{2jk}^{i+1} + c_{33}^{i+1} W_{3jk}^{i+1} + \sum_{\ell=1}^{n_{xy}} a_{\ell 3}^{i} Z_{m(\ell),n(\ell)}^{i} \quad \textbf{[298]}$$

$$Z_4^{i+1} = Z_{2j-1,2k-1}^{i+1} = 4Z_{jk}^{i} - Z_{2j,2k}^{i+1} - Z_{2j,2k-1}^{i+1} - Z_{2j-1,2k}^{i+1} \quad \textbf{[299]}$$

where *W* is a discrete zero-mean, unit variance Gaussian white noise and *m(l),n(l)* are indexing functions traversing in a fixed pattern the $n_{xy} = (2n_x+1)\times(2n_y+1)$ neighborhood of Z_{jk}^{i}. In this implementation, $n_x = n_y = 1$ and the boundary conditions are handled in the same fashion as for the 1-D case. The coefficients $\{a_{lr}^{i}\}$ can be calculated from the linear equations.

$$E\left[Z_{2j,2k}^{i+1} Z_{m(p),n(p)}^{i}\right] = \sum_{\ell=1}^{n_{xy}} a_{\ell 1}^{i} E\left[Z_{m(\ell),n(\ell)}^{i} Z_{m(p),n(p)}^{i}\right] \qquad p = 1,2,\ldots,n_{xy} \qquad \textbf{[300]}$$

$$E\left[Z_{2j,2k-1}^{i+1} Z_{m(p),n(p)}^{i}\right] = \sum_{\ell=1}^{n_{xy}} a_{\ell 2}^{i} E\left[Z_{m(\ell),n(\ell)}^{i} Z_{m(p),n(p)}^{i}\right] \qquad p = 1,2,\ldots,n_{xy} \qquad \textbf{[301]}$$

$$E\left[Z_{2j-1,2k}^{i+1} Z_{m(p),n(p)}^{i}\right] = \sum_{\ell=1}^{n_{xy}} a_{\ell 3}^{i} E\left[Z_{m(\ell),n(\ell)}^{i} Z_{m(p),n(p)}^{i}\right] \qquad p = 1,2,\ldots,n_{xy} \qquad \textbf{[302]}$$

In which the matrices on the right-hand sides are symmetric but no longer Toeplitz in general. The coefficient matrix *ci+1* is assumed to be lower triangular satisfying

$$c^{i+1} \cdot (c^{1+1}) = R \qquad \textbf{[303]}$$

where R is symmetric and given by

$$R_{rs} = E\left[Z_r^{i+1} Z_s^{i+1}\right] - \sum a_{\ell r}^{i} \left[Z_{m(\ell),n(\ell)}^{i} Z_s^{i+1}\right] \qquad r,s = 1,2,3 \qquad \textbf{[304]}$$

Using the indexing notation defined at the extreme left of [281]-[284]. Notice that the assumption of homogeneity vastly decreases the number of coefficients that need to be calculated and stored since $\{a_{lr}^{i}\}$ and c^{i+1} become independent of position. As in the 1-D case, the coefficients need only be calculated prior to the first realization – they can be re-used in subsequent realizations reducing the effective cost of their calculation.

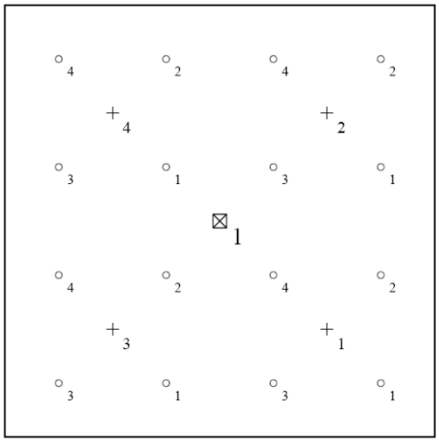

Figure 99 Fist three stages and indexing scheme of the 2D LAS algorithm (Fenton and Griffiths, 2008)

The expectations used in Equations [285] to [289] can be determined from the two-dimensional variance function of the process:

$$\begin{aligned} E\left[Z_{jk}^{i} Z_{j+m,k+n}^{i}\right] = \frac{1}{4}\sigma^2 \Big[& (m-1)^2\left(n-1^2\right)\gamma^i(m-1,n-1) - 2(m-1)^2 n^2 \gamma^i(m-1,n) \\ & + (m-1)^2(n+1)^2\gamma^i(m-1,n+1) \\ & - 2m^2(n-1)^2\gamma^i(m,n-1) + 4(mn)^2\gamma^i(m,n) - 2m^2(n+1)^2\gamma^i(m,n+1) \\ & + (m+1)^2(n+1)^2\gamma^i(m+1,n-1) - 2(m+1)^2 n^2\gamma^i(m+1,n) \\ & + (m+1)^2(n+1)^2\gamma^i(m+1,n+1)\Big] \end{aligned} \qquad \textbf{[305]}$$

where:

$\gamma^i(m,n)$ $= \gamma\left(mT_1^i, nT_2^i\right)$, and

T_1^i, T_2^i =the dimensions of the individual averaging rectangles at stage *i*.

For a quadrant symmetric covariance structure, $\gamma(\bullet)$ is defined by Vanmarcke (1984) to be

$$\lambda(D_1, D_2) = \left(\frac{1}{\sigma D_1 D_2} \right)^2 \int_{-D_1}^{D_1} \int_{-D_2}^{D_2} \left(|D_1| - |\tau_1|\right)\left(|D_2| - |\tau_2|\right) B(\tau_1, \tau_2)\, d\tau_1 d\tau_2 \qquad \textbf{[306]}$$

where

$B(\tau_1, \tau_2)$ = covariance function,

$$B(\tau_1, \tau_2) = \sigma^2 \exp\left(\gamma(D_2)\right) \qquad \textbf{[307]}$$

For the exponential covariance function (185), the value of c should be taken as $\pi/2$. Other forms of this approximate 2-D variance function are given by Vanmarcke (1984).

Although the within-cell covariance structure is reflected exactly by the LAS method, the overall statistics of anisotropic processes are rather poorly preserved. The generated field tends to become isotropic with a scale of fluctuation equal to the minimum scale specified. At this time, it is better to create the anisotropy through post-processing of an isotropic field: generate an isotropic field using a single scale of fluctuation and stretch the resulting field in the direction of the other directional scale of fluctuation to obtain an ellipsoidal correlation structure.

19 APPENDIX B - DYNAMICS - TECHNICAL PREVIEW

19.1 DYNAMICS INTRODUCTION

DYNAMICS is currently in Technical Preview.

Seismic analysis of geotechnical structures involves finding the solution of a set of time-dependent Partial Differential Equations (PDEs) that describe the response of the geotechnical system to a high frequency dynamic excitation, i.e., an earthquake. Earthquake-induced stresses that can be used for stability analysis are also an outcome of seismic analysis. Simplified pseudo-static analysis incorporates the effect of inertial forces into static analysis to provide a valuable insight into some peak values, such as deformations and stresses, that are essential for design. However, many important aspects of a seismic analysis will remain unrevealed unless a fully dynamic analysis, that solves the time dependent PDEs, is performed. The propagation and interaction of seismic waves and the variation of stresses over time can only be captured by means of a dynamic analysis.

DYNAMICS is a finite element analysis package capable of solving two-dimensional dynamic stress-strain models. DYNAMICS performs time-domain dynamic analysis under various types of user-defined dynamic loads. The software can perform seismic analysis using imported earthquake records as well as a combination of dynamic forces and seismic excitations. The availability of a vast choice of boundary conditions provides flexibility for simulating different field conditions such as free surfaces, continuous domains, rigid and semi rigid boundaries, etc. Our user-friendly and efficient interface allows the user to conveniently input the geometry, assign material properties, and define dynamic loads and seismic boundary conditions.

DYNAMICS is a module within the PLAXIS LE software; therefore, geometry can easily be transferred from other modules to DYNAMICS. The output generated by DYNAMICS can be imported to the PLAXIS LE - Slope Stability module to perform dynamic slope stability analysis for two-dimensional models. DYNAMICS uses the PLAXIS LE front-end interface for model setup, PLAXIS LE dynamic finite-element engine for the numerical analysis, and the PLAXIS LE back-end interface for results visualization.

This appendix provides the theoretical basis and the computational approach used by DYNAMICS for performing seismic analysis. The manual, however, does not intend to present an exhaustive review of all theories and numerical techniques associated with seismic analysis. Appropriate citations to the relevant references are provided throughout this manual and the user may refer to those references when in-depth discussions of the theory and numerical techniques are required. For details regarding the software operation and modeling guidelines the user should consult the USER MANUAL and the DYNAMICS TUTORIAL MANUAL, included with the software.

This appendix is organized in the following chapters:

- Chapter 1 presents an overview of DYNAMICS
- Chapter 2 explains the basic principles and concepts involved in the formulation of the governing equations for a general dynamic analysis in DYNAMICS
- Chapter 3 presents the stress-strain relationships and provides information on the selection of appropriate material properties
- Chapter 4 discusses the numerical schemes implemented in DYNAMICS for solving time-dependent systems of PDEs
- Chapter 5 explains the initial conditions and their implementation in DYNAMICS
- Chapter 6 explains the theory and implementation of dynamic boundary conditions in DYNAMICS
- Chapter 7 presents a useful list of references and reading materials

19.1.1 Analysis Types

DYNAMICS can handle the following types of analyses:

Stress variable: Total stress

Stress/strain conditions: (a) 2D plane strain
(b) General 3D stress conditions.

19.1.2 Constitutive Models

DYNAMICS currently allows total stress analysis using a linear elastic constitutive law. More advanced material constitutive models may be added to the DYNAMICS library of constitutive models.

19.1.3 Boundary Conditions

Several types of essential and natural boundary conditions can be defined in DYNAMICS. The vast range of available boundary conditions allow for the enforcement of general fixed and free conditions as well as prescribed values of displacement,

velocity, or acceleration at any boundary of the domain. Different types of non-reflecting boundary conditions can also be defined to simulate truncated domains in a continuum. DYNAMICS is also capable of performing dynamic analysis under various combinations of dynamic loads and seismic motions.

19.2 BASIC PRINCIPLES AND EQUATIONS

DYNAMICS is based on the dynamic analysis theory, applied to two-dimensional (i.e., plane-strain analysis) and three-dimensional models. Dynamic stress analysis can be expressed in terms of time dependent partial differential equations, governing the motion of an infinitesimal differential volume of material.
The equations of motion are combined with constitutive relations and strain-displacement equations to produce a displacement-based formulation. DYNAMICS employs the infinitesimal strains theory for this purpose. Choices of spatial and temporal numerical integration schemes are also required for solving the final set of differential equations, which will be explained in Chapter 4 of this manual.

This chapter explains the basic principles and conventions adopted in DYNAMICS for formulating the governing equations of a general (seismic) dynamic analysis.

19.2.1 Stress/Strain Conditions and Coordinate Systems

Dynamic behavior of a mechanical system is governed by a set of time dependent PDEs solution of which requires the evaluation of spatial and temporal derivatives. The choice of a spatial coordinate system and a time dimension directly affects the solution of the governing equations. Hence, this section explains the conventions adopted in DYNAMICS for the spatial coordinate system and time dimension.

19.2.1.1 Spatial Coordinate System

A two-dimensional Cartesian coordinate system (*x, y*) is used to present the geometry of a 2D plane strain model where the *y*-direction corresponds to the elevation:

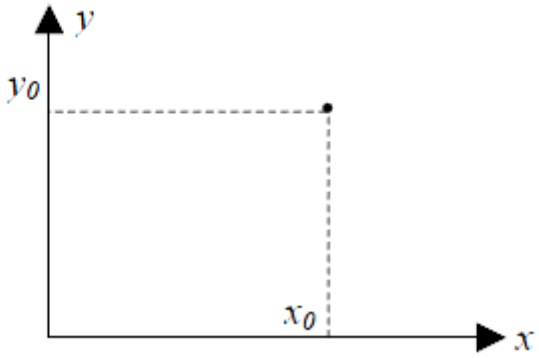

Figure 100 2D Cartesian coordinate system for 2D plane strain analysis in DYNAMICS

Two-dimensional plane strain problems correspond to conditions where the strain in the *z*-direction is zero. Therefore, the stress and strain distributions are independent of the *z*-coordinate. In other words, there is a cross-section of the problem geometry in the *x*-*y* plane that represents the entire problem. Many geotechnical problems can be approximated by a plane strain analysis. Examples of such problems include earth embankments, strip footings, highway embankments, and pipeline foundations.
For general 3D models, a 3D cartesian coordinate system (*x, y, z*) is adopted for presenting the geometry of the model. The z axis corresponds to the elevation in this case.

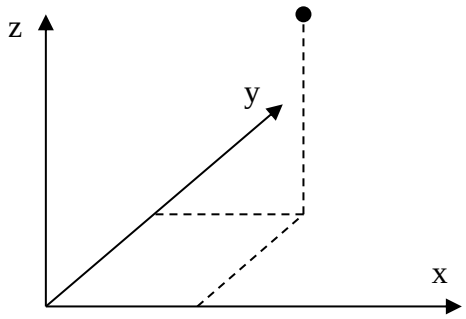

Figure 101 3D Cartesian coordinate system for general 3D analysis in DYNAMICS

The geometry and other conditions of a particular application usually suggests the necessity of using 3D analysis or the possibility of using a simplified 2D model. It is worth mentioning that problems that do not completely conform with the plane strain condition are still often analyzed using the plane strain approach, by selecting representative cross sections. Such approximation is considered common in geotechnical engineering practice but requires engineering judgement.

19.2.1.2 Time Dimension

The time domain in dynamic analysis is a one-dimensional domain with positive values. The time origin (i.e., $t = 0$) in DYNAMICS is assumed to be the time at which a dynamic analysis starts. The initial conditions of the dynamic analysis should be defined at this time.

19.2.2 Sign Conventions

DYNAMICS uses the sign conventions that are most commonly used in geotechnical engineering. The sign conventions adopted are specified in the following sections.

19.2.2.1 Load and Displacement

The sign convention of loads and displacements are defined according to the positive directions of the global coordinate system introduced in the previous section. A force component is considered positive if it is acting in one of the positive directions of the global coordinate system. Similarly, a displacement component that occurs in a positive direction of the global coordinate system is considered positive. For example, a positive force acting in the *x*-direction will be acting towards the right. An upward displacement in a 2D problem will be considered a positive displacement in the *y*-direction. A downward force or displacement in a 3D model will be considered a negative force or displacement in the *z*-direction.

19.2.2.2 Stresses

DYNAMICS follows the standard geotechnical engineering sign convention where compression is positive. To maintain the generality of the topic, in this manual, stress analysis is discussed in the general 3D form and reduced to 2D plane strain conditions when necessary. Consider an infinitesimal differential volume of material, as illustrated in Figure 102. A surface of the differential volume is considered a positive surface if its outward normal vector points in the positive coordinate direction. Similarly, negative surfaces are those whose normal vectors point in the negative coordinate direction. Figure 102(a) illustrates all positive and negative surfaces of a differential volume. The conventions of positive stress components are presented in Figure 102(b). On a positive surface, all stresses that act in the negative coordinate directions are considered positive. On a negative surface, all stresses acting in the positive coordinate directions are positive. Therefore, compression is positive, and tension is negative. The above rule also applies to shear stresses.

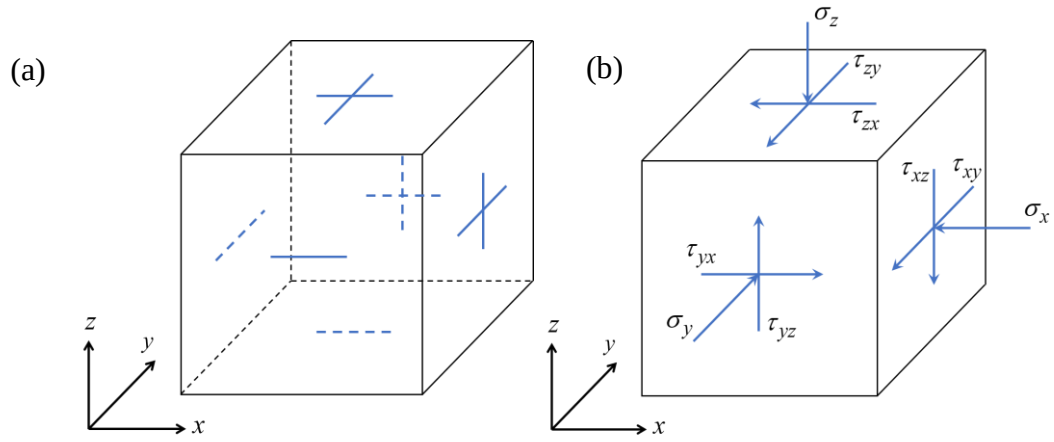

Figure 102 Illustration of the convention for (a) positive and negative surfaces and (b) positive components of stress tensor in DYNAMICS

19.2.2.3 Strains

Normal strains are considered positive when the length in the direction of the strain decreases. When a differential volume is subject to positive shear strains, the right angles between its edges and the extensions of the coordinate axes in the negative directions increase, while the right angles between the positive directions of the coordinate axes and the extensions of the edges in the negative directions decrease.

19.2.3 Units

Seismic analysis in DYNAMICS can be performed in either Metric or Imperial units. The system of units selected dictates the required units when entering material properties, loads, and geometric dimensions.

The following table presents model variables and their units in both Metric and Imperial systems:

Table 3 Model Variable Units in DYNAMICS

VARIABLE	METRIC SYSTEM	IMPERIAL SYSTEM
Distance	meter, *m*	foot, *ft*
Time	second, *s*	second, *s*
Displacement	meter, *m*	foot, *ft*
Velocity	*m/s*	*ft/s*
Acceleration	m/s^2	ft/s^2
Strain	%	%
Force	kilo Newton, *kN*	pound force, *lbf*
Concentrated load	kilo Newton, *kN*	pound force, *lbf*
Spread/line load	*kN/m*	*lbf/ft*
Stress	kN/m^2	lbf/ft^2 (*psf*)
Acceleration of gravity	m/s^2	ft/s^2
Mass	kilogram, *kg*	pound mass (pound), *lbm* (*lb*)
Unit weight	kN/m^3	lbf/ft^3 (*pcf*)
Young modulus	*kPa*	lbf/ft^2 (*psf*)
Poisson ratio	unitless	unitless
Damping ratio	unitless	unitless
Frequency	hertz, *Hz* (s^{-1})	hertz, *Hz* (s^{-1})
Phase	radian, *rad*	radian, *rad*

19.2.4 Stress and strain Tensors

Considering Cartesian coordinates, the general stress and strain tensors, **σ** and **ε** respectively, for a total stress analysis are presented as follows:

$$\boldsymbol{\sigma} = \begin{bmatrix} \sigma_x & \tau_{xy} & \tau_{xz} \\ \tau_{xy} & \sigma_y & \tau_{yz} \\ \tau_{xz} & \tau_{yz} & \sigma_z \end{bmatrix} \quad \text{and} \quad \boldsymbol{\varepsilon} = \begin{bmatrix} \varepsilon_x & \gamma_{xy} & \gamma_{xz} \\ \gamma_{xy} & \varepsilon_y & \gamma_{yz} \\ \gamma_{xz} & \gamma_{yz} & \varepsilon_z \end{bmatrix} \qquad [1]$$

where:

σ_i and ε_j = respectively the normal stress and strain acting on the *i*-plane, in the *i*-direction ($i, j \in \{x, y, z\}$)

τ_{ij} and γ_{ij} = respectively the shear stress and strain acting on the *i*-plane, in the *j*-direction ($i, j \in \{x, y, z\}$)

For 2D plane strain conditions, the normal strains, shear strains, and shear stresses acting in the *z*-direction vanish, and the stress and strain tensors reduce to the following:

$$\boldsymbol{\sigma} = \begin{bmatrix} \sigma_x & \tau_{xy} & 0 \\ \tau_{xy} & \sigma_y & 0 \\ 0 & 0 & \sigma_z \end{bmatrix} \quad \text{and} \quad \boldsymbol{\varepsilon} = \begin{bmatrix} \varepsilon_x & \gamma_{xy} & 0 \\ \gamma_{xy} & \varepsilon_y & 0 \\ 0 & 0 & 0 \end{bmatrix} \qquad [2]$$

19.2.5 Displacement Derivatives

19.2.5.1 Spatial Derivatives

In general 3D conditions, the relationships between the components of strain and displacements can be written, in a Cartesian coordinate system, as follows:

$$\varepsilon_x = \frac{\partial u}{\partial x}\ ,\quad \varepsilon_y = \frac{\partial v}{\partial y}\ ,\quad \varepsilon_z = \frac{\partial w}{\partial z}$$
$$\gamma_{yz} = \frac{\partial v}{\partial z} + \frac{\partial w}{\partial y},\quad \gamma_{xz} = \frac{\partial u}{\partial z} + \frac{\partial w}{\partial x},\quad \gamma_{xy} = \frac{\partial v}{\partial x} + \frac{\partial u}{\partial y} \qquad \textbf{[3]}$$

where:

u, v, z = the displacements in the *x*-, *y*-, and *z*-directions, respectively

For 2D plane strain conditions, the *z* component of displacement and all derivatives with respect to z-coordinates are zero. Hence, the six components of strain reduce to the following three:

$$\varepsilon_x = \frac{\partial u}{\partial x}\ ,\quad \varepsilon_y = \frac{\partial v}{\partial y}\ ,\quad \gamma_{xy} = \frac{\partial v}{\partial x} + \frac{\partial u}{\partial y} \qquad \textbf{[4]}$$

These relationships are derived assuming small strains.

19.2.5.2 Temporal Derivatives

The first and second temporal derivatives of displacement in each direction, respectively represent the values of particle velocity and acceleration in that direction:

$$\dot{u} = \frac{\partial u}{\partial t}\ ,\quad \dot{v} = \frac{\partial v}{\partial t},\quad \dot{w} = \frac{\partial w}{\partial t}$$
$$\ddot{u} = \frac{\partial^2 u}{\partial t^2},\quad \ddot{v} = \frac{\partial^2 v}{\partial t^2},\quad \ddot{w} = \frac{\partial^2 w}{\partial t^2} \qquad \textbf{[5]}$$

where:

$\dot{u}$, $\dot{v}$, and $\dot{w}$ = the values of particle velocity in the *x*-, *y*-, and *z*-directions, respectively

$\ddot{u}$, $\ddot{v}$, and $\ddot{w}$ = the values of acceleration in the *x*-, *y*-, and *z*-directions, respectively

19.2.6 Equations of motion

The motion of an infinitesimal differential element of a continuum under the applied stresses (stresses are illustrated in Figure 102(b)) is governed by the conservation of linear momentum (also known as the equation of motion). The differential element should be sufficiently small such that material properties and measured variables can be considered continuous within the element.

19.2.6.1 General 3D

The equations of motion in the *x*-, *y*-, and *z*-directions, respectively, are presented as follows:

$$\frac{\partial \sigma_x}{\partial x} + \frac{\partial \tau_{xy}}{\partial y} + \frac{\partial \tau_{xz}}{\partial z} + b_x = \rho_s \frac{\partial^2 u}{\partial t^2} \qquad \textbf{[6]}$$

$$\frac{\partial \tau_{xy}}{\partial x} + \frac{\partial \sigma_y}{\partial y} + \frac{\partial \tau_{yz}}{\partial z} + b_y = \rho_s \frac{\partial^2 v}{\partial t^2} \qquad \textbf{[7]}$$

$$\frac{\partial \tau_{xz}}{\partial x} + \frac{\partial \tau_{yz}}{\partial y} + \frac{\partial \sigma_z}{\partial z} + b_z = \rho_s \frac{\partial^2 w}{\partial t^2} \qquad \textbf{[8]}$$

where:

σ_i and τ_{ij} = the total normal and shear stresses ($i, j \in \{x, y, z\}$), respectively,

b_i = the component of body force in the *i*-direction ($i \in \{x, y, z\}$)

The conservation of angular momentum suggests $\tau_{ij} = \tau_{ji}$. The terms on the right-hand side of [6]-[8] represent the inertial forces applied to the differential element, in which:

ρ_s = the average mass density of the solid in the differential element

t = analysis time

19.2.6.2 2D Plane Strain

By default, DYNAMICS creates all two-dimensional models in the *x-y* plane of the Cartesian coordinate system. Therefore, in a two-dimensional plane strain analysis, the component of displacement in the z-direction and all special derivatives with respect to the z-coordinate vanish. Thus, the equations of motion reduce to the following two equations in the *x*- and *y*-directions, respectively:

$$\frac{\partial \sigma_x}{\partial x} + \frac{\partial \tau_{xy}}{\partial y} + b_x = \rho_s \frac{\partial^2 u}{\partial t^2} \qquad [9]$$

$$\frac{\partial \tau_{xy}}{\partial x} + \frac{\partial \sigma_y}{\partial y} + b_y = \rho_s \frac{\partial^2 v}{\partial t^2} \qquad [10]$$

in which, all variables have been defined previously.

The equations of motion, [9] and [10], are time dependent and represent the propagation of two coupled disturbances (waves) in the *x-y* plane. The longitudinal disturbance is known as the Dilatational or Primary wave (P-wave) and the transverse disturbance is known as the Shear or Secondary wave (S-wave). In the general 3D case, the equations of motion, [6]-[8], represent the propagation of one P-wave and two S-waves (known as SH- and SV-wave) in the three-dimensional space. For a detailed discussion about the wave theory, the user is referred to Harris (2001) and Achenbach (1973).

19.2.7 Final Partial Differential Equations

DYNAMICS uses a displacement-based dynamic formulation; therefore, the stress-based equations of motion should be converted to displacement-based Partial Differential Equations by means of the stress-strain constitutive relations.

Let the stress-strain relation in its general form be defined by:

$$\boldsymbol{\sigma} = \mathbf{S}(\boldsymbol{\varepsilon}) \qquad [11]$$

where:

$\mathbf{S}$ = the function that defines the stress-strain relation

This general representation results in an incremental form of the constitutive relation that can be used to express various types of constitutive models. The incremental form of the constitutive equation is obtained by differentiating [11] with respect to the strain tensor:

$$d\boldsymbol{\varepsilon} = \mathbf{D}^{-1} d\boldsymbol{\sigma} \qquad [12]$$

where:

$$\mathbf{D} = \frac{d\mathbf{S}(\boldsymbol{\varepsilon})}{d\boldsymbol{\varepsilon}} = \begin{bmatrix} D_{11} & D_{12} & D_{13} & D_{14} & D_{15} & D_{16} \\ D_{21} & D_{22} & D_{23} & D_{24} & D_{25} & D_{26} \\ D_{31} & D_{32} & D_{33} & D_{34} & D_{35} & D_{36} \\ D_{41} & D_{42} & D_{43} & D_{44} & D_{45} & D_{45} \\ D_{51} & D_{52} & D_{53} & D_{54} & D_{55} & D_{56} \\ D_{61} & D_{62} & D_{63} & D_{64} & D_{65} & D_{66} \end{bmatrix}$$

$$\boldsymbol{\sigma}^T = \left\{ \sigma_x \quad \sigma_y \quad \sigma_z \quad \tau_{xy} \quad \tau_{yz} \quad \tau_{zx} \right\}$$

$$\boldsymbol{\varepsilon}^T = \left\{ \varepsilon_x \quad \varepsilon_y \quad \varepsilon_z \quad \gamma_{xy} \quad \gamma_{yz} \quad \gamma_{zx} \right\}$$

The above generalized relationship is used in this section to present a general format for constitutive models implemented in DYNAMICS. The user is referred to Chapter 3 for a detailed discussion of constitutive models that can be adopted by DYNAMICS. The last step for converting the stress-based equations of motion to displacement-based PDEs is re-writing the components of strain in terms of displacements using the strain-displacement relations presented in section 19.2.5.1.

19.2.7.1 General 3D

Re-writing the components of strain in terms of displacements and substituting stress-strain relations into the equations of motion, the set of PDEs governing the motion of an infinitesimal differential element under general 3D conditions can be re-written as:

$$\frac{\partial}{\partial x}\left[D_{11}\frac{\partial u}{\partial x}+D_{12}\frac{\partial v}{\partial y}+D_{13}\frac{\partial w}{\partial z}\right]+\frac{\partial}{\partial y}\left[D_{44}\left(\frac{\partial v}{\partial x}+\frac{\partial u}{\partial y}\right)\right]+\frac{\partial}{\partial z}\left[D_{66}\left(\frac{\partial w}{\partial x}+\frac{\partial u}{\partial z}\right)\right]+b_x=\rho_s\frac{\partial^2 u}{\partial t^2} \qquad [\ 13\ ]$$

$$\frac{\partial}{\partial x}\left[D_{44}\left(\frac{\partial v}{\partial x}+\frac{\partial u}{\partial y}\right)\right]+\frac{\partial}{\partial y}\left[D_{21}\frac{\partial u}{\partial x}+D_{22}\frac{\partial v}{\partial y}+D_{23}\frac{\partial w}{\partial z}\right]+\frac{\partial}{\partial z}\left[D_{55}\left(\frac{\partial w}{\partial y}+\frac{\partial v}{\partial z}\right)\right]+b_y=\rho_s\frac{\partial^2 v}{\partial t^2} \qquad [\ 14\ ]$$

$$\frac{\partial}{\partial x}\left[D_{66}\left(\frac{\partial w}{\partial x}+\frac{\partial v}{\partial z}\right)\right]+\frac{\partial}{\partial y}\left[D_{55}\left(\frac{\partial w}{\partial y}+\frac{\partial v}{\partial z}\right)\right]+\frac{\partial}{\partial z}\left[D_{31}\frac{\partial u}{\partial x}+D_{32}\frac{\partial v}{\partial y}+D_{33}\frac{\partial w}{\partial z}\right]+b_z=\rho_s\frac{\partial^2 w}{\partial t^2} \qquad [\ 15\ ]$$

in which, all variables have been previously defined.

19.2.7.2 2D Plane Strain

Similarly, the displacement based governing equations under 2D plane strain conditions can be presented as:

$$\frac{\partial}{\partial x}\left[D_{11}\frac{\partial u}{\partial x}+D_{12}\frac{\partial v}{\partial y}+D_{14}\left(\frac{\partial v}{\partial x}+\frac{\partial u}{\partial y}\right)\right]+\frac{\partial}{\partial y}\left[D_{41}\frac{\partial u}{\partial x}+D_{42}\frac{\partial v}{\partial y}+D_{44}\left(\frac{\partial v}{\partial x}+\frac{\partial u}{\partial y}\right)\right]+b_x=\rho_s\frac{\partial^2 u}{\partial t^2} \qquad [\ 16\ ]$$

$$\frac{\partial}{\partial x}\left[D_{41}\frac{\partial u}{\partial x}+D_{42}\frac{\partial v}{\partial y}+D_{44}\left(\frac{\partial v}{\partial x}+\frac{\partial u}{\partial y}\right)\right]+\frac{\partial}{\partial y}\left[D_{21}\frac{\partial u}{\partial x}+D_{22}\frac{\partial v}{\partial y}+D_{24}\left(\frac{\partial v}{\partial x}+\frac{\partial u}{\partial y}\right)\right]+b_y=\rho_s\frac{\partial^2 v}{\partial t^2} \qquad [\ 17\ ]$$

in which, all variables have been previously defined.

19.3 CONSTITUTIVE RELATIONSHIPS

DYNAMICS currently allows total stress analysis using a linear elastic constitutive law. More advanced material constitutive models may be added to the DYNAMICS library of constitutive models.

19.3.1 General

Two important decisions should be made when defining a mathematical model to describe the physical behavior of a material:

1. Selection of a constitutive model that is suitable for the type of behavior being modeled, and,
2. Entry of material behavior parameters applicable to the selected constitutive model.

19.3.2 Isotropic Linear Elastic Law (Total Stress)

The general incremental form of the material constitutive law, [12], for a material with an isotropic linear elastic behavior is reduced to the following format:

$$\boldsymbol{\varepsilon}=\mathbf{D}^{-1}\boldsymbol{\sigma} \qquad [\ 18\ ]$$

where:

$$\mathbf{D}=\begin{bmatrix} D_{11} & D_{12} & D_{12} & 0 & 0 & 0 \\ D_{12} & D_{11} & D_{12} & 0 & 0 & 0 \\ D_{12} & D_{12} & D_{11} & 0 & 0 & 0 \\ 0 & 0 & 0 & D_{44} & 0 & 0 \\ 0 & 0 & 0 & 0 & D_{44} & 0 \\ 0 & 0 & 0 & 0 & 0 & D_{44} \end{bmatrix}$$

$$\boldsymbol{\sigma}^T=\begin{Bmatrix}\sigma_x & \sigma_y & \sigma_z & \tau_{xy} & \tau_{yz} & \tau_{zx}\end{Bmatrix}$$

$$\boldsymbol{\varepsilon}^T = \begin{Bmatrix} \varepsilon_x & \varepsilon_y & \varepsilon_z & \gamma_{xy} & \gamma_{yz} & \gamma_{zx} \end{Bmatrix}$$

$$D_{11} = \frac{E(1-\nu)}{(1+\nu)(1-2\nu)}$$

$$D_{12} = \frac{E\nu}{(1+\nu)(1-2\nu)}$$

$$D_{44} = \frac{E}{2(1+\nu)}$$

where:

E = Young's modulus
ν = Poisson ratio

For a two-dimensional plane strain analysis, ε_z, γ_{xz}, and γ_{yz} are zero. Substituting these values into [18], the out-of-plane components of stress are directly calculated as:

$$\begin{aligned} \sigma_z &= D_{12}\left(\varepsilon_x + \varepsilon_y\right) \\ \tau_{yz} &= 0 \\ \tau_{zx} &= 0 \end{aligned} \qquad \textbf{[19]}$$

Hence, [18] can be expressed only in terms of the in-plane components of stress and strain as follows:

$$\boldsymbol{\varepsilon} = \mathbf{D}^{-1}\boldsymbol{\sigma} \qquad \textbf{[20]}$$

Where:

$$\mathbf{D} = \begin{bmatrix} D_{11} & D_{12} & 0 \\ D_{12} & D_{11} & 0 \\ 0 & 0 & D_{44} \end{bmatrix}$$

$$\boldsymbol{\sigma}^T = \begin{Bmatrix} \sigma_x & \sigma_y & \tau_{xy} \end{Bmatrix}$$

$$\boldsymbol{\varepsilon}^T = \begin{Bmatrix} \varepsilon_x & \varepsilon_y & \gamma_{xy} \end{Bmatrix}$$

The relations in [18] can alternatively be expressed in terms of the bulk and shear moduli of the material, K and G respectively. In that case, one can use the following expressions to convert the values of one set of material properties to another:

$$K = \frac{E}{3(1-2\nu)} \qquad \textbf{[21]}$$

$$G = \frac{E}{2(1+\nu)} \qquad \textbf{[22]}$$

or

$$E = \frac{9KG}{3K+G} \qquad \textbf{[3083]}$$

$$\nu = \frac{3K - 2G}{2G + 6K} \qquad [\ 24\ ]$$

The linear elastic constitutive model is defined in terms of E and ν parameters in DYNAMICS. The value of Poisson ratio is theoretically bounded by 0 and 0.5, respectively representing a fully compressible and a totally incompressible material. To avoid numerical difficulties arising from incompressible mechanics, DYNAMICS has limited the upper bound of Poisson's ratio to 0.499 instead of 0.5.

The P- and S-waves, introduced in Chapter 2, propagate with finite velocities in an elastic domain. The propagation velocities (not to be confused with particle velocity which is the first temporal derivative of displacement at each point of the domain) of P- and S-waves depend on the material properties of the elastic domain and can be calculated by:

$$V_P = \sqrt{\frac{K + \frac{4}{3}G}{\rho_s}} \qquad [\ 25\ ]$$

$$V_S = \sqrt{\frac{G}{\rho_s}} \qquad [\ 26\ ]$$

where:

V_P and V_S = the propagation velocities of P- and S-wave, respectively

It is obvious from [25] and [26] that $V_P > V_S$, as K and G always take positive values.

19.4 DISCRETIZATION AND NUMERICAL SOLUTION

The equations of motion introduced in Chapter 2 describe the propagation of (seismic) waves in the space and time domains. DYNAMICS employs a time-domain dynamic finite element method for solving these equations. To numerically solve the PDEs of motion, appropriate discretization of both space and time domains are required. This chapter explains the numerical techniques used by DYNAMICS to perform (seismic) dynamic analysis.

19.4.1 Discrete form of governing equations

DYNAMICS uses 3-node triangular elements for the discretization of the space domain in 2D problems and 4-node tetrahedral elements for the discretization of the 3D space. Using the Galerkin method (see Zienkiewicz et al. (2013) for more details) and applying the approximation of displacements corresponding to the adopted element type, the partial differential equations of motion are reduced to the following system of Ordinary Differential Equations (ODEs) in terms of the time variable, t:

$$\mathbf{M}\ddot{\mathbf{u}}(t) + \mathbf{K}\mathbf{u}(t) = \mathbf{F}(t) \qquad [\ 27]$$

where:

$\mathbf{M}$ = Mass matrix of the domain
$\mathbf{K}$ = Stiffness matrix of the domain
$\mathbf{F}$ = the vector of all external dynamic forces
$\mathbf{u}$ and $\ddot{\mathbf{u}}$ = the vectors of nodal displacements and nodal accelerations, respectively

For a detailed explanation of finite element approximation and the calculation of the above matrices, the user is referred to Zienkiewicz et al. (2013), Bathe (2006), Cook et al. (1989), or other finite element method references.

It should be noted that using [27] for seismic analysis preserves the kinetic energy of the system during the analysis as no mechanism for the dissipation of energy is incorporated in [27].

19.4.2 Mass matrix

The mass matrix of the model is defined by:

$$\mathbf{M} = \int_{\Omega} \mathbf{N}^T \rho_s \mathbf{N} d\Omega \qquad [\ 28]$$

where:

$\mathbf{N}$ = the matrix of finite element shape functions
Ω = the domain of analysis

In general, [28] introduces a consistent mass matrix representing a continuous mass over the domain of analysis. Alternatively, one can assume that the mass of the domain is discrete and lumped at the nodes of the finite element mesh. This assumption reduces the mass matrix to a diagonal matrix, significantly decreasing the computational cost of matrix inversion when solving the system of equations.

Several techniques exist in the literature for obtaining the lumped mass matrix for a discretized continuum (Zienkiewics et al., 2013). A common and simple though effective mass lumping technique (for domains without discontinuities) replaces the diagonal term of each row of the consistent mass matrix with the sum of its components at that row while setting all off-diagonal components to zero, i.e.:

$$\bar{m}_{ij} = \begin{cases} \sum_{j=1}^{n} m_{ij} & i = j \\ 0 & i \neq j \end{cases} \qquad \textbf{[29]}$$

where:

$\bar{m}_{ij}$ and m_{ij} = components of the lumped and consistent mass matrices, respectively

n = total number of degrees of freedom

i, j = row and column indices of mass matrix components, respectively

DYNAMICS uses a lumped mass matrix in all its (seismic) dynamic analyses.

19.4.3 Damping matrix

The equation of motion shown in [27] represents the motion of a system whose kinetic energy is preserved. In reality, however, the kinetic energy of a system declines over time due to the activation of internal mechanism (e.g., internal friction between soil grains) dissipating the kinetic energy of the system. To account for the energy dissipation, the average effect of all existing dissipative mechanisms is incorporated in the model by adding a viscous damping (i.e., velocity proportional) term to the equation of motion. The matrix representation of the equation of motion for a system with viscous damping can be written as:

$$\mathbf{M}\ddot{\mathbf{u}}(t) + \mathbf{C}\dot{\mathbf{u}}(t) + \mathbf{K}\mathbf{u}(t) = \mathbf{F}(t) \qquad \textbf{[30]}$$

where:

$\mathbf{C}$ = Damping matrix of the domain

The damping matrix, $\mathbf{C}$, represents the average effect of all internal mechanisms that dissipate the kinetic energy of the system. Various assumptions can be made about the structure of the damping matrix based upon the behavior and micro-structure of the material. DYNAMICS uses a common classic format for the damping matrix known as the Rayleigh damping model.

Rayleigh damping model assumes that the damping matrix of a domain can be defined as a linear combination of its mass and stiffness matrices:

$$\mathbf{C} = \alpha\mathbf{M} + \beta\mathbf{K} \qquad \textbf{[31]}$$

where:

α and β = coefficients of mass- and stiffness-proportional damping, respectively

Coefficients, α and β, respectively have units of s^{-1} and s.

The relationship between the damping ratios and natural frequencies of a system damped by a Rayleigh-type damping is given by a set of quadratic expressions in terms of the natural frequencies as follows (Kramer, 1995):

$$\xi_n = \tfrac{1}{2}\left(\alpha \big/ \omega_n + \beta\omega_n \right) \qquad \textbf{[32]}$$

where:

ω_n = the natural frequency corresponding to the nth vibration mode of the system (a.k.a. the nth natural frequency of the system)

ξ_n = the damping ratio of the nth vibration mode of the system

Hence, to determine the Rayleigh coefficients, α and β, one can use [32] for two different natural frequencies of the system and their corresponding damping ratios to determine the two unknowns. In practice, it is common to assume that both modes

have the same damping ratio. Therefore, for a given damping ratio, ξ, corresponding to two different modes of the system with natural frequencies, $\omega_1 = \omega$ and $\omega_2 = \lambda\omega$, Rayleigh coefficients can be directly calculated as:

$$\alpha = \frac{2\xi\lambda\omega}{1+\lambda} \quad \text{and} \quad \beta = \frac{2\xi}{\omega(1+\lambda)} \qquad \textbf{[33]}$$

where:

λ = the ratio of the two natural frequencies of the system

DYNAMICS uses user-defined values for the damping ratio and the minimum and maximum response frequencies of the model to determine Rayleigh damping coefficients from [31].

19.4.4 Time domain discretization and Integration schemes

The equation of motion, [30], represents a set of ODEs with respect to time and should be integrated over the time domain to yield a set of algebraic equations that can be solved for nodal displacements of the system. Once displacements are calculated, a numerical differentiation scheme is required to obtain velocities and accelerations form the displacements.

Numerical integration/differentiation over the time domain requires the time domain to be discretized. The effective size of the time increments is directly dictated by the physical properties of the space domain, such as mass and stiffness, and the numerical algorithm employed for carrying out time integration/differentiation over the time domain.

When an explicit numerical scheme (e.g. Central Difference Method) is employed, the solution is conditionally stable. In this case, the time increment used in dynamic analysis must satisfy the Courant-Friedrichs-Lewy (CFL) condition (Courant et al. 1967) which limits the maximum size of the time increment to a critical value defined as:

$$\Delta t_{cr} = L_{\min} \Big/ V_P \qquad \textbf{[34]}$$

where:

Δt_{cr} = the critical time increment (the maximum admissible value for a time step)

$L_{\min}$ = the smallest distance between any two nodes of the finite element mesh

V_P = velocity of P-wave in the domain

Satisfaction of the CFL condition is a requirement for the stability of the explicit numerical scheme.

When an unconditionally stable implicit scheme (e.g., Constant-average-acceleration Newmark Method) is used, the satisfaction of the CFL condition is no longer a requirement for the stability of the numerical scheme. It is recommended, however, to use time increments close to the value of the critical time increment [34] in order to preserve the accuracy of the results (Bathe, 2006). DYNAMICS generates analysis time arrays according to the sampling frequency of the input signals (defined by the user) and observing the requirements for an accurate dynamic solution.

DYNAMICS presents two powerful implicit schemes for numerical integration/differentiation in the time domain, known as the Newmark method and the HHT-α method.

19.4.4.1 Newmark Method

The Newmark family of methods (Newmark, 1959) has been implemented in DYNAMICS for performing numerical integration/differentiation over the time domain. The values of acceleration and velocity at the $(n+1)$th discrete time step, $t_{n+1} = t_n + \Delta t$, can respectively be calculated, according to the Newmark method, as:

$$\begin{aligned} \ddot{\mathbf{u}}_{n+1} &= a_0(\mathbf{u}_{n+1} - \mathbf{u}_n) - a_1\dot{\mathbf{u}}_n - a_2\ddot{\mathbf{u}}_n \\ \dot{\mathbf{u}}_{n+1} &= \dot{\mathbf{u}}_n + a_3\ddot{\mathbf{u}}_n + a_4\ddot{\mathbf{u}}_{n+1} \end{aligned} \qquad \textbf{[35]}$$

where:

$$a_0 = \frac{1}{\alpha_N \Delta t^2} \quad , \quad a_1 = \frac{1}{\alpha_N \Delta t} \quad , \quad a_2 = \frac{1}{2\alpha_N} - 1$$
$$a_3 = \Delta t\left(1 - \delta_N\right) \quad , \quad a_4 = \delta_N \Delta t$$

with Newmark parameters: $\delta_N \geq 0.50$ and $\alpha_N \geq 0.25\left(0.5+\delta_N\right)^2$

Substituting [35] into the equation of motion, [30], at time $t = t_{n+1}$, the nodal displacement vector of the model is obtained by solving the following system of algebraic equations for the displacement vector, $\mathbf{u}_{n+1}$:

$$\left(\mathbf{K}+a_0\mathbf{M}+a_5\mathbf{C}\right)\mathbf{u}_{n+1}=\mathbf{F}_{n+1}+\mathbf{M}\left(a_0\mathbf{u}_n+a_1\dot{\mathbf{u}}_n+a_2\ddot{\mathbf{u}}_n\right)+\mathbf{C}\left(a_5\mathbf{u}_n+a_6\dot{\mathbf{u}}_n+a_7\ddot{\mathbf{u}}_n\right) \quad \textbf{[36]}$$

where:

$$a_5=\frac{\delta_N}{\alpha_N\Delta t} \quad , \quad a_6=\frac{\delta_N}{\alpha_N}\text{-}1 \quad , \quad a_7=\frac{\Delta t}{2}\left(\frac{\delta_N}{\alpha_N}\text{-}2\right)$$

When the Newmark scheme is chosen for time integration/differentiation, DYNAMICS by default uses $\alpha_N = 0.25$ and $\delta_N = 0.50$ representing the unconditionally stable constant-average-acceleration scheme which is second order accurate and optimum for most problems. Newmark parameters in DYNAMICS can be modified by the user; however, it is highly recommended that the user exercises caution when modifying these parameters. Inappropriately chosen values of Newmark parameters may result in an unstable scheme. Furthermore, choosing a value of $\delta_N > 0.50$ results in an artificial numerical damping that can eliminate some important frequency contents of the dynamic solution (Newmark, 1959), and hence should be used with caution. It is also worth noting that choosing any admissible value of $\delta_N \neq 0.50$ will reduce the Newmark method to a first order accurate scheme.

19.4.4.2 HHT-α method

The Hilber-Hughes-Taylor-α (HHT-α) scheme is a generalization of the Newmark scheme (Hilber, Hughes and Taylor, 1977). The scheme uses the same finite difference equations used by the Newmark method, [35], for relating the kinematics of the system. However, the equation of motion is modified to introduce a time lag, characterized by parameter α, to the contributions of damping forces, internal forces (or stiffness when dealing with linear problems), and external loads:

$$\mathbf{M}\ddot{\mathbf{u}}_{n+1}+(1-\alpha)\mathbf{C}\dot{\mathbf{u}}_{n+1}+\alpha\mathbf{C}\dot{\mathbf{u}}_n+(1-\alpha)\mathbf{K}\mathbf{u}_{n+1}+\alpha\mathbf{K}\mathbf{u}_n=(1-\alpha)\mathbf{F}_{n+1}+\alpha\mathbf{F}_n \quad \textbf{[37]}$$

Like the Newmark scheme, substituting [35] into [37] yields the following system of algebraic equations that will be solved for the displacement vector, $\mathbf{u}_{n+1}$.

$$\begin{aligned}&\left[(1-\alpha)\mathbf{K}+a_0\mathbf{M}+(1-\alpha)a_5\mathbf{C}\right]\mathbf{u}_{n+1}=(1-\alpha)\mathbf{F}_{n+1}+\alpha\mathbf{F}_n\\&+\mathbf{M}\left(a_0\mathbf{u}_n+a_1\dot{\mathbf{u}}_n+a_2\ddot{\mathbf{u}}_n\right)+(1-\alpha)\mathbf{C}\left(a_5\mathbf{u}_n+a_6\dot{\mathbf{u}}_n+a_7\ddot{\mathbf{u}}_n\right)-\alpha\left(\mathbf{C}\dot{\mathbf{u}}_n+\mathbf{K}\mathbf{u}_n\right)\end{aligned} \quad \textbf{[38]}$$

All parameters in [38] have been previously defined.

The HHT-α scheme is at least second order accurate in displacement and unconditionally stable provided that $0 \leq \alpha \leq \frac{1}{3}$ and the following relations between α_N, δ_N, and α are satisfied.

$$\delta_N = 0.50+\alpha \quad \text{and} \quad \alpha_N = 0.25\left(1-\alpha^2\right) \quad \textbf{[39]}$$

The HHT-α scheme reduces to the Newmark scheme for α=0. Increasing α will add an artificial numerical damping to the scheme which dampens out the undesirable high frequency content ($f > 1/2\Delta t$) of the response. For more details about the HHT-α scheme, the user is referred to Hughes (1983). The HHT-α scheme is the default time integration scheme in DYNAMICS.

19.5 INITIAL CONDITIONS

Seismic analysis is an Initial Boundary Value Problem (IBVP). In addition to the boundary conditions of the system at any time t>0, solution of an IBVP requires the initial state of the system (i.e., the state of the system at t=0). The initial conditions for a seismic analysis in DYNAMICS are defined in the form of initial stresses.

19.5.1 Initial Stresses

In DYNAMICS, the model is assumed initially to be in static equilibrium under the applied forces, such as gravity.

Let the initial state of stress in a model under a static equilibrium with all applied forces be denoted by $\boldsymbol{\sigma}_0$. The general form of the constitutive model presented in [11] can be re-written, without loss of generality, to account for the initial state of stress as follows:

$$\boldsymbol{\sigma} = \mathbf{S}(\boldsymbol{\varepsilon}, t) + \boldsymbol{\sigma}_0 \qquad [\ 40\ ]$$

where:

$\mathbf{S}(\boldsymbol{\varepsilon},t)$ = the change in the stress state after the initial state (i.e., during seismic analysis)

Hence, the deformations of the initial state can be discarded, and its stresses can be imported as initial stresses for seismic analysis in the constitutive law. Generally, $\mathbf{S}(\boldsymbol{\varepsilon},t)$, can also be a function of the initial state of stress, $\boldsymbol{\sigma}_0$. However, for a linear elastic constitutive law, $\mathbf{S}(\boldsymbol{\varepsilon},t)$ is independent of $\boldsymbol{\sigma}_0$.

It is imperative that any time-dependent boundary condition defined by the user be consistent, at time t=0, with the above assumption of initial conditions. This means that the initial stresses should be computed considering the boundary conditions of the dynamic model at t=0. In case of an inconsistent boundary condition at time t=0, DYNAMICS gives priority to the initial condition by overriding the boundary condition at time t=0 with the initial condition and applying appropriate corrections to avoid numerical instability.

19.6 BOUNDARY CONDITIONS

This section outlines different types of boundary conditions that can be defined for a dynamic analysis in DYNAMICS.

19.6.1 Dynamic forces

The definition of a dynamic force in DYNAMICS involves determining the location of the boundary on which the force applies, the magnitude of the force, and its time dependency. Time dependency is a function that defines the variation of the force magnitude over time. DYNAMICS uses a separation of variables approach to implement dynamic forces in its finite element formulation. Therefore, a general dynamic force, $\mathbf{F}$, acting at point, $\mathbf{x}$, at time, t, can be defined as:

$$\mathbf{F}(\mathbf{x},t) = \bar{\mathbf{F}}(\mathbf{x})T(t) \qquad [\ 41\ ]$$

where:

$\mathbf{x}$ = the location vector of the point on the boundary at which the force is applied

$\bar{\mathbf{F}}$ = a vector that defines the spatial distribution of the dynamic force

T = a scalar function that defines the variation in the magnitude of the dynamic force over time

Definition of a dynamic force in DYNAMICS requires the user to define the boundary on which the dynamic force is applied, the magnitude of the force, and the distribution of the force over the boundary (i.e., defining $\bar{\mathbf{F}}(\mathbf{x})$) as well as assigning a time dependency to the force (i.e., defining $T(t)$).

19.6.2 Constraints

Dynamic boundary conditions in DYNAMICS can be explained under two major categories: First, the boundary conditions that do not prevent wave reflection into the domain. Second, the non-reflecting boundary conditions that absorb the energy of the outgoing waves and prevent their reflection into the domain.

19.6.2.1 Free, fixed and motion boundary conditions

DYNAMICS allows the use of free and fixed boundaries in each direction of the global coordinate system. In addition to that, the user can prescribe motion on a boundary in the *x*-, *y*-, and *z*-directions to represent seismic excitation of a boundary. Prescribed motions can be defined as time-dependent displacements, velocities, or accelerations.

Defining any of the above-mentioned types of constraint on a boundary will result in the reflection of seismic waves from the boundary into the domain of analysis. While such reflection may be of interest in some cases (e.g., interaction with a rigid base), it may not be desirable in many other cases as the reflected wave can distort the solution within the domain.

Generally, a free boundary condition is suggested to be used on a boundary that represents a free surface, such as the ground surface or the surface of a slope. In this case, the reflection of the waves from the boundary is consistent with the actual behavior of seismic waves interacting with a free surface, and therefore is desirable.

Fixed boundary conditions can be used to represent a layer that is infinitely rigid compared to the domain of analysis. The reflected waves are also desirable in this case as the amount of energy absorbed by the rigid layer is negligible in comparison with the amount of energy reflected into the domain from the rigid boundary.

When an interacting rigid layer transmits motion to the domain, motion boundary conditions can be used to represent the reflection of the waves and transmission of motions at the same time. A motion boundary condition can be defined independently

in each direction on a boundary. In DYNAMICS, defining a motion boundary condition must be followed by assigning a pre-defined motion (displacement, velocity, or acceleration) to the direction in which the motion boundary condition is defined. For example, if a motion boundary condition is defined in the *x*-direction on a boundary, a pre-defined motion must be assigned to that boundary to define the time variation of boundary displacements, velocities, or accelerations in the *x*-direction.

When wave reflection from the boundaries is not desirable, the user should choose non-reflecting boundary conditions as explained in section 6.2.2 of this manual.

19.6.2.2 Non-reflecting boundary conditions

It is common in geotechnical analysis to represent a large or an infinite domain with a truncated finite domain and apply appropriate boundary conditions on the truncation boundaries to resemble the far field behavior. Defining such boundary conditions can be challenging for both static and dynamic analysis. In seismic analysis, the major challenge arising from domain truncation is the elimination of unphysical wave reflections from the boundaries of the truncated domain. The unphysical reflected waves will interact with the waves propagating within the domain and distort the results of analysis.

To overcome this limitation, the boundaries of the model should be chosen far enough such that, the reflected waves do not propagate back to the domain of interest during the analysis. This approach, however, becomes prohibitively expensive in many cases as the propagation velocity of seismic waves is significant in most geotechnical materials.

Alternatively, one can enforce appropriate boundary conditions at the truncation boundary to completely absorb the kinetic energy of the outgoing waves and prevent any reflection from the boundaries. This type of boundary condition is referred to as *non-reflecting* boundary condition.

Non-reflecting boundary conditions in DYNAMICS have been implemented based on the theory developed by Lysmer and Kuhlemeyer (1969) and extended by Joyner and Chen (1975). Lysmer and Kuhlemeyer suggested that enforcing the following set of boundary stresses can provide a perfect absorption of the outgoing waves at the boundary:

$$\sigma_n = \rho_s V_P \dot{u}_n$$
$$\sigma_t = \rho_s V_S \dot{u}_t \qquad \textbf{[42]}$$

where:

subscripts *n* and *t* denote the components in the directions normal and tangential to the boundary, respectively

The values of ρ_s, V_P, and V_S are calculated from the material properties of the domain adjacent to the non-reflecting boundary.

Unlike the boundary conditions explained in section 19.6.2.1, DYNAMICS does not allow the independent application of non-reflecting boundary conditions in different directions on a boundary. When a boundary of a model is defined as non-reflecting boundary, the non-reflecting boundary condition will be enforced to that boundary in *x*-, *y*-, and *z*-directions.

If a motion is assumed to be transmitted from the far-field to the truncated domain, the damping of the outgoing waves and transmission of the far-field motion to the domain can be enforced simultaneously using a formulation like [42]:

$$\sigma_n = \rho_s V_P \left(\dot{u}_n - \dot{u}_n^g\right)$$
$$\sigma_t = \rho_s V_S \left(\dot{u}_t - \dot{u}_t^g\right) \qquad \textbf{[43]}$$

where:

$\dot{u}_n^g$ and $\dot{u}_t^g$ = the components of velocity of the far-field motion in the directions normal and tangential to the boundary, respectively

In this case, DYNAMICS allows the application of independent far-field motions in the directions normal and tangential to the boundary.

It should be noted that both [42] and [43] are used for enforcing a perfect absorption of outgoing P- and S-waves on the non-reflecting boundaries. This assumption is valid when the contrast between the rigidity of the truncated domain and the adjacent material is negligible. Therefore, no reflection occurs at their interface. If the domain is truncated at an interface of two materials with contrasting rigidity (e.g., the interface of a soil column and the underlying rock), it is normal to assume that the energy of the wave is only partially absorbed at the boundary. The remaining part of the wave energy will be transferred to the domain in the form of reflected waves. To account for this effect, Joyner, and Chen (1975) presented a modified version of Lysmer and Kuhlemeyer's formulation, [43], which is used for modeling partially reflecting boundaries:

$$\sigma_n = \rho_s V_P \left(\dot{u}_n - 2\dot{u}_n^g \right)$$
$$\sigma_t = \rho_s V_S \left(\dot{u}_t - 2\dot{u}_t^g \right) \quad \textbf{[44]}$$

It is important to note that the appropriate choice of boundary conditions for (seismic) dynamic analysis should be made by the user based on their engineering judgement. It is the user's responsibility to ascertain that the boundary conditions chosen for (seismic) dynamic analysis are good representatives of the actual conditions for the problem of interest.

19.7 DYNAMICS REFERENCES

Achenbach, J. D. (1973). Wave Propagation in Elastic Solids. North Holland Publishing Company.

Bathe, K. J. (2006). Finite Element Procedures. Klaus-Jürgen Bathe.

Cook, R. D., Malkus, D. S., & Plesha, M. E. (1989). Concepts and Applications of Finite Element Analysis (3rd ed.). John Wiley & Sons, Inc.

Courant, R., Friedrichs, K., & Lewy, H. (1967). On the Partial Difference Equations of Mathematical Physics. IBM Journal of Research and Development 11(2): 215-234.

Harris, J. G. (2001). Linear Elastic Waves. Cambridge University Press.

Hilber, H. M., Hughes, T. J. R., & Taylor, R. L. (1977). Improved Numerical Dissipation for Time Integration Algorithms in Structural Dynamics. Earthquake Engineering and Structural Dynamics 5:283-292.

Hughes, T. J. R. (1983). Analysis of Transient Algorithms with Particular Reference to Stability Behavior. Computational Methods for Transient Analysis, North Holland Publishing Company, 67-155.

Joyner, W. B., & Chen, A. T. F. (1975). Calculation of Nonlinear Ground Response in Earthquakes. Bulletin of the Seismological Society of America. 65(5): 1315-1336.

Kramer, S. L. (1995). Geotechnical Earthquake Engineering. Prentice-Hall, Inc.

Lysmer, J., & Kuhlemeyer, R. L. (1969). Finite-Dynamic Model for Infinite Media. Journal of Engineering Mechanics Division. 95: 859-877.

Newmark, N. M. (1959). A Method of Computation for Structural Dynamics. Journal of Engineering Mathematics, ASCE. 85(EM3): 67-94

Zienkiewics, O. C., Taylor, R., & Zhu, J. Z. (2013). The Finite Element Method: Its Basis and Fundamentals (7th ed.). Butterworth-Heinemann.